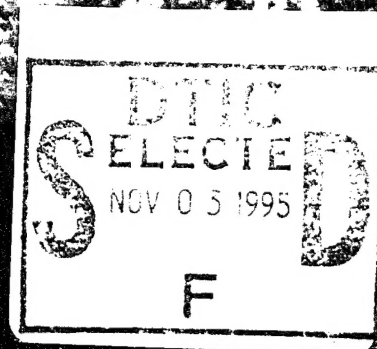


CLOUD IMPACTS ON DOD OPERATIONS AND SYSTEMS 1995 CONFERENCE

U.S. Air Force Phillips Laboratory – Science Center
Hanscom Air Force Base, Massachusetts
24-26 October 1995



DISTRIBUTION STATEMENT A

Approved for public release
Distribution Unlimited

CIDOS – 95

Cloud Modeling and Data for Defense Simulation Activities
"Emphasizing Sufficient Physical Reality in Simulating Clouds"

Front Cover: Daytime color composite image of the Tyrrhenian and Adriatic Seas, Italy, and the western Balkan Peninsula. This image, valid at 1202 UTC on 14 May 1990, is generated by combining data from the 0.63 (visible), 0.86 (near-infrared), and 3.7- μm (mid-wave infrared or MWIR) channels of the NOAA-11 Advanced Very High Resolution Radiometer (AVHRR). Red intensities of the color composite are controlled by the visible reflectivities, green intensities by the near-IR, and blue intensities by the MWIR reflectivities.

During daytime, observed 3.7- μm radiances contain both a reflected solar and emitted thermal component. However, only the reflected component of the MWIR radiances is used to generate this color composite image. The reflected and thermal components of daytime MWIR radiances are difficult to separate precisely, but for this image product a good approximation suffices. Let T_{Br} denote the long-wave infrared (LWIR) 10.7- μm observed brightness temperature for a given AVHRR pixel. Then the reflected component $r_{3.7}$ of the MWIR radiance is estimated as the difference

$$r_{3.7} = I_{\text{obs},3.7} - B_{3.7}(T_{\text{Br}}),$$

where $B_{3.7}(T)$ denotes the Planck radiance at wavelength 3.7 μm for a blackbody of temperature T . Once the distribution of reflected components $r_{3.7}$ is computed for the entire scene, an MWIR image is constructed whose grayshades are linearly proportional to $r_{3.7}$. This image in turn controls the blue intensities of the daytime reflected-solar color composite.

Colors are indicative of spectral signature differences among the three channels. In this image, black denotes open water; blue in the Adriatic Sea denotes sunglint; green denotes vegetated land, while pale blue denotes land with less vegetation; white represents cumuliform water-droplet clouds; yellow represents cirrus, cirrostratus, and cumulonimbus ice-particle clouds; and pale yellow over the Alps denotes snow cover.

(Cover image provided by Robert P. d'Entremont, Atmospheric and Environmental Research, Inc., Cambridge MA 02139; and James T. Bunting, Satellite Analysis and Weather Prediction Branch, PL/GPAB, Hanscom AFB, MA 01731.)

PL-TR-95-2129

Environmental Research Papers, No. 1179

**PREPRINT OF THE CLOUD IMPACTS ON
DoD OPERATIONS AND SYSTEMS
1995 CONFERENCE (CIDOS-95)**

Editor

Donald D. Grantham

1 October 1995

Accession For		1
NTIS	CRA&I	<input checked="" type="checkbox"/>
DTIC	TAB	<input type="checkbox"/>
Unannounced		<input type="checkbox"/>
Justification		
By		
Distribution /		
Availability Codes		
Dist	Avail and/or Special	
A-1		

19951102 035

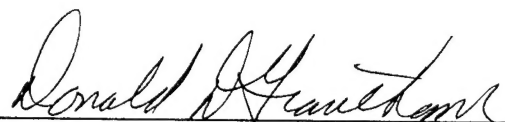
APPROVED FOR PUBLIC RELEASE; DISTRIBUTION UNLIMITED



PHILLIPS LABORATORY
Directorate of Geophysics
Air Force Materiel Command
Hanscom Air Force Base, MA 01731-3010

DTIC QUALITY INSPECTED 8

"This technical report has been reviewed and is approved for publication"



DONALD D. GRANTHAM, Chief
Contract Manager
Atmospheric Structure Branch



ROBERT A. McCLATCHEY, Director
Atmospheric Sciences Division

This report has been reviewed by the ESC Public Affairs Office (PA) and is releasable to the National Technical Information Service (NTIS).

Qualified requestors may obtain additional copies from the Defense Technical Information Center (DTIC). All others should apply to the National Technical Information Service (NTIS).

If your address has changed, or if you wish to be removed from the mailing list, or if the addressee is no longer employed by your organization, please notify PL/TSI, 29 Randolph Road, Hanscom AFB, MA. 01731-3010. This will assist us in maintaining a current mailing list.

Do not return copies of this report unless contractual obligations of notices on a specific document requires that it be returned.

REPORT DOCUMENTATION PAGE			Form Approved OMB No. 0704-0188	
Public reporting burden for this collection of information is estimated to average 1 hour per response, including the time for reviewing instructions, searching existing data sources, gathering and maintaining the data needed, and completing and reviewing the collection of information. Send comments regarding this burden estimate or any other aspect of this collection of information, including suggestions for reducing this burden, to Washington Headquarters Services, Directorate for Information Operations and Reports, 1215 Jefferson Davis Highway, Suite 1204, Arlington, VA 22202-4302, and to the Office of Management and Budget, Paperwork Reduction Project (0704-0188), Washington, DC 20503.				
1. AGENCY USE ONLY (Leave blank)	2. REPORT DATE 1 October 1995	3. REPORT TYPE AND DATES COVERED Scientific-Interim		
4. TITLE AND SUBTITLE CLOUD IMPACTS ON DoD OPERATIONS AND SYSTEMS 1995 CONFERENCE (CIDOS-95)		5. FUNDING NUMBERS PE 62101F PR 6670 TA GS WU 02		
6. AUTHOR(S) D. D. Grantham, Editor				
7. PERFORMING ORGANIZATION NAME(S) AND ADDRESS(ES) Phillips Laboratory/GPAA 29 Randolph Road Hanscom AFB, MA 01731-3010		8. PERFORMING ORGANIZATION REPORT NUMBER PL-TR-95-2129 ERP NO. 1179		
9. SPONSORING/MONITORING AGENCY NAME(S) AND ADDRESS(ES) Military Assistant for Environmental Sciences Office of the Under Secretary of Defense for Acquisition The Pentagon, Washington, DC		10. SPONSORING/MONITORING AGENCY REPORT NUMBER		
11. SUPPLEMENTARY NOTES Supported by Air Force Office of Scientific Research				
12a. DISTRIBUTION/AVAILABILITY STATEMENT Approved for public release; distribution unlimited		12b. DISTRIBUTION CODE		
13. ABSTRACT (Maximum 200 words) The Tri-Service Cloud Modeling Program was established by OUSDR&E and is chaired by the Phillips Lab, Geophysics Directorate. As part of this program, the CIDQS conference is held at 18 month intervals. This forum is attended by researchers and DoD systems designers/users to exchange information on requirements and ongoing research for cloud effects of weapon, communication, and surveillance systems. The theme of CIDOS-95 is "Cloud Modeling and Data for Defense Simulation Activities-Emphasizing Sufficient Physical Reality in Simulating Clouds." Keynote addresses were given by Capt. James W. Hollenbach, US Navy, Director of Defense Modeling and Simulation Office (DMSO) and by Mr. Robert W. Winokur, Assistant Administrator for Satellite and Information Services at the National Oceanic and Atmospheric Administration (NOAA). Three days of CIDOS-95 were devoted to oral and poster presentations in six sessions: (I) Introduction and Program Reviews; (II) Cloud Impacts: Simulation and Applications; (III) Cloud Data Bases; (IV) Measurement Systems and Sensors; (V) Cirrus and Contrail Clouds. Summaries of these presentations are included in this report.				
14. SUBJECT TERMS Clouds, cloud models, cloud simulation, cloud databases, cloud observing, cloud detecting, cloud retrieval, cloud effects			15. NUMBER OF PAGES	
			16. PRICE CODE	
17. SECURITY CLASSIFICATION OF REPORT Unclassified	18. SECURITY CLASSIFICATION OF THIS PAGE Unclassified	19. SECURITY CLASSIFICATION OF ABSTRACT Unclassified	20. LIMITATION OF ABSTRACT SAR	

CIDOS EXECUTIVE COMMITTEE

CAPT Bradley P. Smith, USN

Special Assistant to the Director, Defense Research and Engineering for the Environment

Mr. Donald D. Grantham*

Geophysics Directorate, Phillips Laboratory

Air Force Materiel Command

Dr. Arnold A. Barnes, Jr. *

Geophysics Directorate, Phillips Laboratory

Mr. Sam Brand*

Naval Research Laboratory

Major James T. Kroll*

AFOSR/NM

Major Lauraleen O'Connor*

NPOESS/IPO

Dr. Richard Shirkey*

U.S. Army Research Laboratory

*** Steering Committee Member**

**Preprint of the Conference on
Cloud Impacts on DoD Operations and Systems
Convened at the U.S. Air Force Phillips Laboratory, Hanscom Air Force Base, Massachusetts
24-26 October 1995**

Supported by the
U.S. Air Force Office of Scientific Research

Hosted by the
U.S. Air Force Phillips Laboratory
Hanscom Air Force Base, Massachusetts

Organized and Published by
Science and Technology Corporation
Meetings Division
101 Research Drive
Hampton, VA 23666
Under ESD Contract No. F19628-95-C-005

TABLE OF CONTENTS

CIDOS Executive Committee	v
Preface	xiii
Profile of Captain Bradley P. Smith , U.S. Navy, Assistant for Environmental Sciences, Office of the Director, Defense Research and Engineering	xv
Profile of Captain James W. Hollenbach , U.S. Navy, Director, Defense Modeling and Simulation Office	xvii
Profile of Robert S. Winokur , DOC/NOAA/NESDIS	xix

SESSION I. INTRODUCTION AND PROGRAM REVIEWS

Introductory Address	3
Captain Bradley P. Smith , U.S. Navy, Assistant for Environmental Sciences, Office of the Director, Defense Research and Engineering	
Keynote Address – Future Direction of Modeling and Simulation in the Department of Defense	5
Captain James W. Hollenbach , U.S. Navy, Director, Defense Modeling and Simulation Office	
Overview of DOD Modeling and Simulation Executive Agency for the Air and Space Natural Environment	9
LtCol(s) John M. Lanicci , Headquarters U.S. Air Force, Directorate of Modeling, Simulation, and Analysis	
Synthetic Environments in Synthetic Theater of War (STOW) 97	13
Jeffrey T. Turner , U.S. Army Topographic Engineering Center	
Weather in Distributed Interactive Simulations (WINDS)	17
Vernon M. Stoltz , U.S. Army Topographic Engineering Center; Eric O. Schmidt , TASC	
A Master Environmental Library (MEL) to Support Modeling and Simulation (Including Demo)	21
Richard A. Siquig , Naval Research Laboratory; Captain Bruce G. Shapiro , U.S. Air Force Combat Climatology Center; Martin Miller , USAE Waterways Experiment Station	
Dynamic Environmental Effects Model (DEEM)	23
John R. Hummel , Kathy L. Simunich and John H. Christiansen , Argonne National Laboratory	
The E ² DIS Environmental Manager: Clouds	27
Harry M. Heckathorn , Naval Research Laboratory; Stanley H. Grigsby , ENFO, Inc.	
Survey of Requirements for Effects of the Natural Environment in Military Models and Simulations	31
Thomas M. Piwowar and John Burgeson , Science and Technology Corporation; Donald D. Grantham , Geophysics Directorate, Phillips Laboratory; Sam Brand , Naval Research Laboratory; Alan Wetmore , U.S. Army Research Laboratory	

SESSION II: CLOUD IMPACTS: SIMULATIONS AND APPLICATIONS

Natural Environment Engineering Toolkit	35
Sandra K. Weaver , National Air Intelligence Center; William A. Lanich , USAF Wright Laboratory	

Cloudscape™: Stochastic Cloud Visualization from Volumetric Descriptions	41
John G. DeVore , James H. Thompson and Ross Thornburg, Visidyne, Inc.	
The Cloud Scene Simulation Model—Recent Enhancements and Additions	45
Maureen E. Cianciolo , Eric O. Schmidt and Mark E. Raffensberger, TASC	
Incorporation of Cloud Simulation Into Powerscene	49
Louis Hembree and Sam Brand, Naval Research Laboratory; Mark Deloura, Loral, Inc.; Tom Hickey, Scott Randall and Chip Mayse, Cambridge Research, Inc.; Maureen E. Cianciolo and Eric O. Schmidt, TASC	
Cloud Depiction and Forecast System (CDFS) II Update	53
Major John D. Murphy , Major Don K. Rhudy and Major David J. Zdenek, HQ Air Weather Service; 2Lt Jeff A. Baltes, Anna L. Lathrop and Captain Frank A. Leute IV, Air Force Global Weather Central; Kevin J. Lunn, Michael J. Plonski and Bruce H. Thomas, The Aerospace Corporation	
SBIRS Cloud Measurements, Analysis and Model Validation	57
Captain Michael Pierce, SMC/MTAX; William Blumberg, Phillips Laboratory/GPOS; Ian S. Robinson , The Aerospace Corporation	
Simulated Cloudscapes with Fastview	59
Albert R. Boehm , Hughes STX Corporation	
Radiative Transfer in Scenarios with Multiple Clouds	63
Patti Gillespie, Alan Wetmore and David Tofsted, U.S. Army Research Laboratory	
Realistic Cloud Rendering Using an Auto-Regressive Moving Average (ARMA) Model	65
Robert A. Pilgrim , Murray State University; Andy Bevilacqua, Bevilacqua Research Corporation	
Simulating Clouds Within a Space-Based Doppler Lidar Wind Sounder Simulation Model	69
G. David Emmitt and Sidney A. Wood, Simpson Weather Associates, Inc.	

SESSION III: CLOUD DATABASES

Application of Hypermedia and CD-ROM Technology to the Distribution of Navy Environmental Information for Satellite Image Analysis and Forecasting	75
Marie E. White , Pangaea; Robert Fett, Science Applications International Corporation; Sam Brand, Naval Research Laboratory	
Cloud Data Sets Derived from Combined Geostationary and Polar-Orbiting Environmental Satellite Sensors Using the SERCAA Cloud Model	79
Gary B. Gustafson , Robert P. d'Entremont and Daniel C. Peduzzi, Atmospheric and Environmental Research, Inc.	
Climatological and Historical Analysis of Clouds for Environmental Simulations (CHANCES)—First Year of Products	81
Donald L. Reinke, Thomas H. Vonder Haar , Kenneth E. Eis, Jan L. Behunek, Charles R. Chaapel, Cynthia L. Combs, John M. Forsythe and Mark A. Ringerud, STC-METSAT	
Global Statistics on Cloud Optical Depths from Satellite and Lidar Observations	85
Donald P. Wylie , University of Wisconsin-Madison	

Enhanced Satellite Cloud Analysis by the Development of a Higher Resolution (6-km) Global Geography Data Set	87
1LT R. Radburn Robb and Crystal L. B. Schaaf, Geophysics Directorate, Phillips Laboratory; Daniel C. Peduzzi, Atmospheric and Environmental Research, Inc.; Joan M. Ward, System Resources Corporation	

SESSION IV: MEASUREMENT SYSTEMS AND SENSORS

Detection and Retrieval of Cirrus Cloud Systems Using AVHRR Data: Verification Based on FIRE-II-IFO Composite Measurements	95
Kuo-Nan Liou , Szu-Cheng Ou, N. X. Rao and Y. Takano, University of Utah	
Analysis of Test Results from a Mobile Profiling System	101
James Cogan and Edward Measure, U.S. Army Research Laboratory	
<u>M</u> ulti <u>S</u> pectral <u>P</u> ushbroom <u>I</u> maging <u>R</u> adiometer (MPIR) for Remote Sensing Cloud Studies	105
Gary S. Phipps and Carter L. Grotbeck, Sandia National Laboratories	
A Brief Description of Airborne InfraRed Measurement System (AIRMS)	109
William S. Helliwell , John R. Norris and Betty Rodriguez-Cottle, Science Applications International Corporation	
Cloud Phenomenology Measured from Airborne InfraRed Measurement System (AIRMS) Data	113
William S. Helliwell , John R. Norris and Betty Rodriguez-Cottle , Science Applications International Corporation	
Cloud Radiative and Spatial Properties Using a Ground-Based Infrared All-Sky Imager	117
Robert P. d'Entremont , Ronald G. Isaacs, Jean-Luc Moncet and David B. Hogan , Atmospheric and Environmental Research, Inc.	
Upper Tropospheric Humidity Derived from SSM/T-2 Measurements	119
Michael K. Griffin , Geophysics Directorate, Phillips Laboratory; John D. Pickle, Atmospheric and Environmental Research, Inc.	

SESSION V: CLOUD AND CLOUD RELATED MODELS

A Short-Term Cloud Forecast Scheme Using Cross Correlation: An Update	125
Kenneth F. Heideman and 1LT R. Radburn Robb, Geophysics Directorate, Phillips Laboratory	
Cloud Detection Using Visible and Near-Infrared Bidirectional Reflectance Distribution Models	129
Robert P. d'Entremont , Atmospheric and Environmental Research, Inc.; Crystal L. B. Schaaf, Phillips Laboratory/GPAB; Alan H. Strahler, Boston University	
SERCAA Phase II: Cloud Radiative, Microphysical, and Environmental Properties	131
Ronald G. Isaacs , Gary B. Gustafson, Robert P. d'Entremont and David B. Hogan, Atmospheric and Environmental Research, Inc.; Major Michael Remeika and James T. Bunting, Phillips Laboratory/GPAB	
The Lattice Boltzmann Method: A New Approach to Radiative Transfer Through Clouds	135
Joel B. Mozer and Thomas R. Caudill, Geophysics Directorate, Phillips Laboratory	
Cloud Forecasting Initiatives at Air Force Global Weather Central	139
Raymond B. Kiess and Thomas J. Kopp, Headquarters Air Force Global Weather Central	

Short-Term Cloud Fluctuation Statistics for Central America Using GOES-8 Imagery	141
John G. DeVore , Visidyne, Inc.	
Identification of Thunderstorms in an Operational Global Nephanalysis Using a Convective-Stratiform Technique	145
Thomas J. Kopp , Peter J. Broll and Stephen G. Zahn, Headquarters Air Force Global Weather Central	

SESSION VI: CIRRUS AND CONTRAIL CLOUDS

Four Decades of Cirrus and Contrail Observations	151
Arnold A. Barnes, Jr. , Phillips Laboratory/GPA	
Retrieval of Cirrus Radiative and Spatial Properties Using Coincident Multispectral Imager and Sounder Satellite Data	155
Robert P. d'Entremont , Atmospheric and Environmental Research, Inc.; Donald P. Wylie, University of Wisconsin; Szu-Cheng Ou and Kuo-Nan Liou, University of Utah	
An Ice Crystal Growth Model for Cirrus Cloud Formation	157
Szu-Cheng Ou , Kuo-Nan Liou and D. Frankel, University of Utah	
Thin Cirrus Effects on Hyperspectral Detection of Trace Gases	161
P. Daniel Hestand and Kenneth B. MacNichol, TASC	
Subvisual Cirrus Clouds Associated with Processes in the Natural Atmosphere	165
Eric O. Schmidt , D. Lynch, K. Sassen, G. Grams and J. Alvarez, TASC	
Validation of the Appleman Contrail Forecasting Scheme Using Engine-Specific Aircraft Data	169
Captain David J. Speltz , USAF Environmental Technical Applications Center	
Predicting the Radiative Properties of Nonspherical Particles: Application to Cirrus Clouds	173
David L. Mitchell , Desert Research Institute; Andreas Macke, NASA-Goddard Institute for Space Studies	
Statistics on the Optical Properties of Cirrus Clouds Measured with the High Spectral Resolution Lidar ...	177
Edwin W. Eloranta and Paivi Piironen, University of Wisconsin-Madison	
An Operational Method of Ice Containing Clouds Based on Laboratory and Observational Data Leading to a Numerical Model for Prediction of Radiative Properties	181
Darko Koracin and John Hallett , Desert Research Institute	

POSTER PRESENTATIONS

A Summary of Vertical Cloud Layer Statistics as Derived from Echo Intensities Received by a 35 Ghz Radar	187
James H. Willand , Hughes STX Corporation	
SWIR Cloud Modeling and Data Analysis for the SBIRS Program	191
Joeseeph G. Shanks and Frederick C. Mertz, Photon Research Associates, Inc.; Ian S. Robinson, The Aerospace Corporation; William Blumberg, Phillips Laboratory/GPOS; Edwin W. Eloranta, University of Wisconsin-Madison; James Lisowski, Scitec Corporation	

Global Cloud Cover at Altitude: System Impacts	195
Ian S. Robinson and Susan L. Kafesjian, The Aerospace Corporation	
The Cloud Scene Simulation Model—Parameter Estimation and Preliminary Validation of the Cumulus Model	197
Mark E. Raffensberger , Maureen E. Cianciolo and Eric O. Schmidt, TASC	
Production of Long-Term Global Multi-Layer Water Vapor and Liquid Water Data Sets from Multi-Satellite and Radiosonde Observations	201
Thomas H. Vonder Haar , Mark A. Ringerud, David L. Randel, Graeme L. Stephens, Cynthia L. Combs, Donald L. Reinke and Thomas J. Greenwald, STC-METSAT	
Development of a Cloud Cover Forecast Model	205
Roger D. Dickey , GENCORP/Aerojet; William T. Kreiss, Georgia Tech Research Institute	
A Novel Infrared Imaging Spectroradiometer for Passive Remote Detection of Clouds	207
David M. Sonnenfroh , B. David Green, William J. Marinelli and W. Terry Rawlins, Physical Sciences, Inc.	
Examples of CFLOSA (Cloud-Free Line-of-Sight Aloft) Output	211
Albert R. Boehm , James H. Willand and Marc A. Pereira, Hughes STX Corporation	
Line of Sight Cloud Observations from Haleakala	215
Russell H. Taft , Rockwell Power Systems	
Support of Environmental Requirements for Cloud Analysis and Archive (SERCAA) Integrated Cloud Analysis Validation	219
Kenneth F. Heideman , Phillips Laboratory/GPAB; Robert P. d'Entremont , Jeanne M. Sparrow, Tony S. Lisa and Gary B. Gustafson, Atmospheric and Environmental Research, Inc.	
Cloud Ceiling Climatology Atlas	223
Major James R. Schaefer and Captain Bruce G. Shapiro, Air Force Combat Climatology Center	
Appendix A	225
Agenda	
Appendix B	235
List of Registered Attendees	
Appendix C	247
Author Index	

PREFACE

This preprint contains 60 technical papers that will be presented either orally or as posters at the "*Cloud Impacts on DoD Operations and Systems 1995 Conference*" (CIDOS-95) held at the U.S. Air Force Phillips Laboratory, Science Center, Hanscom Air Force, Massachusetts.

The CIDOS-95 conference is the tenth conference of the DoD community concerned with the impact of clouds on military systems. The first formal meeting of this community was held in 1983 under the name Tri-Service Clouds Modeling Workshop. The name was changed in 1988 to Cloud Impacts on DoD Operations and Systems (CIDOS) to reflect more accurately the intent and purpose of the CIDOS community as a resource for defense-related problems and issues of greater scope and magnitude.

The Theme for CIDOS-95 is "Cloud Modeling and Data for Defense Simulation Activities--Emphasizing Sufficient Physical Reality in Simulating Clouds." The focus of this meeting and the presentations will be simulation and applications, specifically the implications of clouds in distributed interactive simulations for various DoD and civilian areas of interest.

The three day conference will consist of oral and poster presentations. The opening session of DoD overview presentations and program reviews will be followed by technical sessions: Cloud Impacts: Simulations and Applications, Cloud Databases, Measurement Systems and Sensors, Cloud and Cloud Related Models, and Cirrus and Contrail Clouds. A full agenda of the meeting appears in Appendix A.

The CIDOS Steering Committee gratefully acknowledges direction from the CIDOS-95 sponsor, CAPT Bradley P. Smith, USN, Special Assistant to the Director, Defense Research and Engineering for the Environment, and the financial support of the U.S. Air Force Office of Scientific Research. The excellent cooperation and contributions of the session chairs and the presenters is also acknowledged. The conference is hosted by the U.S. Air Force Phillips Laboratory, and the administration organization was carried out by the Meetings Division of Science and Technology Corporation.

Donald D. Grantham
Chairman
CIDOS Steering Committee

Profile of Conference Introductory Speaker

CAPTAIN BRADLEY P. SMITH, UNITED STATES NAVY

Captain Smith was commissioned in 1972 as an Oceanographer through the Naval Reserve Officer Training Corps at the Pennsylvania State University where he received a Bachelor of Science degree in Biochemistry.

His first duty station was as an Oceanographic Watch Officer at Naval Facility, San Nicholas Island. This was followed by tours as the Executive Officer of Oceanographic Unit One aboard USNS BOWDITCH (T-AGS 21), Oceanography Instructor at the Fleet Aviation Specialized Operational Training Group, Atlantic Meteorological Officer with the Naval Support Force Antarctica, Ice Operations Officer at the Navy/NOAA Joint Ice Center, and Meteorological Officer aboard the USS JOHN F. KENNEDY (CV 67). Following his graduation from the Industrial College of the Armed Forces he served tours in the Office of the Chief of Naval Operations and in the Office of the Secretary of the Navy. Prior to his current assignment as the Assistant to the Director, Defense Research and Engineering for Environmental Sciences, Captain Smith was the Commanding Officer of the Naval Polar Oceanography Center and the Director of the Navy/NOAA Joint Ice Center.

Captain Smith graduated "With Distinction" from the Naval Postgraduate School with a Master of Science degree in Meteorology and Oceanography. Captain Smith is entitled to wear Flight Meteorologist Wings. His awards include the Meritorious Service Medal (Gold Star in lieu of third award), Navy Commendation Medal, Navy Achievement Medal, and the Antarctic Service Medal.

Profile of Conference Keynote Speaker

CAPTAIN JAMES W. HOLLENBACH, UNITED STATES NAVY

Captain Hollenbach was raised in New Jersey, graduated from Rutgers University, and worked as an engineer for the Boeing Company before entering the Navy via Aviation Officer Candidate School in 1970. He is a designated Naval Aviator and Acquisition Professional. He has spent most of his career flying carrier-based electronic warfare aircraft (EA-3 and EA-6B) and has served as a strike leader in several carrier air wings. Captain Hollenbach commanded VAQ-135 aboard USS ENTERPRISE. During his shore tours he earned a masters degree in Aeronautical Systems, was an instructor pilot, served as the Navy's Congressional Liaison for Aviation Programs, graduated from the Canadian Forces Command and Staff College and the Defense Systems Management College, and served as Deputy Program Manager for Mission Planning Systems under the Navy's Program Executive Officer for Tactical Aircraft. He assumed his current position as the Director the Defense Modeling and Simulation Office on July 1, 1994.

Profile of Conference Invited Speaker

ROBERT S. WINOKUR

Mr. Robert S. Winokur is the Assistant Administrator for Satellite and Information Services at the National Oceanic and Atmospheric Administration. As the Assistant Administrator, Mr. Winokur administers an integrated program for the development and use of all operational civilian satellite-based environmental remote sensing systems and the national and international acquisition, processing, dissemination, and exchange of environmental data. Prior to November 1993, when Mr. Winokur assumed his current position, he served as the Technical Director in the Office of the Oceanographer of the Navy, Office of the Chief of Naval Operations. Mr. Winokur served in that position from 1985 and was the senior civilian technical manager for the Navy's Operational Oceanography Program. Mr. Winokur has served in various senior management and technical positions, including: Associate Technical Director for Ocean Science and International Programs, Office of Naval Research; Director, Planning and Assessment, Office of Naval Research; Deputy and Special Advisor, Office of the Deputy Assistant Secretary of the Navy for Antisubmarine Warfare; Special Assistant for Acoustics to the Director, Antisubmarine Warfare and Surveillance Programs, Office of the Chief of Naval Operations; and Branch Head and Division Director, Naval Oceanographic Office.

Mr. Winokur has a B.S. degree from Rensselaer Polytechnic Institute and an M.S. degree from The American University. He has published numerous papers and reports in underwater acoustics and Naval oceanography. Mr. Winokur has received numerous awards, including the Presidential Distinguished Executive and Meritorious Rank Awards for senior executives. He was Vice President for Technical Affairs for the Marine Technology Society and is a Fellow of the Acoustical Society of America.

Mr. Winokur has a broad range of experience in satellite remote sensing, underwater acoustics, ocean policy, antisubmarine warfare, undersea warfare and technology, ocean ship management and construction, manned space oceanography, information technology, and national environmental issues.

Mr. Winokur continues to serve on numerous Navy, national and international committees in various capacities. Among these, he is or has been: the Navy representative to the national Environmental Task Force; DoD representative to the Interagency Working Group on Data Management for Global Change; U.S. representative to the NATO Scientific Committee of National Representatives; Executive Secretary, Defense Science Board Study on ASW; DoD representative to the Interagency Arctic Research Policy Study; Executive Secretary, Federal Oceanographic Fleet Coordination Council; and Chairman, Interagency Study on Ocean Bionics. He is currently Vice Chairman of the Interagency Task Force on Observations and Data Management and for the Joint Scientific and Technical Committee of the International Global Climate Observing System.

**SESSION I:
INTRODUCTION AND PROGRAM REVIEWS**

INTRODUCTORY ADDRESS

Captain Bradley P. Smith, U.S. Navy
Assistant for Environmental Sciences
Office of the Director, Defense Research and Engineering
Washington, D.C. 20301-3080

Cloud Impacts on Defense Operations and Systems (CIDOS) Conference has its roots in a request from one of my predecessors, COL Paul Try. He requested the meteorology community to develop standard data bases and methodologies capable of providing a four-dimensional depiction of clouds as well as their impacts on operations. These methodologies were needed for use in both engagement models and wargame simulations. This request led to the formation of the Tri-Service Cloud Modeling Planning Group. One of the initial actions of this Planning Group was to hold the first CIDOS workshop to determine the state-of-the-art in cloud modeling.

We have come a long way in the intervening 12 years, but recognize that we still have a long way to go. As I write this, the articles in the Washington Post are bemoaning the fact that poor weather is hampering the air campaign in Bosnia. Specifically, the presence of low clouds and fog are precluding the use of surgical air strikes which are required by the current tactical and political situation. Air strikes using precision guided munitions are needed to ensure the destruction of the target while eliminating collateral damage. The use of laser guided bombs requires a cloud free line of sight to be effective. Without the ability to employ these precision weapons, the strikes are scrubbed to avoid unwanted collateral damage and civilian casualties. It is almost ironic that despite all the advances in modern weaponry, we remain captive to the operating environment.

In reviewing the minutes of that first meeting of the Tri-Service Cloud Modeling Planning Group, I was struck by a recommendation from a 1982 Defense Science Board Summer Study cited by COL Try. That 1982 Summer Study recommended that OSD require the Services to make more extensive use of models and simulations in evaluating the military worth and cost of systems. COL Try emphasized the need for an accurate depiction of the environment in those models and simulations. Specifically, he was concerned with the accurate depiction of clouds in these simulations. Since that time, the use of models and simulations has grown in virtually all areas within the Department of Defense. The requirement for an accurate depiction of the real operational environment in those models and simulations is greater today than ever before. Among the key parameters which need to be addressed is the accurate, four-dimensional representation of real clouds, not just average clouds.

With the renewed interest in Modeling and Simulation which is manifested, in part, by the establishment of the Defense Modeling and Simulation Office, we decided to make the modeling of clouds for Defense simulation activities the focus of this year's workshop. We are at a critical juncture. As we become more reliant on models and simulations to aid us in making decisions across the full spectrum from determining the utility of a new weapon design to mission planning and rehearsal, it is even more imperative that those simulations have accurate depictions of the battlespace environment, including clouds. Fortunately, the modeling and simulation community is aware of the need and it is up to us, the meteorology community to provide the depictions and models needed for today's and tomorrow's simulations. It is therefore fitting that the keynote speaker for this workshop is CAPT James Hollenbach, the Director of the Defense Modeling and Simulation Office. With the encouragement and support of DMSO, we will be more effective in providing the development and operational communities with the capabilities they need in cloud representations for modeling and simulation.

FUTURE DIRECTION OF MODELING AND SIMULATION IN THE DEPARTMENT OF DEFENSE

CAPT James W. Hollenbach, USN
Director,
Defense Modeling and Simulation Office
1901 North Beauregard Street, Suite 504
Alexandria, Virginia 22311

ABSTRACT

The declining Department of Defense (DoD) budget and increased emphasis on Joint operations emphasize the need for development of a common technical framework for modeling and simulation. The resulting ability to produce efficient and effective models and simulations will facilitate interoperability and promote reuse of data and software components within the DoD modeling and simulation (M&S) community. The technical framework consists of three major components: a high level architecture (HLA) to which models and simulations must conform; conceptual models of the mission space (CMMS) which provide the basis for coherent development of distributed interoperable and reusable simulation representations (synthetic environments, systems, and human behaviors); and data standardization which will generate certified common, interchangeable data for M&S use.

1. INTRODUCTION

Traditionally, Department of Defense (DoD) models and simulations have been developed in isolation from one another. Perceived and actual differences in requirements and the absence of a common technical infrastructure have created a variety of "stovepipe" solutions that are not designed to interact or interoperate. While these legacy systems have typically served their intended purpose, they currently do not adequately or efficiently interoperate with each other and generally fail to satisfy the full scope of the operational and training needs of theater commanders and the acquisition needs of command and control and weapon system developers.

Declining defense funding combined with an increased emphasis on Joint operations, has reemphasized the need for interoperability and reuse among simulations and model developers. The Defense Modeling and Simulation Office (DMSO) is sponsoring development of a technical framework that will identify and build on common underlying information technology to facilitate simulation interoperability and promote reuse of critical M&S system components.

2. DoD VISION

The DoD Vision for Modeling and Simulation states that M&S must provide readily available, operationally valid synthetic environments for use by DoD Components in support of operations and acquisition.

This vision will be realized when operational forces can train at "home-base" locations using real-world command, control, communications, computers, and intelligence (C4I) systems while models, running at distributed sites, provide common synthetic environments that replicate real-world events. These synthetic "mission space" environments will serve as laboratories to test new or modified doctrine in operational scenarios against highly capable simulated threats. Warfighters need to plan and rehearse missions in realistic synthetic environments prior to responding in crisis situations. Command authorities must be able evaluate alternative courses of action in accredited M&S environments.

Use of synthetic environments and virtual prototyping in the acquisition process will allow new concept exploration and system requirements definition and design at significantly reduced cost. Virtual prototypes should be used to evaluate the impact of variable system and environmental parameters on overall battlefield performance thus providing a more cost-effective and complete examination of engineering design trade-offs.

Synthetic environments must be used to create more comprehensive test scenarios that enable test events over the full range of operational climates and in otherwise dangerous and destructive conditions (e.g., live munitions, nuclear and/or chemical environments). Use of distributed simulation will provide concurrent evaluation of system logistics and maintenance demands in a greatly accelerated process to provide a more comprehensive view of life-cycle support requirements and costs.

3. COMMON TECHNICAL FRAMEWORK

Achieving the DoD Vision requires the use of efficient and effective models and simulations across DoD. A common technical framework for M&S must be developed to facilitate interoperability and promote reuse. The DMSO is sponsoring development of such a technical framework comprised of: a common high level architecture (HLA) to which models and simulations must conform; conceptual models of the mission space (CMMS) to support coherent development of distributed interoperable and reusable simulation representations (synthetic environments, systems, and human behaviors); and data standardization to generate certified common, interchangeable data for M&S use.

This strategy for DoD Modeling and Simulation is comparable to city planning. Substituting HLA, CMMS (common world view), and data standards for city ordinances, street plans, and building codes presents an inviting analogy. City planners provide a framework which allows residents the ability to pursue many and diverse activities in many different building styles and locations. Such a concept for DoD M&S with access to services and utilities (common environmental representations; communication network (e.g., the Defense Simulation Internet (DSI)); verification, validation and accreditation (VV&A) methods; repositories (the Modeling and Simulation Resource Repository (MSRR) system; and help desks) will provide the common technical framework to support a community of simulation systems.

4. HIGH LEVEL ARCHITECTURE

The concepts of the HLA are based on the belief that no single model or simulation system can satisfy all uses and users in the DoD. Therefore, the HLA must provide a framework for a configurable federation of systems (interacting simulations supporting a community of common interest), each with an implementation appropriate to their needs, but working together based on a common set of protocols, and specifications. A common set of "rules" coupled with an interface specification and object model template define the HLA. The HLA Rules facilitate interoperability and promote reuse by describing the federation responsibilities of simulations and of the supporting runtime infrastructure. They refer to: 1) functions required of simulations to interact with other simulations; and 2) functions required of the infrastructure to support the interaction of simulations. These rules must be followed in the simulation development phase to achieve proper interaction of simulations in the execution phase. The HLA Interface Specification defines the required interface functions between the runtime infrastructure and compliant simulations. The Object Model Template prescribes a common method for recording the information contained in the HLA Object Model required of each compliant federation and simulation.

A key element of the HLA is the runtime infrastructure (RTI) component that serves as the backbone for interface among simulations. The RTI provides data management (attribute ownership), filtering services (intelligent data routing), distribution services (interfaces to communications), and time synchronization services (coordination for runtime and after action analyses).

5. CONCEPTUAL MODELS OF THE MISSION SPACE

While the HLA addresses system technical constraints, the CMMS process addresses the system's unique representation of the real-world. As a whole, the CMMS defines a first abstraction of the real-world and serves as a frame of reference for simulation development by capturing the features of the problem space. Those features are the entities involved in any mission and their key actions and interactions. The CMMS is a situation-neutral view of the real-world and serves as a bridge between the warfighter, who owns the combat

process and is the authoritative source for validating CMMS content, and the simulation developer. Additionally, the CMMS provides a common viewpoint and serves as a vehicle for communication among warfighters, doctrine developers, C4I system developers, analysts, and simulation developers. This common view allows all concerned parties to be confident that DoD simulations are anchored in operational realism.

M&S system developers (and the users who provide the requirements) expend considerable time in "knowledge acquisition" activities designed to capture the real-world processes they intend to simulate. To provide common definitions and facilitate interoperability in common functions the CMMS effort is developing standard descriptions of the Universal Joint Task List (UJTL). These conceptual models, each addressing broad mission areas (e.g., conventional combat operations, operations other than war, manufacturing, engineering, analysis, etc.), will provide both a framework and the necessary detail to permit development of consistent, interoperable, and authoritative representations of environments, systems, and human behaviors in DoD simulation systems.

6. DATA STANDARDIZATION

If DoD M&S is to directly support the operational world then the M&S and C4I communities must share common data and data standards. The data standardization effort includes establishing data standards; accurate, verified, validated and certified (VV&C) data methods; and data security. The benefits of data standardization are: to promote reuse of data and interoperability of M&S and C4I by overcoming data mapping problems and expensive data translation; to enable data suppliers to provide certified data which will improve the quality of M&S results; and to protect data while still promoting accessibility through the appropriate level of control.

To facilitate the sharing of metadata, data, algorithms, models, simulations and tools, the DMSO is sponsoring development of a distributed M&S Resource Repository (MSRR) system. This development is being coordinated with the Defense Information Systems Agency (DISA) Data Administration Program Office and will be compatible with the DoD data repository system. The MSRR will be a distributed system designed to serve M&S clients who develop and use models and simulations, and access and acquire data from classified and unclassified sources.

7. SYNTHETIC ENVIRONMENTS

Common representation of the natural environment is a major factor in achieving interoperability and an absolute requirement for reuse. Establishing common synthetic environments (SE) involves defining standards for common SE components of HLA object models (what constitutes an SE object, attribute, or event?) and basic services (e.g., look up elevation/soil type/feature, calculate line-of-sight (with and without obscuration), determine surface trafficability, vehicle mobility, and illumination). These issues are being addressed by M&S Executive Agents (MSEAs) designated by the Under Secretary of Defense (Acquisition and Technology). The Director, Defense Mapping Agency is the MSEA for Terrain and has established a Terrain Modeling Project Office as a DoD M&S community resource for executing programs. The Oceanographer of the Navy and the Air Force Deputy Chief of Staff, Plans and Operations are in the process of final designation as the MSEAs for Oceans and Aerospace respectively.

8. CONCLUSIONS

The common M&S technical framework, briefly discussed in this paper, is outlined in greater detail in the DoD Modeling and Simulation Master Plan, DoD 5000.59P. Issues and supporting actions with milestones are listed and offices of primary responsibility are identified. Major challenges lie ahead in fulfilling the DoD Vision for Modeling and Simulation. Technology exchange in M&S conferences must continue to play a key role in addressing those technology challenges. Information on the developing common technical framework for M&S as well as other DMSO activities is available through an internet home page at url: <http://www.dmsomil/dmsomil>.

OVERVIEW OF DOD MODELING AND SIMULATION EXECUTIVE AGENCY FOR THE AIR AND SPACE NATURAL ENVIRONMENT

John M. Lanicci
Headquarters U.S. Air Force
Directorate of Modeling, Simulation, and Analysis
Washington, D.C. 20330-1510

ABSTRACT

This paper outlines the preliminary DoD strategy for modeling and simulation (M&S) activities in the Air and Space Natural Environmental areas. This strategy takes the form of an Executive Agency (EA) for M&S of Air and Space Natural Environment. The EA will be described in terms of long-term vision for M&S of air and space natural environment, proposed organizational structure, and strategic objectives and timelines for attaining the vision.

1. INTRODUCTION

The Draft DoD M&S Master Plan¹ outlines the strategy for making dramatic improvements in the ways M&S is applied to DoD mission areas. A part of the strategy calls for appointing Executive Agents (EAs) for natural environmental domains such as terrain, oceans, atmosphere, and space. The EA would have management responsibility and delegated authority for the development and maintenance of the specific domain of expertise. In June 1995, the Executive Council for Modeling and Simulation (EXCIMS) endorsed EAs for oceans (U.S. Navy), and atmosphere and space (U.S. Air Force) representations (earlier this year the Defense Mapping Agency was officially appointed EA for terrain representation).

This paper briefly describes the proposed multi-Service EA for M&S of the air and space natural environment. The EA's vision will be presented, followed by the proposed organization, strategic objectives, and timelines.

2. EXECUTIVE AGENT'S VISION

2.1 DEFINITION OF AIR AND SPACE NATURAL ENVIRONMENT

For the EA's domain of responsibility, the formal definition of air and space natural environment is given below:

"The temporal and spatial state of the atmosphere, which includes the region from the surface of the Earth, through the troposphere and stratosphere, upper atmosphere, radiation belts, Interplanetary Medium, to the surface of the Sun. These state conditions include parameters such as pressure, temperature, density, wind velocity, moisture, cloud cover, and effects/impacts (natural and man-made) such as electro-optical weapons lock-on range, battlefield obscurant concentration/distribution, satellite drag, etc."

The domain of air and space natural environment does not include oceans and terrain. However, interactions between the air and Earth's surface will be jointly addressed between the EAs for these domains. Additionally, the natural environmental EA will not address the M&S of objects (e.g., aircraft, satellites) operating in the air and space natural environment. However, the effects and impacts from the natural environment will certainly be included in representations of those objects operating there.

2.2 THE EXECUTIVE AGENT'S VISION FOR M&S

The paradigm for describing the hierarchy of M&S is often represented by a pyramid. The pyramid shows the basic foundation for M&S is the System/Subsystem/Component level (often called the "Engineering" level). From this foundation the pyramid builds upward, at increasing levels of model aggregation, until the Campaign level is reached. In our EA domain, the Engineering level includes simulation of environmental effects on individual system/platform

performance, especially important during system design and testing. At the Campaign level, the environmental interface is *exploitation*, defined as the use of knowledge about our environmental sensitivities (and those of our adversary) to optimize employment of land, sea, and air forces against the enemy's weaknesses. An example of environmental exploitation is the use of smoke in the old Soviet military doctrine of *maskirovka*² (camouflage, concealment, and deception). At the engagement level, the Soviets used smoke as a means of concealing their ground forces during World War II. Smoke usage was such an important part of Soviet ground combat strategy that it became part of their doctrine at the Campaign level. Their use of this strategy in a potential East-West conflict could have caused big problems for target detection using U.S. and NATO smart weapons technology. Our ability to model the impacts that their concealment strategy would have had on our weapons employment strategy is virtually non-existent, and *must* be integrated into M&S applications in order for M&S to become a true force multiplier.

The previous discussion of the M&S hierarchy provides a good lead-in to our vision statement:

"The thorough integration of air and space natural environmental M&S into all aspects of mission-area M&S, by realistically representing environmental effects and impacts from the Engineering level through the Theater level, using environmental exploitation in Campaign-level simulations, and building the capability to employ environment/environmental effects M&S in real-time operations."

Another useful paradigm incorporates the M&S hierarchy, but interfaces it with mission areas and types of simulations to form a cube, as illustrated in Figure 1 below:

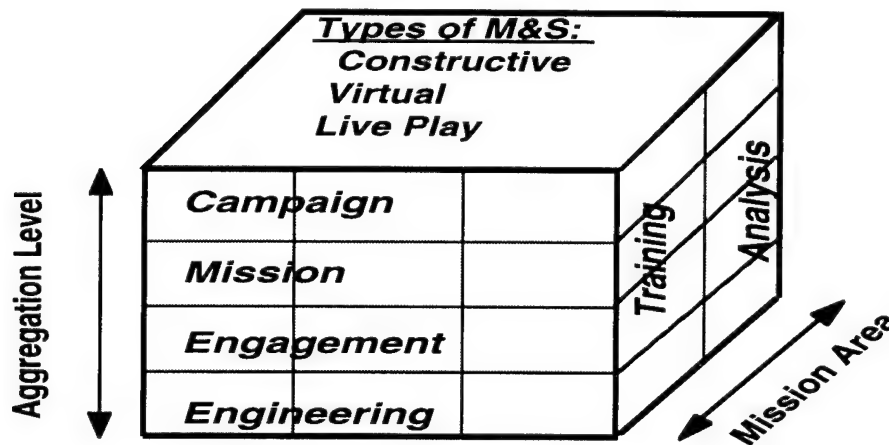


Figure 1 - Air and Space Natural Environmental M&S Paradigm

As seen from Figure 1, there are eight possible combinations of M&S which we can analyze for both user requirements and assessment of environmental capabilities to support the requirement. For example, we can examine the category "Campaign models used for analysis" to analyze the current "state-of-the-art" in environmental effects representation. At the present time, there are few models that employ any type of weather/weather effects representation. However, there may be a real need in the operational community to have such a capability in order to perform analytical studies of potential conflict regions such as Southwest Asia or the Korean peninsula. Therefore, we identify a technological shortfall in this category of M&S. Incidentally, the third side of the cube, illustrating the types of M&S, really depicts the solution for the category from the other two sides. In our campaign level model for analysis example, it is quite likely the solution is a constructive model. However, if our mission area were training, then it is possible the solution may be either live play or virtual (or even a combination). The cubic paradigm forms the basis for the strategic objectives outlined in the next section.

3. EXECUTIVE AGENT STRATEGIC PLAN

There are three primary functional areas in the proposed EA organization: 1) Requirements analysis; 2) Technology Integration; and 3) Standardization.

Requirements analysis is the foundation upon which the EA will implement the M&S vision. It consists of collecting and validating user requirements and matching them against the environmental community's technological capabilities. This analysis will employ the cubic paradigm from Figure 2 to identify technology shortfalls, which will be used to drive the planning and programming of new projects to satisfy these long-term needs.

Technology integration involves identification of promising new technologies for solving the shortfalls identified during the requirements/capabilities analysis. This task has two focus areas: 1) short-term projects; and 2) long-term projects. The first focus area is difficult because it will certainly involve investment in systems considered to be "legacy" in nature. The challenge will be evaluating these risks against the current user needs that cannot wait until the next-generation M&S systems are fielded. The second focus area is somewhat easier to plan and program, but here again, choices must be made within the framework of a shrinking fiscal environment.

Standardization is a parallel effort which will be evolving and maturing while both the requirements/capabilities analysis and technology integration projects are continuing. Since software costs constitute the vast majority of system life-cycle costs today, it is very important that future technology conforms to industry standards for software, data storage, and hardware. The challenge here will be to evolve a set of environmental M&S standards while at the same time planning and developing new technologies for delivery and implementation to support DoD mission areas.

The strategic plan for implementing the EA vision, using the three functional areas above, is shown in Figure 2:

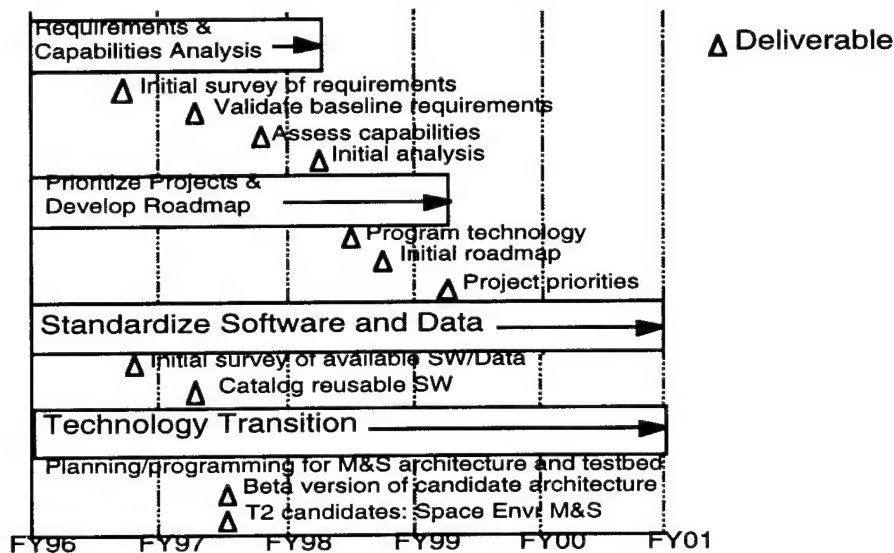


Figure 2 - Execution schedule for major EA objectives. Milestones are indicated by triangles.

4. CONCLUSIONS

This paper briefly described the Executive Agency for M&S of Air and Space Natural Environment. At the present time, plans are being made for including personnel from various DoD Agencies in the proposed EA. Although there are numerous challenges ahead in building a robust air and space natural environmental M&S capability for DoD, we believe it is absolutely critical for National security that this capability gets developed properly. With the increased emphasis on M&S throughout DoD, it is very likely that our future land, sea, and air component commanders will have used M&S extensively in their training and preparation for combat. If we do not recognize this opportunity and take advantage of it quickly, an entire generation of military leadership could emerge which does not understand the impacts of the natural environment on military operations such as Command, Control, Communications and Intelligence, nor has the proper knowledge of how to exploit the natural environment to the advantage of friendly forces. The present state of M&S is comparable to the early days of the Space Program. While there were many 'false starts' in those early days, the future held promise; this is a good analogy to keep in mind in the months and years ahead.

5. REFERENCES

1. Draft DoD Modeling and Simulation Master Plan, January 1995, Under Secretary of Defense (Acquisition and Technology), Washington D.C. (Obtainable through DTIC, Cameron Station, Alexandria VA 22304-6145, or from NTIS, 5285 Port Royal Rd., Springfield VA 22161)
2. Smoke-An Integral Part of Soviet Maskirovka, 1986, Ebersole, J.F., Klimek, W., and A. Van de Wal, 1986; Tactical Weather Intelligence Conference, White Sands Missile Range, NM.

SYNTHETIC ENVIRONMENTS IN SYNTHETIC THEATER OF WAR (STOW) 97

Jeffrey T. Turner
U.S. Army Topographic Engineering Center
7701 Telegraph Road
Alexandria, VA 22315-3864, USA

ABSTRACT

In 1997 the STOW Synthetic Environment program will demonstrate a robust DIS capability by 1) dynamically collecting, integrating, and distributing geo-specific weather data; 2) governed by this data simulate within ModSAF and visual simulators the state of the environment to include changing atmospheric states and dynamically changing physics-based feature models; and 3) simulating dynamic terrain and objects through a series of combat engineering related ModSAF scenarios. These technologies will demonstrate an interoperable system level architecture solution supporting weather distribution, weather simulation, environment feature modeling, and dynamic terrain.

INTRODUCTION

The Synthetic Theater of War (STOW) 97 is an Advanced Concept Technology Demonstration (ACTD) jointly sponsored by the Advanced Research Projects Agency (ARPA) and the United States Atlantic Command (USACOM). The successful implementation of STOW 97 technologies will mark the full operational capability of USACOM's Joint Training, Analysis and Simulation Center (JTASC). The STOW Program seeks to demonstrate technologies enabling the integration of war-fighting virtual and constructive simulations from diverse locations into a common synthetic battlespace through communication via high speed/bandwidth networks. This overview serves to address STOW 97 Synthetic Environment (SE) component technologies in the virtual and constructive domain. The SE Program is executed out of the SE Program Office within the Topographic Engineering Center (TEC) under the direction of ARPA SE Program Manager, Mr. George Lukes.

Current computer image generators (CIGs) and semi-automated force (SAF) applications in Distributed Interactive Simulations (DIS) have not, in general, simulated the environment. In virtual simulators today clouds, fog, haze, and rain are generally simulated via simple graphic display techniques to offer the effect of an environment. Smoke, obscurants, vehicle dust, explosions, flares, and fire are, in general, canned animations. Dynamic terrain events such as breaching of anti-tank ditches, minefields, and other complex obstacles are generally considered formidable technology barriers for today's simulators. In constructive simulations (Modular Semi-Automated Forces (ModSAF) for instance) the presence of true environment modeling is even more immature. The computational burden of an added environment on real time attenuation of sensors and line of sight calculations have been major factors in limiting the environment in the past. These problems are key focus issues for the Synthetic Theater of War (STOW) Synthetic Environment Technology Development program.

The principle charter of the SE program is to develop a system level interoperable first generation physics-based synthetic environment within ModSAF and Stealth virtual simulators.

Stealth simulators being enhanced include Naval Postgraduate School's NPSNET and Loral Advanced Distributed Simulation's VISTAWORKS. Both NPSNET and VISTAWORKS are software image generators running on Silicon Graphics Onyx Reality Engine work stations.

Three efforts described herein were initiated by TEC on October 1, 1994. SE research and development will continue through March, 1997. Integration of SE components with other STOW components will begin in May, 1995 and continue through final demonstration of STOW technologies in November, 1997. These efforts include: 1) Weather in DIS; 2) Dynamic Environment Modeling; and 3) Dynamic Terrain and Object Modeling.

WEATHER IN DIS (WINDS)

TASC of Reading, MA is developing the architecture necessary to provide tactically significant weather (Wx) to participants in DIS exercises. Two principle components form the core WINDS program. First, TASC will develop a Wx Integrator to blend disparate sources of meteorological data from live observations, forecast models, and/or historical archives into a consistent, manageable, and distributable format. Secondly, TASC is developing a Wx Distributor to provide the meteorological data to individual simulators at appropriate levels of detail and abstraction.

The Wx Integrator will rely on data sources such as weather prediction and forecast outputs (e.g., NORAPS), radar data, surface observations, upper air soundings, satellite radiances, and cloud analyses. Wind data will be enhanced in resolution with the Army Research Laboratory (ARL) High Resolution Wind (HRW) model. Other atmospheric state information, coarse in spatial resolution initially (e.g. 10km grids), will be enhanced to sub 1km gridded resolution using the ARL Battlefield Forecast Model (BFM).

The Wx Distributor will (a) support distribution of atmospheric states during an exercise; (b) support pre-distribution of Wx data; (c) minimize network loading by distributing only the requested data and by using compression and incremental updates; (d) provide capabilities to run feature models (e.g., clouds) at the server; and (e) support generation and distribution of multi-fidelity Wx fields.

Analysis of the atmospheric state and Wx events during a simulation exercise will be supported by a Wx Viewer augmented into the existing ModSAF Plan View Display.

Wx data will be distributed to simulation components both prior to simulations as well as in real-time via environmental Protocol Data Units (PDU). Requirements for Wx data stem primarily from the Dynamic Environment Modeling program where Wx dependencies reside. For instance, vehicle dust, flares, and battlefield obscurant (smoke) models require wind vector inputs; atmospheric transmittance models require temperature, humidity, dewpoint, precipitation state, and extinction type and amounts; and cloud models require basic atmospheric state information, cloud bottom height, cloud top height, and cloud cover percent.

DYNAMIC ENVIRONMENT MODELING

Loral Advanced Distributed Simulation (LADS) of Bellevue, WA and Cambridge, MA are integrating environment effects and feature models within ModSAF and Stealths. Types of effects being added or enhanced include battlefield smoke (obscurants), atmospheric transmittance, time of day, shadowing, signal and illumination flares, vehicle dust, clouds, thunderstorms, precipitation, dust clouds and storms, explosion and weapon effects, trafficability and mobility, and hydrology modeling. Successful environmental representation in ModSAF will include facilitation of appropriate weapon system effects and entity behaviors that respond to or exploit to some degree each environmental effect. Successful environmental representation in the Stealths will include

correlation to the ModSAF representation, acceptable Stealth performance benchmarks, and accurate visual correlation to real-world environmental phenomenon. All environmental phenomenon are dependent upon the input provided by the WINDS weather distributor.

DYNAMIC TERRAIN AND OBJECT MODELING

A third component of the SE Program, also under contract to LADS, is developing ModSAF and Stealth capabilities supporting two levels of dynamics (a) Level I - dynamic terrain in which terrain database geometry is manipulated during simulation run-time; and (b) Level II - multi-state objects supporting various health states for objects such as buildings and bridges (i.e. healthy bridge, damaged bridge, destroyed bridge). Requirements for Level I dynamic terrain are principally focused on combat engineering requirements. Namely cratering, minefield breaching, anti-tank ditch breaching, and breaching of other combat emplaced obstacles. Level II dynamic terrain is based on the requirement for a more computationally inexpensive, highly scalable architecture to globally reflect dynamic properties in all placeable simulation database objects.

The architecture supporting dynamic terrain has been a controversial subject over the past five years. Point solutions developed in the past have provided excellent case studies for the most recent STOW architecture design process. A rigorous evaluation of the current dynamic terrain architecture by government and industry subject matter experts in both SAF and CIG domains have convened throughout 1995. These meetings have addressed potential deficiencies in the design while addressing a "System Level" solution capable of supporting interoperability within a heterogeneous suite of simulators both virtual and constructive.

CONCLUSIONS

In 1997 the STOW Synthetic Environment program will demonstrate a robust DIS capability by 1) dynamically collecting, integrating, and distributing geo-specific weather data; 2) governed by the weather data simulate within ModSAF and CIGs the state of the environment to include changing atmospheric states and dynamically changing physics-based feature models; and 3) simulate dynamic terrain and objects through a series of combat engineering related scenarios.

ACKNOWLEDGMENTS

These programs are being executed under the direction of the U.S. Army Corps of Engineers, Topographic Engineering Center, 7701 Telegraph Road, Alexandria, VA 22315-3864.

WEATHER IN DISTRIBUTED INTERACTIVE SIMULATIONS (WINDS)

Vernon M. Stoltz
U.S. Army Topographic Engineering Center
Alexandria, VA 22315-3864

Eric O. Schmidt
TASC
Reading, MA 01867-3297

ABSTRACT

The ability to provide tactically significant weather to participants in Distributed Interactive Simulations (DIS) exercises is one of the major components of the Synthetic Theater of War (STOW) Synthetic Environments program. Weather in DIS, or WINDS program, is being designed to ingest meteorological data from a variety of sources, assimilate this data to produce a coherent description of the state of the atmosphere, store that data in data fields and then distribute those fields to the various exercise participants. Weather data will be distributed through environmental Protocol Data Units (PDUs) at appropriate levels of detail and abstraction. The WINDS architecture can be easily extended to include other aspects of the environment.

Introduction

The Weather in DIS, or WINDS program, is one of several efforts under the STOW '97 Synthetic Environment (SE) program. The goal of WINDS is to provide DIS-compliant weather information to STOW exercise participants. TASC of Reading, Mass., is designing the architecture and developing the software under this effort. WINDS is sponsored by the Advanced Research Projects Agency (ARPA) and the U. S. Atlantic Command (USACOM). The SE Program Office is located within the U.S. Army Topographic Engineering Center (TEC) under the direction of George Lukes, ARPA SE program manager. Initial terrain data base construction has focused on a high-resolution Ground Maneuver Box area and a 2 by 4 degree, low-resolution region known as "Area 2" which contains a land/ocean interface (See Figure 1).

Architecture

The WINDS architecture consists of five basic software modules: an integrator, a data base, a distributor, a viewer and a simulator. These modules were developed using object oriented design and C++ to promote maximum flexibility, efficiency and robustness. These five modules can be functionally organized into a client-server representation and into different subsystems for purposes of testing and validation. The WINDS architecture is shown in Figure 2.

Integrator

The weather integrator will receive data from various sources including forecasts, radar data, surface observations, upper air soundings, satellite radiances and cloud analyses. The primary source for this data will be the Master Environmental Library (MEL), a program under development through the Naval Research Laboratories. A Naval Operational Regional Atmospheric Prediction System (NORAPS) run providing horizontal resolution of 20 km with one-hour interval resolution was performed for a period of high precipitation from Jan 9-11, 1995. This run will be augmented by both a Coupled Ocean-Atmosphere Mesoscale Prediction System (COAMPS) run providing 5 km resolution and oceanographic data provided by the Princeton Oceanographic Model (POM). A second dataset covering a summer monsoon for the same Southwest region

will be delivered later in 1995. Future data sets will include data coincident with the final location of the STOW exercise area.

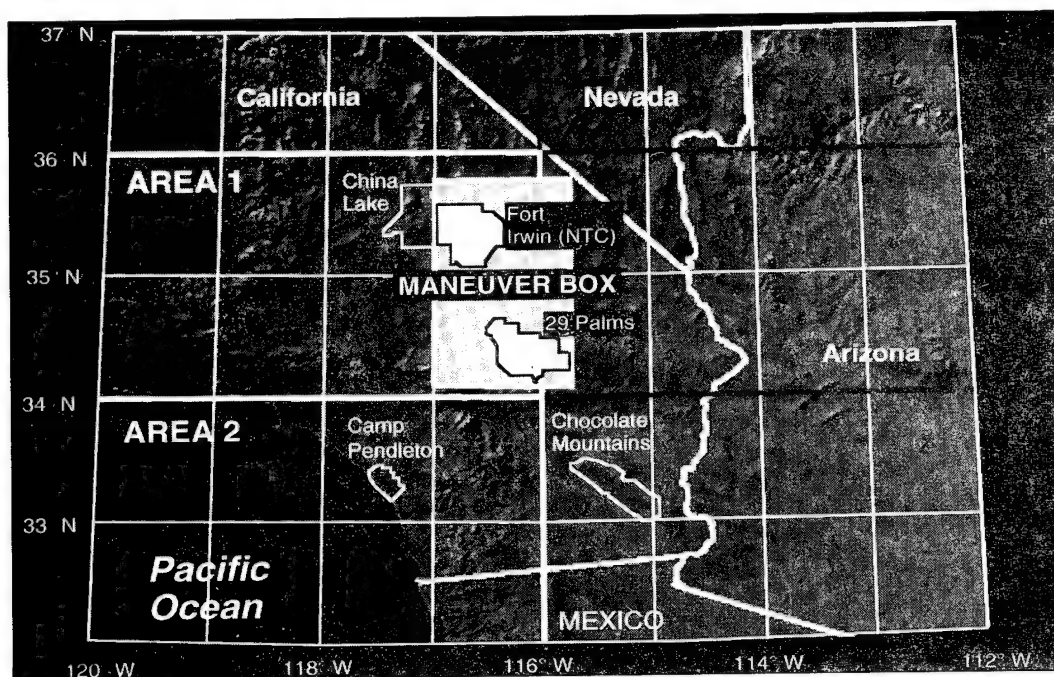


Figure 1. The Southwest United States terrain data base. Initial construction has focused on the maneuver box and Area 2, which contains a significant portion of the Pacific Ocean.

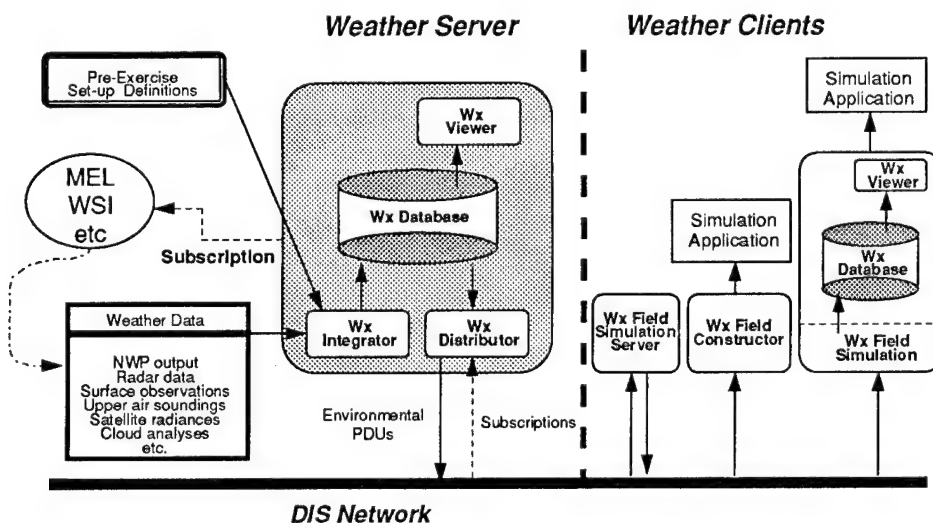


Figure 2. Overview of the WINDS Architecture Design

Database

The various input data sources each have their own unique coordinate representations. These data sets will be transformed into a single internal representation latitude-longitude-pressure height through the use of various assimilation techniques, including a Barnes algorithm. This common representation will provide the native coordinate representation for the weather data base, where other weather data can be derived. An Applications

Programmer Interface (API) will be provided to allow other STOW developers easy access to the environmental data stored in a local data base through the WINDS software.

Distributor

The weather distributor will support multi-fidelity transmissions. If a DIS user needs weather information for only a small area of the data base at 12 hour intervals, he would not need to receive the entire data set. A Real-time Information Transfer and Networking (RITN) architecture, which supports data subscription and publication of environmental PDUs in a multicast mode, will be used to help minimize network loading of any single node. The weather data base will support the dynamic update of weather data as the scenario evolves in time.

Viewer

A weather viewer, currently augmented into an existing Modular Semi-Automated Forces (ModSAF) Plan View Display, allows users to view the contents of the 3-D gridded data base. Field constructor software will allow users elsewhere on the DIS network to read the PDUs and reconstruct selected portions of the data base at their own location. The weather viewer could then be used to view this reconstructed dataset. Users not using ModSAF will still be able to read distributed PDUs. The distributor architecture does not depend on ModSAF. The ModSAF software is used only to browse and examine the environmental data, not to distribute or reconstruct it.

Simulator

The simulator portion of WINDS will include the use of the Army Research Laboratory's (ARL) High Resolution Winds (HRW) model to provide wind speed and vectors at high resolution. ARL's Battlefield Forecast Model (BFM) may also be used to enhance the resolution of the weather data. Many applications are unable to process large amounts of raw gridded weather data, such as temperature and humidity fields. Because of this, WINDS will investigate using feature extraction techniques to provide more basic information such as cloud boundaries, water content, or possibly atmospheric transmission coefficients.

Ocean Environment

It had been sufficient to have the environment represented only by an atmospheric component when DIS exercises were limited to small landlocked areas. In this case, land-based trainers had their own data bases created and maintained, focusing only on those factors affecting terrain. Likewise, Naval participants had their own unique data base, focusing only on factors concerning the ocean. DIS exercises have since expanded to cover much larger areas that contain both terrain and ocean areas. With the accompanying emphasis on joint exercises, it becomes critical that all participants using environmental data reference a single common environmental representation.

The WINDS program has been expanded to include ocean data in addition to the original atmosphere data. Oceanic and atmospheric data are similar in that both are made up of often sparse 3-D gridded fields which slowly transition to different states over time. This structural similarity makes it easy to add ocean data without redesigning the basic architecture of WINDS. A common, cohesive solution at the ocean/atmosphere interface will help assure that the various players within each realm are working together on a consistent, correlated basis.

CONCLUSION

The WINDS architecture provided a solid basis on which to build a common representation of the environment. Its architecture design will support the addition of more robust and scientifically sound algorithms as they become available. The environmental data provided will enable developers many opportunities to enhance their models, resulting in more realistic and valuable DIS training exercises.

A MASTER ENVIRONMENTAL LIBRARY TO SUPPORT MODELING AND SIMULATION

Richard A. Siquig
Naval Research Laboratory
Monterey, CA 93943-5502 USA

CAPT Bruce Shapiro
Air Force Combat Climatology Center
Scott Air Force Base, IL 62225-5116 USA

Martin Miller
USAE Waterways Experiment Station, CERC
Vicksburg, MS 39180 USA

ABSTRACT

The Master Environmental Library project funded by the Defense Modeling and Simulation Office has a two fold purpose, to provide a library structure linking dissimilar autonomous regional sites of environmental data through a common interface at a master site, and to populate the library with consistent realistic environmental data sets for DoD modeling and simulation. A prototype has been developed on the World Wide Web, linking environmental data bases for the Navy, Air Force, and Army. Future extensions will include security safeguards, enhanced data visualization tools, and incorporate other regional sites.

1. INTRODUCTION

No DoD standard oceanographic, atmospheric, or near-space data bases exist today which provide detailed, *consistent*, natural environments in a standard format from an accessible searchable library for modeling and simulation (M&S). The Defense Modeling and Simulation Office (DMSO) Master Plan has set objectives that promote joint service standards and capabilities for M&S. To support this end, DMSO has funded the Master Environmental Library (MEL) project, a FY95 new start, to prototype an initial distributed environmental data base repository with a common interface usable by all service M&S users and to be a component of the Modeling and Simulation Resource Repository (MSRR).

The MEL project is a joint service (Navy, Air Force, Army) effort, with a central focus of analyzing, designing, implementing, testing, and enhancing a common user-friendly library structure for distributed dissimilar data base systems of environmental data within DoD with possible extensions to non-DoD data bases. MEL will allow the user to search for arbitrarily formatted data stored at the regional sites, visualize the data to some degree, reformat desired data (possibly subsetted) in an appropriate standard transfer format, and finally retrieve the data in a timely fashion. To meet the goals and timelines for the prototype, the MEL structure is based on World Wide Web (WWW) utilities including browsers such as Mosaic/NetScape and metadata search systems such as the Wide Area Information Servers (WAIS). The MEL structure can be separated into two main components, the master site (where the MEL system is accessed by the user) and the regional sites (where the data resides).

2. MASTER SITE

A HyperText Markup Language (HTML) user interface has been developed that includes a MEL home page and related links to other necessary or desirable HTML pages. User options are extensive and helpful to a range of users and include, e.g., help options, glossary, documentation, related software, extensive query features (e.g., by time, geographic domain, parameter, project, site, case studies, etc.), several logical approaches to the data, links to other library systems, and a comment/feedback option. All implementations are intended to be as user friendly as possible. Explanatory hypertext links will provide

progressively more detailed levels of explanation to serve a community of users with a wide range of expertise in networking skills and familiarity with environmental data.

A MEL search scheme was developed that utilizes the strengths of widely available and rapidly evolving Internet utilities, such as indexed WAIS servers. Common gateway interface (CGI) scripts were written to facilitate searching and displaying metadata records stored at the participating regional sites and then, if desired, to request data, including subsetting the data if that is possible at the originating site. Data security has been addressed only in a preliminary way so far. Initially, this may require encryption safeguards for unclassified environmental data subject to releasability constraints.

3. REGIONAL SITES

Regional site software consists of a WAIS server and an order/extraction/delivery system. The WAIS server searches WAIS indexed metadata files that describe available datasets. MEL uses the Federal Geospatial Data Committee (FGDC) Content Standards for Digital Geospatial Metadata. Regional sites maintain their own metadata which can describe an individual dataset or a class of datasets. Each regional site runs a suite consisting of order parser, access control, scheduler, data extractor/formatter, and delivery modules. Orders arrive via electronic mail from the master site or direct from users (batch mode). They are parsed and submitted for extraction. The customizable access control module must approve the request before order processing. Access control can be tailored to provide human approval, user authentication, cost and accounting, etc. Once approved, the scheduler submits the job to the extractor/formatter. This module is customized to extract data using the local data access methods and to format data into the desired delivery format, which may include GRIB for gridded data, BUFR for non-gridded data, and NITFS for image data. The scheduler then triggers the data delivery system to deliver data per user request (ftp, email, mail, etc.). In addition, each regional site may have its own MEL regional home page which describes the types of data available and provides access to a local data search and browser if they exist. Regional sites might have search engines capable of finer grain searching than the generalized MEL metadata-based search.

The initial regional sites are NRL Monterey, the Air Force Combat Climatology Center, and the Army Coastal Engineering Research Center. These MEL sites have data bases that are consistent among themselves. For example, the ocean models use surface winds derived from the atmospheric model data bases.

4. FUTURE DEVELOPMENT

Long term requirements for MEL will include tools to register data from disparate sources or data bases to some common representation for greater utility to the user. Later versions will consider more powerful client-server methods. Generic viewers for data in standard transfer formats may eventually be required for improved user visualization capabilities.

5. CONCLUSIONS

A prototype library structure has been developed that utilizes WWW technologies to provide a common interface for data query, search, access, and delivery of environmental data at distributed dissimilar DoD sites. The strengths of this approach are that regional sites retain full control over their data and the rapidly evolving Internet technologies allow rapid cost effective prototyping. The drawbacks are mainly possible security weaknesses, which are being addressed for future enhancements.

6. ACKNOWLEDGMENTS

The Master Environmental Library (MEL) project is funded by the Defense Modeling and Simulation Office (DMSO) under the Director of Defense Research and Engineering (DDRE).

DYNAMIC ENVIRONMENTAL EFFECTS MODEL

John R. Hummel, Kathy L. Simunich, and John H. Christiansen

Decision and Information Sciences Division

Argonne National Laboratory

Argonne, IL 60439-4832

ABSTRACT

The Dynamic Environmental Effects Model (DEEM) is a simulation architecture that has been developed to provide a flexible framework for multidisciplinary modeling of terrestrial, aquatic, and atmospheric processes. The modeling domain of DEEM is flexible, determined by the library of objects available within DEEM and by the collection of legacy models which have been gathered by users to address specific modeling concerns. One application that will be highlighted is the use of DEEM as a simulation architecture for a theater level weather forecast model being developed for the U.S. Air Force.

1. INTRODUCTION

The Dynamic Environmental Effects Model (DEEM) is a software framework intended to facilitate holistic multidisciplinary modeling of terrestrial, aquatic, and atmospheric processes. These processes are modeled in DEEM as interrelated actions caused by and affecting the collection of diverse real-world objects represented in a simulation. The modeling domain of DEEM is flexible, determined by the library of environmental and other objects available within DEEM. The modeling domain is also enhanced by the collection of legacy models which have been gathered by users to address specific modeling concerns.

The DEEM concept was adopted in mid-1993 by the Joint Chiefs of Staff/J-8 for use in developing a prototype terrain reasoning and synthetic terrain generation system. In addition, DEEM has been selected by the USAF Air Weather Service as the software framework for a multidisciplinary environmental modeling effort in support of theater-level mesoscale weather forecasting. Development efforts for DEEM have been sponsored by a number of agencies including the Joint Chiefs of Staff/J-8, US Marine Corps, Defense Modeling and Simulation Office, USAF Air Weather Service, US Transportation Command, and the Department of Energy, among others.

2. SUMMARY OF THE DEEM ARCHITECTURE

Figure 1 shows the top-level architecture of DEEM. An external Graphical User Interface (GUI) is used to input commands as well as display results from a simulation. The DEEM Context Manager is used to interpret the requests and instructions supplied by the user and identify the DEEM resources to be utilized during the course of a simulation, such as objects from the DEEM Object Library, databases, and models. During the execution of a simulation, the Context Manager controls the interactions between objects and models using a rules-based expert system.

The DEEM architecture is a fully object-oriented system that contains a library of reusable objects. This system supports distributed, dynamic representations of interlinked processes and behaviors at variable scales of resolution and aggregation. The environmental taxonomy developed for DEEM has also been used as the basis of the environmental components in the Joint Warfare Simulation Object Library and the Joint Task Force Advanced Technology Development Program. DEEM is also designed to be able to easily interface with existing models. In this way, DEEM can import the various physics and process models that are required to provide the functionality for a given simulation. The majority of these models already exist within the DOD R&D community. The models remain in their native language when integrated into DEEM. The interface between DEEM and the model is primarily through a description of the data needs for a particular model and its interaction with DEEM objects.

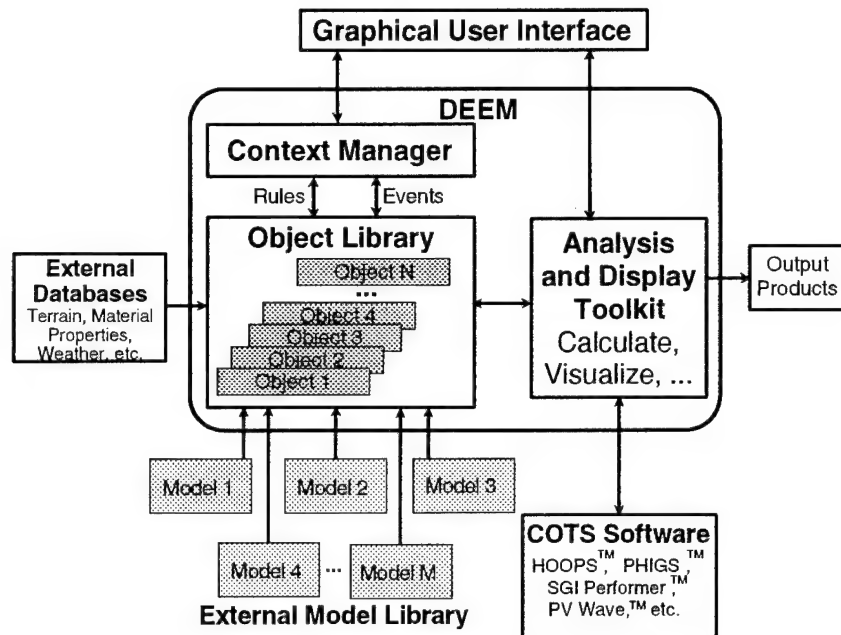


Figure 1. Top Level Architecture of the Dynamic Environmental Effects Model

3. DEEM APPLICATIONS

The majority of the applications utilizing DEEM to-date have focused on understanding the impacts of the environment on military operations. For example, for the work being performed for the Joint Chiefs Staff/J-8, models related to mobility and trafficability have been integrated into the DEEM framework. These models calculate vehicle speeds and their impact on the determination of mobility corridors, avenues of approach, etc. as a function of different weather conditions and terrain. In another effort being performed for USA Forces Command, DEEM technology is being used to determine the role of the environment in making mobilization assessments and force generation predictions.

In the effort being performed for the U.S. Air Force Air Weather Service, DEEM is being used as a software "shell" for a suite of models being used to develop an advanced theater level weather forecast model. This theater level forecast model will enable Air Force forecasters to better predict weather conditions in a theater of operations, thereby improving the data given to commanders for use in mission planning. Figures 2 and 3 show examples of the output produced by the prototype version of the system for the Korean peninsula. In Figure 2, the relative humidity fields at the surface are displayed on a 33 km grid. Figure 3 shows the same 33 km grid with wind vectors overlaid with an isosurface of the predicted cloud water mixing ratio for Typhoon Faye.

4. CONCLUSIONS

The Dynamic Environmental Effects Model (DEEM) is a simulation architecture that has been developed to provide a flexible framework for multidisciplinary modeling of terrestrial, aquatic, and atmospheric processes. The modeling domain of DEEM is flexible, determined by the environment objects available within DEEM and by the collection of models which have been gathered by users to address specific modeling concerns.

Future legacy models to be integrated into the DEEM framework will be utilized to provide information on how clouds impact military operations. For example, models capable of calculating cloud-free lines-of-sight and atmospheric transmittance and radiance are planned to be added to the DEEM library of legacy models in the upcoming months. With the addition of these models, DEEM will be able to provide a powerful system for studying the impact of the environment on military operations.

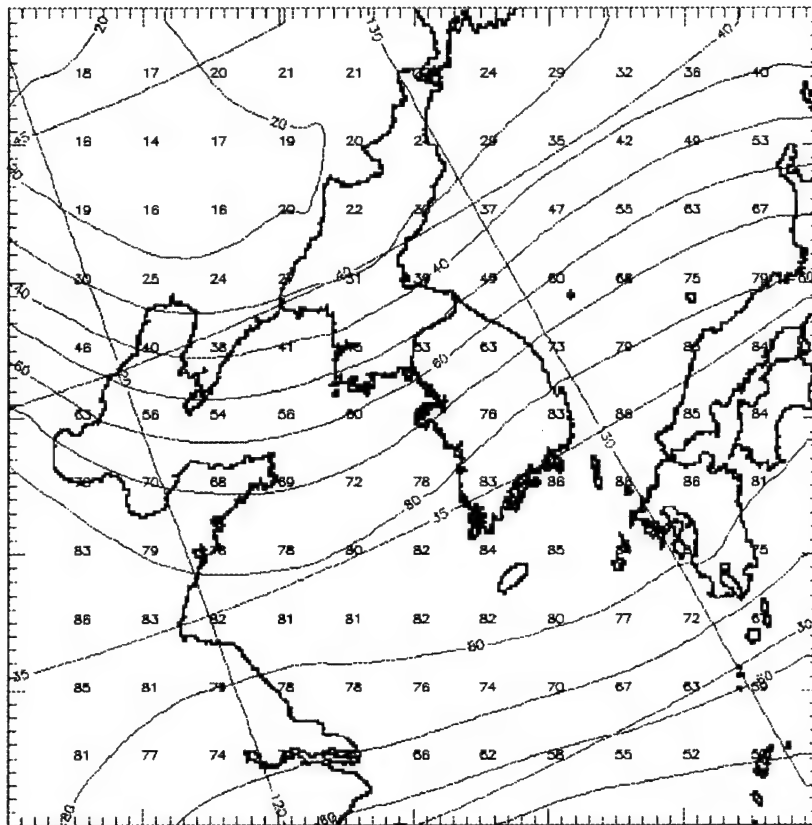


Figure 2. Example of the Relative Humidity Fields Produced by the Prototype Version of the Advanced Theater Level Weather Forecast System. The Results Shown are From a 36 hour Forecast Produced With Data Taken at 12 Z on 14 November 1995.

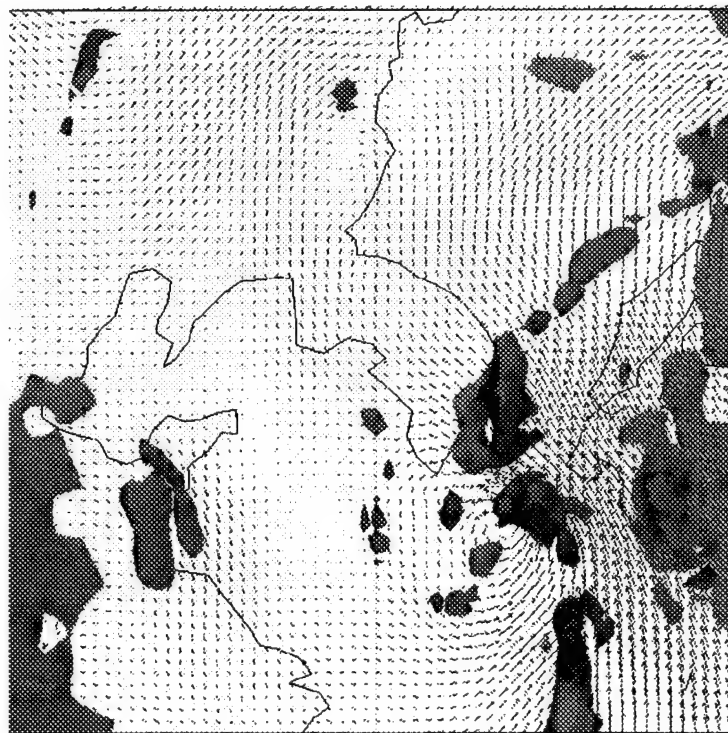


Figure 3. Typhoon Faye Shown With Wind Vectors Overlaid With Cloud Water Mixing Ratio Isosurface. The Results are From a 48 hour Forecast Produced With 22 July 1995 Data Taken at 0 Z.

THE E²DIS ENVIRONMENTAL MANAGER: CLOUDS

Harry M. Heckathorn
Naval Research Laboratory
Washington, D.C. 20375-5352

Stanley H. Grigsby
ENFO, Inc.
Alexandria, VA 22314

ABSTRACT

The E²dis architecture consists of a runtime infrastructure, standard interfaces between environmental models and the runtime infrastructure, object model design rules, and the environmental manager. The environmental manager contains the models, databases, and management software required to provide simulation of the representations and effects of the atmosphere, terrain, ocean, and other entities in the environment. Management of the execution of the environmental representation and environmental effects is provided through a hierarchy of software managers. This paper describes the cloud portion of the E²dis environmental manager and its role within the E²dis architecture.

1. INTRODUCTION

The *DIS Vision* document states that, "Obtaining environmental correlation may be the most complex challenge facing the DIS community."¹ The E²dis project has developed a method to address this issue that consists of two components.^{2,3,4} The first is an architecture, called the runtime infrastructure, RTI, that provides synchronization and control of the players in a distributed simulation.^{5,6} The other component is an environmental manager consisting of environmental players on each of the nodes operating under this architecture.⁷

2. ARCHITECTURE

The E²dis architecture is composed of a runtime infrastructure (RTI), the environmental manager, standardized interfaces between all the players and the RTI, and standardized object model descriptions. The RTI provides the delivery system for the E²dis environmental effects and representations. Through a hierarchy of management functions the RTI provides synchronization and control that guarantees the proper order and timeliness of message transmission and receipt. For a complete description of the E²dis architecture see the E²dis paper entitled, "An Architecture to Support Large N, Highly Interactive, Distributed Simulations".⁶

3. ENVIRONMENTAL MANAGER

The RTI provides the delivery system that insures messages are passed (*i.e.* sent and received) at the correct time and in the correct order among players. Therefore making the environment a player allows it to take advantages of the RTI infrastructure in order to provide synchronization and control and hence correlation. The environmental manager is the name given to the distribution of environmental players located on each node

A key assumption in the development of the E²dis concept is that the environment can be considered, for a large part, deterministic. This means that a 4D description of the natural environment is a sufficient description and is the basis for the further computation of more highly detailed environmental effects. This description can be precomputed and predistributed to all of the environmental players resident on the nodes of the simulation. This predistribution allows for a major reduction in the information that would otherwise occupy bandwidth during an exercise. Because one of the dimensions of this description is time, the only requirement to maintain consistency of this portion of the environment is that all of the environmental players be synchronized. The portion of the environment that is not deterministic is

superimposed on or imbedded within the deterministic portion. Only the messages necessary to trigger these non-deterministic portions must be exchanged among the nodes in a distributed simulation.

The non-deterministic portion of the environment includes features such as smoke and dust clouds, and the information about the other players in the simulation. This information about the other players is maintained in an object called the spatial manager, part of the environmental player.

The flexibility of the architecture provides for a high degree of modularity and information hiding, therefore the requesting player need not know, and thus not concern itself with how the environmental information is produced. Because of encapsulation, the specific computations within the environmental player are hidden from other players (information hiding) and objects within the environmental player. As long as the interface standards are adhered to, this architecture provides great flexibility when building and modifying the environmental player. It is therefore possible to use a precalculated 4D database or real-time data as the basis for the environmental player.

A simple implementation of the environmental player was developed by E²dis. Only portions of the atmosphere, terrain and the spatial manager, as highlighted in Figure 1, were included in this initial implementation. There are two players in this implementation: a Fiber Optic Guided Missile, FOG-M, and the environment. This implementation is the result of decomposing a system currently running as a single model into the parts related to the FOG-M and the terrain within that model. The terrain database was removed and placed on the environmental player. The FOG-M simulator then used the E²dis architecture to access the terrain data from the environmental player. Atmospheric codes were included in the environmental player to provide cloud shadow information to the rendering of the terrain. All of this is considered deterministic and is computed prior to the simulation. Rendering is done through the FOG-M visualization tool, PV3i. The spatial manager contained the state variables for each player. In this experiment those state variables are the position and velocity. The attributes of the players are then position in x, y, and t, and the velocity components in x, y, and t.

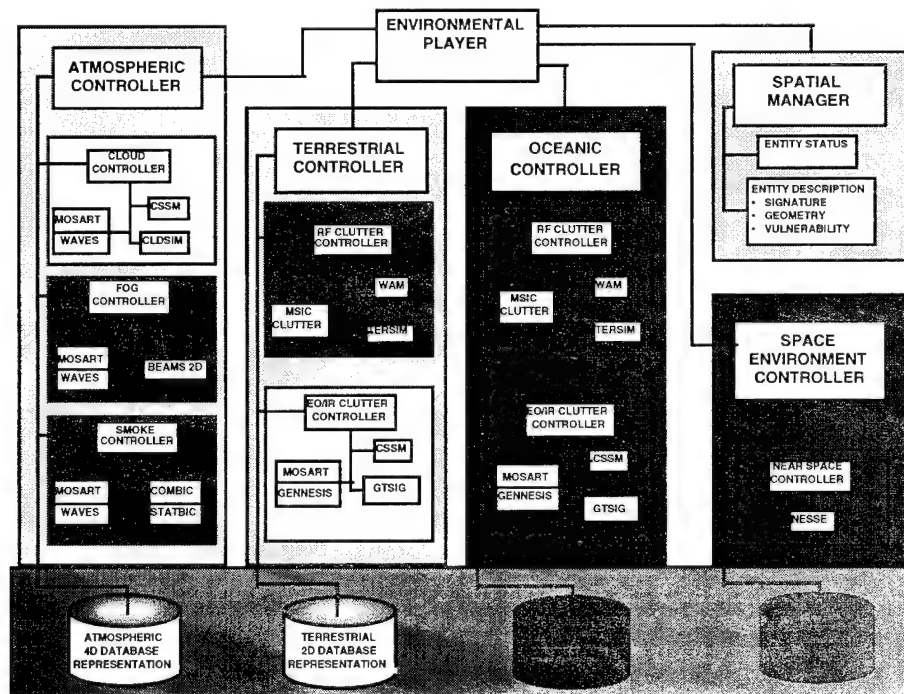


Figure 1

The cloud player is included in the environmental player which is then included in the distributed simulation as shown in Figure 2. As stated earlier the details of this implementation are given in other E²dis papers.^{6,7} The modular nature of this design provides a mechanism for including cloud information from various sources without modifying design of the environmental player. The information hiding or encapsulation aspect of this object oriented design allows modification of the details in the development of the cloud information, or any other part of this player, without modifying the player that uses this

information. This is made possible through the use of standard interface definitions and the control exerted by the various managers within the environmental player.

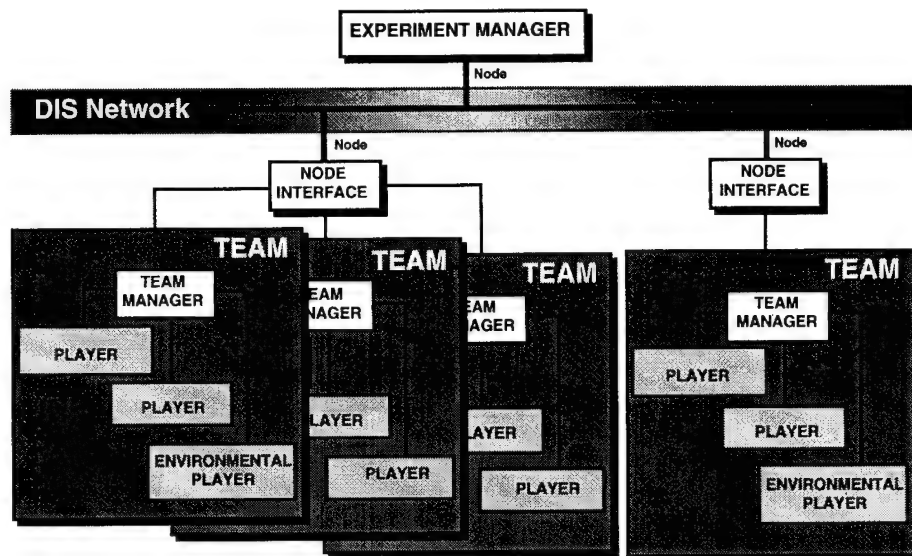


Figure 2

4. CONCLUSIONS

Cloud information, correlated in time, space, and phenomena, can be delivered to distributed simulations by the E²dis architecture. This correlation is a result of deriving the effects from a common 4D environmental database that is maintained by an environmental manager running under the control of the E²dis RTI. The object oriented design of this architecture allows modification to the models used by the environmental player or any player without modification to other players. Information hiding as a part of the concept and standardized interfaces in the implementation provide this capability.

5. REFERENCES

1. DIS Steering Committee, The "DIS Vision - A Map to the Future of Distributed Simulation," IST-SP-94-01, Institute for Simulation and Training, University of Central Florida, May 1994.
2. Berg, S.L., S.H. Grigsby, H. Heckathorn, J.C. Herbst, D. Anding, J. H. Kirkland, "Improving the Fidelity of Distributed Simulations Through Environmental Effects", 13th Workshop on Standards for the Interoperability of Distributed Simulations, Position Paper 95-13-108, September 1995.
3. "E²DIS Program Requirements Document," Version 0.1, April, 1995.
4. "E²DIS Object Oriented Analysis," Version 0.9, November, 1994.
5. Herbst, J.C., S.L. Berg, J.H. Kirkland, D. Anding, H. Heckathorn, S.H. Grigsby, R. Graves, "The Approach for Providing Environmental Effects to DIS," 12th Workshop on Standards for the Interoperability of Distributed Simulations, Position Paper 95-12-111, March 1995.
6. Herbst, J.C., J.H. Kirkland, S.L. Berg, S.H. Grigsby, H. Heckathorn, "An Architecture to Support Highly Interactive, Large N, Distributed Simulations," 13th Workshop on Standards for the Interoperability of Distributed Simulations, Position Paper 95-13-079, September 1995.
7. Grigsby, S.H., J.C. Herbst, J.H. Kirkland, S.L. Berg, H. Heckathorn, D. Anding, "The E²dis Environmental Manager," 13th Workshop on Standards for the Interoperability of Distributed Simulations, Position Paper 95-13-090, September 1995.

SURVEY OF REQUIREMENTS FOR EFFECTS OF THE NATURAL ENVIRONMENT IN MILITARY MODELS AND SIMULATIONS

Thomas M. Piwowar and John Burgeson
Science and Technology Corporation
Washington, DC

Donald D. Grantham
Geophysics Directorate, Phillips Laboratory
Hanscom Air Force Base, Massachusetts

Sam Brand
Naval Research Laboratory
Monterey, California

Alan Wetmore
U.S. Army Research Laboratory
White Sands Missile Range, New Mexico

As a result of DMSO interest in better incorporation of the natural environment into modeling and simulation, research laboratories of the Military Services have begun to focus on gaining a better understanding of the requirements for natural environmental effects in military modeling and simulation efforts. The first coordinated step by the Services in gaining this better understanding was started with the DMSO-funded Environmental Effects for Distributed Interactive Simulation (E²DIS) Project Survey Task.

A strategy to survey the four Services for environmental effects requirements was developed and executed. A questionnaire and personal interview process was used to document, understand and verify requirements and to provide the basis for a compilation of the qualitative findings and quantitative results. Emphasis was placed on identifying critical environmental factors and the parameter/fidelity/accuracy requirements for the warfighting models and simulations surveyed. Some unexpected findings and results materialized that have far-reaching implications for the military M&S community. For example, some widely used warfighting models do not incorporate environmental effects and environmental data at all, others incorporate the environment in an inconsistent manner. In addition, some modeling and simulation developers were not aware of the role that the natural environment could play in their modeling and simulation efforts, and some were not aware that technology currently exists to provide more realistic results. An analysis of the parameter/fidelity/accuracy requirements for the models and simulations surveyed will be presented.

A complimentary survey was also conducted as part of the E²DIS Project Survey Task in order to determine "capabilities" that exist within the environmental community to meet the environmental "requirements" of M&S. These two compilations provide the basis for the necessary "roadmaps" needed to solve many of the environmental/environmental effects issues in the M&S world.

Manuscript not available at time of printing. Please contact author for information.

SESSION II:
CLOUD IMPACTS: SIMULATIONS AND APPLICATIONS

NATURAL ENVIRONMENT ENGINEERING TOOLKIT

Sandra K. Weaver
National Air Intelligence Center
Wright-Patterson AFB, OH 45433-5635
Telephone: 513/25-77071; FAX: -79888

William A. Lanich
USAF Wright Laboratory
Wright-Patterson AFB, OH 45433-7700
Telephone: 513/25-55292; FAX: -56144

ABSTRACT Pity the poor engineer. Tradeoffs are his life blood, but tradeoffs aren't available to him for the most potent influence on the performance of his mission avionics system—at least not in a form which he can conveniently use, except with outside expert guidance. This paper is a plea for environmental influence engineering tools, with some notions about what they might look like, how they might behave, and how they might be developed.

BACKGROUND

Think about the engineering involved in developing and making use of new military technology. Think about how tradeoffs are the essence of the iterative, recursive engineering process. Consider the engineering processes involved in designing, testing, and applying new technology.

When designing a mission avionics subsystem, the engineer has access to computational tools which portray how much benefit is to be expected from, say, increasing the aperture size of an antenna or lens, or from improving the noise figure of an amplifier. And good tools are available which make it straightforward to establish the performance envelope of a subsystem comprising various combinations of typical 'good' or 'bad' detectors with typical 'good' or 'bad' preamps, as expected from production tolerances. Understanding of the influences of these variables is well in hand, and computational tools are available for making tradeoffs. But where are the tools which allow the engineer to trade increments in the performance of his hardware to compensate for the performance decrements which will be caused by the natural environment?

New technology is always given real-world testing. But testing in every combination of conditions which will be experienced by an operational system is simply not possible. So a series of tests is conducted over what is intended to be a gamut of conditions which will suggest the operational performance of the system. Each test gives one or two points on an infinitude of curves. Extrapolations and interpolations are not intuitive. Thus, when

trying to understand the implications of the results of testing new technology in real-world conditions, the question should always be "How typical was this experience?" That is, was the experienced combination of environmental influences extreme—too easy, or too difficult? Or was it representative of the many locations where the system will operate? But the meaning of "representative" must be expressed in engineering terms—how often the system will work better or worse than it did during the test experience.

Planners and tacticians must make deployment and employment decisions.

Deployment decisions involve deciding where in the world it makes the most sense to situate various systems, so their capabilities will be most effective, and so they will produce the most return on investment.

Employment decisions involve, for example, deciding what time tomorrow which system will be most effective against a given target in a given background. But the advice must be expressed in engineering terms—where and when the system will work how well how often. Where are the tools to support complicated deployment decisions? A tool is available which gives advice to tacticians: the operational version of the 'Tactical Decision Aids' developed by Wright Lab for Phillips Lab. (And Wright Lab has attempted to use the Research-Grade version of these TDAs to suggest tradeoffs when designing and testing new systems. They are awkward for this purpose, but the RGTDA technology is being incorporated in the Wright Lab Advanced Electromagnetic Model for Aerial Targeting (AEM*AT), where they will better support such tradeoffs.)

THE NEED FOR TOOLS

So, there are good, well-understood, engineering tools available for predicting the way system performance is influenced by changes in subsystem and component performance. There are no similar tools for use by the engineer in trading off the influences of the natural environment. It is important for DoD to build smart and invest smart, and that means it is essential to be able to predict the performance of systems (and variations on systems) in what an engineer might think of as good-, typical-, and bad-weather scenarios. But even environmental experts don't agree on what constitutes a 'good' or 'bad' weather scenario—or even what 'typical' means.

In the absence of such tools, a Staff Meteorologist is essential. But the skill and judgment of the StaffMet are not always available; and even the most insensitive engineer eventually gets embarrassed by repeatedly asking dumb questions: "Well, OK, StaffMet, now what happens if I tweak *this* parameter by 10%?" Yet the business of engineering implies tradeoffs, and that implies 'what-ifs' and 'cut and try'. (Usually expressed as "a systematic exploration of technical options which is designed to converge on a solution optimized among many variables" — cut and try.)

An engineer isn't interested in met data. Even the most complete and perfect compilation of weather numbers is not engineering information. Information emerges when that data is turned into decision-support tools. This paper is a plea for natural environmental engineering tools (NEETs?), with some notions about what they might look like, how they might behave, and how they might be constructed.

WHAT THE QUESTIONS ARE

At the last CIDOS Conference, the question was asked, "Will your sensor be able to detect a MiG fighter flying at 5000 feet over Cambodia at 12 midnight on the 31st of December?" This real-life scenario is an example of the demands presented to the modeling and simulation community by sensor designers and operational planners. Unfortunately, we still don't know the answer to this question.

Pretend we are interested in a thermal imaging system—a FLIR. We need to know which of the factors below are the most important influences on the day-to-day targeting range of this system.

- aircrew skills
- sensor operating altitude
- daytime/nighttime operation

- target operating state
- maintenance actions
- target camouflage
- target aspect
- weather

What's your estimate?

Our experience with numerous systems in laboratory, test, and operational conditions suggests that reasonable performance ratios for a system not exposed / being exposed to these influences are:

- daytime/nighttime operation....2:1
- aircrew skills.....4:1
- maintenance actions.....8:1
- target operating altitude.....10:1
- target operating state.....20:1
- sensor aspect.....100:1
- target camouflage500:1
- weather10,000:1

Of course the individual values are arguable. And some positions will change. But always and by far, weather will be the dominant influence.

So our customer wants to know, "How much I can offset the effects of changing operating location from the Middle East to North East Asia by increasing detectivity through aperture size and/or detector improvements. How about Middle Europe? How often will I have a detection range of less than 99km? If I double my aperture, how often? How big must my aperture be to achieve 99km at least 80% of the time in the Middle East?; South East Asia?; Middle Europe?"

The DoD modeling and simulation community needs to determine how extant databases and those that are being developed—which are based on surface observations, upper air soundings, and satellite data—are going to satisfy their engineering needs. In order to fully represent the effect of the natural environment in electro-optic and radar simulations, we must develop databases of clouds, basic meteorological parameters, aerosols, and surface weather history that are cross-correlated with one another and merged with models of solar insolation and cloud-free line-of-sight. We can then use these databases/models to create tools for the engineer to use in answering questions like these:

- If I build sensor X, will it be able to detect a Scud over Riyadh in the summer at noon?
- Would sensor X be better than sensor Y for the same scenario?
- If my only flight test data for sensor X is at Edwards AFB against an F-16 in August at 0900, how can I translate these results to a

situation over Bosnia in December at 1300?

- How can I plan, reduce, and compare flight test data to earlier, modeled performance?
- Given the type of clouds that my troops will encounter in North Korea in November at 2 AM, will sensor X or sensor Y find my ground-based target?
- How do I prepare my pilot to use sensor X when he gets into an engagement over Libya at 15 kft in June?
- How can I calculate the effect on the typical detection range performance of this system as I vary the
 - aperture size between 10 cm and 25 cm.
 - operating location between the Middle East and Northeast Asia.

(Note that these questions will arise during requirements definition, concept exploration and definition, demonstration/validation, deployment, and operation. The difference is the fidelity needed in the answer we must deliver, and whether it is based on measured, forecast, or historical met data.)

Then the question for any member of the military met community should be, "Given the data sources that I have, how can I develop tools that can be used by R&D engineers, flight test planners, field commanders, and trainers, to give accurate representation of how a sensor system will work in the real world environment?" It is the job of the meteorological community to translate its extant databases and models into usable tools for the modeling and simulation community.

But this must be a joint responsibility. The met community can not be expected to guess at what the engineering community considers usable forms. (But it cannot simply offer the system engineer a menu of data in forms it has found convenient in the past for supporting farming or flight operations.) On the other hand, the engineers aren't capable of defining what they need because they aren't proficient in weather techniques and jargon.

The authors, one a meteorologist, one a system engineer, have worked together for a number of years. (Many StaffMets have contributed to beating back the boundaries of ignorance in the engineer.) As a result, the questions are becoming better-defined. They have begun to develop a wish list of tools which are expressed in terms both can understand. You will see some of them here.

WEATHER-RELATED INPUTS TO SIMULATION

Our CIDOS-93 paper noted that many inputs to current models are affected by the natural environment, including the atmosphere, the celestial dome, and the underlying terrain. This table is reprinted as Table 1 for

your reference. Note that the effect of these variables is needed anywhere and anytime.

Table 1 Required Inputs to an Aerial Targeting Simulation

Bold items are affected by the environment, needed anywhere and anytime.

- **Sky backgrounds** — how evolved, spectral & edge characteristics, horizon
- **Terrain backgrounds** — temp, BRDFs, DEs, conductivities, permittivities, polarization, spatial/spectral distribution, *etc.*
- **Sea backgrounds** — temp, BRDFs, DEs, conductivities, permittivities, polarization, spatial/spectral distribution, *etc.*
- Hardbody geometry — aircraft, missiles, stores, ships, ground vehicles, buildings, LoCs, airdromes, HVTs
- **Target materials** — BRDFs, DEs, conductivities, permittivities, polarization, abrasion, *etc.*
- **Sensor optical materials** — wavelength-dependent transmissivity, dispersion, abrasion (all w/w/o coatings)
- Sensor stabilization — gimbal & IMU
- **Atmospheric mechanical turbulence**
- **Path obscurants** — wet/dry aerosols, clouds, *etc.*
- **Atmospheric shimmer** — beam wander, wavefront distortion, scintillation
- **Aerodynamic heating**
- **Propulsion** — cycle decks, CFD, hot parts, plumes, contrails, ingestion
- Flyout — range, altitude, attitude vs. time

In an end-to-end model, the effects are seen on the target and background, the intervening atmosphere, and again as effects on the sensor hardware itself. The task is to relate the normally reported atmospheric variables to environmental effects on the scene.

The variables historically reported by the met community are such things as temperature, pressure, relative humidity, cloud cover, visibility, surface weather history, *etc.* We must relate other remotely sensed databases, such as those satellite-derived, to these normally recorded data sets to provide a realistic 4-D picture of a scene. Maybe we will discover a need to measure some parameter not currently measured. We acknowledge the need for improved modeling techniques for linking historical parameters to the needed quantities, and for inferring the parameters we need but cannot measure. Only then will we have accomplished what we set out to do.

The effort must include the cross-correlation of the various parameters with each other and with the accompanying remotely sensed databases. Real 'snapshots' in time of what occurred at a given location lead to variables that are naturally correlated with each other. However, any other type of normal statistical treatment of meteorological data does not necessarily include the cross-correlation of such variables; hence, a realistic result is only accidental, and is unlikely. And,

although a 'snapshot day' gives fully-correlated met parameters, it does not suggest how the day fits on a scale of 'good-typical-bad', or how its influence on systems fits on a scale of 'easy-typical-difficult'.

With today's tools you may need to 'fly' your sensor/weapon system through a database of 10 years or more of real 4-D data to get how it would perform over a long period of time. Better to use a fairly sophisticated computer simulation that does your cross-correlations among the conditions for the various variables, so that you can relate a few experiences now, to any encounter in the future.

For example, consider an 'average day' temperature-wise. Can you assume that the amount of water vapor present on that day is also average? And are the wind direction/speed and inherent air mass aerosol characteristics also 'average' for that day? The chances of having such a day and saying that it would really occur are slim.

To fully define the scene, we need the variables mentioned in Table 2. Many papers are being presented in this forum regarding the development of databases for one or many of the mentioned parameters; however, we have not seen an attempt to do the proper correlations with the other databases or models needed to present a fully coherent, accurate representation of the real-world environment. Some of these databases are attempting to solve the problem by 'getting all the data there is'. Others are looking at regionalizing the data to present 'typical' criteria for life-time store types of questions. Some simulators are also looking at the 'snapshot in time' concept of capturing all of the weather for a specific type of condition for various regions of the world. We suggest that we need to turn our attention to answering the question, 'What do we do next?'

Table 2 Defining the Environment

- Basic Met parameters
 - with cross-correlation parameters for 'good' and 'bad' days
 - statistical significance
 - upper-level moisture
- 3-D to 4-D Clouds
 - convert satellite databases to 'typical' clouds for 'average', 'good', and 'bad' days
 - correlated to basic met database
 - input to first-principles cloud model
- Aerosols
 - boundary layer
 - stratospheric
- Cloud-Free Line-of-Sight Models
- Solar Insolation Databases / Models
- Surface Weather Effects Databases

PROGRESS

Since the last CIDOS meeting, some organizational progress has been made toward the goal of completely defining the environment. We have an organization for real-time simulation efforts, such as the E2DIS community. And there is the semblance of an organized effort at defining what needs defining, as per the E2DIS Survey. Also, the Aerospace Weather executive agent is tasked to find or develop solutions to this very problem in the near future. Many efforts at creating databases have been started.

But military meteorologists are still grappling with what will transform the databases they need into what they will be like when they end up in the hands of the non-weather user. It is the intent of this paper to help 'nudge' our met and engineering communities into a purposeful look at what has been and what is being developed, and how we are going to bridge the huge gap between what we've been doing so far and where we should be

A NEET SOLUTION

Based on the needs of our customers in the DoD R&D and Modeling & Simulation (M&S) Communities, we suggest a 'Natural Environment Engineering Toolkit' be developed by the meteorological community interacting with the end-user. NEETs will 'hold the hand' of the engineer toward using an accurate representation of the environment when making decisions.

One difficulty in devising NEETs is that the end-users will be many and varied, from the engineer doing design work, to the flight test engineer doing Verification & Validation (V&V) work, to the operational commander's planner doing operational engagement simulations, to the new aircrew doing sortie training in his training wing. The end-product of our efforts must be of high enough fidelity to accurately represent how our sensors being developed will respond in actual combat engagements. This implies that the databases must be accurate across the electromagnetic spectrum and even in data denied areas. We have a long way to go. Our success will eventually be measured by the success in battle of our aircrews using sensor-based weapons systems.

After realistically looking at the data and data sources we have now, we need to map a route to getting there: from data to information to NEETs. Since truly accurate 'virtual reality' fidelity is not attainable until our remote sensing abilities come to fruition, what can we do now to help those who needed the data yesterday?

Some suggestions are listed in Table 3. Consider an example of how a NEET and a model might work together: As the result of the application of the NEET by the model, a decision-maker is given model outputs comprising equations which display multi-dimensional curve-fits: hardware parameters on some axes, met influences on others, some axes containing information on how often, some on the 'tudes' (latitude, longitude, altitude), one on seasons, and *etc.*.

Table 3 Natural Environment Engineering Toolkit

- Environment Envelopes
- Environmental Scene Driver
- Test Advisor
- Scenario Transplanter
- Maintenance Monitor

Environment Envelopes NEETs will satisfy a request that StaffMets hear often from design and test engineers: "Give me values that bound the problem, i.e., 'typical', 'good', and 'bad' conditions that I might encounter in Bosnia during the winter." And when a General must decide whether or not to support a new mission, the decision will be better if s/he is supplied with some way to include percent frequency of occurrence statistics for the correlated ensemble of weather influences.

A NEET needed for many applications is an *Environmental Scene Driver* — a scheme which enables mapping of the environment data onto 3-D materials databases. A model designates a 3-D location and the DB says *e.g.*, 'asphalt', or 'dirt', or 'stucco' or 'deciduous', and this response for many points, with the NEET, is used to produce fully-defined, authentic scenes that evolve with the diurnal cycle and weather history. The data for such a NEET would comprise real data, which must be correlated.

Lab, field and flight tests will be cheaper and more productive when a *Test Advisor* NEET is available for test design, results forecasting, and near-real-time comparison of the outputs of the test instrumentation or the Device Under Test with outputs predicted by prior modeling and simulation. Test design requires that models and simulations have access to detailed, correlated climatologies with new NEETs to apply them to support development of a test matrix which explores the envelope with just-adequate redundancy. Field and flight test planning requires new NEETs and models with the proper hooks to employ weather statistics for the test location *vs.* time-of-day/day-of-year, and to ingest on-line forecasts, so testers may compare expected test results in different scenarios of the test matrix and select the smartest next

test scenario. Near Real Time test monitoring and direction requires new NEETs and models with the proper hooks to ingest realtime weather streams so the test team can compare incoming test results with those predicted using models (as above), and those estimated in NRT using on-line weather data.

The *Scenario Transplanter* would give designers and operators an engineering basis to translate an experience in one set of particular test or engagement conditions at one location/geometry/walk-through to that for another place/time. Such comparisons would work well for Cost and Operational Assessments (COEAs), a common request in these days of shrinking budgets.

The *Maintenance Monitor* will give operational field support organizations a way to decide if their systems are working as well as they should. When an aircrew writes up a system for, say, too short a lock-on range, the maintenance organization, with the support of the wing weather officer, can check the performance which it should have delivered, considering the influences of the natural environment. If the only reason it didn't perform well was because weather prevented it, then the aircrew has learned something, and the maintainers have avoided costly replacement and downtime.

THE PAYOFF

The US meteorological community and US military weather service are the best overall in the world. But they are grossly underutilized by the end users. We believe the reasons are the difficulties described above. If we are successful at producing the Natural Environment Engineering Tools that the engineering community needs, the payoff will be weapon systems that perform well and without surprises in the real world. We'll develop them smarter, operate them smarter, and buy them smarter. Ultimately, we will have a better-equipped, more effective, more affordable fighting force. We'll win more easily and at less cost.

ONGOING EFFORTS

There are some ongoing efforts which will incorporate new meteorological tools for supporting engineering decision-making.

AEM*AT (Advanced Electromagnetic Model for Aerial Targeting) is a ten-year program of Wright Lab Avionics Directorate to develop a comprehensive end-to-end model of the aerial targeting situation (target/background signatures, path and environmental influences, sensors/processing), with an

expert system and knowledge-based interface to permit correct, efficient use by topic experts and by non-experts making investment decisions and tradeoffs for design, development, testing, deployment, and intelligence, and to use this modeling architecture as a means to capture and disseminate extant and new knowledge developed for the Government in a *practicable form* to the communities of analysts, avionics and vehicle designers, seeker designers, contract specifiers, buyers, suppliers, old crows, operators, maintainers, strategists, and tacticians. The AEM*AT Program Office knows that the natural environment is one of the strongest influences on the performance of electromagnetic sensor systems, but believes it is not readily available for engineering tradeoffs to the community for which AEM*AT is intended. So an important aim of AEM*AT is to support work in environmental databases and modeling, and tools which put tradeoff capabilities in the hands of decision makers.

IRIAM (Integrated Radar/Infrared Analysis Model) is a 7M\$ DMSO-funded joint USN/USAF/USA/DIA program to develop workstations for the national ranges comprising powerful models with visualization tools to aid in planning tests and analyzing results. AEM*AT is an important part of IRIAM, and will make consideration of natural environmental influences easy for test engineers and their clients.

PLExUS (Phillips Lab Expert-assisted User Software) is a knowledge-based, highly user-oriented software platform that integrates and widens the accessibility of the DoD-standard Phillips Lab family of atmospheric and astronomical background codes. It provides a single Graphical User Interface access for selecting, setting up, running, and analyzing the outputs of all codes.

There are several ongoing efforts which will provide the meteorological community new tools for supporting engineering decision-making. If new software is created, some of these can be used in NEETs.

MEL (Master Environmental Library) is a 6M\$ 2-year DMSO project to produce and demonstrate a prototype of 4-D environmental representations of ocean, atmosphere, and near-space environments.

Climate Spreading Plan is an Air Force Combat Climatology Center (AFCCC, née ETAC) effort with St. Louis University to develop a feasibility demonstration of a scheme—using statistical methods, and considering terrain effects on the local small-scale environment—for spreading mesoscale data from coarse grid points into 5–25 km regions

giving basic parameters in five altitude levels, and yielding a 40GB database for the planet.

PRISM (Oregon State U) is a spreading technique for precipitation and temperature data using summary of the day information.

ExPeRT (Extreme and Percentile Reference Tables) is an effort of Wright Lab / Phillips Lab / AFCCC to produce single-site CD-ROM databases of regional climatologies expressed as durations, percentiles, and risk factors comprising land, ocean, upper-air, and MIL-STD-210C.

GENeSis (Global Environmental Simulations) is an effort by Wright Lab StaffMets to support modeling and simulation by producing CD-ROM regional climatologies and continuous data on a 5 to 25 km grid with 'extra' parameters (e.g., aerosols, sulfur dioxide, ozone, carbon di- and monoxides), and comprising more than mere averages, together with algorithms which correlate parameters.

CONCLUSIONS

For meteorologists, the old way of doing business is no longer adequate because engineers are finally revising their old way of doing business—considering the environment last. They are now realizing it is essential that they consider the influences of the natural environment on their systems during every level of development: concept exploration, requirements definition, demonstration/validation, deployment, operation, and support. But met tools are not available for the engineer to efficiently make decisions.

The authors (a meteorologist and a system engineer) feel obligated to warn engineers that the correct incorporation of weather influences is a very complicated business. We suggest that users be suspicious of schemes we have seen which offer simple operation and unequivocal answers. If it seems too easy, it's likely to be giving you bad advice—but you won't know it. Talk to your StaffMet.

We have described our evolving wish list of tools. We solicit help from others to perfect the questions, and to suggest approaches to the answers. We'd like to begin a dialogue with others who think they know some of the questions, or believe they have some of the answers. Let's begin on ARPAnet, and if that looks fruitful, perhaps follow with a brainstorming session at Wright Lab. Our eMail addresses:

skw111@naic.wpafb.af.mil
lanichwa@aa.wpafb.af.mil

CLOUDSCAPE™: STOCHASTIC CLOUD VISUALIZATION FROM VOLUMETRIC DESCRIPTIONS

John G. DeVore and James H. Thompson
Visidyne, Inc.
Goleta, CA, 93117, USA

Ross J. Thornburg
Visidyne, Inc.
Huntsville, AL, 35801, USA

ABSTRACT

This paper describes CloudScape™, a prototype code for the 2-dimensional visualization of natural clouds from 3-dimensional, volumetric descriptions. CloudScape™ employs simplified, physics-based models of radiative transfer to produce radiometrically realistic simulations at wavelengths in both the visible and infrared. CloudScape™ calculates cloud shadowing and scattering of solar and terrestrial radiation as well as thermal emission. An overview of the modeling, sample images, and a comparison with observations from an AFGL aircraft are presented.

1. INTRODUCTION

CloudScape™ is the product of a Phase I SBIR effort with the Phillips Laboratory¹ to demonstrate a physics-based approach to quantitatively modeling the reflectivity, emissivity, and transmissivity of natural clouds. The archetypal application for CloudScape™ is simulating the natural cloud environment as viewed by sensors involved in DIS (Distributed Interactive Simulation) exercises. Operation in DIS means that the model must fairly represent the effects of clouds as viewed (1) by a variety of sensors, (2) in a range of spectral bands, and (3) from any perspective. Hence the underlying models in CloudScape™ are (1) radiometric, (2) physics-based, and (3) start with the 3-dimensional distribution of liquid water in the atmosphere. CloudScape™ calculates cloud shadowing and scattering of solar radiation, which are important in the visible and short-wave infrared spectral regions during the daytime, and thermal emission and transmissivity, which are important at night and in the mid- to long-wave infrared.

The primary Phase I objective of demonstrating a prototype code for applying a surface radiometric model to a 3-dimensional volumetric cloud description has been met. A robust Mie model for generating scattering patterns for prescribed particle size distributions coupled with the Slab model for calculating bidirectional reflectivity and thermal emissivity were successfully adapted to provide valid characterizations of the radiometric properties of a 3-dimensional distribution of cloud liquid water content. CloudScape™ calculations were found to agree well with data taken by Brian Sandford.

2. MODELING

The Phillips Laboratory has recognized the importance of modeling cloud properties and sponsored the development of the Cloud Scene Simulation Model² (CSSM). The prototype version of CloudScape™ employs a simple 3-dimensional model of cloud liquid water content similar to that of CSSM. Although CloudScape™ starts with a volumetric description, it models clouds radiatively as surface scatterers and emitters. In employing a surface description CloudScape™ is following the lead of CLDSIM³, a version of which is incorporated in the Strategic Scene Generation Model (SSGM)⁴. CLDSIM, one of the few physics-based cloud visualization models, was designed originally for space-based sensors viewing (down) in atmospheric molecular absorption bands.

Cloud radiometrics are governed by scattering, absorption, and the inverse of absorption, emission (Figure 1). What makes the problem challenging is that these processes depend nonlinearly on cloud thickness. The Slab model⁵ was developed for the Defense Nuclear Agency for treating the radiative effects of particulate clouds. Its internal volume emission and scattering formulas are exact to the first scattering interaction; then an approximate build-up factor is used for multiple scattering contributions. The Slab model has been extensively validated with the exact isotropic results of Chandrasekhar⁶, the Monte Carlo results of Kattawar and Plass⁷, and the standard set of six cases presented by Lenoble⁸. Figure 2 depicts the application of the Slab model to a point on a cloud being viewed. The slab is oriented

parallel to the cloud surface at the point being viewed.

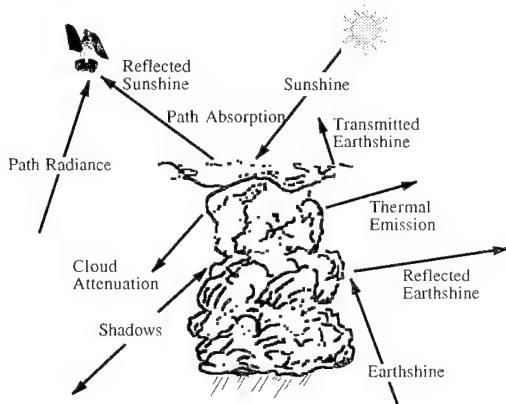


Figure 1. Processes involved in radiometric cloud visualization.

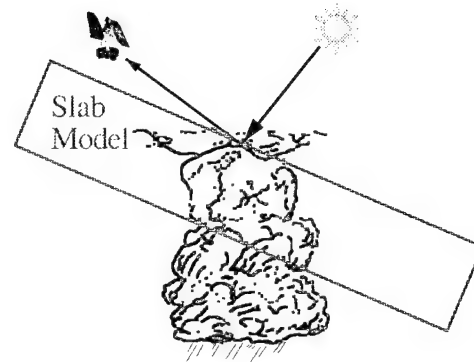


Figure 2. Application of the Slab model of reflectivity, emissivity, and transmissivity.

CloudScape™ is organized to facilitate its incorporation in DIS applications. Figure 3 illustrates an architecture suitable for cloud models operating within DIS applications. CloudScape™ models are prototypes for the Dynamic Cloud Manager and Dynamic Cloud Modeler modules (the shaded boxes).

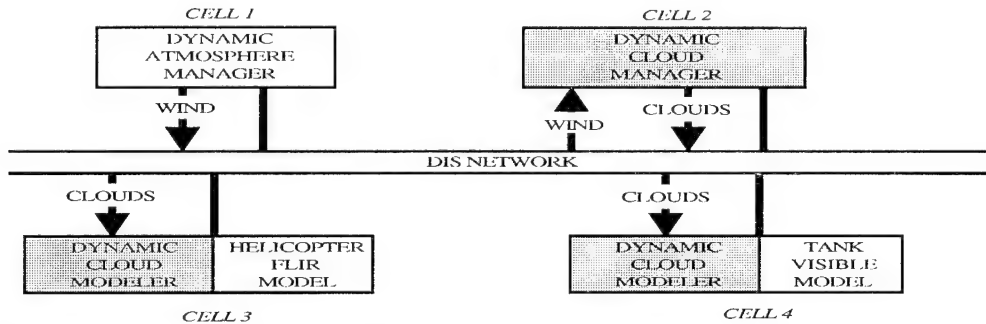


Figure 3. An architecture suitable for cloud models operating within DIS applications.

3. SAMPLE CLOUD IMAGES

CloudScape™ produces images in radiance units ($W/cm^2/sr$). CloudScape™ images are shown below using a subjectively chosen gray-scale, with white corresponding to bright and black to dark regions.

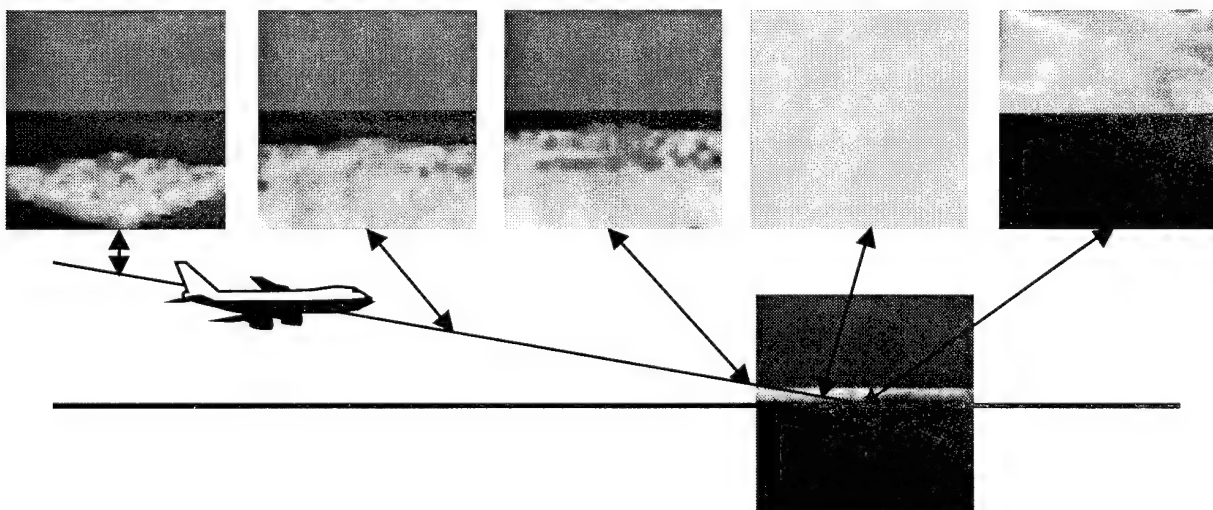


Figure 4. CloudScape™ visualization of flying through a stratocumulus cloud layer.

Figure 4 shows CloudScape™ views in the visible of a stratocumulus cloud deck situated between 0.5 and 2.0 km altitude as seen from an aircraft on a landing approach through the deck. The field of view initially encompasses a region broader than the 32 km by 32 km grid modeling the cloud. The sun is at a 60° elevation angle, e.g., 10:00 am local time, and to the viewer's right. Note the "whiteout" as the viewer enters the cloud and the softer appearance of the cloud deck seen from below.

Figure 5 compares CloudScape™ calculations in the visible (0.38-0.68μm), MWIR window (3.6-3.9μm), and LWIR (9-12μm) bands for two of the frames shown in Figure 4.

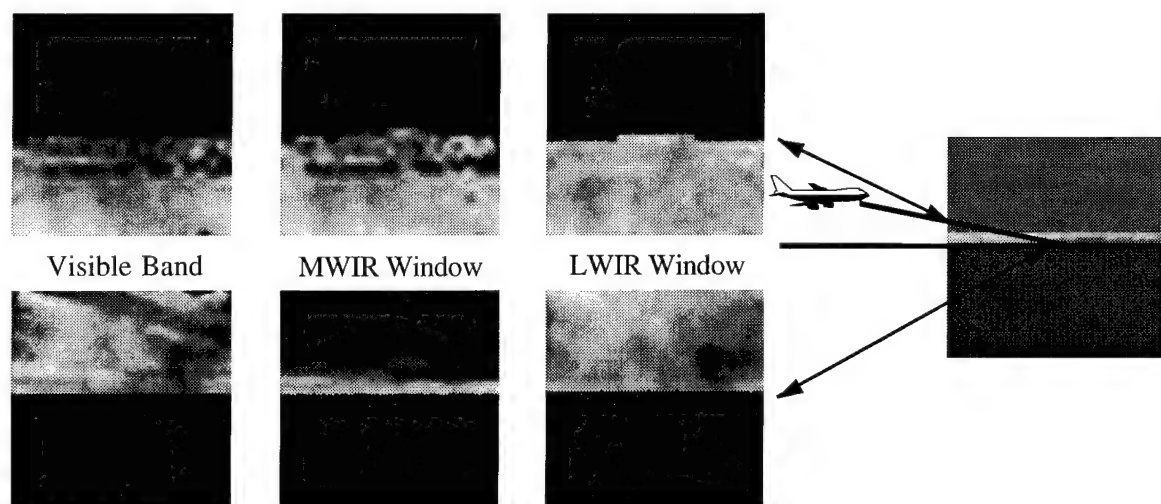


Figure 5. Comparison CloudScape™ calculations in the visible, MWIR window, and LWIR bands.

The texture of cloud images depends upon a variety of parameters, including both macroscopic ones associated with the cloud liquid water distribution as well as microscopic ones associated with the cloud drop size distribution. Figure 6 compares CloudScape™ images of stratus and cumulus clouds as seen from below in the visible.

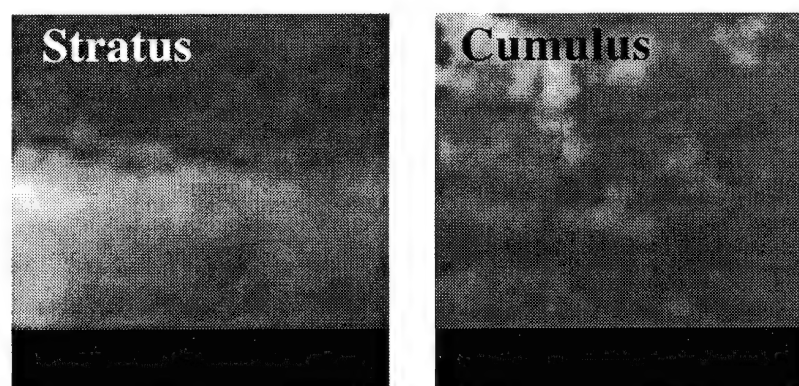


Figure 6. CloudScape™ stratus and cumulus clouds seen from below in the visible.

4. DATA COMPARISON

A number of cloud radiance spectra were obtained by the Air Force Geophysics Laboratory (AFGL) during the course of the Background Measurement Program. Zachor, Holzer, and Smith⁹ reported on case 726/7/FB43 involving an unusually uniform and flat stratus layer off the coast of central California near San Luis Obispo. The AFGL aircraft flew at 6.0 kft viewing the top of the thick stratus layer at 3.0 kft.. The solar elevation angle was 8.88° while the line of sight depression angle was 5.0°. Spectra were reported between 1800 and 3600 cm⁻¹ for four sun-viewer relative azimuths varying from approximately 5° to 185°. CloudScape™ calculations were made in the 3.70-3.85μm band to minimize path absorption effects. The match shown in Table 1 used a mean droplet size parameter of 10 μm, midway between the values of 8 and 16μm used by Zachor, Holzer, and Smith. The good comparison with these data demonstrate the radiometric fidelity achievable with the modeling approach adopted in CloudScape™. However, more such data are required to validate the model fully.

TABLE 1. COMPARISON OF CLOUDSCAPE™ CALCULATIONS WITH AFGL DATA.

Record	Azimuth	Measured	Calculated
	(deg)	(W/cm2/sr)	(W/cm2/sr)
175	94.5	5×10^{-6}	4×10^{-6}
176	175.5	1×10^{-5}	1×10^{-5}
177	95.5	4×10^{-6}	4×10^{-6}
178	5.5	3×10^{-5}	5×10^{-5}

5. UPGRADE PLANS

CloudScape™ is currently a prototype tool. Planned model upgrades include incorporating a more sophisticated liquid water content model, such as CSSM, adopting the PL/GPOS MOSART code for calculating atmospheric path transmission and radiance, and replacing equivalent-volume Mie calculations with tables of scattering intensity versus scattering angle for ice crystals. A major focus of Phase II efforts will be the acceleration of the rendering process by exploiting the specialized graphics capabilities of Silicon Graphics™ workstations. Attention will also be given to using Geophysics Directorate observational data for model verification and validation.

6. ACKNOWLEDGEMENTS

The authors are pleased to acknowledge the kind support and encouragement of Dr. William Blumberg and Dr. Laila Jeong.

7. REFERENCES AND FOOTNOTES

- ¹ The prototype version of CloudScape™ was developed under Phase I SBIR contract F19628-94-C-0071 with the Geophysics Directorate of the U.S. Air Force Phillips Laboratory.
- ² Ciancolo, M. E., and R. G. Rasmussen, 1992, Cloud Scene Simulation Modeling, The Enhanced Model, PL-TR-92-2106, Phillips Laboratory, Hanscom AFB, MA.
- ³ Mertz, F. C., and D. C. Anding, 1990, "Simulation of Background Cloud Images for Sensor System Design and Evaluation", in Proceedings of the Cloud Impacts on DoD Operations and Systems 1990 Conference, Monterey.
- ⁴ Photon Research Associates, 1992, Strategic Scene Generation Model, Release 4.0, Technical Reference Manual, Photon Research Associates, R-068-92.
- ⁵ Thornburg, R. J., J. G. DeVore, and J. H. Thompson, 1993, Review of the CLDSim Cloud Radiance Simulator, VI-2186, Visidyne, Inc., Huntsville, AL.
- ⁶ Chandrasekhar, S., 1960, Radiative Transfer, Dover Publications, Inc., New York, NY.
- ⁷ Kattawar, G., and G. N. Plass, 1968, "Influence of Particle Size Distribution on Reflected and Transmitted Light from Clouds", Applied Optics, **7**, 869-878.
- ⁸ Lenoble, J. (ed), 1985, Radiative Transfer in Scattering and Absorbing Atmospheres: Standard Computational Procedures, A. Deepak Publishing.
- ⁹ Zachor, A. S., J. A. Holzer, and F. G. Smith, 1979, IR Signature Study, AFAL-TR-79-1012, Air Force Avionics Laboratory, Wright-Patterson AFB, OH.

THE CLOUD SCENE SIMULATION MODEL — RECENT ENHANCEMENTS AND ADDITIONS

Maureen E. Cianciolo, Eric O. Schmidt, Mark E. Raffensberger
TASC
Reading, Massachusetts USA 01867

ABSTRACT

Development continues on the Cloud Scene Simulation Model (CSSM) to support high-fidelity environmental simulations. The CSSM is a parametric model which relies on fractal field generation techniques, simple convection dynamics, and climatological distributions to simulate the cloud environment based on user-specified background atmospheric conditions. Output fields contain cloud water density, rain rate, and droplet size distribution parameters that together describe the synthetic cloud and rain field environments. This paper provides an overview of model input, output, and methodology with a focus on recent CSSM enhancements implemented to satisfy the requirements of a growing simulation community. We describe those enhancements as well as improvements to the cumulus physics model, internal model parameters, event processing, and memory management. On-going and future development tasks are also outlined.

1. CSSM OVERVIEW

The CSSM is an empirical model that generates high-resolution, four-dimensional (three spatial and time), multi-layer cloud fields (including cirriform, stratiform, and cumuliform types) consistent with large-scale input weather conditions. It was originally developed to support the Smart Weapons Operability Enhancement (SWOE) Program. Since that time, TASC has continued to develop the CSSM to extend the model's physical realism and utility to support a growing list of modeling and simulation application areas such as personnel training, mission rehearsal, and sensor test and evaluation as required by the Distributed Interactive Simulation (DIS) communities. The CSSM provides a realistic atmospheric background in which to simulate various weather sensitive operations. The newest version of the model supports larger simulation domains, longer simulation periods, more complete specification of the background environment, and emphasis on high-speed processing. These growing requirements have led to several significant changes to the model (e.g., a movable domain origin, gridded input fields, initialization with numerical model output, conversion to an ANSI C language environment, and the addition of particle size distribution and rain models).

1.1 Methodology

The CSSM simulates realistic structure (typical resolutions of 10-100 meters) within a domain defined by general meteorological characteristics (Figure 1). One field is generated for each specified output time and contains cloud water density values, particle size distribution parameters, and rain rates arranged on a regular volumetric grid.

The model uses a fractal algorithm to specify the horizontal distribution of cloud elements across the user-specified model domain, where algorithm parameters are tuned to fit observed cloud data. Preliminary comparisons with observed data have shown that the model captures the characteristically complex internal and external structure of cloud fields found in nature. Additional validation is currently underway. The vertical growth of the clouds is modeled using convection physics and knowledge of atmospheric structure. Recent enhancements to the model physics include location-dependent entrainment rates, orographic cloud types, and heat-dependent parcel sizes used in the convection model. In addition, we have modified the CSSM to work on a box-by-box geometry. That is, the CSSM creates clouds consistent with each individual cloud input gridpoint (box) and ensures continuity between each box. This more efficient use of computer memory allows the user to simulate larger regions and longer time periods, such as those required in the upcoming Synthetic Theater of War (STOW) exercises. One of the most significant changes to the CSSM is the addition of models that further describe the atmospheric environment: a rain model and a model of the particle microphysics (i.e., size distribution parameters) within the cloud field. The microphysics model provides information critical for wavelength-dependent visualization and analysis.

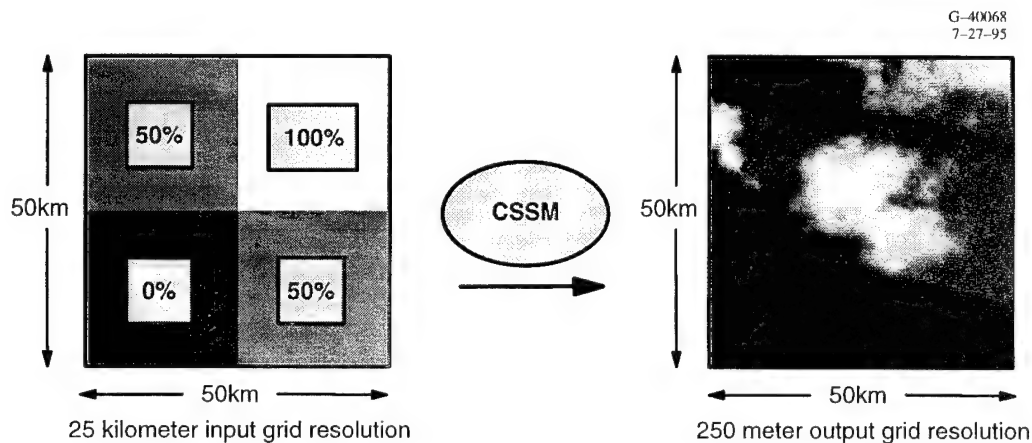


Figure 1 CSSM Methodology. High-resolution Cloud Scenes are Generated Consistent with Coarse-resolution Inputs. Here a 250 Meter Resolution Stratus Layer is Generated from a 25 Kilometer Resolution Cloud Analysis Field.

1.2 Input Variables

The CSSM is initialized with three primary categories of data specified either on a grid or as a single measurement valid across the domain (other general simulation parameters required as input are outlined in Table 1):

- atmospheric state variables (temperature, dewpoint temperature, u and v wind components)
- terrain elevation and type (ocean, land, coast, etc.)
- cloud features by layer (amount, type, base and top heights).

Table 1 General CSSM input parameters

Atmospheric state variables:	Temperature Dewpoint temperature u and v wind components Z geometric height of pressure levels
Cloud variables (by layer):	Amount Base and top heights Type
Terrain variables:	Elevation Type (not currently used)
Domain parameters:	Origin Resolution Extent
Miscellaneous parameters:	Number seed Root name of output file Output variable toggles (water content, rain rates, size distribution parameters)

The CSSM is initialized with these data at a relatively coarse resolution. It then creates a higher-resolution cloud scene consistent with these inputs. Atmospheric state variables are sampled from a numerical weather prediction (NWP) model, analysis model, or observed atmospheric profile (typical resolution of 20–50 km). The current version of the CSSM accepts output fields from the Navy's Operational Regional Atmospheric Prediction System (NORAPS) or single values from a sounding or similar source. Future versions of the CSSM will accept COAMPS, MM5, or other NWP model output. Cloud features are estimated from observations, satellite imagery, or NWP output fields. Future development efforts will add the capability to initialize the CSSM with cloud layers estimated from satellite-based cloud analysis algorithms (such as those under development in the SERCAA program).

1.3 Output Fields

CSSM output fields are specified on a regular Cartesian volumetric grid. Output fields consist of one or more of the following components as selected by the user:

- liquid/ice water content
- rain rate
- particle size distribution.

A recent enhancement to the CSSM allows the location of the output grid to vary over time. This results in greater efficiency for those simulations in which the area of interest moves (e.g., an aircraft moving across the larger simulation domain). Continuity is conserved in the model to ensure that identical cloud formations are produced for mobile and static users. The output fields listed above can be rendered or analyzed using a variety of commercial graphics tools or specialty simulators. Methods to translate the CSSM physical variables to wavelength-dependent scenes are currently under development.

2. CURRENT STATUS

As of the writing of this paper, final extensions to the CSSM are under development. The model will be available to members of the DoD community in early or mid 1996. The model is written in ANSI C and will be tested on a variety of common workstations in a UNIX environment. Figure 2 shows a sample output scene generated with the previously-released SWOE version of the CSSM for reference. The scene was rendered by combining the CSSM output water content grid with terrain imagery of the Sarajevo area built from Landsat and Digital Terrain Elevation Database.

3. ACKNOWLEDGMENTS

Sponsorship for model development is provided by the U.S. Air Force Phillips Laboratory, the U.S. Army Topographic Engineering Center, and the Defense Modeling and Simulation Office as one part of the Dynamic Environment and Terrain in Distributed Interactive Simulation (DETDIS) Program.

4. REFERENCES

1. Cianciolo, M. E., and R. G. Rasmussen, Cloud Scene Simulation Modeling — The Enhanced Model, Technical Report, PL-TR-92-2106, April 1992.
2. Saupe, D., Point Evaluation of Multi-Variable Random Fractals, *Visualisierung in Mathematik and Naturwissenschaft*, H. Jurgens and D. Saupe, Eds., Springer-Verlag, Heidelberg, 1989.

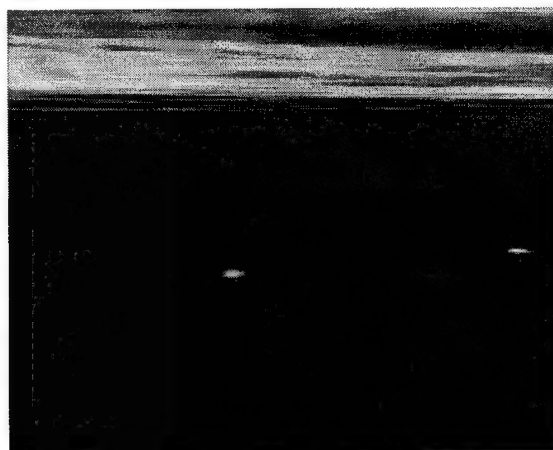


Figure 2 A Sample Cirrus Output Scene Generated with the SWOE Version of the CSSM

INCORPORATION OF A CLOUD SIMULATION INTO POWERSCENE

Louis Hembree and Sam Brand
Naval Research Lab
Monterey, CA 93943

Mark DeLoura
Loral Inc.
Bellevue, WA 98005

Tom Hickey, Scott Randall, and Chip Mayse
Cambridge Research Inc.
McLean, VA 22102

Maureen Cianciolo and Eric Schmidt
TASC
Reading, MA 01867

ABSTRACT

Current aircraft mission rehearsal systems operate with no environmental information. One environmental parameter that has a large impact on aircraft missions is cloud cover. This paper describes an initial attempt to incorporate clouds into a mission rehearsal system that runs in real time. A cloud scene simulation model (CSSM) has been developed by TASC and was reported on in previous CIDOS meetings. Loral developed C++ application program interfaces (APIs) for the CSSM and visualization tools. These were incorporated into PowerScene by Cambridge Research. PowerScene incorporates off-the-shelf hardware to provide photo realism to a wide range of applications including mission planning, preview, rehearsal, debrief, and training. It can use standard or helmet mounted display technology. This allows the user to train in both clear and cloudy conditions and evaluate the impact of clouds on the mission.

1. INTRODUCTION

The role of Modeling and Simulation (M&S) in tactical aircraft training, mission rehearsal, and mission planning is increasing. There are several reasons for this. A pilot cannot fly over the target and study it at his leisure to familiarize himself with the target to pick the best approach and egress routes. With a mission rehearsal simulation the pilot can "fly" simulated missions and examine various options. To date most M&S systems do not include any environmental information or impacts. In actual missions the environment can play a critical role in the success or failure of the mission. Clouds can obscure the target; fog and smoke can decrease visibility. Detection and lock on ranges can be decreased significantly. The objective of this effort is to incorporate simulation of realistic clouds into a mission rehearsal system. Figure 1 illustrates the concept. The CSSM was developed by TASC. Loral developed an interface, and Cambridge Research is integrating the cloud model into PowerScene.

2. CLOUD SCENE SIMULATION MODEL

The Cloud Scene Simulation Model (CSSM) was developed by TASC under the sponsorship of the Air Force Phillips Laboratory and ARPA. CSSM uses stochastic field generation techniques and knowledge of atmospheric structure and physics to model four-dimensional (three spatial, and one temporal) cloud scenes. It can simulate up to four cloud layers. The environmental conditions are provided by the user. Environmental information required includes cloud type, cloud fraction, cloud thickness and an atmospheric sounding. The domain size and resolution must also be provided.

The model simulates the internal water density perturbation field which is then converted to absolute liquid water contents (LWC). The conversion is performed using computed field statistics and a mean LWC profile. The LWC fields are then used by the visualization routines to produce cloud representation for use in simulations.

3. INTERFACE AND VISUALIZATION

Loral developed a generalized interface and visualization tools for CSSM with sponsorship from ARPA and the Navy's Naval Research Laboratory. The interface allows the simulation system to specify the environmental parameters, the domain and resolution, and the frequency of the update fields. The visualization approach used by Loral uses a simple geometric primitive aggregation. That is, angle-oriented textured polygons are aggregated to produce the cloud scene. This approach uses a disk that is oriented perpendicular to the viewer's line of sight, and is textured with a spherical texture pattern. The texture pattern makes the disk appear more spherical or realistic and gives some subtle shading and depth to the cloud.

4. INTEGRATION INTO POWERSCENE

PowerScene is a mission rehearsal system developed at Cambridge Research with sponsorship from the Naval Air Systems Command (NAVAIR). PowerScene provides complex free-play flight in seamless country-sized databases. It allows the users to rehearse their missions and become familiar with the mission areas. It creates high fidelity, geo-specific perspective scenes from raw DTED data and image data from a variety of sources. Image resolution varies from as low as 10 meters for terrain to better than 1 meter for targets. NAVAIR has recognized the need for environmental information and some users have stated that clouds and smoke would provide a more realistic and useful mission rehearsal system.

With sponsorship from the Naval Research Laboratory Marine Meteorology Division, Cambridge Research is integrating the CSSM and Loral interface into PowerScene. To integrate the software into PowerScene, several additional steps have to be taken. The initial software runs in real time mode, while PowerScene uses display lists. Therefore the programs had to be converted. The high level of detail (LOD) is needed when the pilot is near the clouds. However the full detail level is not needed when the pilot is far from the clouds. An approach to control the LOD is also being developed. In addition, a method is being developed to filter out cloud elements that are hidden from view by other clouds or other obstacles. This would include cloud elements on the far side of a cloud that are not seen because of the intervening cloud elements. Without control of the LOD and filtering of hidden cloud elements, the number of polygons needed to render the clouds would be so large that the simulation would be slowed significantly and real-time fly through would not be possible.

5. SUMMARY

The integration of the CSSM into PowerScene marks the first time that the integration of realistic cloud simulations into a mission planning system has been attempted. This will provide PowerScene with the capability to incorporate realistic clouds into mission rehearsal, thereby allowing the impact of clouds on the mission. This was made possible by leveraging the work of previous unrelated projects from other sponsors and the cooperation of the PowerScene sponsor. The integration is still on going.

6. REFERENCES

- Soderberg, B., and M. DeLoura, 1996: "Adding Cloud Visualization to a Real-Time Simulator," Loral Final Report, Contract DACA76-91-C-0006, May, 1995.
- Cianciolo, M. and B. Soderberg: "Modeling the Cloud Environment in Distributed Interactive Simulations," 16th Interservice/Industry Training Systems and Education Conference, Nov. 1994.

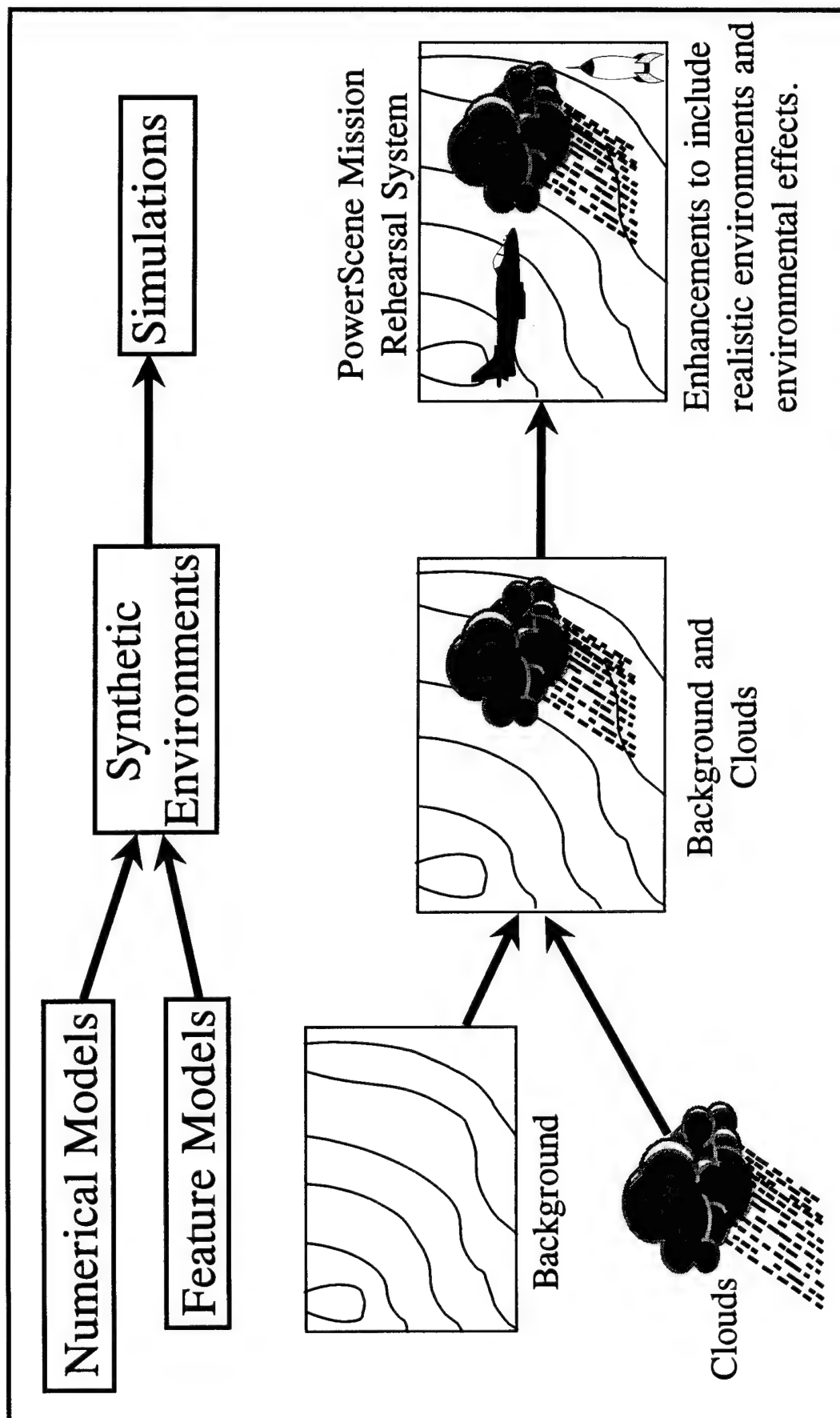


Figure 1: Illustration of using feature models in conjunction with model outputs to create synthetic environments for use in simulation systems.

CLOUD DEPICTION AND FORECAST SYSTEM (CDFS) II UPDATE

Maj. John D. Murphy
Maj. Don K. Rhudy
Maj. David J. Zdenek
HQ Air Weather Service
Scott AFB, IL 62225

2Lt Jeff A. Baltes
Anna L. Lathrop
Capt. Frank A. Leute IV
Air Force Global Weather Central
Offutt AFB, NE 68113

Kevin J. Lunn
Michael J. Plonski
Bruce H. Thomas
The Aerospace Corporation
El Segundo, CA 90245

ABSTRACT

The Air Force's Air Weather Service (AWS) is procuring a new cloud analysis and forecast system, Cloud Depiction and Forecast System (CDFS) II, to be installed at its weather central, Air Force Global Weather Central (AFGWC). CDFS II is expected to be fully operational, supporting worldwide military and national users, in 2001, with development starting this year. The CDFS II will enhance the functionality currently provided by CDFS I, and will provide a centralized database. CDFS II will include a multi-source, multispectral database of weather satellite data, a new three dimensional cloud analysis model, and a worldwide cloud forecast model. The CDFS II system will also include a comprehensive development environment to maintain and enhance the meteorological models well into the next century. Software modifications will allow current resident applications to run on the new hardware and use the new central database. This paper will present an overview of the CDFS II system.

1. BACKGROUND

The current AFGWC CDFS I is comprised of three mainframe computers (a suite of Unisys 1100/91 series computers) with associated software which processes polar orbiter weather satellite data, merges satellite and surface weather data into three-dimensional cloud analyses and cloud forecasts, and supports classified operations. The three mainframes consist of a satellite processor (System 5), classified applications processor (System 3), and a developmental (as well as backup) mainframe processor (System 6). The satellite processor was originally sized to process two polar orbiting satellites (primarily DMSP), a Real Time NEPHanalysis (RTNEPH) model^{1&2} and a long range cloud forecast model. Requirements have placed increasing demands on the satellite processor which have added processing loads causing the mainframe to become saturated. Enhancements to the cloud analysis and forecast models (computationally expensive algorithm enhancements and/or additional data sources) have not been possible due to the processor's saturation.

Processing and storage limitations on the older mainframes prohibit using the satellite data at its full resolution. System 5 stores the satellite data, both visual and infrared (IR), in a Satellite Global Data Base (SGDB). The SGDB contains only two channels of DMSP and limited NOAA AVHRR (2 channels) data and thus multispectral techniques are limited within the RTNEPH. Data in the SGDB is re-mapped from 1.5 NM raw resolution to a 3 NM polar stereographic grid (true at 60 degrees latitude)^{3&4}. Additional satellite data degradation occurs due to the data being stored in 6 bits limiting the IR data to a 1.9 degree Kelvin thermal sensitivity. The limiting thermal resolution of the IR data limits cloud detection in the RTNEPH's IR thresholding cloud detection scheme^{1&2}.

The SGDB is used as an input to the RTNEPH and has additional data age problems when the RTNEPH is run on a worldwide spatial domain. The RTNEPH processes data in two ways: 1) It produces cloud analyses over the regions that are covered by polar orbiting data as it arrives at AFGWC. 2) Every three hours it produces worldwide cloud analyses from the most recent data in the AFGWC databases. The satellite data in hemispheric databases is asynoptic (data over the world not valid at the same time). This causes difficulties in using worldwide cloud analyses as inputs to worldwide cloud forecast models.

2. CDFS II ENHANCEMENTS

2.1 SATELLITE INGEST PROCESSING AND STORAGE

CDFS II will acquire and ingest satellite data, at full spatial and bit resolution, from up to 5 polar orbiting satellites (DMSP and NOAA TIROS) and 5 geostationary satellites (GOES IJK/LM GMS, METEOSAT, 1 future GEO) simultaneously. Processing the satellite data includes calibration, geolocation, and storing the data in the centralized database at scan line (satellite) resolution.

2.2 HOURLY WORLDWIDE CLOUD ANALYSIS

The RTNEPH will be replaced by a worldwide cloud analysis model (CDFS II - NEPH) combining portions of the Support of Environmental Requirements for Cloud Analysis and Archive (SERCAA) model⁵, developed at Phillips Lab, and the RTNEPH. The CDFS II - NEPH will produce hourly worldwide cloud analyses and forecasts on a 25 NM polar stereographic grid (true at 60° latitude) for each hemisphere. It will produce cloud analyses for individual satellites and merge them together, along with conventional observations, into a worldwide cloud analysis. The CDFS II - NEPH will process each satellite channel based on its native resolution, eliminating the current system shortfalls. This requires a tremendous increase in processing power and throughput in order to support the near real time needs of operational customers.

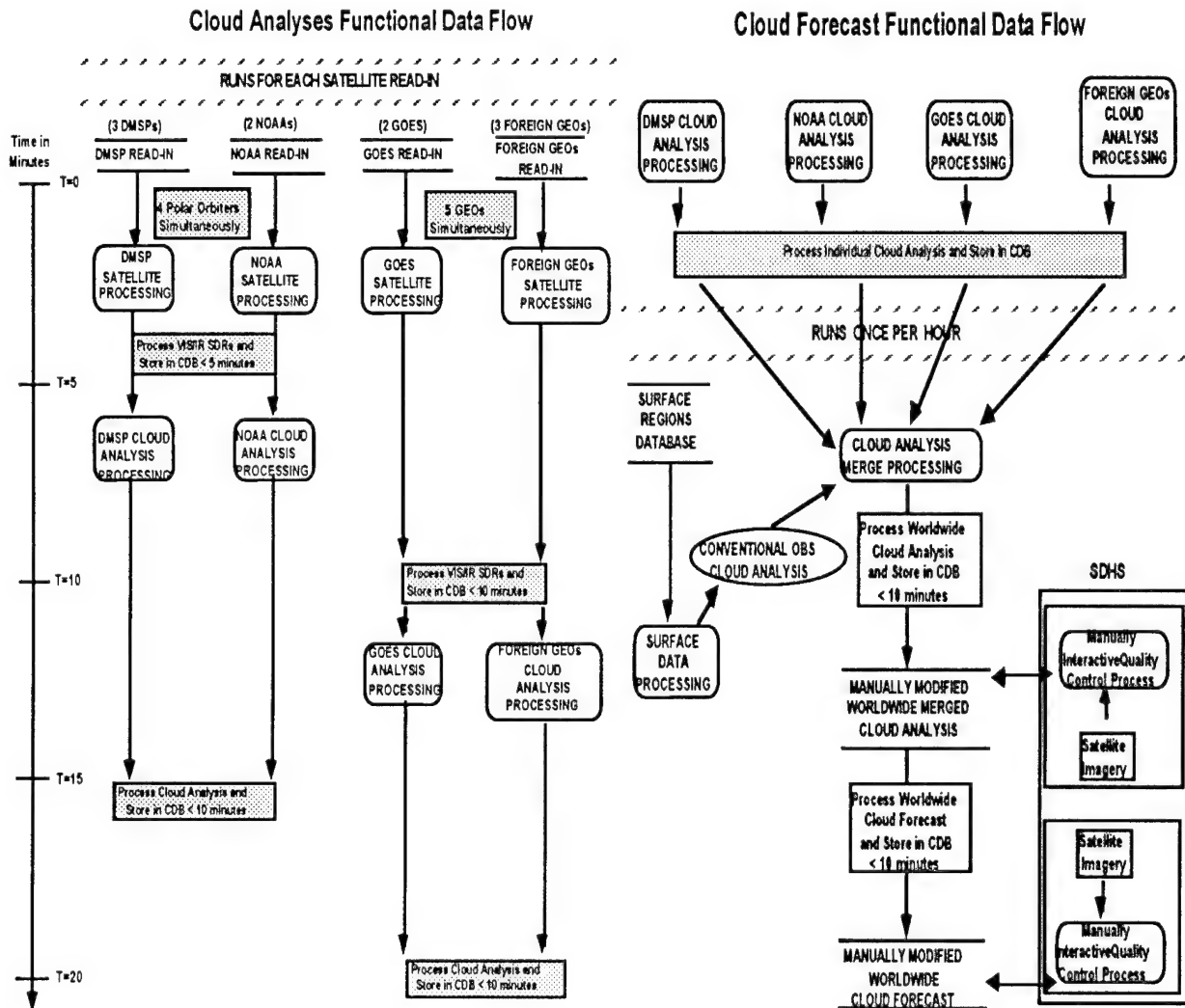


Figure 1. Cloud Analysis/Forecast Functional Data Flow

2.3 HOURLY WORLDWIDE CLOUD FORECASTS

CDFS II will operationally implement a worldwide cloud forecast model that replaces the current cloud forecast models: High Resolution Cloud Prognosis (HRCP⁶), the long-range cloud forecast model called 5LAYER⁷, and the tropical persistence cloud forecast model known as TRONEW⁷. This model will have worldwide coverage by increasing the spatial domain of the short-range cloud forecast model (HRCP). The model will be run hourly to produce short-range forecasts out to 12 hours, in hourly increments from the base time of the worldwide merged cloud analysis, and be output on a 12.5 NM polar stereographic grid. The model will also run every six hours to produce long-range forecasts from 15 to 48 hours in three hourly increments from the base time of the worldwide merged cloud analysis, and be output on a

50 NM polar stereographic grid. Figure 1 depicts the data flow for the cloud analysis and forecast models.

2.4 CENTRALIZED DATABASE

AFGWC is converting from a "flat file" data management system (DATMAN) where redundant copies of data files (packed 36 bit words) exist on each mainframe, to a new commercial centralized database management system. CDFS II will create one logical Central Database (CDB) providing a shared database resource for all computing platforms within AFGWC. The CDB shall contain all meteorological data currently stored in the existing CDB and the additional CDFS II created items. It will provide for the monitoring, insertion, retrieval and temporal management of selected satellite sensors, graphic, text and numeric data within the CDFS II system. It will support combined input/output data access throughput of at least 33 Gigabytes (GB)/hour from CDFS II production processors and existing systems. Additionally the CDB will support at least 100 simultaneous users, and be capable of storing 200 GB, exclusive of redundant storage required to meet fault tolerance.

2.5 CDFS II Computer System.

CDFS II will replace the existing UNISYS mainframes, connected by a Hyperchannel backbone and custom communications protocols, with a network of DEC Alpha workstations and servers connected by Fiber Distributed Data Interface (FDDI) backbones and Transmission Control Protocol/Internet Protocol (TCP/IP) communications protocols. CDFS II is one of the programs helping AFGWC migrate from a proprietary computer network to an open systems environment. CDFS II will also install a test database and network of development workstations, that are fully integrated with the production environment, to allow meteorologists and programmers to enhance and maintain the meteorological models. The computing environment is being designed with expandability as a key requirement of the system.

3. CONCLUSION

Through the CDFS II program, AFGWC will eliminate known cloud analysis and forecast system weaknesses. The new system will exploit multi-source and multispectral satellite data at full satellite resolution with more accurate processing algorithms every hour. The improved cloud analysis techniques will improve the initial conditions for the cloud forecast models. The expandability of the hardware in CDFS II will allow for future enhancements after delivery of the initial system.

4. REFERENCES

1. Kiess, R.B. and W.M. Cox., 1988: The AFGWC Realtime Cloud Analysis Model. AFGWC Tech. Note AFGWC/TN-88/001, Air Force Global Weather Central, Offutt AFB, 82 pp.
2. Hamill, T.M., R.P. d'Entremont, and J.T. Bunting, 1992: A description of the Air Force real-time nephanalysis model, Wea. Forecasting, 7, 288-306
3. Callahan, K.P., R.B. Kiess, J.M. Lanicci, and T.J. Neu, 1993: Cloud Analysis and Forecasting at Air Force Global Weather Central Under the Cloud Depiction and Forecasting System II: Proceedings of the Cloud Impacts on DOD Operations and Systems 1993 Conference (CIDOS-93)
4. Hoke, J.E., J.L. Hayes, and L.G. Renniger, 1981: Map Projections and Grid Systems for Meteorological Applications, AFGWC Tech. Note AFGWC/TN-79/003, Air Force Global Weather Central, Offutt AFB, 86 pp.
5. Gustafson, G.B., et al, 1994: Support of Environmental Requirements for Cloud Analysis and Archive (SERCAA): Algorithm Descriptions. Phillips Laboratory Tech. Report, PL-TR-94-2114, Directorate of Geophysics, Air Force Materiel Command, Hanscom AFB, 100 pp.
6. Kiess, R.B., K.P. Callahan, and J.M. Lanicci, 1993: The Air Force Global Weather Central's Short Range Cloud Forecast Model: Preprints of the 5th Conference of Aviation Weather Systems, Vienna, VA, AMS, 290-294.
7. Crum, T.D., 1987: AFGWC Cloud Forecast Models. AFGWC Tech. Note AFGWC/TN-87/001, Air Force Global Weather Central, Offutt AFB, Nebraska, 66 pp.

SBIRS CLOUD MEASUREMENTS, ANALYSIS AND MODEL VALIDATION

Captain Michael Pierce
SMC/MTAX
Los Angeles Air Force Base, California

William Blumberg
The Phillips Laboratory, PL/GPOS
Hanscom Air Force Base, Massachusetts

Ian S. Robinson
The Aerospace Corporation
Los Angeles, California

The Space-Based Infrared Systems (SBIRS) Program office is supporting a number of cloud measurements and analysis efforts to quantify the impact of clouds as a clutter source and as obscurants.

The cloud related efforts have two primary goals. The first goal is to assess the spatial variability of background radiance in spectral bands between 2 and 5 microns at geometries of relevance to the SBIRS constellation. Clouds are assumed to be important contributors to the overall background radiance structure, particularly in spectral bands that do not penetrate to the ground. Measurements will be made by the IR imaging spectrometer/radiometer aboard the Airborne Remote Earth Sensing Program's WB-57, the dual IR focal planes aboard the MSTI-III satellite, and with the SPIRIT-III radiometer/interferometer to be flown on the Mid-Course Space Experiment (MSX).

It is recognized that cloud models complement measurements by providing the capability to synthesize conditions that have not specifically been measured. The SBIRS program is supporting the validation of cloud scene generation models. The validation effort requires the collection of cloud "truth" data. The primary source of cloud "truth" data will be combined measurements by ground-based lidars at the University of Wisconsin. SBIRS is exploring the use of alternate sources of "truth" data as well.

The second goal is to determine the frequency of occurrence of clouds at altitude. Optical depth or opacity information is also of interest. The impact of clouds on a high reliability surveillance system is dependent on how frequently severe clutter and obscuration occur. Cloud altitude is an important factor in assessing the magnitude of clutter and determines the volume of space blocked by an (obscuring) cloud.

This paper will describe the plans to accomplish the stated goals, identify the participants, and summarize results to date.

Manuscript not available at time of printing. Please contact author for information.

SIMULATED CLOUDSCAPES WITH FASTVIEW

Albert R. Boehm
Hughes STX Corporation
Lexington, Massachusetts 02173

ABSTRACT

FASTVIEW is a scene generator for the FASTPROP line-of-sight propagation simulator being developed by the US Army and Strategic Defense Command for implementation in the Extended Air Defense Simulator (EADSIM). FASTVIEW is designed to give consistent ultra-fast propagation calculations from any angle or altitude. Basic cloud structure is given by HEFeS (Hierarchical Environmental Feature Structure) which uses a series of stages to specify clouds at various scales. The location of intricate detail is done by Stochastic Indexing which uses the repeatability of random number generators to store information. Propagation and rendering are quickly done using the Morficon set of algorithms which use morphed icons to allow for various viewing angles.

1. SIMULATION GOAL

The FASTVIEW goal is to provide ultra-fast propagation algorithms for simulation and in particular for inclusion in the EADSIM (Extended Air Defense Simulator) simulation. FASTVIEW will provide cloud scenes in the IR, millimeter, and visual.

2. BASIC PRESUMPTIONS

These facts and premises are simply stated here. Justification is found in Boehm (1994), Boehm (1995), and LaMar et al. (1995).

1. The purpose of a constructive simulation is to quantify the effectiveness of a system in operational usage. In an operational simulation, numerous calculations of propagation are required. The large number is due to moving targets and sensors and to the number of sensors and targets. Contrast this with a sensor simulation which can sometimes use a single simulation to see if it works or not.

2. The atmosphere does have layers that are effectively uniform with respect to transmission, but there are other layers, particularly those with clouds, that have intricate detail. It is the intricate detail that is hardest to specify and often has the strongest effect on propagation.

3. Current physical fluid dynamic methods are unable to specify intricate details in the atmosphere. This is not due to lack of computer power nor observations of initial or boundary conditions. It is due to lack of proper physical principles with respect to the stress tensor, water droplet/crystal/vapor transformation, and radiation flux in clouds.

4. Current archived observations fall far short of specifying intricate detail in the atmosphere.

5. Current methods of calculating propagation are much too slow for operational simulation. MODTRAN running on a high end work station would take several days to calculate the radiances in a single picture.

6. A propagation beam is affected by structure of many scales - from a single droplet on a sensor lens to a complete cloud field when viewed from hundreds of kilometers away.

7. There are numerous statistical and stochastic models of the atmosphere that have been validated for specific purposes. These range from simple rain/no rain Markov chains to complex four dimensional non-homogeneous anisotropic global models such as CFARC which produce minute by minute results for decades.

8. Clouds and associated rain contribute the most to the variability of propagation yet are poorly measured. Standard observations give only fractional cover and type; no information is recorded on orientation, shape of gaps, or physical properties. Cloud types are based on visual appearance. The liquid water per cubic meter can vary over an order of magnitude within the same cloud type.

3. FASTVIEW DESIGN

In order to overcome these deficiencies, three methodologies have been developed: HEFeS (Hierarchical Environmental Feature Structure), stochastic indexing, and the Morficon. Together HEFeS, stochastic indexing, and the Morficon form a weather expander. This weather expander takes a small set of input and using stochastic generators produces a complete weather scenario. A cloud scene with varying instability is shown in figure 1.

4. HEFeS

HEFeS (Hierarchical Environmental Feature Structure) provides a statistical and stochastic description of the atmosphere at all scales of interest. HEFeS is extensive, that is, the number of object scales and the number of objects in each scale can vary depending on the simulation requirement.

HEFeS consists of a statistical description of weather objects and the statistics of interaction between them. The description consists of statistical distributions of size, shape, location and physical characteristics such as temperature, wind, etc. The statistics of interaction consists of conditional probabilities which allow a consistent selection of objects in a instantiation.

5. STOCHASTIC INDEXING

Stochastic indexing uses the repeatability of random number generator sequences to quickly select the same object if viewed from different angles or if the instantiation must be repeated. Stochastic indexing effectively stores a myriad of detail in zero storage.

6. THE MORFICON

The Morficon is a computer method of storing propagation data so that transmission along a line-of-sight or a image can be rapidly generated. Each Morficon object has propagation parameters that are precalculated and stored as part of the Morficon. A Morficon object can be a layer, a cloud, a cloud puff, etc. Thus, a specific view can be generated very rapidly. The essence of the Morficon algorithm can be inferred from the two formulas in figure 2.

REFERENCES

- Boehm, A., 1994: Visual Translucent Algorithm (VISTA), *Simulation*, 62, No. 2, 91-97.
- Boehm, A., 1995: Objective Analysis Using A Hierarchy of Climate Features, Preprint Sixth International Statistical Climatology Meeting, University of Galway, Ireland.
- LaMar, C., Boehm, A., Gebhart, W., and Cook, W., 1995: Implementing Realistic Weather Effects On Line-Of-Sight Propagations For Constructive Simulations, 12th Workshop on Standards for the Interoperability of Distributed Simulations, Institute for Simulation & Training, Orlando, FL.

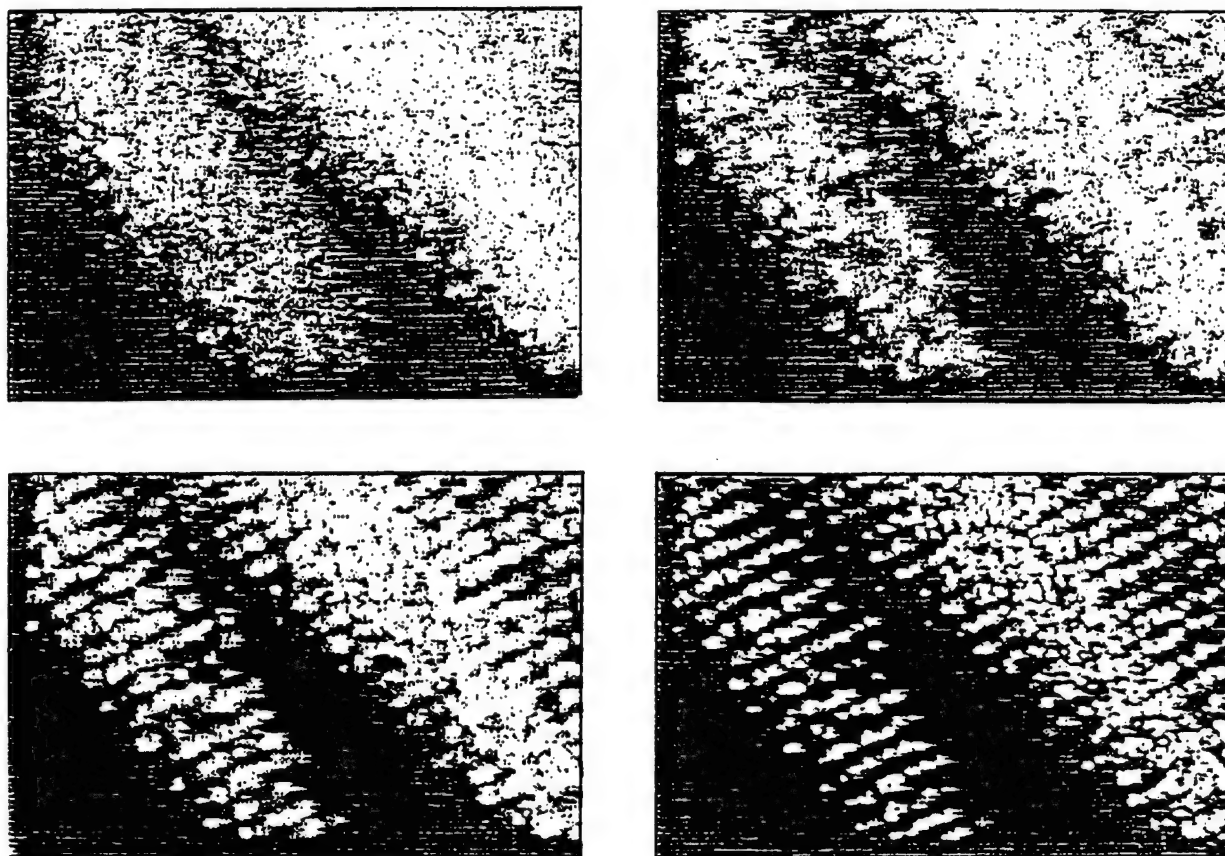


Figure 1 HEFeS produced clouds with varying instability.

MORFICON TRANSMISSION

$$I_s = I_t e^{\int_s K dx}$$

I_s is illumination at sensor s
 I_t is illumination at target t
 K is absorption coefficient
 x is along line of sight

For n homogenous or linear gradient objects

$$I_s = I_t e^{\sum_{i=1}^n K_i \Delta x_i} \quad \text{or} \quad \ln(I_s) = \ln(I_t) + \sum_{i=1}^n K_i \Delta x_i$$

Δx is distance along line of sight through object
 K_i is $(K_{\text{enter}} + K_{\text{exit}})/2$ for linear gradient object

Figure 2 Transmission at single wavelength shown in general in top equation and with Morficon objects in bottom equation. If objects accurately portray structure than calculation is exact.

ACKNOWLEDGMENTS: This work is supported by Geophysics Directorate of Phillips Lab. with Mr. Donald Grantham as contract monitor for contract No. F19628-93-C-0051 and The US Army Space and Strategic Defense Command with Mr. Chuck LaMar as project leader.

RADIATIVE TRANSFER IN SCENARIOS WITH MULTIPLE CLOUDS

Patti Gillespie, Alan Wetmore and David Tofsted
U.S. Army Research Laboratory
Battlefield Environment Directorate
White Sands Missile Range, New Mexico

The Battlefield Environment Directorate has been developing a suite of models, Weather and Atmospheric Effects for Simulation (WAVES). One of these models is an atmospheric radiative transfer code, Boundary Layer Illumination and Radiative Balance, BLIRB, is to be used in calculating radiance and illumination in inhomogeneous, partly-cloudy sky conditions. The model, BLIRB, has recently been compared with Monte-Carlo calculations for several different cloud configurations as part of the validation of the WAVES suite. The agreement of these comparisons indicate that the BLIRB model handles the radiative transfer calculations within the atmosphere well, including calculations for multiple cloud conditions. A description of the BLIRB code, the testing scenarios used, and results of the comparisons will be presented.

Manuscript not available at time of printing. Please contact author for information.

REALISTIC CLOUD RENDERING USING AN AUTO-REGRESSIVE MOVING AVERAGE (ARMA) MODEL

Robert A. Pilgrim
Computer Science and Information Systems Department
Murray State University
Murray, Kentucky

Andy Bevilacqua
Bevilacqua Research Corporation
Huntsville, Alabama

ABSTRACT

This paper describes a technique for realistic rendering of clouds and other environmental effects in rear real-time based on an auto-regressive moving average (ARMA) technique. This algorithm creates complexity using a combination of fixed and random coefficients. The ARMA generated cloud scenes are maintained in a separate pixel plane and are rapidly integrated with background and object scenes using a radix masking approach. The technique was originally applied to the simulation of cloud modeling for strategic discrimination studies and has been extended to simulate cluttered backgrounds, clouds, and obscurants. The baseline algorithm is currently being modified to render clouds and other effects in three dimensions and to add basic first-principles effects under a Phase I, Small Business Innovative Research (SBIR) program contract, administered out of the Mathematics and Computer Sciences Division of the Army Research Office.

1. INTRODUCTION

The ARMA approach was first applied to clouds and obscurants as a method of specifying clutter characteristics in scenes. Following this application, the technique was next applied to the generation of cloud scenes with specified clutter coefficients. Later methods were developed to simulate cloud movements and diffusion due to wind. Currently the ARMA cloud rendering technique is being modified to generate real-time animated 3-D cloud scenes at various levels of fidelity. The inclusion of first-principles effects for non-visible sensors is also being implemented using mapping functions which relate visible cloud density and composition to self-emission and transmission in specified passbands.

1.1 MATHEMATICAL BACKGROUND

Consider the generation of a two-dimensional array M of values for which $M_{i,j}$ represents the value of the i th row and the j th column. In Equation 1 the a_k are members of a set of constants whose sum is unity, r_k and c_k represent the indices of elements of the array in the neighborhood of $M_{i,j}$, $\rho_{\mu,\sigma}$ is a stochastic variable of the desired distribution, and α is a coefficient indicating the relative level of correlation between $M_{i,j}$ and its neighborhood.¹ This is the first-order auto-regressive (AR) model.

$$M_{i,j} = \alpha \left[\sum_{k=1}^N a_k M_{r_k, c_k} \right] + (1 - \alpha) \rho_{\mu,\sigma} \quad (1)$$

The stochastic function $\rho_{\mu,\sigma}$ can have a fixed or varying distribution. In a moving-average (MA) model, for example, the mean of ρ is not constant. Ahuja and Schachter provide an excellent description of AR, MA and ARMA.²

In our context, Equation 1 indicates the operation to be performed on every element of a matrix used to represent the cloud clutter level at a specified time. Changes in the set a_k and the magnitude of α are used to control clutter characteristics. For purposes of illustration, let $N=2$, $a_1=a_2=1/2$, $r_1=i$, $c_1=j-1$, $r_2=i-1$, and $c_2=j$. So that,

$$M_{i,j} = \frac{\alpha}{2} [M_{i,j-1} + M_{i-1,j}] + (1-\alpha)\rho_{\mu,\sigma} \quad (2)$$

1.2 SOFTWARE IMPLEMENTATION

In general, a basis must be provided for every $M_{i,j}$ in Equation 1 that cannot be defined recursively. The software implementation of Equation 2 requires special consideration for the first row and the first column of M . Equation 3 shows how this is done for linear propagation through M .³

$$\begin{aligned} M_{1,1} &= \rho_{\mu,\sigma} \\ M_{1,j} &= \alpha M_{1,j-1} + (1-\alpha)\rho_{\mu,\sigma} \quad \text{for } j > 1 \\ M_{i,1} &= \alpha M_{i-1,1} + (1-\alpha)\rho_{\mu,\sigma} \quad \text{for } i > 1 \\ M_{i,j} &= \frac{\alpha}{2} [M_{i,j-1} + M_{i-1,j}] + (1-\alpha)\rho_{\mu,\sigma} \quad \text{for } i, j > 1 \end{aligned} \quad (3)$$

2. CLOUD SCENE RENDERING

The generation of synthetic cloud imagery requires a mathematical model that can provide both randomness and persistent structure. The auto-regressive moving average (ARMA) is such a stochastic model. Let the matrix $M_{i,j}$ of Equation 1 represent a two-dimensional image in which each matrix element defines a corresponding image pixel. In this image, every pixel value is updated using the indicated operation.

2.1 VISIBLE EFFECTS

To simulate the dynamics of clouds or other obscurants at desired locations in the image, selected elements of M are "seeded" with values at the beginning of each frame. The rate of diffusion and direction of motion of clouds in the image are determined by the relative magnitudes of the correlation coefficients a_k and the stochastic function $\rho_{\mu,\sigma}$. Using a method analogous to the one presented in Equation 3, every pixel is updated in every frame. In those regions where clouds are not present the model simply propagates zero values. The values of the elements of M are used to determine the cloud density. The cloud image M is integrated with the background image B to create the scene S .

$$S_{i,j} = \beta [\tau B_{i,j} + (1-\tau)M_{i,j}] + (1-\beta)\rho_{\mu,\sigma} \quad (4)$$

where τ is the transparency of the cloud at $M_{i,j}$. The coefficient β represents the magnitude of an overall noise component in the observation. Its inclusion has the visual effect of softening the boundary between cloudy and clear image regions.

2.3 FIRST PRINCIPLES MODELING

A preliminary analysis has indicated that with the addition of a mapping function as illustrated in Figure 1, the visible effects described in 2.1 above can be extrapolated into other passbands. For a specified set of environmental conditions and for known constituents of an obscurant, a deterministic mapping between visible cloud density, cloud transparency and self-emission/reflection can be established for other spectral passbands. The salient parameters needed to reduce the standard deviations in such mappings are currently being evaluated.

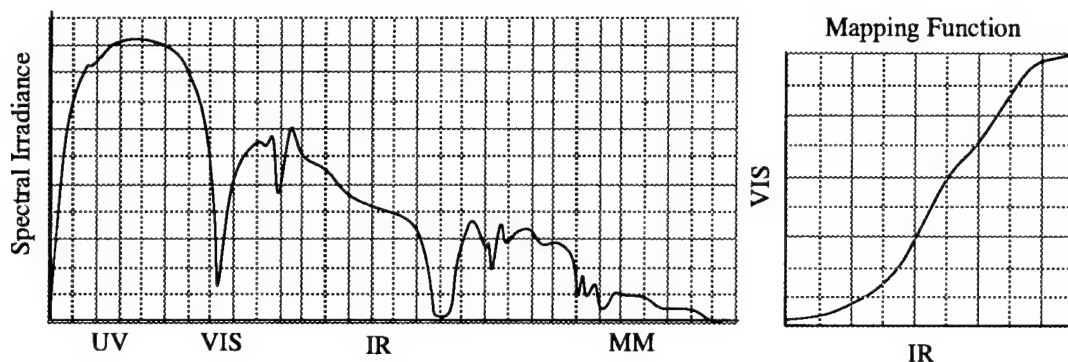


Figure 1. For clouds and other obscurants of known composition, there is a deterministic relationship between the visible characteristics and those of other spectral passbands.

2.3 THREE DIMENSIONAL MODELING

The ARMA cloud generation model can be extended to three-dimensions in a number of ways. The level of fidelity needed depends of the dynamics of the engagement scenario. Table I lists the conditions being considered in the current study and the preferred modeling method.

TABLE I. ARMA EXTENSIONS REQUIRED FOR 3-D MODELING

Viewing Platform Position	Observation Line-of-Sight	ARMA Method
FIXED	FIXED	Single plane with scale change only
FIXED	MOVING	Single plane with extended FOR only
MOVING	FIXED	Single plane with scale change and extended FOR
MOVING	MOVING	Multiple planes with scale change and extended FOR

Each of these conditions places a different demand of the level-of-fidelity of the cloud rendering model. If the viewing platform is stationary, a 3-D cloud model can be developed by attaching a range or scale-factor to each seed. If the viewing platform is moving but the line-of-sight (LOS) is inertially fixed, then the scale-factor must change with the platform position and the cloud image must be generated for an extended FOR.

CONCLUSIONS

Extending the ARMA model to include first-principles effects appears to be straightforward. The ability to model clouds in three dimensions can be accomplished for some scenarios. When both the viewing platform and the line-of-sight are unrestricted, the ARMA cloud rendering model must be modified to render clouds in multiple planes and then transformed into the current LOS.

REFERENCES

1. Young, Tzay Y., and King-Sun Fu, "Handbook of Pattern Recognition and Image Processing," pp. 285-288, Academic Press, Inc., NY, 1986.
2. Ahuja, N., and B. J. Schachter, "Pattern Models," pp. 232-233. John Wiley & Sons, NY, 1983.
3. Bevilacqua, A. T. and R. A. Pilgrim, "Clutter Metric Specification Using An Auto-Regressive Moving Average (ARMA) Model, U.S. Army Tank-Automotive Command RD&E Technical Report, Warren Michigan, 1993.

SIMULATING CLOUDS WITHIN A SPACE-BASED DOPPLER LIDAR WIND SOUNDER SIMULATION MODEL

G. David Emmitt and Sidney A. Wood
Simpson Weather Associates, Inc.
Charlottesville, VA 22902

ABSTRACT

An end-to-end performance simulation model for space-based Doppler lidar wind sounders is being developed under a Phase II SBIR contract. The Defense Lidar Simulation Model (DLSM) uses operational weather forecasting models (ECMWF/T106 and ETA/28 km) to generate LOS atmospheres for individual lidar shots. In addition to providing shot-by-shot aerosol backscatter, molecular attenuation, and atmospheric turbulence, the DLSM atmosphere generation model (AGM) produces cloud coverage, backscatter and porosity.

The AGM cloud model is, in general, based on the Slingo cloud parameterization scheme¹. The Slingo approach provides distinctions between high and mid-tropospheric stratiform clouds, convective clouds with and without anvil cirrus, and low level clouds driven by weak vertical motion or inversion capped moist boundary layers.

1. CONVECTIVE CLOUD

The convective cloud is inferred, for example, from 3 hour integrated precipitable water from the 3-D model meteorological profiles. A critical threshold value of 0.14 mm/day must be met for a convective cloud to be present. The top of the convective cloud layer is a function of the base layer convective cloud amount and the tropopause height. If the top of the convective cloud is above the 400 mb layer and the integrated precipitable water more than 3.4 mm/day, then an anvil is defined. All anvil clouds are considered to be optically thick cirrus layers.

2. HIGH NON-CONVECTIVE CLOUDS

All non-convective high clouds are derived as a function of relative humidity from the 3-D model meteorological profiles. A high layer cloud is only derived when the tropopause height is higher than the 400 mb layer. All high non-convective cloud is considered to be thin cirrus and thus semi-transparent to the laser beam.

3. MIDDLE NON-CONVECTIVE CLOUDS

All non-convective middle clouds are derived as a function of relative humidity from the 3-D model meteorological profiles. If there was a convective cloud or a high layer cloud, the AGM dries out the relative humidity profile and thus reduces the likelihood of middle cloud. Like the high cloud algorithm, the AGM finds the highest relative humidity in the profile and uses a relative humidity threshold for cloud occurrence.

4. LOW NON-CONVECTIVE CLOUDS

The estimate of low level non-convective clouds is based upon two parameters: vertical velocity and the potential temperature profile. From vertical velocity, the AGM finds the layer with the largest negative vertical velocity and computes the critical relative humidity for the layer.

5. GLOBAL STATISTICS AND EMPIRICAL ADJUSTMENTS

We expect that clouds will be in the field-of-view (FOV) of a space-based lidar 70-80% of the time. This

estimate is based upon the reported analysis of two years of HIRS data², the cirrus climatology derived from SAGE data³ and the ISCCP global cloud climatology⁴. Much (30-40%) of this cloud coverage is high cloud (above 400-500 mb) and is semi-transparent. Very thin or subvisual cirrus ($\tau < .07$) not detected by HIRS or AVHRR may be occasionally represented in the SAGE observations. We conclude that the occurrence of very thin to subvisual cirrus is underestimated in current global cloud climatologies.

Of particular interest to any program involving space-based lasers are the semi-transparent and optically thin cirrus clouds, since they may provide strong returns without full extinction. When one considers that the statistics given above are, in most cases, exclusive - i.e., they do not provide a good representation of coincident clouds at different altitudes, it is very likely that there are many occasions when there are multi-layers of thin clouds underlain by opaque clouds (e.g., the recent WWW pictures on the LITE home page (<http://arbs8.larc.nasa.gov/LITE/litehome.html>)).

The distribution of clouds (over a $1^\circ \times 1^\circ$ area) based upon the ECWMF total cloud coverage as a function of latitude are shown in Figure 1. The total coverage is quite reasonable and compares well with the satellite statistics. While not evident in the figure, the amount of midlevel cloud forecast for the tropics is considerably less than the 30-40% reported using the satellite data. This discrepancy is an ongoing point for discussion and study within the modeling community, with some researchers suggesting that the interpretation of midlevel cloud in satellite imagery may be faulty.

ONE DAY GLOBAL AVERAGE INTEGRATED CLOUD AMOUNTS FOR 10 DEGREE LATITUDE BANDS

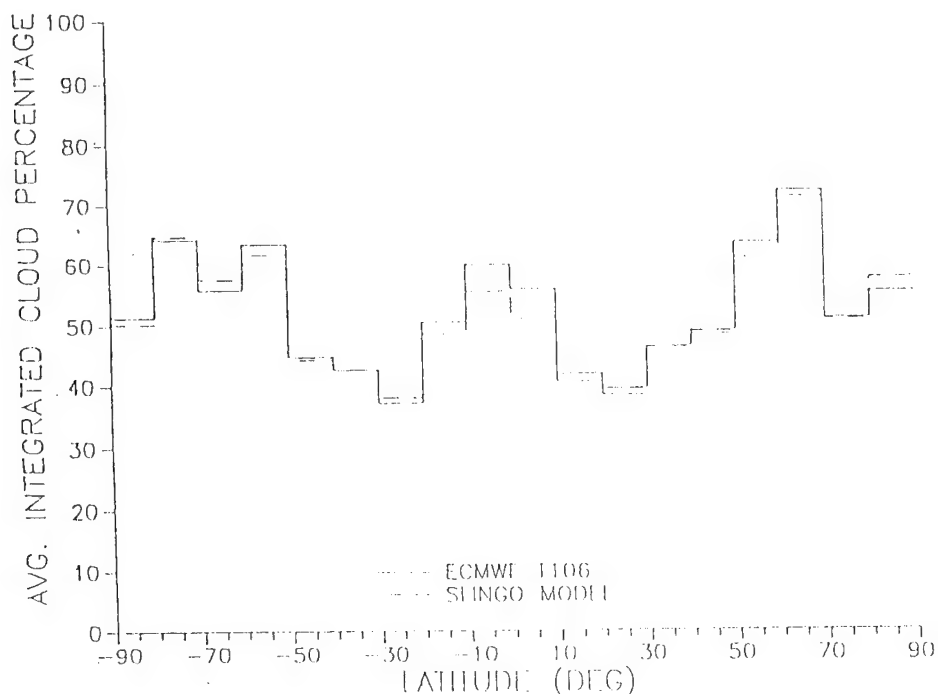


Figure 1. Comparison of the global average integrated cloud cover from the Slingo model to the AGM integrated cloud amount.

6. CLOUD OPTICAL PROPERTIES

All opaque cloud backscatter values are defaulted in the AGM to be $10^{-6} \text{ m}^{-1} \text{ sr}^{-1}$. We believe this value is properly conservative, since recent midlayer cloud backscatter, measured with a lidar in the Antarctic, range from 10^{-6} to $10^{-4} \text{ m}^{-1} \text{ sr}^{-1}$ ⁵. Once a lidar shot gets a return from an opaque cloud, the shot is considered to be fully attenuated and its propagation terminated. Cirrus cloud backscatter is computed using the LOWTRAN⁶ cirrus model. For cirrus cloud layers, however, we allow all the shots a finite probability to pass through to the next model layer. The cirrus cloud attenuation model is a modified version of the analytical LOWTRAN cirrus algorithm⁶,

$$\tau = e^{-0.14 \cdot L^2}$$

where

τ = the cirrus transmittance

L = the cirrus cloud thickness .

Since the AGM is restricted to a coarse vertical resolution, it uses the Slingo algorithm cirrus cloud percentage as a surrogate for cirrus cloud optical thickness. The major assumption is that while the Slingo model derives a percent cirrus cloud coverage (e.g., 30%) from an average relative humidity within a grid volume, it is just as reasonable to interpret an optical thickness tendency from the same fields. Validation of this approach is ongoing. Instead of using the percent coverage as literally meaning that 30% of the grid has cirrus cloud and 70% is totally cloud-free, the AGM assumes that the whole grid area is covered by a cirrus cloud that has an optical thickness that scales to the percent coverage. The cirrus cloud attenuation is defined as

$$ci_{att} = 10^\alpha \cdot (CLD_{\%} \cdot 10)^2$$

where

ci_{att} = the cirrus cloud attenuation

α = the LOWTRAN cirrus attenuation coefficient for a 1 km thick layer

$CLD_{\%}$ = the cirrus cloud percentage cover .

7. CLOUD POROSITY

Experience with airborne lidar systems has shown that visually dense and unbroken cloud fields are often fractionally (0-30%) transparent to a laser beam⁷. Detailed analysis of SPOT and LANDSAT imagery⁸ also revealed that scenes (multi-pixel) classified as 100% covered, were more likely 10-30% porous for 10-20 m diameter beams. While the supporting data is rather sparse, the DLSSM does allow the users to assign a porosity to model clouds based upon their type and physical thickness. A porosity of 25% for stratiform clouds makes a significant difference in the number of times a space-based lidar can make measurements in the PBL. We are currently evaluating techniques for validating the porosity assignments.

REFERENCES

- ¹Slingo, A., R.C. Wilderspin and S.J. Brentnall, 1987: Simulation of the diurnal cycle of outgoing longwave radiation with an atmospheric GCM. *Mon. Wea. Rev.*, 115, 1451-1457.
- ²Menzel, W.P., D.P. Wylie and K.L. Strabala, 1992: Seasonal and diurnal changes in cirrus cloud as seen in four years of observations with the VAS. *J. Appl. Meteor.*, 31, 370-385.
- ³Woodbury, G.E. and M.P. McCormick, 1986: Zonal and geographical distributions of cirrus clouds determined from SAGE data. *J. Geophys. Res.*, 91, 2775-2785.
- ⁴Rossow, W.B. and R.A. Schiffer, 1991: ISCCP cloud data products. *Bull. Amer. Meteor. Soc.*, 72, 2-20.
- ⁵Del Guasta, M., M. Morandi and L. Stefanutti, 1993: One year of cloud lidar data from Dumont d'Urville (Antarctica), 1. General overview of geometrical and optical properties. *J. Geophys. Res.*, 98, 18575-18587.
- ⁶Kneizys, F.X., E.P. Shettle, L.W. Abreu, G.P. Anderson, J.H. Chetwynd, W.O. Gallery, J.E.A. Selby and S.A. Clough, 1983: Users guide to LOWTRAN 7. Air Force Geophysical Laboratory, Hanscom AFB, MA, Contract AFGL-TR-88-0177 (Rept. ADA206773).
- ⁷Menzies, R.T., D.M. Tratt and P.H. Flamant, 1994: Airborne carbon dioxide coherent lidar measurements of cloud backscatter and opacity over the ocean surface. *J. Atmos. Oceanic Technol.*, 11, 770-778.
- ⁸Emmitt, G.D. and G. Séze, 1991: Clear line of sight (CLOS) statistics within cloudy regions and optimal sampling strategies for space-based lidars. Paper presented at the AMS 71st Annual Meeting, Seventh Symposium on Meteorological Observations and Instrumentation, Special Session on Laser Atmospheric Studies, New Orleans, LA, January.

**SESSION III:
CLOUD DATABASES**

APPLICATION OF HYPERMEDIA AND CD-ROM TECHNOLOGY TO THE DISTRIBUTION OF NAVY ENVIRONMENTAL INFORMATION FOR SATELLITE IMAGE ANALYSIS AND FORECASTING

Marie E. White
Pangaea
Pebble Beach, CA, 93953, U.S.A.

Robert Fett
Science Applications International Corporation
Monterey, CA, 93940, U.S.A.

Sam Brand
Naval Research Laboratory
Monterey, CA, 93943, U.S.A.

ABSTRACT

Computer technology is undergoing tremendous advances with regard to information delivery. One important development is the ability to convert written materials into an electronic hypermedia format, and then publish these materials on CD-ROM or the Internet. This technology provides new capabilities for use in training, operations, and R&D. The Naval Research Laboratory in Monterey utilized this technology with the *LaserTAG* project, an electronic compendium of the Navy Tactical Application Guides. The attributes of the *LaserTAG* project are as follows: (1) the compact format of the materials; (2) application development and publication cost reduction; (3) stability of CD-ROM for long-term storage; and (4) enhanced user capabilities including user-defined studies, keyword searches, annotations, and bookmarks. The importance of this project lies not only in its value to Navy users but also in the applicability of this technology to other projects that need to effectively publish large quantities of graphical, textual, or numeric information.

INTRODUCTION

Eleven Navy Tactical Application Guide (NTAG) volumes were developed from 1977 to 1992 for the purpose of aiding Navy weather forecasters using satellite analysis. The NTAG materials are unique for two reasons: (1) exceedingly high quality photographic images from the DMSP satellite system were used in the NTAG construction; these images were fully documented by conventional charts and observations; and (2) the NTAG materials focused on the operationally most relevant phenomena of concern to Navy decision makers. The NTAG volumes were divided by region to cover all main areas of Navy operation throughout the world. Information in the volumes included satellite and sensor technical information, atmospheric and oceanographic case studies, and graphics. More than 3500 satellite images, charts, and graphs were included in the volumes.

The NTAG volumes have remained valuable documents for both land and sea-based use of environmental information. New information technologies now permit the NTAG series to be enhanced. The purpose of the *LaserTAG* project was to incorporate these new technologies by developing a hypermedia implementation of the NTAG volumes on CD-ROM. By converting the paper copy of the NTAG volumes into a computer-based application on CD-ROM, three feet of shelf space is saved and replaced by two CD-ROM discs. CD-ROM discs are more durable than hard-copies and have lower publication costs. Hypermedia implementation provides advantages to users through search capabilities, user-defined studies, and creation of bookmarks and annotations. The hypermedia implementation allows users to easily move from the Table of Contents to a specific topic. Users can read case studies and view graphics simultaneously (Figure 1). Bookmark and annotation files can be targeted for a single user or for multiple users when exchange or turnover of information is desired.

METHODOLOGY

The first part of the LaserTAG project focused on determination of the appropriate technology to utilize; this was followed by the development of a prototype application. Various software packages were analyzed and a proprietary hypermedia authoring tool, Guide, was chosen. This software provided multiple windowing tools, good graphical display capabilities, and free run-time versions. Next, the design of the file naming system and directory structure were determined. Design was based on requirements of both the hypermedia software and CD-ROM technology. The prototype hypermedia document, consisting of two NTAG volumes, was then developed. The prototype process required about one and half man years, for procurement, development, and integration of the appropriate technologies.

Following review and analysis of the prototype, development of the hypermedia implementation of the entire NTAG series was begun. The first step was to digitize all the textual information, graphics, and images. Text was digitized by NRL Monterey using a desktop flatbed scanner with Optical Character Recognition software. Line art (2 bit color) was also scanned with the desktop flatbed scanner using scanning and image enhancement software. Grayscale and color images were contracted out to a scanning firm. The hypermedia application then was developed following the original design of the NTAG volumes.

The final part of the LaserTAG project was to transfer the hypermedia application to CD-Recordable (CD-R) disc. Data files were written to an image file using premastering software; the image file was then written to CD-R disc. Dedicated hard disk partitions were used for image and data files. The use of CD-R media enabled testing of the hypermedia application for robustness and quick distribution of the application for review.

PROJECT STATUS AND FUTURE WORK

Beta evaluation of the LaserTAG was conducted by the Commander, Naval Meteorology and Oceanography Command in Summer, 1995. Based on the beta evaluations, revisions will be made to the LaserTAG in Fall, 1995. The expected project completion is Spring, 1996.

The Naval Research Laboratory in Monterey is currently working on other hypermedia and multimedia applications. Specifically, NRL is developing a prototype satellite training application using Hypertext Markup Language (HTML) and World Wide Web (WWW) browsers. Development is targeted both for stand alone machines and networked environments. The advantages of this approach are the cross-platform and network capabilities. Proprietary multimedia and hypermedia software, as the one used in the LaserTAG, remain valuable development tools depending on the demands of the application. Applications best suited for these tools are those requiring multimedia capabilities or large numbers of graphics.

CONCLUSIONS

The LaserTAG project accomplished its pre-defined goals. These included: compact format for technical materials; reduction in the cost of development and publication; stable long-term storage of data; and enhanced user capabilities including the ability to define an individual learning program, conduct searches, and create annotations and bookmarks. This technology can prove very valuable to any project that seeks to accomplish similar goals and is especially important for projects that need to effectively provide large quantities of graphical, textual, or numeric information for training, operational support or R&D.

ACKNOWLEDGMENTS

Funding for the prototype research for the LaserTAG project was provided by Space and Naval Warfare Systems Command (PMW-175). Funding for the operational development was provided by Commander, Naval Meteorology and Oceanography Command.

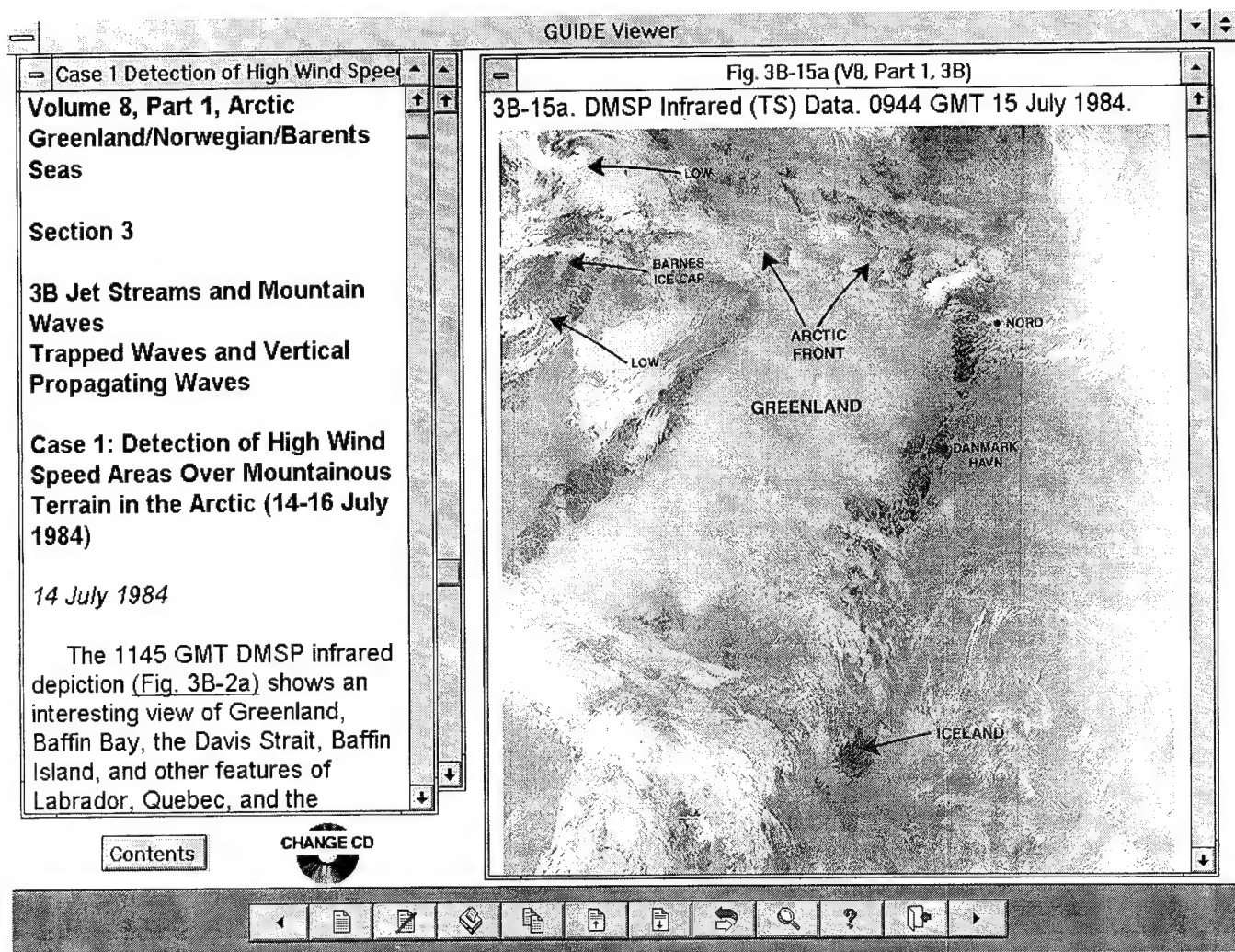


Figure 1. Screen capture of the LaserTAG showing a Case Study window and the associated Graphic Window. The Table of Contents window is mostly hidden behind the Case Study window. The text, Fig. 3B-15a, in the Case Study window is a hypermedia link to the DMSP Infrared image. The control panel, seen at the bottom of the screen capture, provides navigation, search, and help capabilities.

CLOUD DATA SETS DERIVED FROM COMBINED GEOSTATIONARY AND POLAR-ORBITING ENVIRONMENTAL SATELLITE SENSORS USING THE SERCAA CLOUD MODEL ¹

Gary B. Gustafson, Robert P. d'Entremont and Daniel C. Peduzzi
Atmospheric and Environmental Research, Inc.
Cambridge, Massachusetts

The Cloud Depiction and Forecasting System II (CDFS II) is a major new initiative that will transition the Air Force Global Weather Central (AFGWC) to a new satellite data processing environment and include extensive changes in cloud analysis and forecasting. The present cloud analysis model, the RTNEPH, combines reduced resolution DMSP OLS or NOAA AVHRR data with conventional observations. The RTNEPH domain and analysis frequency are limited by its dependence on polar-orbiting satellites. In the CDFS II era (1998+), AFGWC cloud forecast models will benefit directly from improved automated nephanalysis capabilities from multiplatform sensor data. The Support of Environmental Requirements for Cloud Analysis and Archive (SERCAA) project is a research effort sponsored by the Strategic Environmental Research and Development Program (SERDP) to provide both the next generation nephanalysis model for CDFS II and a new global cloud algorithm for use in determining the radiative and hydrological effects of clouds on climate and global change. The SERCAA cloud model operates on multiplatform multispectral satellite sensor data for the purpose of retrieving cloud location and the vertical distribution of amount, height, and type. Data sources include the civilian NOAA AVHRR and TOVS; military DMSP OLS, SSM/I, SSM/T, and SSM/T2; and international GMS, GOES, and METEOSAT geostationary imaging sensors. In the now completed first phase separate cloud analysis algorithms were developed for each imaging sensor in order to best exploit the information content unique to the individual data sources. A new and innovative analysis integration approach based on NWP data assimilation techniques was developed to combine the separate nephanalysis results from the temporally spatially, and spectrally inconsistent sources into a single logically consistent analysis. Using real satellite data from NOAA 11 and 12, DMSP F10 and F11, GMS 4, GOES 7, and METEOSAT 3, 4, and 5, SERCAA cloud analysis products have been generated for a series of ten-day data sets taken from March and July of 1993 and 1994 over four large and widely dispersed geographic regions. These data sets are being used to support development of a new global cloud forecast model under a Defense Nuclear Agency sponsored research and development program. Intermediate and integrated nephanalysis products have been evaluated for accuracy and consistency. Results show that while the sensor-specific algorithms produce accurate intermediate cloud analyses when compared to imagery from the respective data source, platform-dependent differences do occur, particularly in the analysis of low cloud and optically thin cirrus. For example, analyses of high-resolution multispectral AVHRR data tend to identify more thin cirrus than can be detected from the coarser-resolution one- or two-channel geostationary data. The analysis integration algorithm minimizes inconsistencies between the various input sources through the application of source-specific weights and persistence criteria designed to maximize the internal consistency of the integrated analysis while simultaneously exploiting the respective temporal, spatial, and spectral information content of the various data sources.

¹This work is supported under contracts F19628-92-C-0149 and F19628-94-C-0106 by the Geophysics Directorate, Phillips Laboratory (AFMC), Hanscom AFB, MA.

Manuscript not available at time of printing. Please contact author for information.

CLIMATOLOGICAL AND HISTORICAL ANALYSIS OF CLOUDS FOR ENVIRONMENTAL SIMULATIONS (CHANCES) - FIRST YEAR OF PRODUCTS

Donald L. Reinke, Thomas H. Vonder Haar, Kenneth E. Eis, Jan L. Behunek,
Charles R. Chaapel, Cynthia L. Combs, John M. Forsythe, Mark A. Ringerud
STC-METSAT

Fort Collins, Colorado, 80521, USA

ABSTRACT

The STC-METSAT CHANCES project is an Small Business Innovative Research Phase II effort that produced a 1-yr, global, hourly, 5-km resolution, satellite-derived cloud product. The global cloud database has been built at a higher spatial and temporal resolution than any previous Department of Defense cloud product, using almost two orders of magnitude more data than the United States Air Force (USAF) Real-Time NEPHAnalysis (RTNEPH) cloud product.

Input for the database includes satellite imagery from four geostationary and four polar orbiting vehicles and ancillary input from the USAF Surface Temperature database and the U.S. Navy Snow/Ice database. The input geostationary satellites include GOES, GMS, and two Meteosat vehicles. The polar satellite input is from two DMSP and two NOAA vehicles. The CHANCES output products include a cloud/no cloud image, a quality assessment image, and visible and infrared radiance images.

1. INTRODUCTION

The current Department of Defense (DoD) cloud database is not meeting the demands for cloud input to high time and space resolution simulation models. It is based on cloud data taken from the United States Air Force (USAF) Real Time NEPHAnalysis (RTNEPH). This 46-km, 3-hour resolution database has been built since 1973 (Kiess and Cox, 1988) with its primary input from surface observations and one satellite system, the Defense Meteorological Satellite Program (DMSP) polar orbiter. High Resolution Satellite Cloud Climatology (HRSCC) studies by Reinke et al., (1992) supported the generally accepted position that there is a striking diurnal variability in cloud cover that is missed when a polar orbiting system is used as the primary input to a cloud analysis model.

The Climatological and Historical ANalysis of Clouds for Environmental Simulations (CHANCES) project was sponsored by an Small Business Innovative Research (SBIR) Phase II grant. The purpose of Phase II was to produce a 1-yr, 1-hr, 5-km resolution, global cloud/no cloud (CNC) database product (shown in Fig. 1). The intent of the CHANCES project was not to produce new and innovative algorithms for cloud detection and analysis. That work is being done, most notably, by the International Satellite Cloud Climatology Project (ISCCP) group (Rossow et al., 1991) and by the DoD sponsored Support of Environmental Requirements for Cloud Analysis and Archive (SERCAA) project (Gustafson et al., 1994). The primary challenge for STC-METSAT was a systems engineering issue; to implement such cloud analysis algorithms in a working system that is designed to ingest and process the massive amounts of satellite imagery that are required to produce a global product for every hour.

2. INPUT DATA

Raw satellite imagery that served as input to the CNC processing was archived on 8-mm tape in various formats depending on the source of the data. Table 1 shows the platforms, wavelengths, and resolutions of the satellite data that were used as input for the CHANCES project. Three supportive

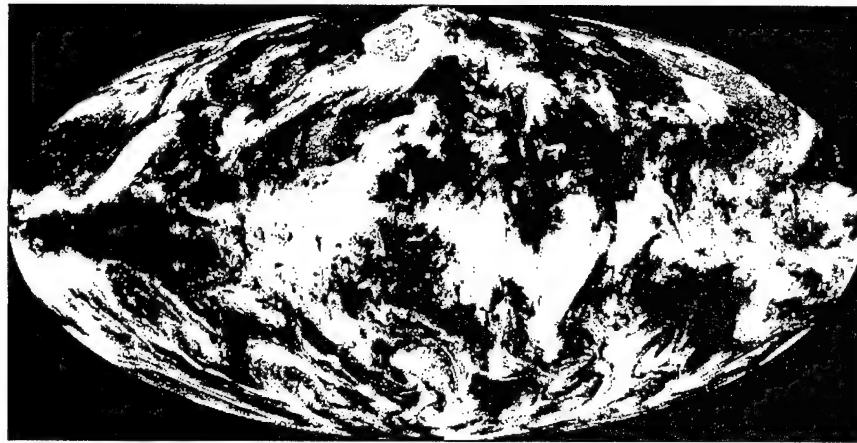


Figure 1. CHANCES global CNC image.

databases used in this project are the USAF Surface Temperature database, the USAF Snow/Ice database, and the U.S. Navy ETOPO5 10-km resolution topography database.

	DMSP	GMS	GOES	METEOSAT	AVHRR
Visible Wavelength (μm)	0.4-1.1	0.50-0.75	0.55-0.75	0.40-1.1	0.58-0.68
Infrared Wavelength (μm)	10.5-12.6	10.5-12.5	10.5-12.6	10.5-12.5	10.3-11.3 3.55-3.93
Nominal subpoint resolution of raw CHANCES imagery (km)	2.7	5	VIS - 4 IR - 6.8	5	4
Approximate geo resolution at 55° from subpoint (km)		12	10	11	

Table 1. CHANCES input satellite data specifications.

3. IMAGE DATA PROCESSING

A detailed description of image data processing is given in Reinke et al., (1995). The CHANCES products include a CNC image, visible and infrared radiance images, and a Quality Analysis (QA) image.

The QA image contains information about the satellite ID, whether a particular point was filled due to missing data, and CNC flags for visible, infrared, and combined logic CNC processing.

Visible data are processed by building a visible background image that represents the cloud-free radiance that is expected for each hour. The visible images are compared to this background to determine if the measured radiance is colder (brighter) than the background with the assumption being that a colder signature denotes the presence of a cloud. A detailed description of this procedure can be found in Reinke et al., (1992) and Rossow et al., (1991). Special attention was given to shadows, deserts, snow/ice, terminator, and sunglint.

Infrared imagery was processed to identify cloudy pixels using a bispectral, dynamic threshold technique. Background temperature, spatial variability, and temporal variability tests were run in a manner similar to that used for the ISCCP processing described by Rossow et al., (1991). Because of the availability of additional spectral channels, the National Oceanic and Atmospheric Administration (NOAA) Advanced Very-High Resolution Radiometer (AVHRR) data were processed using a trispectral

dynamic threshold technique. In addition to the visible data, AVHRR infrared channels 3 and 4 were used for detection of low clouds over snow and ice.

The CHANCES final global output image files are formed by merging the intermediate output from five geostationary (GOES 7, GMS-4, Meteosat-3, and Meteosat-4 and 5) and six polar (DMSP F10, F11, and F12, NOAA 11, 12, and 13) satellites into a single global product. All of the final product images are mapped onto a mollweide projection (Fig. 1) scaled to provide a nominal 5-km resolution. Missing data is filled in by applying a spatial or temporal interpolation of available data or, as the lowest priority, persistence (either forward or backward in time).

4. FUTURE WORK

STC-METSAT has submitted proposals to produce an additional four years of the CHANCES Phase II database and two additional cloud products. The first product is a Global Layered Cloud and the second is a Global Cloud Climatology. In addition, a spin-off global radiance background database is planned for both the visible and infrared image data sets.

5. ACKNOWLEDGMENTS

For the first time ever, the STC team has delivered an innovative new cloud database product for the USAF. STC-METSAT acknowledges the support and helpful discussions provided during the course of this work by Dr. Kenneth Champion and Dr. Arnold Barnes, the USAF Technical Representatives. Special thanks are extended to USAF Maj. Steve Musto for assistance in the development of the CHANCES database specifications, and Dr. Garrett Campbell and Mr. Kelly Dean for their assistance with the geostationary satellite data ingest and archive. This work was supported under USAF SBIR Phase II contract F19628-93-C-0197.

6. REFERENCES

- Kidder, S.Q. and T.H. Vonder Haar, 1995: *Satellite Meteorology: An Introduction*. Academic Press, 456 pp.
- Kiess, R.B. and W.M. Cox, 1988: *The AFGWC Automated Real-Time Analysis Model*. AFGWC/TN-88/001, AFGWC, Air Weather Service (MAC), Offutt AFB, Nebraska, 82 pp.
- Reinke, D.L., C.L. Combs, S.Q. Kidder, and T.H. Vonder Haar, 1992: Satellite Cloud Composite Climatologies: A New Tool in Atmospheric Research and Forecasting. *Bull. Amer. Meteor. Soc.*, **73**, 278-285.
- Reinke, D.L., T.H. Vonder Haar, K.E. Eis, J.L. Behunek, C.R. Chaapel, C.L. Combs, J.M. Forsythe, M.A. Ringerud, 1995: *Climatological and Historical ANALYSIS of Clouds for Environmental Simulations (CHANCES) Database - Final Report*. PL-TR-95-2101, Phillips Laboratory, Hanscom AFB, Massachusetts, 44 pp. plus 5 Appendices.
- Rossow, W.B., L.C. Gardner, J.P. Lu., and A.W. Walker. 1991: *International Satellite Cloud Climatology Project (ISCCP) Documentation of Cloud Data WMO/TD - No. 266*, World Meteorological Organization, Geneva, 76 pp. plus 3 Appendices.

GLOBAL STATISTICS ON CLOUD OPTICAL DEPTHS FROM SATELLITE AND LIDAR OBSERVATIONS

Donald Wylie
Space Science and Engineering Center
University of Wisconsin-Madison
Madison, Wisconsin

Six years of cloud data have been collected globally from the NOAA satellite series. The High Resolution Infrared Radiometer Spectrometer (HIRS) data were used to detect clouds and estimate their optical depths in the 11 micron infrared window. The cloud detection algorithm has been called the CO2 Slicing Algorithm because it uses the 13-15 micron infrared channels where partial CO2 absorption occurs, to detect partially transparent clouds and correctly determine their altitude. This algorithm is designed to be sensitive to upper tropospheric cirrus clouds which are difficult to detect. The frequency of these clouds along with their global distribution and seasonal changes have been reported at past CIDOS conferences.

The optical depths of semi-transparent cirrus clouds from the CO2 Slicing data. A detailed comparison of infrared optical depths derived from satellite data to optical depths measured by the University of Wisconsin's High Spectral Resolution Lidar (HSRL) has been made. The HSRL is discussed in a separate paper by E. Eloranta in these proceedings. Coincident satellite and lidar optical depth data were collected on 21 days in the past two years. The optical depth comparison exhibited scatter because of differences in which each sensor scanned the clouds. The satellite scanned over a large area with a lower resolution field of view; typically 1-8 km in diameter, while the lidar scanned a narrow line through the cloud < 1 m wide from the wind advection of the cloud over the lidar. The spatial variability of cloud density produced most of the disagreement between the two measurements. The mean optical depths, however, did agree after accounting for differences in the radiative physics of scattering and absorption between the visible and infrared measurements. A satellite bias toward larger optical depths was found for very thin cirrus clouds at the minimum detectable density of the satellite system. This bias occurred because very thin clouds had to be at least 2 K colder than surrounding cloud free backgrounds to be distinguished from noise and natural scene variability on the satellite images. This constraint imposed a minimum IR optical depth of 0.05 (0.10 in the visible) which is near the "invisible cirrus" category.

Thicker clouds appeared to be correctly measured by the satellite in spite of the fact that they are often 3-5 km thick and composed of multiple layers.

Manuscript not available at time of printing. Please contact author for information.

**ENHANCED SATELLITE CLOUD ANALYSIS
BY THE DEVELOPMENT OF A HIGHER RESOLUTION (6-KM)
GLOBAL GEOGRAPHY DATA SET**

1LT R. Radburn Robb and Crystal Barker Schaaf
Geophysics Directorate, Phillips Laboratory
Hanscom AFB, MA 01731

Daniel C. Peduzzi
Atmospheric and Environmental Research, Inc.
Cambridge, MA 02139

Joan M. Ward
System Resources Corporation
Burlington, MA 01803

ABSTRACT

An improved global 6-km raster geography based on an Air Force vector product, several terrain data sets, and human interpretation has been produced at the Air Force Phillips Laboratory, Hanscom AFB, MA. Additionally, desert surface types were identified using background brightness values from satellite measurements. Use of this improved geography data has dramatically improved cloud analysis, particularly over coastal areas. This data set was produced as part of the SERCAA (Support of Environmental Requirements for Cloud Analysis and Archives) global cloud detection and analysis algorithms. These algorithms utilize the capabilities of both polar orbiting and geosynchronous satellites. Since detailed knowledge of the underlying surface is critical to the cloud/no-cloud decision process, a necessary component of the cloud analysis effort is a fine-resolution geography database that determines information on surface characteristics such as land-water boundaries, deserts, and lakes. Such geographical data has also been used to retrieve surface skin temperatures, thus further increasing the accuracy of the thermal infrared section of the cloud detection algorithm.

1. INTRODUCTION

Under the Support of Environmental Requirements for Cloud Analysis and Archives (SERCAA) project, the Air Force Phillips Laboratory has developed global cloud analysis algorithms that utilize the capabilities of both polar orbiting and geosynchronous satellites.¹ During algorithm development, a detailed knowledge of the underlying surface was found to be more critical to the cloud/no-cloud decision process than originally anticipated. The production of a higher-resolution geography database that better delineated both ocean and lake coastlines, and defined deserts, became a necessary component of the cloud analysis effort. The resulting 6-km global geography is based on the vector coastlines currently used at Air Force Global Weather Central (AFGWC), Offut AFB, NE, Defense Mapping Agency (DMA) Digital Terrain Elevation Data (DTED) based sea-level heights, and extensive human interpretation. Desert surface types were identified using background brightness values from satellite measurements. These enhanced geography data sets have dramatically improved cloud analysis, particularly over coastal areas.

The Earth Observing System (EOS) Moderate Resolution Imaging Spectroradiometer (MODIS)

science team is also making use of SERCAA algorithms in its work with cloud masking algorithms. This group has found that the use of even higher-resolution land/water masks further improves cloud analyses.² They are using a new 1-km land/water data set developed by the United States Geological Survey (USGS) Earth Resources Observation Systems (EROS) Data Center that is based on the rasterized Digital Chart of the World (DCW) and World Vector Shoreline (WVS) data sets.³

2. DATA SOURCES

The 6-km geography data set is based on a rasterized version of the vector coastline data set currently in use at AFGWC. For the northern-hemisphere, these data were merged with sea-level (zero elevation) contour data from a 6-km terrain data set based primarily on DMA 3-arc-second data.⁴ Extensive human interaction refined this product generating an accurate 6-km geography raster data set, complete with large inland lakes. Since very little DMA DTED data were available for the southern-hemisphere, the data set relied alone on the AFGWC data and once again on detailed human interpretation. In addition, locations of deserts and coastal deserts in both hemispheres were identified and cataloged from satellite background brightness values. Both the northern and southern hemisphere sets were mapped to a 6-km hemispheric standard polar stereographic projection true at 60 degrees latitude, as used under SERCAA.

3. CLOUD ANALYSIS ENHANCEMENTS

SERCAA cloud analysis products are provided at 24-km resolution, but the actual cloud/no-cloud decisions are made on a pixel-by-pixel basis. When processing all of the timely satellite data available for a location, different cloud detection algorithms are selected for use depending on whether the pixel is located over land, water, shorelines, or desert. Originally, the use of a supporting geography database with a resolution similar to that of the cloud analysis products (such as the Navy 10-minute data set) was thought to be sufficient to select the appropriate cloud detection algorithm. However, there were difficulties, particularly in geographic transition regions such as coastlines, where either obvious cloud went undetected or spurious cloud was added to the analysis. By using the new 6-km geography database, these problems were minimized. Furthermore, by using the geography data sets to enhance other crucial supporting data, such as the 48-km resolution surface skin temperatures used by the thermal infrared cloud detection algorithms, the geographic information also improved results indirectly.

4. RESULTS

In Figure 1, a DMSP OLS visible image contains a thick cloud bank over the islands of Japan. In Figure 2, the land/ocean boundaries of the region are depicted, at both 10-minute (black) and 6-km resolution (white). Using the coarser-resolution data set, several regions along the coast are incorrectly identified as boxy clouds (Figure 3). This effect is considerably lessened when the finer 6-km resolution geography is used (Figure 4). This example of a SERCAA cloud analysis over Japan demonstrates the improvement in cloud detection that occurs due to the implementation of finer-resolution geography databases.

5. CONCLUSIONS

Higher-resolution background geography data sets are a necessary component of satellite cloud analysis. A 6-km global geography raster data set has been constructed at the Air Force Phillips Laboratory in support of the SERCAA cloud analysis project. Since the SERCAA algorithms have

been chosen as part of the current Cloud Depiction and Forecast System II (CDFS II) procurement at AFGWC, this geography data set will be used operationally. As the EOS remote sensing instruments go on-line, and as higher resolution mapping data are being made available, even higher-resolution data sets are being produced. Some of these, such as the 1-km land/water raster data set recently produced by USGS, have been implemented with SERCAA based algorithms and shown sufficient improvements to warrant further evaluation.

6. REFERENCES

1. Neu, T.J., R.G. Isaacs, G.B. Gustafson, and J.W. Snow, 1994: Improved Cloud Analysis for CDFS II through the SERCAA Research and Development Program. Preprints, Seventh Conference on Satellite Meteorology and Oceanography, AMS, Jun. 6-10, Monterey CA., 239-242.
2. Ackerman, S., 1995: MODIS Science Data Products - Cloud Mask (MOD35).
<http://cloud.ssec.wisc.edu/modis/cldmsk/cldmask.html>
3. Eidenshink, J.C. and J.L. Faundeen, 1994: The 1-km AVHRR Global Land Data Set: First Stages in Implementation. *Int. J. Rem. Sens.* 17, 3443-3462.
<http://sun1.cr.usgs.gov/landdaac/1KM/1kmhomepage.html>
4. Ward, J.M., D.C. Peduzzi, and C.B. Schaaf, 1994: Development of 6-km Global Geography and Terrain Elevation Databases for Satellite Cloud Analysis. Preprints, Seventh Conference on Satellite Meteorology and Oceanography, AMS, Jun. 6-10, Monterey CA., 452-454.



Figure 1: DMSP OLS visible image over Japan and Korea valid for 0807 UTC on May 24, 1993.

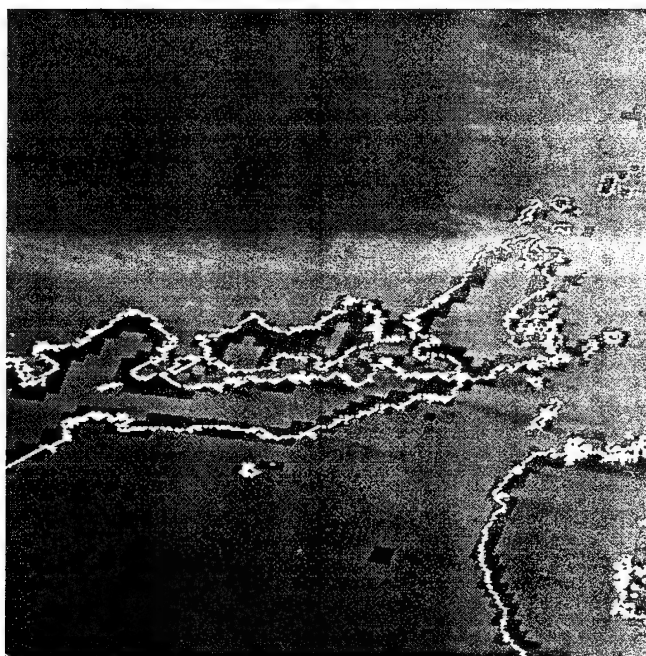


Figure 2: 10-minute (black) and 6-km (white) coastline flags for the image in **Figure 1**.

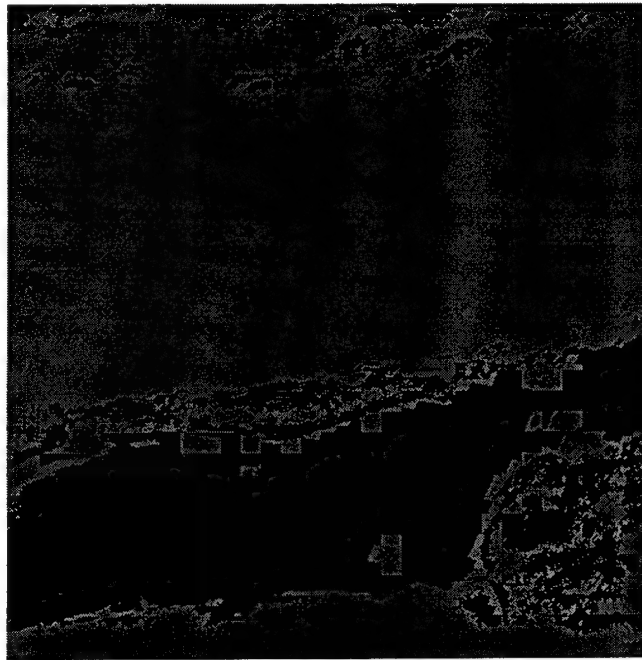


Figure 3: Cloud detection results for the image in **Figure 1** using the 10-minute geography database. Gray denotes cloudy pixels and black denotes clear pixels.

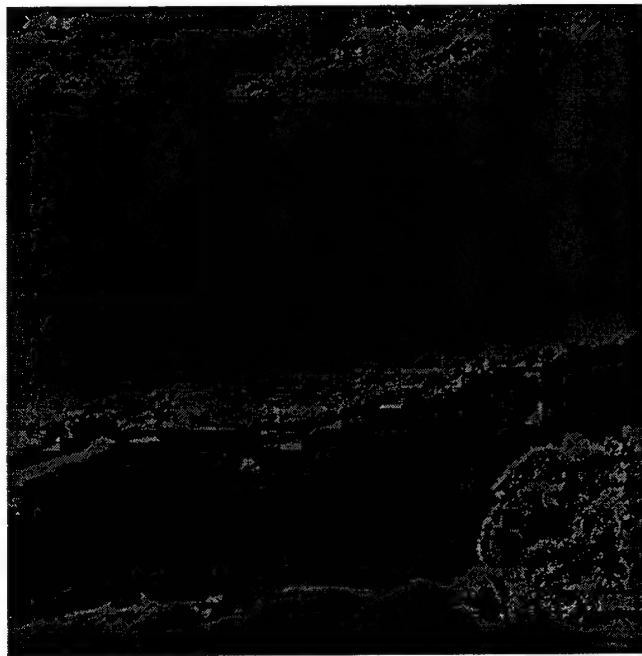


Figure 4: Cloud detection results for the image in **Figure 1** using the 6-km geography database. Note the improvement in the analysis near coastlines. Gray denotes cloudy pixels and black denotes clear pixels

SESSION IV:
MEASUREMENT SYSTEMS AND SENSORS

DETECTION AND RETRIEVAL OF CIRRUS CLOUD
SYSTEMS USING AVHRR DATA:
VERIFICATION BASED ON FIRE-II-IFO COMPOSITE MEASUREMENTS

K.N. Liou, S.C. Ou, N.X. Rao, and Y. Takano
University of Utah
Department of Meteorology/CARSS
Salt Lake City, Utah 84112

ABSTRACT

We have developed a detection scheme to identify single and multilayer cirrus cloud systems based on the physical properties of the AVHRR Chs. 1-2 reflectances and ratios, the brightness temperature differences between Chs. 4 and 5, and the Ch. 4 brightness temperatures. Clear pixels are first separated from cloudy pixels, which are then classified into three types: cirrus, cirrus/low cloud, and low cloud. This scheme has been applied to the NOAA satellite data collected over the FIRE-II-IFO area, Kansas, during nine overpasses within seven observation dates (November - December 1991). We have validated the detection results against the cloudy conditions inferred from the collocated and coincident ground-based lidar and radar images, balloon-borne replicator data, and NCAR-CLASS humidity soundings on a case-by-case basis. We show that the satellite detection results are consistent with the cloudy conditions inferred from these independent and complementary measurements. We have also modified our retrieval scheme for the determination of cirrus optical depth and ice crystal size in multilayer cirrus cloud systems. A case study using FIRE-II-IFO data is reported.

1. INTRODUCTION

Cirrus clouds have been recognized to play a key role in the global radiative energy balance and climate change (Liou 1986). Information on cirrus cloud parameters is critically important to the development of cirrus cloud formation models, the upgrade of real-time global cloud analyses, and the computation of atmospheric and surface radiative parameters in climate and general circulation models.

In recent years, our research group has developed a novel and comprehensive remote sensing algorithm for the retrieval of cirrus cloud temperature, optical depth, and mean effective ice crystal size using AVHRR data (Ou et al. 1993; Rao et al. 1995). Validation of this cirrus remote sensing program has been carried out using the local daytime satellite data collected during FIRE-I-IFO and FIRE-II-IFO (Rao et al. 1995; Ou et al. 1995a). A very important procedure in determining cirrus cloud parameters is the detection of the sky condition within the field-of-view of satellite radiometers. Our detection and retrieval schemes have been developed primarily for applications to single-layer cirrus clouds.

Surface observations show that multilayer clouds frequently occur in the frontal areas where cirrus clouds overlay boundary layer convective or stratus clouds. In this paper, we describe a numerical scheme for detecting multilayer cirrus pixels using AVHRR Chs. 1 ($0.63 \mu\text{m}$), 2 ($0.86 \mu\text{m}$), 4 ($10.9 \mu\text{m}$), and 5 ($12.0 \mu\text{m}$) data. Moreover, we also present a preliminary investigation for the retrieval of cirrus cloud optical depth and ice crystal size in multilayer cloudy conditions. Verifications of the detection as well as retrieval schemes utilize the composite data sources available from FIRE-II-IFO.

2. DETECTION AND RETRIEVAL OF MULTILAYER CIRRUS CONDITIONS

2.1 DETECTION

During daytime, with the availability of visible channel data, differentiation between clear and cloudy conditions over various types of surfaces can be made using the following criteria. First, the AVHRR Ch. 1 reflectance must be less than a threshold value as a necessary condition for the presence of clear pixels. Second, we can define a ratio $Q = r_2/r_1$, where r_2 and r_1 are reflectances for Chs. 2 and 1, and use two thresholds Q_1 and Q_2 , determined from the Q histograms, to identify cloudy and clear pixels over land and water surfaces, respectively. Third, the Ch. 4 brightness temperature for a clear pixel must be higher than that for a cloudy pixel so that a threshold temperature can be established for identification. Fourth, over clear regions, because of the behavior of Planck functions and atmospheric transmissions for Chs. 4 and 5 the brightness temperature difference is less than a prescribed value. We find that the preceding four criteria that use visible radiances and IR brightness temperatures are necessary and sufficient to identify the clear condition.

After all the cloudy pixels are identified, they are further classified into three classes: cirrus, cirrus/low cloud, and low cloud. First, we use the Ch. 4 brightness temperatures to detect optically thick cirrus clouds. Pixels with temperatures less than 233 K are identified as thick cirrus. Second, the visible-channel reflectances for low clouds are generally larger than those for cirrus clouds because the former are composed of water droplets with relatively small sizes and high number concentrations and are generally optically thicker than the latter (Liou 1992, Table 4.2). For this reason, a visible-channel threshold (~ 0.2) can be established to filter out those pixels that contain low clouds. Third, the Q -ratio for low clouds is usually smaller than the Q -ratio for cirrus clouds. For cirrus over land this ratio is larger than that for cirrus over low clouds. Moreover, the Q -ratio for cirrus over water is smaller than that for cirrus over low clouds. Thus, we can set threshold values to separate cirrus from either low cloud or cirrus/low cloud.

The preceding three criteria are used to separate single layer cirrus from cirrus/low cloud and low cloud alone conditions. Finally, we establish a threshold for the brightness temperature difference between Chs. 4 and 5 to differentiate the presence of nonblack cirrus overlapping low cloud and black low cloud. Moreover, the Ch. 4 brightness temperature can also be used to separate cirrus/low cloud and low cloud, because the latter temperature must be higher than about 253 K. More detailed descriptions of the detection scheme are presented in Ou et al. (1995b).

2.2 PRELIMINARY RETRIEVAL

Retrieval of the cirrus cloud optical depth and ice crystal size in multilayer cirrus condition using the AVHRR 0.63, 3.7, and 10.9 μm channels follows the numerical procedures developed by Ou et al. (1993), Rao et al. (1995), and Ou et al. (1995a). In brief, the 3.7 and 10.9 μm thermal radiances are used to retrieve the cloud temperature and emissivity from which the ice crystal size and optical depth can be determined on the basis of cloud microphysics and radiative transfer parameterizations. Removal of the solar component in the 3.7 μm radiance for applications to daytime satellite data is then made by correlating the 3.7 μm (solar) and 0.63 μm reflectances. The numerical scheme is primarily developed for single cirrus cloud systems. Validation of the algorithm has been performed by using various datasets that were collected during FIRE-II-IFO.

We have modified the preceding retrieval program to include the presence of low cloud. If its area coverage is larger than cirrus, then the upwelling radiances reaching the cirrus cloud base can be determined from the statistical histogram analyses similar to the single-layer cirrus case. The low cloud albedo can also be determined from the visible radiance for input to the removal-retrieval program developed by Rao et al. (1995). However, if both cirrus and low clouds have the

same coverage, information of the thermal upwelling radiances in the 3.7 and 10.9 μm channels as well as the low cloud albedo is unknown and must be assumed a priori. In this case, we use the climatological microphysics data for stratus to perform theoretical calculations to obtain the required inputs in retrieving the cirrus optical depth and ice crystal size. We can then compute the visible radiances at the top of the atmosphere and compare with observed radiances to assess the reliability of the calculated optical depth for low cloud. Subsequently, iterations can be developed to derive a consistent set of optical depths for both cirrus and low clouds.

3. VALIDATION OF THE DETECTION AND RETRIEVAL SCHEMES USING FIRE-II-IFO DATA

The FIRE-II-IFO was carried out near Coffeyville, Kansas, during November and December 1991. There were a number of dates during which multilayer cloudy conditions occur. For the detection of cirrus cloud pixels, the high-resolution (HRPT) AVHRR data from NOAA-11 and NOAA-12 polar-orbiting satellites are used. We have acquired ground-based lidar and radar images, balloon-borne replicator data, and NCAR-CLASS humidity soundings on a case-by-case basis. From the available datasets, we have selected seven representative dates (nine overpasses) for our study, including clear, cirrus, and cirrus/low cloud conditions. For each case, we compare cloud types identified from satellite radiances with those derived from ground-based composite instruments.

Table 1 summarizes the results of the comparisons. Columns 2-6 list the required parameters for numerical processing determined from satellite data, while columns 7-11 depict cloudy conditions obtained from satellite data and various ground-based and in situ instruments. Overall, the satellite detection scheme successfully differentiates among clear (12/6b), cirrus (11/26b and 12/5b), and cirrus/low cloud conditions. These results are consistent with the cloudy conditions identified from the independent and complementary ground-based measurements.

We have selected the cirrus/low case that occurred on 29 November 1991 for testing the retrieval scheme. Figure 1(a) displays the temperature and relative humidity profiles obtained from the NCAR-CLASS sounding launched at 1343 UTC. The cirrus cloud base and top heights derived from the replicator, PSU 94 GHz cloud radar, and visible lidar are ~ 6 (-20°C) and 9 km (-41°C), respectively. A moist layer roughly corresponding to the cirrus cloud layer is evident. Moreover, another moist layer ($\text{RH} > 90\%$) existed between ~ 1 and 2 km, corresponding to a low-level cloud layer detected by the PSU radar. Temperature inversion occurred at the low-level cloud top and near the peak of the relative humidity around 7 km. The mean retrieved cloud temperature is 233 K, which is the average of 62 pixels within the $0.1^\circ \times 0.1^\circ$ area. The standard deviation is 5.8 K, indicating that cloud temperatures were not uniform within the retrieval domain. Moreover, the mean cloud height determined from the temperature sounding is 9.2 km, which is near the cloud top.

On 29 November 1991, there were only three levels of replicator measurements available. At 9.13 km, ice particles are composed of bullet rosettes, columns, and irregular crystals with the maximum dimensions ranging from 25 to 425 μm . The size distribution peaks at 75 μm with a number concentration of $0.24\text{ L}^{-1}\mu\text{m}^{-1}$. At 8.18 km, the ice crystal size distribution is similar to that at 9.13 km. However, the upper limit of the measured sizes increases to 575 μm . The size distribution also peaks at 75 μm , but with a smaller value of number concentration of $0.1\text{ L}^{-1}\mu\text{m}^{-1}$. The level at 7.46 km corresponds to a local peak in the relative humidity profile. The size distribution with an upper limit of 875 μm is broader than the previous two. The ice crystal shapes include bullet rosettes and aggregates. The derived mean effective sizes for these three levels are 96, 116, and 146 μm from top to bottom. The vertically averaged mean effective ice crystal size is 134.6 μm (solid vertical bar in Fig. 1b). The retrieved mean effective size from satellite radiances is

130.9 μm . On the bottom scale are shown the replicator derived and the satellite retrieved optical depths, which are 2.21 and 2.44, respectively.

We are in the process of improving and refining the retrieval program for the determination of cirrus optical depth and mean ice crystal size. More comprehensive analyses and validations will be reported in the future.

4. ACKNOWLEDGEMENTS

This work was supported by the Air Force Geophysics Directorate Contract F19628-95-K-002 and NASA Grants NAG5-1050 and NAG1-1719.

REFERENCES

- Liou, K.N., 1986: Influence of cirrus clouds on weather and climate processes: A global perspective. Mon. Wea. Rev., 114, 1167-1199.
- Liou, K.N., 1992: Radiation and Cloud Processes in the Atmosphere: Theory, Observation, and Modeling. Oxford University Press, New York, 487 pp.
- Ou, S.C., K.N. Liou, W.M. Gooch, and Y. Takano, 1993: Remote sensing of cirrus cloud parameters using advanced very-high resolution radiometer 3.7 and 10.9 μm channels. Appl. Opt., 32, 2171-2180.
- Ou, S.C., K.N. Liou, Y. Takano, et al., 1995a: Remote sounding of cirrus cloud optical depths and ice crystal sizes from AVHRR data: Verification using FIRE-II-IFO measurements. J. Atmos. Sci., FIRE-II Special Issue (accepted and in press).
- Ou, S.C., K.N. Liou, and B. Baum, 1995b: Detection of multilayer cirrus cloud systems using AVHRR data: Verification based on FIRE-II-IFO composite measurements. J. Appl. Meteor., (accepted and in press).
- Rao, N.X., S.C. Ou, and K.N. Liou, 1995: Removal of the solar component in AVHRR 3.7 μm radiances for the retrieval of cirrus cloud parameters. J. Appl. Meteor., 34, 482-499.

Table 1. Results of the satellite-based cloud detection compared with ground-based radar, lidar, and balloon-borne replicator measurements.

r_1 : Ch. 1 reflectance
 Q : Ratio of Ch. 2 to Ch. 1 radiances
 BT45: Brightness temperature difference between Ch. 4 and Ch. 5
 T_4 : Ch. 4 brightness temperature
 a: NOAA-12 overpass (~ 1400 UTC)
 b: NOAA-11 overpass (~ 2100 UTC)

Date	number of pixels	Parameter Values				Cloudy Condition				
		$r_1(\%)$	Q	BT45(K)	$T_4(K)$	satellite	PSU radar	ETL lidar*	LaRc lidar*	soundings
12/6b	117	12.1	1.22	0.92	287.0	clear	clear	clear	clear	---/dry
12/5b	89	32.1	1.07	3.04	249.4	cirrus	cirrus	cirrus	cirrus	ice/dry
11/26b	79	24.2	1.10	2.73	271.6	cirrus	cirrus	cirrus	cirrus	ice/dry
11/22a	93	57.7	0.91	0.46	244.7	ci/low	ci/low	cirrus	cirrus	ice/low
11/29a	52	45.6	0.89	1.18	249.7	ci/low	ci/low	---	---	ice/low
11/28a	100	23.8	0.91	2.09	272.1	ci/low	ci/low	cirrus	cirrus	ice'/low
11/28b	85	20.0	1.04	1.77	284.2	cirrus	cirrus	cirrus	cirrus	ice'/dry
11/27a@	5200	44.5	0.91	0.80	246.0	ci/low	ci/low	---	---	---/low
11/27b	67	63.5	0.93	3.74	262.7	ci/low	ci/low	---	---	---/low

- *: Both ETL lidar and LaRc lidar measured signals from the backscattering of boundary layer aerosols and low cloud particles. These signals were not included in the images analyzed in this study.
 +: Based on replicator measurements between the two satellite overpasses.
 @: Satellite cloud detection results are based on data over $1.0^\circ \times 1.0^\circ$ area around 38.5° N, 96.5° W.

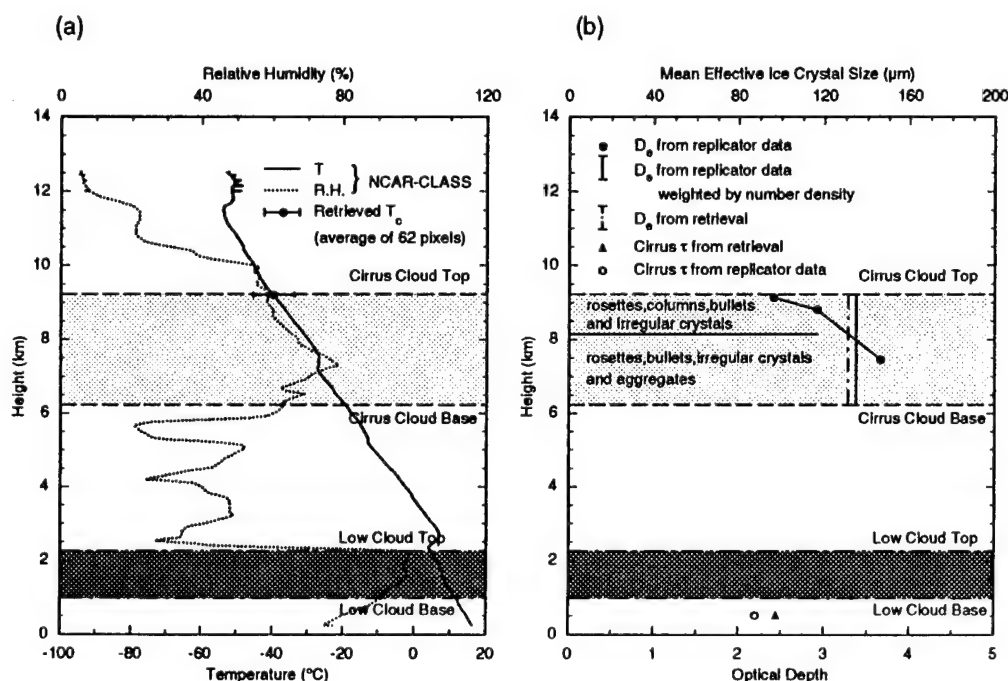


Figure 1. (a) Cloud base and top heights for cirrus and stratus determined from lidar, radar and sounding data, as well as temperature and humidity profiles obtained from the NCAR CLASS sounding system at 1343 UTC, 29 November 1991. Overlapped with the temperature profile are the mean retrieved cirrus cloud temperature over $0.1^\circ \times 0.1^\circ$ domain around Coffeyville, Kansas, and (b) Display of the replicator-derived mean effective ice crystal size at selected height levels, their vertical average, and the retrieved value. Also shown on the bottom scale are the optical depths derived from the replicator data and from the retrieval.

Analysis of Test Results from a Mobile Profiling System

James Cogan and Edward Measure
Army Research Laboratory
White Sands Missile Range, NM 88002-5501

1. INTRODUCTION

A mobile profiling system capable of probing the atmosphere from the surface to over 30 km was developed by the Battlefield Environment Directorate of the Army Research Laboratory and the Environmental Technology Laboratory of the Environmental Research Laboratories, National Oceanic and Atmospheric Administration. The present version of the Mobile Profiling System (MPS) combines ground based instruments, including a five beam 924 MHz radar wind profiler, a Radio Acoustic Sounding System (RASS), and two passive microwave sounders (virtual temperature and moisture parameters, respectively), with a receiver and processor for meteorological satellites. Software in the MPS produces profiles from the surface to the highest satellite sounding level by combining profiles generated from the suite of ground based sensors with those from a meteorological satellite. The MPS has operated successfully in different climates, including operations during the Los Angeles Free Radical Experiment (LAFRE) in Claremont, CA, and tests at White Sands Missile Range (WSMR), NM, Erie, CO, Ft. Sill, OK, and Wallops Island, VA.

The MPS has certain common elements with fixed site systems described by Parsons et al (1994) and Stokes and Schwartz (1994), but has a number of additional features as well as software for processing and quality control of data from the ground based sensors, and for combining satellite soundings with ground based profiles. Wolfe et al (1995) provide details on the MPS as configured and operated during the LAFRE and present examples of the various data processing and output available. Cogan (1995) presents additional samples of output and gives preliminary quantitative results.

2. ANALYSIS

The MPS produces graphical and ASCII output in a variety of formats. A number of programs produce text output describing, for example, comparison of profiler and rawinsonde output for individual sounding pairs and by atmospheric layer for a series of sounding pairs. Various meteorological messages may be produced in real time or from archived data (e.g., WMO format) for display or input to mesoscale models via land line or satellite link. Much of the ASCII and other output may be displayed in graphical form as shown in Wolfe et al (1995) and Cogan (1995). In the current configuration the MPS can generate a sounding every 3 to 4 minutes with a minimum vertical resolution of 100 m (60 m resolution possible with minor changes). With the further addition of the radiometer the system can produce virtual temperature (T_v) soundings with a vertical resolution of 30 m in the lowest kilometer. Table 1 from Cogan and Wolfe (1995) shows T_v accuracies from the LAFRE where period refers to the Julian day for 1993, and layers to the number of data layers. There were a maximum of 36 comparison pairs for the first period (7-11 Sep 1993) and a maximum of 12 for the second (17-23 Sep 1993).

TABLE 1. Average means and standard deviations of T_v differences (K) for 300 m layers (merged sounding relative to rawinsonde).

Mean	Std Dev	Layers	Period
-0.18	1.37	20	250-254
0.38	1.16	23	260-266

Two separate radiometer systems, one designed and built by the Jet Propulsion Laboratory of CalTech, and the other designed and built by Ophir Corporation, were in use for the Wallops Island test. Each measured brightness temperatures in both the Oxygen complex from 50-60 GHz and near the water line at 22.235

GHz, although there were extensive differences in system design and choice of specific frequencies measured. Results from the two radiometers were compared to a simultaneous radiosonde observation. Each system incorporated a separate surface sensor package.

Preliminary results indicate that the separate surface sensor suites gave very different answers for the surface temperature. This may be in part due to the slightly different siting of the instruments, but clearly contaminates the comparisons, since the retrieved radiometer temperature depend on the surface values.

TABLE 2. Root Mean Square (RMS) of T_v (K) for the ARL (PMTP) and Ophir radiometer (NGR). Height is in meters AGL.

Height	PMTP	NGR
4	1.1	2.0
34	2.4	1.7
65	1.2	2.9
95	0.8	2.7
156	0.7	1.6
216	0.8	0.7
307	0.9	0.8
459	1.1	1.2
762	2.4	0.8
1216	3.9	1.1
1823	4.5	3.0
3034	6.5	5.5
4549	5.0	6.2

For wind speed the results were not as close for the same periods, location, and maximum number of comparisons as shown in table 3.

TABLE 3. Average means and standard deviations of wind speed differences (ms^{-1}) for 300 m layers (merged vs. rawinsonde). From Cogan and Wolfe (1995).

Mean	Std Dev	Layers	Period
3.78	3.89	20	250-254
4.43	2.80	17	260-266

However, as shown in table 4, most of the difference between merged sounding and rawinsonde arose from the satellite wind

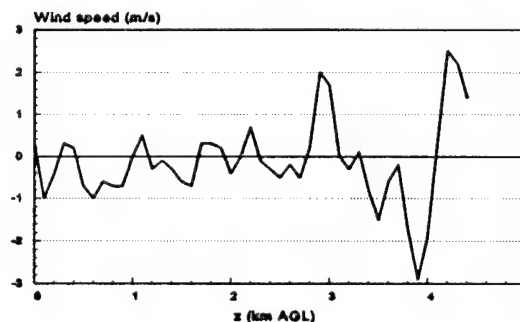
estimates. As noted by Miers, et al (1992) in a fairly comprehensive review, geostrophic wind estimates using satellite data differ on average from actual measurements by rawinsondes by ± 4 to 14 ms^{-1} . In table 4 the satellite values were modified at the lowest 3 satellite layers by the method noted in Cogan (1995).

TABLE 4. Average means and standard deviations (Std Dev) of wind speed differences (ms^{-1}) for 300 m layers (indicated sensor vs. rawinsonde). From Cogan and Wolfe (1995).

Radar Profiler / Satellite			
Mean	Std Dev	Layers	Period
0.75/10.84	1.88/8.60	14/6	250-254
1.53/8.61	2.75/2.88	11/6	260-266

The "error" in profiler data relative to the rawinsonde may arise, for example, from differences between measurement techniques (volume vs. running average along a line, respectively), assumptions in the profiler algorithms (e.g., uniform flow in a volume ≥ 100 m thick and a few km in diameter at 5 km), instrument errors in the profiler, and errors in the rawinsonde relative to the true wind velocity. At the LAFRE two rawinsonde systems received data from one sonde. The comparison between output from these two systems, Cross-chain Loran Atmospheric Sounding System (CLASS) and Marwin, gives a rough estimate of data processing differences. These differences are not meant to suggest which processing technique is "better." Figure 1 from Cogan and Wolfe (1995) presents differences in wind speed for one ascent on 9 September 1993. The rawinsonde transmitter was cut off near 4.5 km.

Figure 1. Wind speed difference (ms^{-1}) between CLASS and Marwin tracking the same sonde.



The roughly periodic pattern is not unusual in other data examined to date. The large differences near and above 3 km are on the high side, but values around $\pm 1 \text{ ms}^{-1}$ are not uncommon. This type of comparison suggests that standard deviations of profiler wind around $\pm 1 \text{ ms}^{-1}$ relative to rawinsonde may be close to the "best" one could expect. Differences in T_v from comparisons using one sonde averaged around ± 0.2 to 0.4 K with maximum differences of about $\pm 1 \text{ K}$. The "least" difference to be expected from a comparison with RASS or other sensors may, therefore, be around the aforementioned average value.

4. CONCLUSION

The MPS is a mobile system that combines the capabilities of several types of sensing systems to provide atmospheric soundings with a rapid refresh rate that greatly reduces error caused by time staleness. The MPS can generate input for the rapid update of models, analyses, and forecasts. The ability of the ground based instruments in the MPS to generate a picture of very short patterns and changes in atmospheric variables in the lower troposphere can lead to a better understanding of the atmosphere and better modeling at smaller scales. Future work aims to reduce the size of the MPS to a shelter carried on a standard pick-up truck plus a trailer, co-locate the radar and RASS antenna, combine the two ground based radiometers in one smaller but more capable unit, and upgrade the processing software.

5. REFERENCES

Cogan, J. (1995). Test results from a Mobile Profiler System, *Meteor. Appl.*, in press.

Cogan, J., and D. Wolfe (1995). The Mobile Profiler: Data Analysis and Display. *27th Conf. On Radar Meteorology*. Amer. Meteor. Soc., Vail, CO, in press.

Miers, B., J. Cogan, and R. Szymler (1992). *A Review of Selected Remote Sensor Measurements of Temperature, Wind, and Moisture, and Comparison to Rawinsonde Measurements*. ASL-TR-0315, Army Atmospheric Sciences Laboratory, 41 pp.

Parsons, D., W. Dabberdt, H. Cole, T. Hock, C. Martin, A. Barrett, E. Miller, M. Spowart, M. Howard, W. Ecklund, D. Carter, K. Gage, and J. Wilson (1994). The integrated sounding system: description and preliminary observations from TOGA COARE. *Bull. Amer. Meteor. Soc.*, **75**: 553-567.

Stokes, G. M., and S. E. Schwartz (1994). The atmospheric radiation measurement (ARM) program: programmatic background and design of the cloud and radiation testbed. *Bull. Amer. Meteor. Soc.*, **75**: 1201-1221.

Wolfe, D., B. Weber, D. Weurtz, D. Welsh, D. Merritt, S. King, R. Fritz, K. Moran, M. Simon, A. Simon, J. Cogan, D. Littell, and E. Measure (1995). An overview of the mobile profiler system (MPS): preliminary results from field tests during the Los Angeles free radical study, *Bull. Amer. Meteor. Soc.*, **76**, 523-534.

MULTI SPECTRAL PUSHBROOM IMAGING RADIOMETER (MPIR) FOR REMOTE SENSING CLOUD STUDIES

Gary S. Phipps and Carter L. Grotbeck
Sandia National Laboratories
P.O. Box 5800 MS0980
Albuquerque, New Mexico 87185-0980 USA
gsphipp@sandia.gov
(505) 845-8269

ABSTRACT

A Multi Spectral Pushbroom Imaging Radiometer (MPIR) has been developed as a well-calibrated, imaging radiometer for studies of cloud properties from an Unmanned Aerospace Vehicle (UAV) platform. The instrument is designed to fly at altitudes up to 20 km and produce data from nine spectral detector modules. Each module has its own telescope optics, linear detector array, spectral filter, and necessary electronics. Cryogenic cooling for the long-wavelength infrared modules as well as temperature regulation of the visible modules is provided by a liquid nitrogen system designed to operate the system for multi-day missions. Spectral channels are optimized to obtain maximum information about cloud physical and micro-physical properties, as well as reflected and radiated energy. Pre- and post-flight calibration, combined with an on-board calibration chopper provide an instrument with state-of-the-art radiometric measurement accuracies. Each module has a $\pm 40^\circ$ across-track field-of-view and images a curved footprint onto its linear detector array. The long-wavelength array types have 256 detector elements while the short-wavelength arrays can have 512 elements. All are co-aligned so that they view the same object space. The nine telescopes provide a modular design allowing individual spectral bands to be changed to match the requirements for a particular mission.

1. INTRODUCTION

A Multi Spectral Pushbroom Imaging Radiometer (MPIR) has been developed as a relatively inexpensive (~\$1M/copy), well-calibrated, imaging radiometer for aircraft studies of cloud properties. The instrument is designed to fly on an Unmanned Aerospace Vehicle (UAV) platform at altitudes from the surface up to 20 km. MPIR is being developed to support the Unmanned Aerospace Vehicle portion of the Department of Energy's Atmospheric Radiation Measurements program (ARM/UAV). Radiation-cloud interactions are the dominant uncertainty in the current General Circulation Models used for atmospheric climate studies. Reduction of this uncertainty is a top scientific priority of the US Global Change Research Program and the ARM program. While the DOE's ARM program measures a number of parameters from the ground-based Clouds and Radiation Testbed sites, it was recognized from the outset that other key parameters are best measured by sustained airborne data taking. These measurements are critical in our understanding of global change issues as well as for improved atmospheric and near space weather forecasting applications.

2. OPTICAL DESIGN

MPIR requires that a $\pm 40^\circ$ across-track field-of-view be imaged onto a 25.6 mm-long linear detector array. The forward motion of the UAV provides the 'pushbroom' motion to form a two-dimensional image of

the scene as depicted in Figure 1. Each spectral band has its own detector with separate optics, detectors, and electronics packaged as an interchangeable module. Co-registration is provided by aligning all modules so that they image the same scene footprint. The all-reflective optics design chosen is a derivative of WALRUS² which provides the needed wide field-of-view in a compact design. The optical elements are rotationally symmetric allowing the aspheric surfaces to be manufactured by a relatively inexpensive diamond turning process. All of the mirrors were diamond turned, nickel plated, diamond turned a second time, and post polished under interferometric control. Optical surface coatings are silver for the shortest wavelengths and gold for the infrared. The design has several interesting optical features. The pupil size increases with off axis distance, an effect that helps to counteract the natural cosine falloff. The barrel distortion in the image plane has multiple consequences: The instantaneous field-of-view (IFOV) in the scene changes as a function of field position in a manner that helps compensate for the normal IFOV variations expected from a comparable whiskbroom imager. Also, since image magnification varies laterally, by adjusting the position of the linear array the magnification in the image can be exactly matched to the specific array being used. One disadvantage is that for a linear detector array, the distortion results in a curved footprint in the cross track direction, a pixel at the edge of the field (+40° degrees off-axis) has an along track angular displacement of 11.4°. The image reconstruction process must re-map the curved lines onto a Cartesian grid.

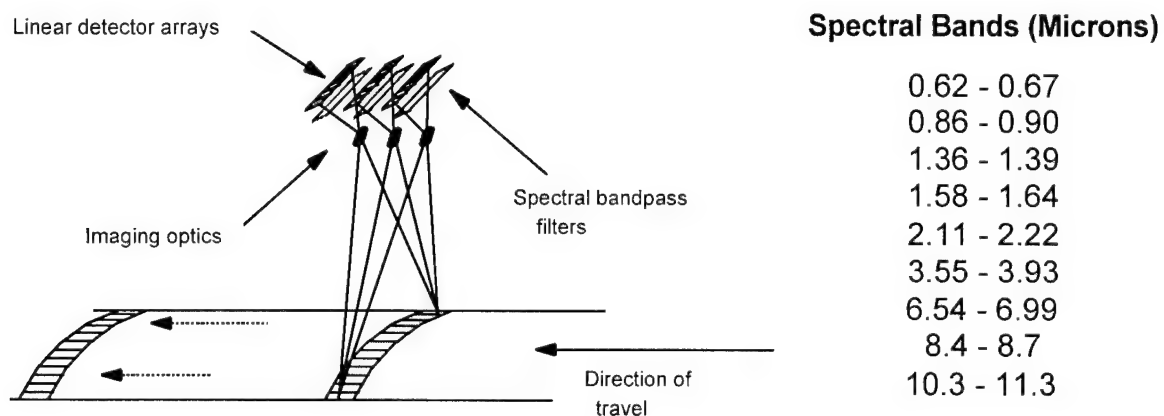


Figure 1. Schematic of Coincident, Spectral Imaging Using the MPIR Instrument

3. MECHANICAL DESIGN

The major components of a detector module are illustrated in Figure 2. The diamond-turned mirrors have a common axis of symmetry tilted by 55° from the center of the field-of-view. The system is f/3.5, with a 5 mm on-axis entrance pupil diameter and is nearly telecentric in image space allowing the interference filters to operate at near normal incidence over the entire FOV. At visible wavelengths the 50 µm detector element spacing was determined by geometric aberrations: 86% of the energy from a visible, collimated input beam is contained within a 50 µm square. The long-wavelength pixel size of 100 µm was chosen to match the diffraction limited performance: at 11 microns 85% of the energy falls within a 100 µm-square pixel. Spectral bands between 0.4 and 12 microns are defined by internal, cooled interference filters used with one of the four different detector module types: Silicon, InGaAs, InSb, and HgCdTe. The cooling system allows each module to be individually and optimally controlled at any temperature from room temperature to 80K. High emissivity chopper blades coated with Orlando Black³ are used to provide a dark reference for the short wavelength channels and a calibration reference for the thermal channels. The chopper blades are mounted on a torsionally-suspended, momentum-compensated structure driven at its 4 Hz resonate frequency. Each module views and measures its own chopper blade every 0.25 seconds. The temperature of each thermally isolated blade is precisely measured and is used as an on-board blackbody calibration source for the infrared channels. This on-board calibration update in conjunction with extensive pre- and post-flight ground and

laboratory calibration⁴ is used to achieve the radiometric accuracy design goals of 1% in the infrared and 3% in the visible wavelengths. A goal of the mechanical design was to allow interchangeability between the modules. Diamond turning of all critical surfaces within each module allowed for a mechanical "bolt-together" optics alignment while attention to mechanical detail during assembly allows for fully interchangeable modules.

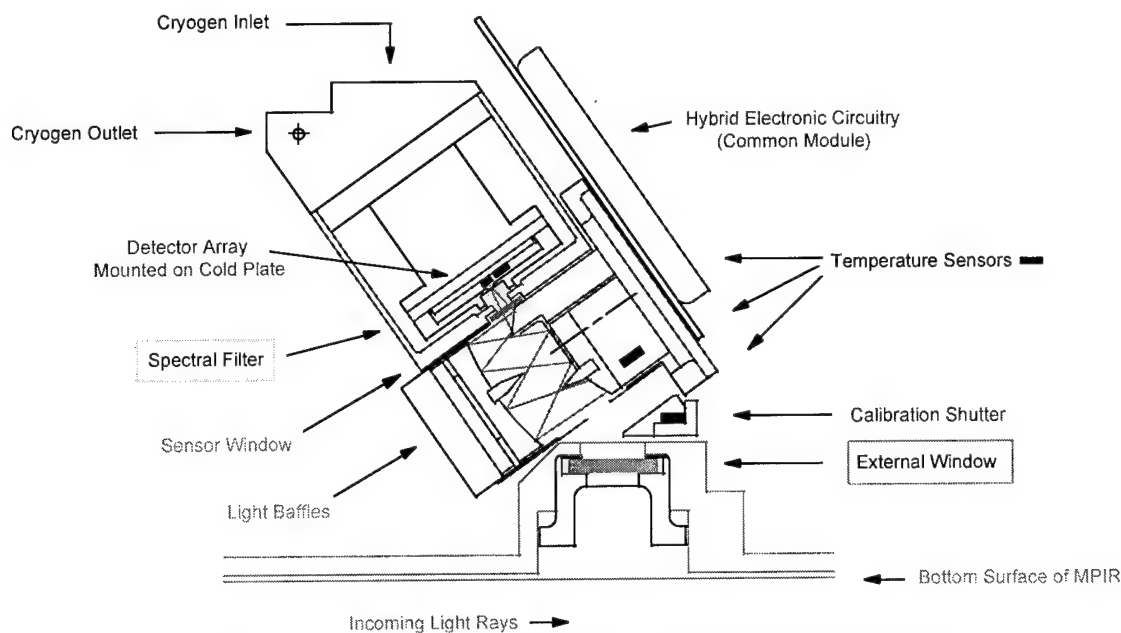


Figure 2. Internal Details of an MPIR Detector Module

The down-looking optical modules, associated electronics, and cooling hardware are included in the MPIR chassis illustrated in Figure 3 (the external LN₂ storage dewar is not shown). The amount of required LN₂ storage depends upon the mission length and type of modules flown. The 80K infrared modules require more cooling, and thus a larger supply of LN₂, than do the warmer visible modules. The standard five liter dewar is designed to operate MPIR for a 48-hour mission with the standard complement of infrared modules. Total power consumption is 50 watts; main box weight is 30 kg. A filled, five liter storage dewar adds an additional 8 kg.

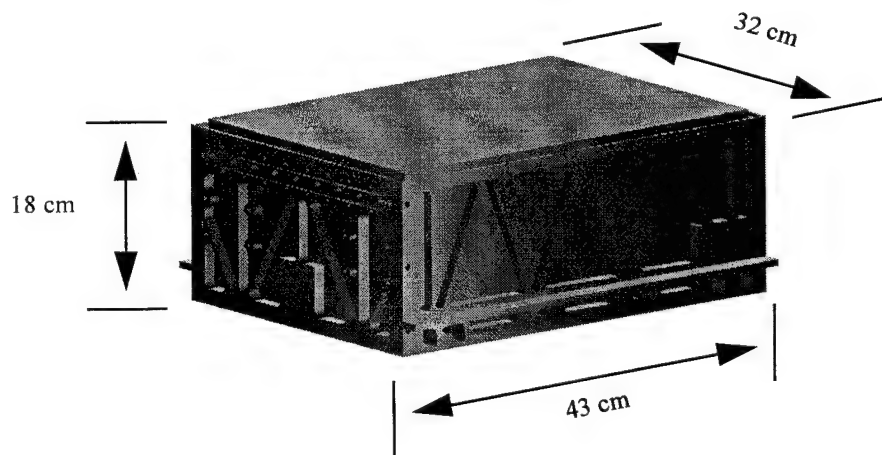


Figure 3. The 9-Channel MPIR Instrument

4. DATA ISSUES

Each module has its own microprocessor controlled 'array specific' board with signal conditioning, detector read electronics, 12-bit digitization, and data communications capabilities. A main processor communicates with each module via a serial data link. The main processor controls all data queuing and communications, collecting sensor and temperature data for all nine modules, and combining it all into an 80 kbit/second serial data stream. The final serial data is telemetered to a ground receiving station for storage and later data analysis. The nine spectral bands have been chosen to answer questions about tropospheric clouds, provide a means for energy balance measurements, and also potentially allow re-calibration of presently used satellite sensors. A list of the spectral bands with the derived data products includes:

λ in μm	Extracted Data Products
0.62 - 0.67	Cloud identification, amount, thickness, particle size, and phase. Ground reflectance.
0.86 - 0.90	Cloud identification and amount, Ground reflectance.
1.36 - 1.39	Upper tropospheric water vapor, daytime cirrus detection.
1.58 - 1.64	Cloud microphysics and phase.
2.11 - 2.22	Cloud particle size, and phase.
3.55 - 3.93	Cloud particle size, microphysics, and phase.
6.54 - 6.99	Cloud top temperature and (indirectly) height of cloud tops
8.40 - 8.70	Cloud identification and amount, nighttime cirrus, cloud and surface temperatures
10.3 - 11.3	Cloud identification and amount, nighttime cirrus, cloud and surface temperatures

5. CONCLUSIONS

MPIR is a relatively inexpensive radiometric imager capable of collecting accurate data in nine simultaneous wavelength bands over the range of 0.4-12 μm . Each detector module has its own detector array, filter, reflective optics, and electronics making a highly modular design that can be reconfigured for the differing optimum detection wavelengths necessary for a particular task: cloud radiometry, crop assessment, detection of environmental contamination, satellite calibration, etc.

6. ACKNOWLEDGMENTS

MPIR is being developed for the DOE's ARM/UAV program with funding from the Strategic Environment Research and Development Program under direction of the ARM/UAV Technical Director, Dr. John Vitko, Sandia National Laboratories/California, Department 8102.

7. REFERENCES

1. Atmospheric Radiation Measurement Program Plan, February 1990, U.S. Department of Energy, Office of Energy Research, Office of Health and Environmental Research, DOE/ER-0441
2. U. S. Patent # 4,598,981 (1986)
3. A proprietary, ultra-black, dendritic copper coating produced by Lockheed Martin Corp., Orlando, FL.
4. Radiometric ground calibration of MPIR and other ARM/UAV instruments is being performed by NIS-2, Los Alamos National Laboratory, Los Alamos, NM.

A BRIEF DESCRIPTION OF AIRMS

William S. Helliwell, John R. Norris, and Betty Rodriguez-Cottle
Science Applications International Corporation
San Diego, California, 92121, USA

ABSTRACT

AIRMS (Airborne InfraRed Measurement System) incorporates a 24 inch aperture infrared sensor on a modified Boeing 720B. Operating altitudes are up to 42000 feet. The sensor and electronics were built by Hughes Aircraft Company, El Segundo, CA. ARPA selected AIRMS to collect infrared signature and cloud data to support the Air Defense Initiative program. SAIC was selected to oversee the flight planning, data collection, sensor characterization, and data analysis. This paper gives a brief description of the AIRMS hardware and summarizes the results of the characterization effort. The system is operating at or better than all specifications. A complete list of all flights and data collected to date is included.

1. INTRODUCTION

As part of the Air Defense Initiative (ADI) program, the Advanced Research Projects Agency (ARPA) is investigating the feasibility of applying infrared imaging technology for future air defense needs. This includes the long range detection and tracking of aircraft and tactical missiles. An advanced infrared imaging sensor was built by Hughes Aircraft Company in El Segundo, CA. It was installed on a modified Boeing 720B. The Airborne InfraRed Measurement System (AIRMS) was selected by ARPA to collect various types and combinations of cloud, sky, ocean, terrain, and target imagery. AIRMS has been in operation since November of 1993 and has made close to 50 flights.

1.1 AIRMS HARDWARE DESCRIPTION

The sensor description is summarized in table 1. The sensor and aircraft are shown in figure 1. More information is contained in reference 1.

TABLE 1. SENSOR DESCRIPTION

Optics		Detector	
aperture diameter	24 inches	type	extrinsic Si:Ga
telescope effective focal length	75 inches	geometry	4 horiz. in time delay integrate, 1500 vert.
IR spectral bands (selected by filter wheel)	1: 8.2 - 9.3 μm	instantaneous field of view	16 x 16 μ radians
	2: 10.0 - 12.2 μm		
	3: 3.5 - 4.4 μm		
	4: 8.2 - 12.2 μm	time between samples	32 μ sec @ 8.7 Hz
	5: 5.7 - 6.8 μm		
	6: 4.35 - 5.3 μm	sample integration time	28 μ sec @ 8.7 Hz
field of regard	+ -10 deg horizontal	fpa temperature	19 deg K
	+5 -10 deg vertical	filter temperature	100 deg K
Scan Mirror		Output Frame	
scan direction	horizontal	pixel size	8.4 x 8.4 μ radians
frame rates	14.7, 8.7, 5.0, 2.8, 1.4, 0.727, 0.366, 0.183, 0.092 Hz	size in pixels	2239 x 1500
		total field of view	1.1 x 0.72 deg



Figure 1. AIRMS Sensor Platform. Modified Boeing 720B aircraft.

1.2 SUMMARY OF AIRMS CHARACTERIZATION RESULTS

A list of key parameters is in table 2, both the spec value and the achieved value are shown.

TABLE 2. KEY PARAMETERS

	spec	achieved
mtf at 20 cy/millirad	0.2	0.25
absolute pointing (deg)	0.25	0.05
scan linearity (pixel)	<1	0.5
scan repeatability (drift μ rad/sec)	<2	0.2
intraframe jitter (pixel rms)	0.75	0.5
interframe jitter (pixel rms)	0.75	0.5
ner 8.2-12.2 at 8.7 Hz ($\text{w/m}^2\text{-sr-}\mu$)	0.03	0.02
calibration stability 1 hour (% of full scale)	<10	0.6

Calibration is done onboard the aircraft and can be redone by the analyst. There are three thermal reference sources (TRS) that can be imaged upon command from the operator.

Mtf, pointing and jitter were measured from images containing a hot plate installed at the top of Mammoth Mountain located in the Sierra Nevada Mountains, CA. An image is shown in figure 2. Other parameters were measured from various scene, TRS, and auxiliary data collected during flight.

The goal was to have no more than 1 defective pixel per frame. Even after two years of sensor operation this goal is still met. There are a few bad detector elements that the sensor ignores. In no case are four detector elements that contribute to one pixel all bad. The net result is that all pixels are valid samples of the scene and a few pixels have slightly higher sensor noise than all the rest.

A complete description of all parameters and sensor anomalies is given in reference 2.

1.3 LIST OF FLIGHTS AND DATA

As many as 6000 frames are collected during a flight. Cloud images are shown in figures 3-5. Table 3 contains a complete list of all flights and a brief description of the data collected to date.

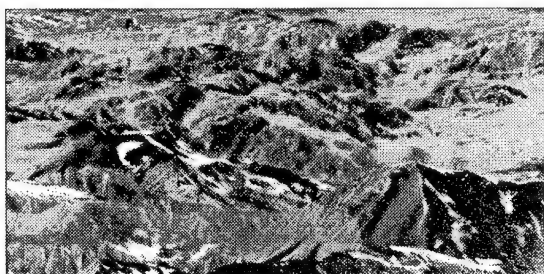


Figure 2. Flight 12 Mammoth mountain image.

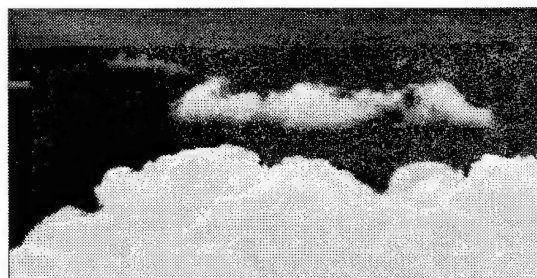


Figure 3. Flight 12 calibrated cloud image.

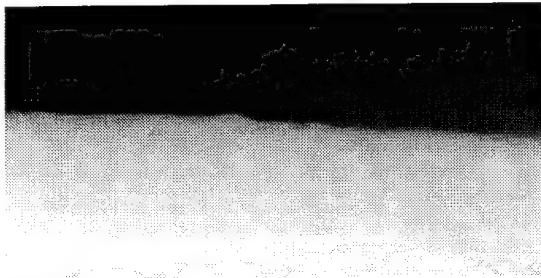


Figure 4. Flight 40 calibrated cloud image.

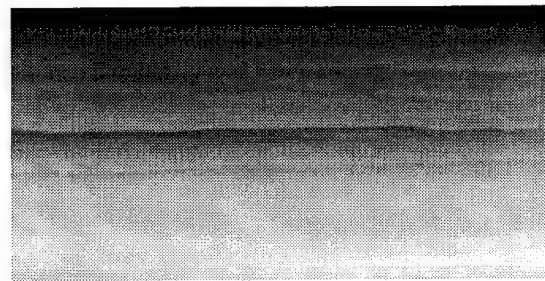


Figure 5. Flight 40 calibrated cloud image.

TABLE 3. AIRMS FLIGHTS

#	Date	Description	#	Date	Description
1	951129	Airworthiness	26	941211	Diablo Canyon, Clouds
2	931214	Airworthiness	27	950119	Mojave
3	940105	Sensor functional checkout	28	950202	ALCM, F-16, Terrain, Clouds
4	940119	Sensor functional checkout	29	950207	Terrain, Clouds
5	940225	Sensor functional checkout,	30	950221	Telescope Peak, Clouds, Sky
6	940315	Mammoth Mtn, Telescope Pk	31	950301	Clouds, Targets of opportunity
7	940329	Telescope Peak, Clouds/Sky	32	950302	Clouds, Wash. DC
8	940412	Telescope Peak, Clouds/Sky	33	950304	Clouds, Wallops, Aries Plume
9	940503	Mammoth Mtn, Telescope Pk	34	950305	Clouds
10	940517	Moon, Mojave, Clouds	35	950328	Passive Ranging, Desert
11	940507	Mammoth Mtn, GII B, Buoys	36		Special collection
12	940508	Mammoth Mtn, Clouds, Hill AFB	37		No imagery collected
13	940713	Mammoth Mtn, Cloud/Sky, Moon	38	950525	Mojave AFB, Clouds
14	940729	Mammoth Mtn, Clouds, GII, T-39	39	950614	GII, Clouds
15	940809	Mammoth Mtn, Clouds, GII, T-39	40	950615	GII, T-39, Clouds
16	940816	Clouds, F4G, F16C, Terrain	41	950711	GII, Clouds, Mtn Terrain
17	940823	Cruise Missile, Terrain, Sky	42	950712	Telescope Pk, GII, T-39, Clouds,
18	940909	Mammoth Mtn, T-39, Nellis AFB	43	950802	Mojave, Edwards AFB, Clouds
19	941006	Mountains, Sky, Diablo Canyon	44	950803	No imagery collected
20	941018	Mojave Hangar, Clouds	45	950815	GII, T-39, Clouds
21	941019	Ocean, Clouds, (Duck, NC)	46	950816	GII, T-39, Clouds, Mtn Terrain
22	941108	GII, T-38, T-39, Telescope Peak	47	950830	Fighter IRST emulation
23	941123	GII, T-38, T-39, F-16	48		
24	941205	Edwards AFB, Clouds	49		
25	941206	Vandenberg AFB, Clouds	50		

2. ACKNOWLEDGMENTS

This work was funded by ARPA. The program manager is Tom Wiener, ARPA-STO, 4001 N. Fairfax, Suite 410, Arlington, VA 22203, phone (703) 243-9830, fax (703) 524-2957, e-mail twiener@arpa.mil. For information about flights and data contact Stephen Farmer, NAWC, Code 472120D, China Lake, CA 93555, phone (619) 939-8297, fax (619) 939-0099, e-mail stephen.farmer@chinalake.navy.mil.

3. REFERENCES

1. AIRMS System Technical Description, Rev. A, GM Hughes Electronics Electro-Optical Systems Technical Report, 31 Oct. 1994.
2. Airborne Infrared Measurement System (AIRMS) Final Report, SAIC Technical Report, 30 Dec. 1994.

CLOUD PHENOMENOLOGY MEASURED FROM AIRMS DATA

William S. Helliwell, John R. Norris, and Betty Rodriguez-Cottle
Science Applications International Corporation
San Diego, California, 92121, USA

ABSTRACT

AIRMS (Airborne InfraRed Measurement System) consists of a 24 inch aperture gimbaled IR sensor mounted inside a modified Boeing 720B passenger jet aircraft. Sequences of 200 frames (23 seconds) at LW (8.2-12.2 microns) of two cloud types at different ranges and altitudes are analyzed. Two dimensional Fourier analysis is used to characterize the two spatial dimensions and the time dimension. The spatial power spectral density shape follows that of a Butterworth spectrum. Roll-off wavenumber and roll-off rate are estimated from the data. The temporal decorrelation is found to be a function of spatial wavenumber. The exponential form $\exp(-\alpha k^m t^n)$ is fit to the data where α , m , and n are parameters, k is spatial wavenumber, and t is time.

1. INTRODUCTION

AIRMS has been used to collect a variety of cloud data. Usually the aircraft operates at 12 km and so is looking down on clouds. This is in contrast to ground based IRAMMP data that looks up at clouds. Previous analysis of IRAMMP data (1) found that the spatial power spectral density of clouds followed a power law with exponent around 4. Temporal analysis found that high wavenumbers decorrelated faster than low wavenumbers, consistent with turbulence theory.

In this paper LW (8.2-12.2 m meter) imagery of two different cloud scenes are analyzed. For both data sets the frame rate was 8.7 Hz and 200 frames (23 seconds) were collected. Every tenth frame was used in the temporal analysis. The nature of the spatial and temporal structure is found to be similar to that found in the IRAMMP analysis, even though the viewing geometry is substantially different.

One set of images is of a cirrus cloud deck. This data was collected during flight 40 on 15 June 1995. From geometry the clouds are estimated to be at 10 km altitude and at a range of 160 km. A subset of the full field of view was selected. The first frame from the 200 frame sequence is shown in figure 1. The other set of images is of a cumulus cloud deck collected during flight 12 on 8 May 1994. These clouds are estimated to be at 6 km altitude and at a range of 150 km. The first frame of the subset selected for analysis is shown in figure 2.

1.1 SPATIAL ANALYSIS

The spatial analysis was done on a single frame. The two dimensional power spectral density (psd) was estimated using the Fourier transform squared. The spatial scales are estimated from the range to the clouds and the pixel size of 8.4 μ radians. For both scenes the cloud clutter power dropped below the sensor noise well before the sampling frequency of 0.38 cycles per meter. Contour plots of the middle portion of the spectra are shown in figures 3 and 4. It is clear that the cumulus cloud scene has significantly more structure than the cirrus scene, and some anisotropy is evident as well.

To investigate the cloud spectra the modulation transfer function (mtf) of the sensor is removed from the data. Cuts along the azimuth and elevation wavenumber axes are shown in figure 5 and 6. The sensor noise floor is easily seen in the cirrus scene psd cuts. The sensor noise floor just barely appears at the right side of the plots for the cumulus psd cuts. The fall off rate for the cumulus psd cuts is fairly constant, whereas the cirrus rate appears fast then slow. A Butterworth spectrum was fit to each of the

cuts, $P(k) = A / (1 + (k/k_0)^r)$ where k is one dimensional wavenumber. The parameters found are listed in table 1.

TABLE 1. SPATIAL PSD PARAMETERS

	A	k_0	r
cirrus			
azimuth	43.3	0.001	5.5
elevation	43.3	0.005	5.5
cumulus			
azimuth	13.4	0.002	3.0
elevation	13.4	0.006	3.5

The anisotropy is estimated from the observed offset between the elevation and azimuth psd cuts. For the cirrus scene it is about 5:1 and for the cumulus scene about 3:1. From grazing angle alone the aspect ratio is more than 30:1. The discrepancy is due to the fact that clouds are not opaque to LW.

1.2 TEMPORAL ANALYSIS

In order to avoid mixing up too different scales, a region only 32 pixels in elevation was extracted from the frames. Frames were registered to remove the apparent motion of the clouds. Two dimensional Fourier transforms were taken. Temporal correlation was estimated for small extents of wavenumbers. Small boxes were selected along the azimuth wavenumber axis only. Length scales can then be estimated from range and pixel size without having to involve grazing angle. The coherences obtained are plotted in figures 7 and 8. The wavenumber range over which coherences can reliably be calculated is limited for the cirrus data. Even so, the faster decorrelation of higher wavenumbers is seen. Shorter scales can be analyzed for the cumulus scene, going down to 20 meter wavelengths. For high wavenumbers and long separation times the calculated correlation is noisy and is not plotted.

An exponential was fit to the coherence, $C(k,t) = \exp(-\alpha k^m t^n)$. A simple turbulence model predicts $m=n=2$. The values found by curve fitting are listed in table 2. Not only do the estimated exponential values differ from the simple turbulence model predictions, but they differ between cloud types.

TABLE 2. TEMPORAL COHERENCE PARAMETERS

	α	m	n
cirrus	566.	2.0	0.5
cumulus	49.	1.5	1.0

2. CONCLUSIONS

It has been shown that data collected by AIRMS can be used to investigate temporal and spatial characteristics of clouds. At ranges around 160 km spatial scales down to 20 meters can be seen. Spatial structures follow a Butterworth spectral shape. Temporal analysis indicates that short wavelengths decorrelate much faster than long wavelengths. The mechanism for this does not appear to be turbulence only and uncovering it needs more analysis.

3. REFERENCES

1. Farber, M. S., Hemple, S. J., Eckstein, B. A., "Characterization of IRAMMP data using scene registration," Proc. IRIS Targets, Backgrounds and Discrimination, 1991, Vol. I.



Figure 1. AIRMS flight 40 cirrus image



Figure 2. AIRMS flight 12 cumulus image

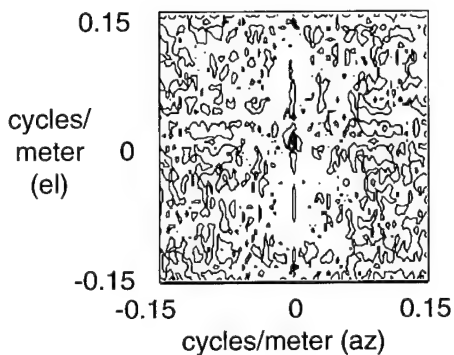


Figure 3. Cirrus image PSD (dB)

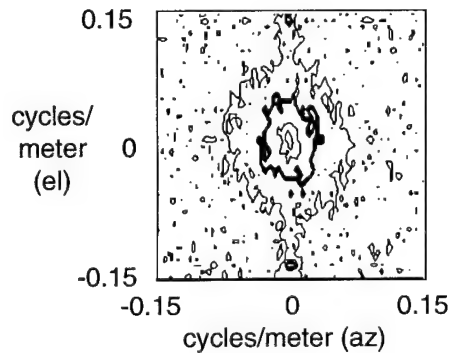


Figure 4. Cumulus image PSD (dB)

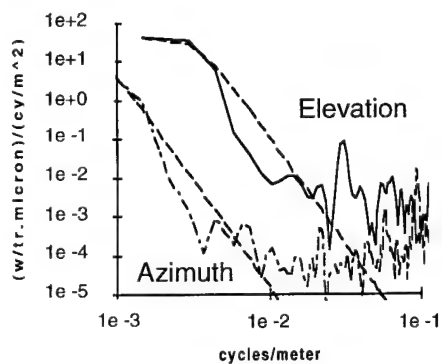


Figure 5. Cirrus image PSD cuts

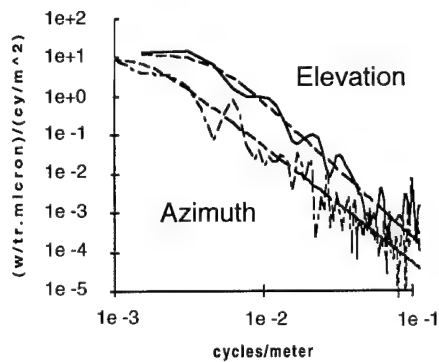


Figure 6. Cumulus image PSD cuts

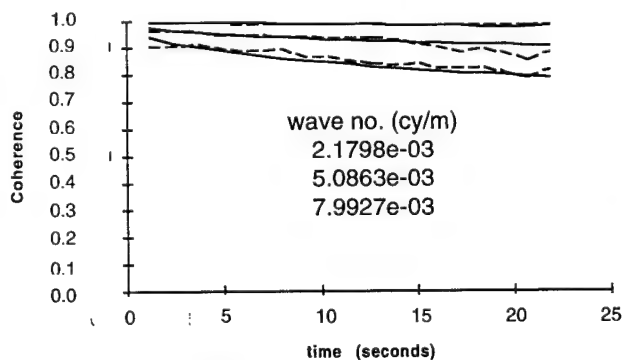


Figure 7. Cirrus image coherence

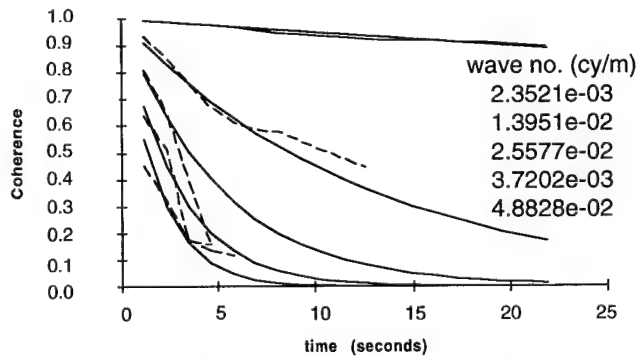


Figure 8. Cumulus image coherence

Cloud Radiative and Spatial Properties Using a Ground-Based Infrared All-Sky Imager

Robert P. d'Entremont, Ronald G. Isaacs,
Jean-Luc Moncet, and David B. Hogan
Remote Sensing Group
Atmospheric and Environmental Research, Inc.
840 Memorial Drive, Cambridge, MA 02139-3794

Comprehensive radiative transfer calculations were performed to establish the sensitivity of measured downwelling infrared radiances to cloud phase, cloud fraction, cloud base height, liquid water content, and mode radius of the cloud particle size distribution. The simulations are for middle-wavelength infrared (MWIR, 3-5 μm) and longwave infrared (LWIR, 8-13 μm) narrow-band and broad-band channels. Atmospheric properties including relevant gas absorption profiles and aerosol scattering extinction profiles drive the calculation of gas absorption as a function of altitude within the atmosphere. Aerosol properties are also accounted for. Analogous cloud properties are based on Mie scattering calculations using specified cloud-type-dependent modified gamma droplet size distributions for cloud particles. Estimation of cirrus optical properties is based on the parameterization of the cirrus particle size spectrum using ambient temperature and ice water content. These specification data are input to a discrete-ordinate-method (DOM) multiple-scattering radiative transfer program that computes scattering, absorption, and thermal emission in a vertically inhomogeneous, non-isothermal atmosphere. The adding-doubling DOM simultaneously accounts for gaseous, aerosol, and cloud optical properties.

Deterministic sensitivities were found to all parameters except liquid water content. Based on these sensitivity results, a prototype algorithm has been developed that retrieves the desired parameters from an infrared all-sky imager data stream by exploiting its spectral, angular, spatial, and temporal properties.

Results from this study can be used to define IR all-sky imager sensor attributes. An IR all-sky imaging system would have numerous applications for DoD line-of-sight operational and research needs, military and civilian flight safety, and surface-atmosphere radiation budget studies for climate modelers. IR all-sky imager data can also be used in conjunction with satellite overpasses to develop and verify models that retrieve cloud radiative properties from space-based platforms.

UPPER TROPOSPHERIC HUMIDITY DERIVED FROM SSM/T-2 MEASUREMENTS

Michael K. Griffin

*Phillips Laboratory, Geophysics Directorate
Hanscom AFB, MA 01731-3010 USA*

John D. Pickle

*Atmospheric and Environmental Research, Inc.
Cambridge, MA 02139 USA*

ABSTRACT

A procedure was developed to generate fields of upper tropospheric humidity from the 183 ± 1 GHz channel on the DMSP SSM/T-2. The technique consisted of the following steps: 1) obtain temperature profiles from coincident radiosonde observations, 2) use the temperature profiles as input to a microwave radiative transfer model varying the input moisture profiles from 0 to 100% relative humidity (RH), and 3) match the computed brightness temperatures (T_b s) and associated RH with the observed SSM/T-2 T_b s. In this manner, RH as a function of T_b is obtained which is valid over a limited region around the temperature profile. The technique was applied to DMSP F-11 pass segments over the East Coast of the United States in which both cloud and precipitation information was available.

1. INTRODUCTION

While the retrieval of atmospheric temperature and to a lesser extent atmospheric water vapor profiles has been obtained for a number of years utilizing infrared (IR) satellite sensors, they have always suffered from the inability to sense through clouds. With the launch of the F-11 spacecraft in November, 1991 and F-12 in August, 1994, a new microwave sensor, the Special Sensor Microwave Water Vapor Sounder (SSM/T-2), ushered in a new era of atmospheric water vapor measurements. While not totally transparent to clouds and their constituents, microwave measurements are much less sensitive to liquid and solid hydrometeors. This attribute has proven useful for probing precipitating systems normally opaque to IR sensors¹. Much effort has been devoted to understanding the information content of the raw radiance or brightness temperatures of the SSM/T-2 channels^{2,3}.

With the focus in this study of retrieving upper tropospheric humidity (UTH), a simple and efficient physical retrieval scheme was devised utilizing a microwave radiative transfer model along with satellite-based T_b measurements. Estimation of the UTH can be useful in various research efforts such as condensation trail and cirrus cloud studies. In the following sections, the UTH estimation technique will be detailed and applications of SSM/T-2 data will be discussed.

2. UTH METHODOLOGY

The technique for the retrieval of UTH utilizes a single channel measurement from the SSM/T-2 sounder. The SSM/T-2 is a five channel, cross-track scanning, sun-synchronous, passive, total power microwave radiometer system. The SSM/T-2 senses radiance at 91.655 GHz considered a window channel in this portion of the microwave spectrum, 150 GHz which is sensitive to near-surface moisture, and three channels located on the 183.31 GHz water vapor absorption line. The channel located nearest the peak of the absorption line (183 ± 1 GHz) with the highest peaking weighting function of the five channels (see Figure 1) is used to obtain the UTH in this study. At an orbital altitude of approximately 870 km, the 183 ± 1 GHz channel FOV is 48 km in diameter at nadir. The sensor makes 28 measurements across a scan line at 3° increments ($\pm 40.5^\circ$) with a swath width of approximately 1480 km.

SSM/T-2 data used in the derivation of the UTH (direct read-out orbital pass segments oriented over the East Coast of the United States) was obtained from the AIMS (AFGL Interactive Meteorological System) DMSP satellite ingest system. The direct-readout satellite ingest system provides both the microwave instrument data (SSM/I, SSM/T-1 and SSM/T-2) and the OLS (Operational Linescan System) Visible and Infrared imagery useful for cloud depiction. Surface-acquired data is routinely collected and archived by AIMS as part of the meteorological information retrieval and archive program at the Phillips Laboratory, Geophysics

Directorate. Manually Digitized Radar (MDR) data included in the standard meteorological data stream available to AIMS was used as a verification of precipitation occurrence over the contiguous U.S. For this study, radiosonde profiles of atmospheric temperature from NWS sites along the East Coast of the U.S. and within the SSM/T-2 sensor measurement swath were collected and matched with each SSM/T-2 FOV. Radiosonde humidity measurements also provided a source (albeit questionable) of UTH comparison data.

The methodology for computing the UTH is patterned after a technique derived for use with GOES VAS data at the University of Wisconsin (Wu, personal communication). For each 183 ± 1 GHz observation, an iterative RT approach was used to obtain the UTH. All RT model runs were performed utilizing the collocated temperature profile and an isohumic (constant RH) moisture profile. Initially, model estimates of the outgoing 183 ± 1 GHz T_b at the RH extremes of 5 and 100 percent were made. In most cases, if the SSM/T-2 measured T_b was found to be colder than the model-calculated values, it was an indication of a precipitation event and was treated as such. If the T_b was warmer than the warmest model value (at 5 percent RH) it signified a very dry atmosphere with a possible contribution from the surface (normally insignificant for this channel). Otherwise, using a Newton-iterative technique, the RH profile was adjusted until the model-calculated channel T_b agreed with the satellite measured value to within 0.2 K (typically 4-5 iterations). The final RH profile value was defined as the UTH. As an example, the full range of model-calculated T_b s versus RH was calculated for three radiosonde profiles and is shown in Figure 2.

3. CASE STUDY

Coincident F-11 SSM/T-2 observations, OLS imagery, radiosonde profiles and MDR data were collected during March, 1994. Figure 3 is a four panel graph displaying the 183 ± 1 GHz channel T_b , OLS Visible Image, estimated UTH values and the MDR precipitation depiction for one pass on March 2, 1994. The SSM/T-2 channel T_b features are denoted by dark (warm) and light (cold) regions which are similar in extent to the final UTH image. Missing data was evident as white line segments near the center of the image. The OLS visible image depicts reflective cloud fields as bright and clear regions as dark. A late season snowfall was evident in the Carolinas and Georgia and in the Great Lakes region. Clouds extended over much of the Eastern U.S. from Alabama to New York State. The MDR image depicts the regions of precipitation which correspond relatively well with the visible cloud cover. Ellipses in the image define the approximate radar areal coverage for each reporting station. Black dots depict the edge of the SSM/T-2 scan for reference purposes.

Gradients in the UTH field parallel the cloud boundary extending from southeastern Indiana to just north of Lake Erie and covering all points east as regions of 70 percent or greater humidities. The clear snow-covered region along the southeast coast is depicted correctly as supporting low humidities. An artifact of the technique is the effect of precipitation on the SSM/T-2 measurements. Precipitating regions tend to display reduced T_b s loosely proportional to the precipitation intensity. In the UTH image this is depicted as increased humidity; in some cases the estimated humidity is 100 percent. Regions of precipitation displayed in the UTH image matched well with the MDR observations especially over southern New England and the New York City area.

Comparisons of the derived UTH with those obtained from radiosonde humidity measurements yielded an RMS difference of 14 percent for non-precipitating conditions. The comparison was limited by the small number of East Coast radiosonde sites encompassed by the satellite sensor swath (12). Quality of the radiosonde humidity measurements at low humidity and cold temperatures is suspect and undoubtedly affects the accuracy of the comparison.

4. SUMMARY

A technique has been described which allows for the estimation of the upper tropospheric humidity on a regional scale. The technique utilizes available temperature profiles (radiosondes) as the only measured quantity input into a microwave radiative transfer model. Using an iterative technique, the humidity profile is modified to allow the calculated 183 ± 1 GHz T_b to match the measured SSM/T-2 channel T_b . Applying the technique to all SSM/T-2 FOVs yields a UTH field which accurately depicts the moisture variations observed in DMSP OLS visible and MDR imagery. A regional case study displays a close correlation between the UTH and cloud field boundaries. Precipitation events are depicted as areas of enhanced UTH (cold T_b s). While lacking independent verification information, the technique produced UTH values that were reasonable (RMS difference of 14 percent at radiosonde sites) and spatially accurate when compared with collocated cloud and precipitation information. The technique has recently been applied on a global scale utilizing SSM/T-1 retrieved temperature profiles. Preliminary results are encouraging.

5. REFERENCES

- ¹ Hollinger J.P. and the DMSP SSM/I CalVal Team, 1991: DMSP special sensor microwave/ imager calibration/validation, final report. *Naval Research Laboratory*, 1, Washington, D.C.
- ² Conlee, D.T. and T.T. Wilheit, 1994: Information content and non-profiling applications of the SSM/T-2. *Preprints of the Seventh Conference on Satellite Meteorology and Oceanography*, AMS, Monterey, CA, June 1994, pp 124-127.
- ³ Griffin, M.K., V.J. Falcone, J.D. Pickle and R.G. Isaacs, 1994: SSM/T-2 brightness temperature signatures. *Preprints of the Seventh Conference on Satellite Meteorology and Oceanography*, AMS, Monterey, CA, June 1994, pp 110-113.

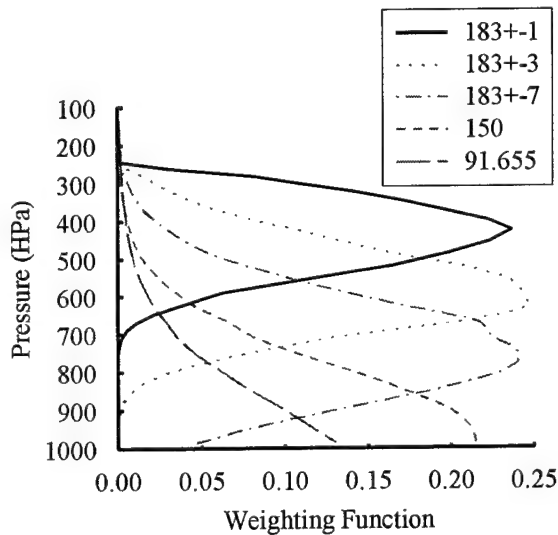


Figure 1. Weighting functions for the five SSM/T-2 channels valid for a midlatitude summer atmosphere.

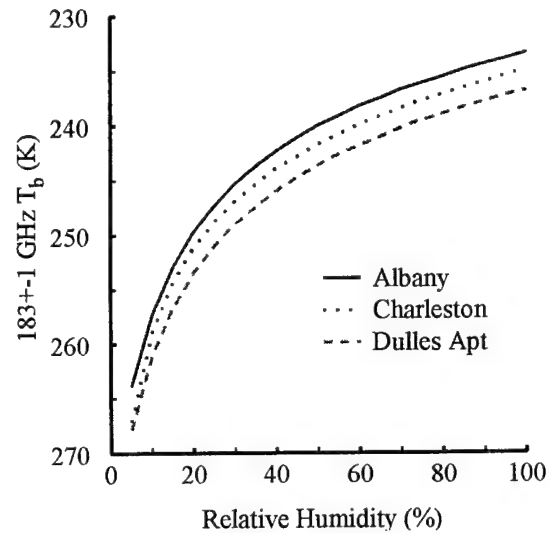


Figure 2. Graph of model-calculated T_b versus UTH for three radiosonde temperature profiles.

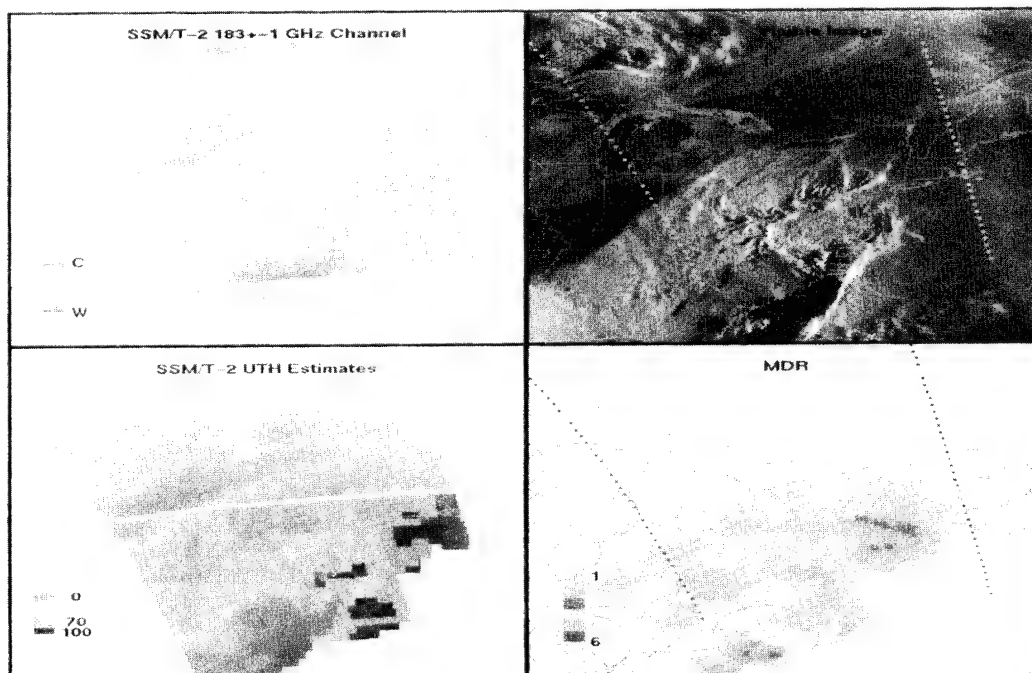


Figure 3. Four panel display showing clockwise from top left: SSM/T-2 183±1 GHz T_b , OLS Visible Image, MDR reports and UTH field for a single F-11 pass segment over the East Coast of the U.S. on March 2, 1994.

**SESSION V:
CLOUD AND CLOUD RELATED MODELS**

A SHORT-TERM CLOUD FORECAST SCHEME USING CROSS CORRELATIONS: AN UPDATE

Kenneth F. Heideman and 1LT R. Radburn Robb
Geophysics Directorate, Phillips Laboratory
Hanscom AFB, MA 01731

ABSTRACT

A trajectory-based cloud forecast technique based on lag cross correlations was initially described at CIDOS-93. The technique generates a set of loopable forecast IR images nearly indistinguishable from the real images and can be run in a few minutes on current generation workstations. Advective velocities are generated through the cross correlation of multiple subsets of the two frames. The cross-correlation technique is considered to be an excellent candidate for transition to operational use in base weather station environments and as a "first-in" tool, when the use and/or availability of many conventional data sources may be restricted; the only data required to produce forecast images several hours into the future are two IR satellite images of the same scene not more than one hour apart. Recent work has focused on improving the scheme by eliminating (or reducing) previously reported limitations, including spurious advection of terrain features, contamination at the edges of the image domain, and lack of any mechanism to infer cloud development and dissipation. This paper describes our approach to solving these problems.

1. INTRODUCTION

Accurate nowcasting and very short range forecasting of cloud features has long been a top priority of the Air Force. In response to this need, Phillips Laboratory (PL) has sponsored an on-going effort to develop a capability to produce 0-5 hour forecasts of geostationary satellite imagery in data-restricted environments. The technique used, cross correlation, is trajectory-based and requires only two consecutive geostationary infrared or visible images and a basic workstation to produce loopable forecast images up to five hours in advance. The work discussed here is based on IR imagery to take advantage of 24-hour coverage; brightness temperatures are converted to greyscale values for display purposes. A previous CIDOS paper¹ describes the details of the cross correlation technique, and documents its superiority to persistence and other techniques (such as cloud advection using 500-mb winds) in generating accurate forecast images when advective processes predominate. Readers are urged to peruse that paper to gain an understanding of the fundamentals of the technique, as lack of space precludes an adequate treatment here.

Application of the cross-correlation technique to the cloud forecasting problem was done under contract by Atmospheric and Environmental Research, Inc. (AER), in 1993. Upon successful completion of the contract, AER identified several problems with their working version of the cross-correlation code that could be corrected fairly easily given time, such as a.) lateral boundary contamination, b.) advection of terrain features in addition to clouds, and c.) excessive smoothing of cloud features at longer forecast intervals. Beyond these problems, which would require only software fixes (and in some cases increased computation time) to solve, Hamill et. al. discussed the fundamental limitation of the technique itself, namely an inability to forecast cloud development and dissipation. Subsequent research on cross correlation at PL has followed up on the AER work, and addresses the aforementioned problems and the development/dissipation limitation; our attempts to improve the technique by dealing with these issues provide the framework for this paper.

2. THE BASIC PROBLEMS

The basic problems with the cross-correlation technique identified by Hamill et. al.¹ and in-house attempts to correct them are described below:

2.1 LATERAL BOUNDARY CONTAMINATION

Inaccuracies and distortions along the boundary of any limited-area domain are to be expected. In the case of cross correlation, advection of pixel gray shade values based on a recent history of their positions is the essence of the technique; there is no such information outside the domain, and advection right at the boundary is zero. The result is often distorted cloud features that don't move in synch with rest of the forecast images when looped. The only proper solution is to enlarge the domain over which the technique is applied but to display and calculate error statistics only on the inner "protected" domain of the original size. We have uniformly worked with 256 X 256 pixel IR images with 8-km resolution. In attempting to minimize the border problem, the question of how large the additional buffer should be is an important one, as the computational expense of increasing the domain is non-trivial. The primary consideration was that it be large enough that contamination at the edge of the buffer domain in the first forecast image not advect into the inner domain during the 5-hour forecast period. As a result, we settled on a working domain of 384 X 384 pixels, displaying the inner 256 X 256, and thus providing a buffer of 64 pixels on each side. To date, testing suggests that the approach is very effective, with RMSE due to boundary contamination reduced by an average of 15-20%. The cost of the improvement, however, has been a 25% increase in computer time, bringing the run time to nearly 25 minutes on a VAX4000 workstation.

2.2 ADVECTION OF TERRAIN FEATURES

Hamill and Nehrkorn² show what can happen when clear pixels are interpreted as cloud because their IR temperature is sufficiently different from the background IR temperatures; the water in Lake Michigan is shown to "advect" to the east in forecast cross-correlation images. While many examples of terrain advection are not as dramatic, it represents a significant problem. Hamill and Nehrkorn suggest that an initial nephanalysis be run on the second of the two observed IR images used to initialize the cross-correlation process, and to advect only those upstream pixel values that were identified as cloudy by the nephanalysis. In such cases, the downstream pixel that would have received the upstream greyshade value can maintain the value it had in its previous image, or revert to a climatological value adjusted for sun angle. In applying this suggestion, we have used archived nephanalyses produced by the Support of Environmental Requirements for Cloud Analysis and Archives (SERCCA) project³ over North America and eastern Asia. Among other parameters, SERCAA provides cloud/no-cloud determinations on a pixel by pixel basis. Testing over areas containing terrain features most likely to be spuriously advected confirm that this approach works and effectively eliminates the problem, with very little computational expense.

2.3 EXCESSIVE SMOOTHING OF CLOUD FEATURES

When using the backwards trajectory scheme described in Hamill et. al.¹ to obtain forecast greyshade values, displacement vectors are followed back to their origin in the previous frame, which may or may not lie directly on a pixel. Bilinear interpolation has been used to compute the forecast pixel value in such cases. This is certainly a reasonable approach, but may result in a subtle smoothing of cloud features on forecast imagery that increases with increasing forecast interval. As Hamill and Nehrkorn² point out, one alternative would be to round the trajectory calculation to the nearest pixel

instead of using bilinear interpolation; this would result in sharper images but at the expense of accuracy. However, our tests show a sufficiently consistent reduction in RMSE using bilinear interpolation to eliminate this as a viable option. A second approach would be to use a non-iterative trajectory technique; originally, a forecast for Frame 3 was based on Frame 2, a forecast for Frame 4 was based on Frame 3, etc. Alternatively, trajectory origins are all traced back to their origins in Frame 2, resulting in less smoothing of the forecast fields with time. Implementation of this scheme has indeed produced sharper looking forecast images without sacrificing accuracy.

3. DEVELOPMENT AND DISSIPATION OF CLOUD

Attempting to parameterize developmental and dissipative processes in the cross correlation technique (particularly while preserving its ability to provide forecast satellite images fairly quickly and with a minimum of outside data sources) is a daunting task indeed, if it is possible at all. Efforts at PL to include some capability to forecast development and dissipation currently require no additional data and no parameterization of cloud growth and decay, and can thus be expected to result in only partial success. At the heart of these is a method which requires development of a ten-day "climatology" of cloud-fraction and/or greyscale values for 25-km boxes over our 256 X 256 pixel region of interest in eastern Asia (provided by SERCAA). The average climatological and/or greyscale value for each 25-km box is then averaged for each hour over the entire data set (10 days), yielding 24 hourly means. The domain we are working with is tropical in nature, with fairly regular convection. This "climatology" does reflect the strong diurnal signal that drives the convection and it is hoped that these results can be used to nudge each forecasted pixel greyscale value toward its climatological value. Testing of this method is in process and results should be available at the time of the conference.

4. CONCLUSIONS

Efforts to improve the cross correlation technique for satellite image extrapolation are continuing at Phillips Laboratory. The approach involves both fine-tuning the original working version of the routine and attempting to broaden the capabilities of the technique to include cloud growth and dissipation. This work is motivated by the belief that the enhancements to the cross correlation technique currently being incorporated will facilitate its operational implementation in the field. Research and testing suggest that, as a routinely available tool, forecast satellite images generated by the cross-correlation technique will be an asset to forecasters.

5. REFERENCES

1. Hamill, T.M., T. Nahrkorn, and K.F. Heideman, 1993: A Short-Term Cloud Forecast Scheme Using Cross Correlations. Proceedings, Cloud Impacts on DoD Operations and Systems 1993 Conference, Nov. 16-19, Fort Belvoir, VA., 346-351.
2. Hamill, T.M., and T. Nahrkorn, 1993: A Short-Term Cloud Forecast Scheme Using Cross Correlations. *Weather and Forecasting*, 8, 401-411.
3. Neu, T.J., R.G. Isaacs, G.B. Gustafson, and J.W. Snow, 1994: Improved Cloud Analysis for CDFS II through the SERCAA Research and Development Program. Preprints, Seventh Conference on Satellite Meteorology and Oceanography, AMS, Jun. 6-10, Monterey CA., 239-242.

Cloud Detection Using Visible and Near-Infrared Bidirectional Reflectance Distribution Models

Robert P. d'Entremont

*Atmospheric and Environmental Research, Inc.
840 Memorial Drive, Cambridge, MA 02139-3794*

Crystal L. B. Schaaf

*Phillips Laboratory / GPAB
29 Randolph Road, Hanscom AFB, MA 01731-3010*

Alan H. Strahler

*Department of Geography
Boston University, Boston, MA 02215*

Bidirectional reflectance distribution functions (BRDFs) quantify the manner in which surfaces reflect incident solar radiation as a function of the satellite view and solar illumination geometries. BRDFs allow for directional correction (normalization) of satellite radiance data via anisotropic correction factors to a standard view and illumination geometry. Clear-scene anisotropic correction factors are of use in automated cloud detection models. Modeled BRDFs allow for prediction of visible and near-infrared satellite radiances for a particular location on the Earth's surface prior to the actual measurements of the satellite radiances themselves. These predictions are used to estimate the clear-scene radiance for each 1-km pixel in a New England AVHRR scene. Next, the observed radiance in each pixel is compared to the predicted radiance and any value that exceeds the predicted clear-scene value is flagged as cloud. Cloud detection results will be compared digitally to 26 cloud-cleared AVHRR images taken over New England during a 17-day period in September 1994.

NOAA AVHRR data are to be cloud-cleared and atmospherically corrected for subsequent use in formulating visible/near-IR BRDF models. The data must be cloud cleared (atmospherically corrected) to ensure that the scattering effects of clouds (the atmosphere) do not enter into the BRDF estimations. AVHRR cloud clearing tests that exploit the multispectral IR signature of clouds will be used. The cloud detection tests use daytime 0.63, 0.86, 3.7, 10.7, and 11.8 μm HRPT data. The IR cloud tests are part of a global cloud detection and analysis model called Support of Environmental Requirements for Cloud Analysis and Archive (SERCAA). BRDF cloud detection techniques are also a part of the SERCAA Phase II development effort. This cloud model has been extensively validated, is scheduled for operational implementation in 1998, and is being used to help augment planned EOS MODIS cloud-clearing techniques.

SERCAA PHASE II: CLOUD RADIATIVE, MICROPHYSICAL, AND ENVIRONMENTAL PROPERTIES

Ronald G. Isaacs, Gary B. Gustafson, Robert d'Entremont and David B. Hogan
Atmospheric and Environmental Research, Inc.
Cambridge, Massachusetts 02139 USA

Micheal Remeika and James T. Bunting
Phillips Laboratory/ GPAB
Hanscom AFB, Massachusetts 01731 USA

ABSTRACT

The Support of Environmental Requirements for Cloud Analysis and Archives (SERCAA) program is a two phase basic research program to develop techniques for analysis of multi-source multi-spectral satellite sensor data for the purpose of estimating cloud fractional amount, location, height, and type. Data sources for this work include NOAA AVHRR and TOVS; DMSP OLS, SSM/I, SSM/T, and SSM/T2; and geostationary imaging sensors. In the now completed first phase, separate cloud analysis algorithms were developed for each imaging sensor in order to best exploit the information content unique to the individual data sources. A major innovation was development of an analysis integration approach based on NWP data assimilation techniques to combine the separate algorithm results from the temporally, spatially, and spectrally inconsistent sources into a single logically consistent analysis.

1. INTRODUCTION

The ensemble of SERCAA Phase 1 algorithms will provide an unprecedented capability to exploit the cloud cover, layer, type, and height information content of existing civilian and military meteorological polar and geosynchronous platforms. These algorithms will be implemented at the Air Force Global Weather Central to replace the current RTNEPH¹ under the auspices of the Cloud Depiction and Forecasting System (CDFS II) program and operational in the late 1990s². The principal objectives of SERCAA are: (a) to incorporate high-resolution sensor data from multiple military and civilian satellites, polar and geostationary, into a real-time cloud analysis model, (b) to demonstrate multispectral cloud analysis techniques that improve the detection and specification of clouds, especially cirrus and low clouds, (c) to provide augmented parameter, algorithm, and data base specifications for an improved cloud retrieval model, and (d) to design and prototype a global archive of these cloud analysis products in support of climate research.

SERCAA algorithms include a number of processes to accomplish integration of cloud analyses from multiple platforms into a single analysis product³. These processes include: (a) SERCAA total cloud algorithms for DMSP, AVHRR, and geostationary platforms, (b) SERCAA cloud layer and type algorithms, and (c) SERCAA analysis integration algorithm. The analyzed parameters or SERCAA data products include: (a) cloud cover, (b) cloud layers, (c) cloud type (d) cloud height, and (e) analysis confidence level. The Phase 1 algorithm functional flow is illustrated in Figure 1.

2. SERCAA PHASE 2

In the current, SERCAA Phase 2 program, work has been expanded to include algorithms for retrieval and estimation of the cloud physical and optical properties such as phase, drop size distribution, optical thickness, and emissivity. Also under investigation are cloud environment parameters including vertical profiles of temperature and moisture available from sounding sensors. Other parameters of interest, such as surface temperature and cloud liquid water content, may be retrievable from the SSM/I microwave imager. SERCAA Phase 1 employs only cloud imager data and provides output for cloud spatial properties only (coverage, layering, type). Current cloud analysis approaches underutilize available satellite remote sensing

data and lack the potential to fully exploit the next generation of satellite sensors. For example, onboard the two U.S. polar orbiting satellite platforms, DMSP and NOAA, there are two different multispectral imagers, four different microwave sounders, and a multi-channel infrared sounder. The planned Earth Orbiting System (EOS) will add an even greater number of sensor suites. The amount and accuracy of environmental information obtainable by passive remote sensing is dependent upon the number of quasi-independent radiance measurements made. The spectral diversity of satellite sensors is great, providing the potential to infer significant high quality cloud information. Current technology does not combine the cloud information measured by diverse sensors.

The SERCAA Phase 2 algorithms will supplement the cloud spatial properties available from the Phase 1 algorithms with:

- cloud environmental properties (temperature and moisture profiles, cloud liquid water content)
- cloud radiative properties (optical thickness, emissivity)
- cloud microphysical properties (mode radius, effective particle size, and phase)

The relationship between Phase 1 and Phase 2 parameters is illustrated in Figure 2.

3. CONCLUSIONS

The success of overall cloud depiction and forecast improvements for short and extended ranges dependent on characterization of atmospheric state. The SERCAA Phase I algorithms provide the basis to address requirements for improved specification of cloud initial state for short range forecasts by improving initialization of cloud macrophysics: cloud cover, layers, and heights. The SERCAA Phase 2 algorithms complete the cloud depiction with enhanced parameters such as cloud environment, microphysics, and radiative parameters which are required for cloud forecasting over longer time scales. These SERCAA Phase 2 cloud characteristics are of interest to the scientific community at large and can be made available through a global cloud climatology archive⁴.

4. ACKNOWLEDGEMENTS

This work is supported by Contract F19628-92-C-0149 from the Phillips Laboratory, Geophysics Directorate at Hanscom AFB, MA to AER.

5. REFERENCES

1. Hamill, T. M., R. P. d'Entremont and J. T. Bunting, 1992: A description of the Air Force Real Time Nephanalysis model. *Wea. Forecasting.*, **7**, 288-306.
2. Neu, T.J., R.G. Isaacs, G.B. Gustafson and J.W. Snow (1994) Improved cloud analysis for CDFS II through the SERCAA research and development program. *Preprints, 7th Conference on Satellite Meteorology and Oceanography*, June 6-10, Monterey, CA, 239-242.
3. Gustafson, G.B., R.G. Isaacs, R.P. d'Entremont, J.M. Sparrow, T.M. Hamill, C. Grassotti, D.W. Johnson, C.P. Sarkisian, D.C. Peduzzi, B.T. Pearson, V.D. Jakabhazy, J.S. Belfiore, and A.S. Lisa, 1994: Support of environmental requirements for cloud analysis and archive (SERCAA): Algorithm Descriptions. PL-TR-94-2114, Scientific Report #2, Phillips Laboratory, Directorate of Geophysics, AFMC, Hanscom AFB, MA 01731-3010.
4. Isaacs, R.G. (1993). Remote sensing of cloud for defense and climate studies: an overview. In SPIE Proceedings Vol. 1934, Conference on Passive Infrared Remote Sensing of Cloud and the Atmosphere, 13-15 April 1993, Orlando, FL.

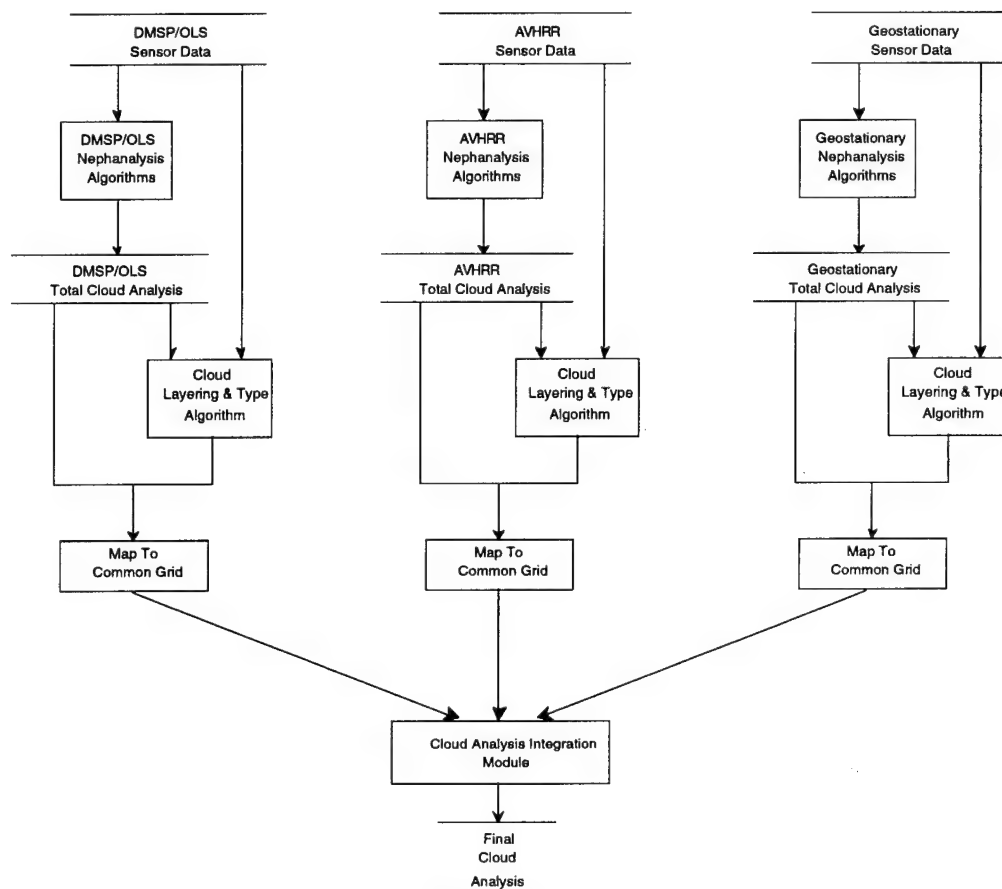


Figure 1. SERCAA Phase 1 flow chart.

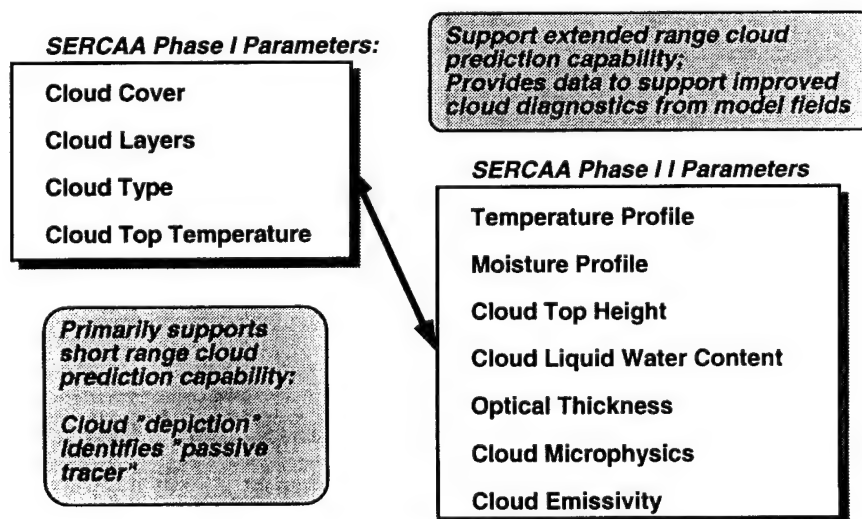


Figure 2. Relationship of SERCAA Phase 1 and Phase 2 parameters.

THE LATTICE BOLTZMANN METHOD: A NEW APPROACH TO RADIATIVE TRANSFER THROUGH CLOUDS

Joel B. Mozer and Thomas R. Caudill
USAF Phillips Laboratory, Geophysics Directorate
Hanscom AFB, MA 01731, USA

ABSTRACT

The Lattice Boltzmann method is a new tool for studying radiative transfer. This method stems from cellular automata techniques in which the dynamics of discrete particles interacting on a multidimensional discrete lattice are described. A particular cellular automata method known as Lattice Gas Automata (LGA) has been used in recent years as an alternative to traditional methods of modeling Navier-Stokes fluid dynamics. Lattice Boltzmann (LB) methods extend LGA by treating dynamics of ensemble averages of the discrete dynamics directly. The principal advantage of LB methods is that they are amenable to parallel computation. This paper describes a new application of the LB method to 3-D radiative transfer through inhomogeneous media. In this case the particles represent discrete scattering, absorption and emission events. We show that this is a particularly useful treatment of radiative transfer through a field of broken cumulus clouds.

1. INTRODUCTION

Solutions to the radiative transfer equation, particularly for three dimensional geometries, have been a topic of interest to the atmospheric science community for nearly three decades. This interest has intensified over the past few years as shortcomings in the radiative parameterizations of clouds in the global circulation models have been examined (see review article by Levi, 1995). Current models do not adequately describe cloud effects, which include 3-D variability of optical depth, particle size, LWC, etc. Another problem is how to account for the randomness of cloud fields including cloud interactions and shadowing (Newman et al., 1995; Zuev and Titov, 1995). In a recent paper, Kuo et al. (1995) give a good general description and evaluation of the existing solution techniques for 1-D radiative transfer. Each of the approaches is evaluated for application to 3-D problems and all have some problems. Gabriel et al. (1993) gives a fairly comprehensive list of techniques developed for 2- and 3-D geometries between 1975-1992. In addition, Li et al. (1995) present a perturbation method for solving the 3-D radiative transfer equation with periodic inhomogeneity. The analytical approaches mentioned are clearly most efficient for relatively simple geometries but are very computationally intensive for realistic atmospheric conditions.

Another group increasingly interested in cloud issues is the Modeling and Simulation community. The ability to visualize three-dimensional clouds in a physically accurate manner at high frame rates is a current obstacle to the inclusion of atmospheric effects into interactive, real-time system simulations. Presently, there are two fundamentally different methods for visualizing volumetric objects on modern computer hardware. The first requires that a three-dimensional surface be constructed by building a mosaic of connected, two-dimensional, polygonal surfaces which serve as a basis for radiosity calculations. The second method involves the direct simulation of the interactions between the radiation and the volumetric objects through ray-tracing techniques. Of these two methods, the former is typically much faster due to the capabilities of modern computer graphics rendering hardware and the latter is generally more realistic because of the physical accuracy which can be included in the calculations. For real-time simulation applications where realistic clouds are desired, one is generally prohibited from the use of ray-tracing techniques because of a lack of computational resources. However, the polygonalization of clouds generally leads to an unrealistic and non-physical rendition of the scene since they are treated as surfaces as opposed to volumes.

Here we present an alternative to conventional ray-tracing techniques for cloud scene rendering which is computationally efficient and therefore very fast. This so-called Lattice Boltzmann (LB) method involves the direct simulation of the interaction of photons with atmospheric media (including clouds). The Lattice Boltzmann method has its foundations in Lattice Gas Automata (LGA) techniques (c.f., Frisch et. al, 1986) and is a novel approach to atmospheric transmission and visualization problems; however, it has proven

to be a useful and efficient method for solving a variety of other physical problems, most notably that of multi-dimensional fluid flows (c.f., Chen, 1993).

In general, a LGA calculation is a construction of a simple micro-dynamical system in which space, time and velocity are all discrete. Fictitious microscopic particles which reside at nodes in this discrete space are tracked as they interact with each other and with obstacles in the lattice according to a well-defined set of interaction rules. These rules are chosen to conserve certain properties. For the case of Navier-Stokes flow, mass, momentum and energy are the appropriate conserved quantities. For a properly chosen set of interaction rules, macroscopic averaging of the trajectories of individual particles leads to an evolving field which represents a physical system. LGA and related techniques are therefore an alternative to traditional finite-difference approximations as a method for solving a system characterized by a set of partial differential equations. Unfortunately, like all particle methods, LGA calculations are inherently noisy due to the randomness of the particles unless a large amount of averaging is taken over space or time. LGA methods also require prohibitively large amounts of memory in three or more dimensions due to the nature of the collision rules.

The Lattice-Boltzmann method circumvents the above undesirable features. Here, the individual particles (binary variables) are replaced by the single particle distribution functions (real variables). In this way one goes from modeling individual particles on the microscopic scale to modeling particle populations on the mesoscopic scale. Equilibrium distributions of particles replace explicit collision rules thus eliminating the need for large collision lookup tables. As with LGA methods, the LB methods lead to proper physical simulation on the macroscopic scale as long as the proper particle interactions are chosen. Since the LB method directly models ensembles of particles, it is free from noise. However, for the same reason, correlations between individual particles are lost in LB calculations. Also, with LB methods, one is not guaranteed absolute numerical stability as with LGA methods.

The extension of the LB method to the modeling of radiative transport phenomena is new. In this case, the elementary particles represent discrete packages of radiation and the lattice nodes represent volumes where scattering, absorption and emission occurs. The fundamental physics of the radiative transfer is captured in how the particles interact but with these volumes. This approach is akin to Monte Carlo techniques. However, LB calculations are much more efficient since all the "photons" synchronously travel along the lattice. LB calculations are also view-independent since all incident photons interact with the optical medium, not just those arriving at the image plane.

2. METHOD

The first step to posing a radiative transport problem in terms of the Lattice Boltzmann method is to construct a proper discretization of the physical space. This lattice, in its most simple form is just a Cartesian grid where a regular array of nodes are connected to their nearest neighbors. A set of lattice vectors, \hat{e}_i , are constructed which point along each of the i lattice directions. At each lattice node, the distribution of the particles in each of the directions \hat{e}_i is given by f_i .

For each time step, t , the distribution of particles are modified via the kinetic equation,

$$f_i(\mathbf{x} + \hat{e}_i, t + 1) - f_i(\mathbf{x}, t) = \Omega_i$$

where, \mathbf{x} , represents the location of the node in the lattice and Ω_i represents the rate of change of particle density in a given direction. In practice, this can be considered two separate operations—a collision representing the local redistribution of particles via Ω and a free streaming as the particles move from one node to another. Because these operations occur in lock-step fashion, and involve only local information, the procedure is very efficient in parallel computer environments.

The essential physics calculation is captured in the way in which the collision term, Ω is chosen. For simplicity, we consider the single-time relaxation model,

$$\Omega_i(f) = -\frac{1}{\tau}(f_i - f_i^{eq}), \quad (1)$$

where f_i^{eq} represents a local equilibrium distribution of particles and the parameter τ controls the rate at which the system relaxes to equilibrium. For radiative transport application, τ , may be a function of space and contains information about the optical properties of the medium (e.g. optical depth). The equilibrium distribution function, f_i^{eq} represents the scattering phase function relevant for an interaction of a beam of light with the volume element represented by the lattice node. For isotropic scattering, $f_i^{eq} = const.$; for more general cases, f_i^{eq} is a function of the discrete angles inherent in the lattice geometry. For Rayleigh scattering,

$$f_i^{eq} = Af_i \sum_{j=1}^B [1 + (\frac{\hat{e}_i \cdot \hat{e}_j}{\hat{e}_i \hat{e}_j})], \quad (2)$$

where A is a constant chosen to produce conservative scattering and B is the number of lattice directions. Other scattering phase functions may be represented through the equilibrium distribution function, however as the angular distribution becomes more complex, more lattice directions will be required. The increase angular resolution comes at the cost of higher memory and communication requirements in the calculation.

It is evident from (1) and (2) that f_i^{eq} is equivalent to the scattering phase function and the parameter τ controls the relative amount of scattering which takes place. For an inhomogeneous cloud, $\tau = \tau(\mathbf{x})$ thus allowing for spatial variation in the optical properties of the cloud. Absorption and emission by the media is accomplished simply by adding sources and sinks of particles to the collision operator Ω .

3. DISCUSSION

We have begun to explore a new method for rapid visualization of three-dimensional clouds using a technique which exploits parallel processing architectures. We have described the application of the Lattice Boltzmann technique to 3-D radiative transfer through inhomogeneous media. Preliminary comparisons of the radiometric calculations made using this method with traditional Monte Carlo techniques indicate that LB techniques offer an efficient alternative where fast visualization is required. This offers a particularly useful treatment of radiative transfer through a field of broken cumulus clouds. Further investigations are underway to test the applicability of the method to three dimensional variability of optical characteristics (i.e. optical depth, particle size, LWC, etc.). We intend to eventually extend the method to arbitrary cloud geometries and to examine the effects of cloud-cloud interactions.

Chen, H., 1993: Discrete Boltzmann systems and fluid flows, *Comp. in Phys.*, 7, 632-637.

Frisch, U., B. Hasslacher, and Y. Pomeau, 1986: Lattice-Gas Automata for the Navier-Stokes Equation, *Phys. Rev. Lett.* 56, 1505-1508.

Gabriel, P. M., S. -C. Tsay and G. L. Stephens, 1993: A Fourier-Riccati approach to radiative transfer. Part 1: Foundations, *J. Atmos. Sci.*, 50, 3125-3147.

Kuo, K. -S., R. C. Weger and R. M. Welch, 1995: The Picard iterative approximation to the solution of the integral equation of radiative transfer - Part I. The plane-parallel case, *J. Quant. Spectrosc. Radiat. Transfer*, 53, 425-444.

Levi, B. G., 1995: Clouds cast a shadow of doubt on models of Earth's climate, *Physics Today*, 48, 21-23.

Li, J., D. J. W. Geldart and P. Chylek, 1995: Second order perturbation solution for radiative transfer in clouds with a horizontally arbitrary periodic inhomogeneity, *J. Quant. Spectrosc. Radiat. Transfer*, 53, 445-456.

Newman, W. I., J. K. Lew, G. L. Siscoe, R. G. Fovell, 1995: Systematic effects of randomness in radiative transfer, *J. Atmos. Sci.*, 52, 427-435.

Zuev, V. E. and G. A. Titov, 1995: Radiative transfer in cloud fields with random geometry, *J. Atmos. Sci.*, 52, 176-190.

CLOUD FORECASTING INITIATIVES AT AIR FORCE GLOBAL WEATHER CENTRAL

Raymond B. Kiess and Thomas J. Kopp
HQ AFGWC/SYSM
Offutt AFB, NE, 68113-4039

ABSTRACT

The Air Force Global Weather Central provides customers with cloud forecasts from a suite of three models that either use semi-lagrangian advection of an initial cloud field or diurnal persistence. We are making three significant changes to this model suite. The first change is to combine the three models into a single model, initially increasing the horizontal resolution from 191 km to 48 km in 1996 and eventually to 24 km in 2000. The second change is to forecast daytime boundary layer clouds by using a one dimensional boundary layer cloud model. The third change is to use a cloud diagnosis algorithm on numerical weather prediction fields. The first two changes benefit the shorter range forecasts while the third helps longer range forecasts.

INTRODUCTION

The Air Force Global Weather Central (AFGWC) has provided operational customers with cloud forecasts since the 1970s using a model suite consisting of the 5LAYER, HRCF, and TRONEW models. The 5LAYER and HRCF use a semi-lagrangian advection of an initial cloud field specified by the Real-Time Nephanalysis Model (RTNEPH) while TRONEW uses diurnally persisted RTNEPH fields. 5LAYER and TRONEW each use 191 km horizontal grid spacing covering most or all of each hemisphere and three hour temporal forecasts out to 48 and 24 hours, respectively. HRCF uses 48 km horizontal grid spacing covering an area bounding a quarter-orbit pass of polar-orbiting satellite data and produces three hour temporal forecasts out to nine hours. These models work well for shorter range forecasts as advection is usually the dominant cloud change process, but break down in convective and longer range forecast scenarios as they lack the physics to develop and dissipate clouds. Our customers' requirements demand improved forecast quality and resolution, hence we are pursuing a multi-prong approach that builds upon existing capabilities to improve our products.

APPROACH

Our approach is to make three significant enhancements. First, we will combine the advective models into a single model with increased horizontal and temporal resolution. Second, we will use a one-dimensional planetary boundary layer (1DPBL) model to forecast daytime boundary layer clouds. Finally, we will use a cloud diagnosis scheme on numerical weather prediction (NWP) fields to improve longer range forecasts.

We have developed a prototype model called ADVCLD that is designed to be the single advection model. There are two versions, each using a different horizontal grid spacing. ADVCLD-A uses 48 km RTNEPH data for input and provides forecasts on a 48 km horizontal grid spacing out to 12 hours and a 96 km grid spacing out to 48 hours. Its temporal resolution is hourly out to 12 hours and three-hourly thereafter. ADVCLD-B uses 24 km Support of Environmental Requirements for Cloud Analysis and Archive (SERCAA) data for input and provides forecasts on a 24 km horizontal grid spacing with hourly output to 12 hours. We

validated each model against RTNEPH or SERCAA data. Results show we meet or exceed current model skill. We are planning to implement ADVCLD-A in 1996 to replace the 5LAYER and TRONEW models. ADVCLD-B will be implemented by contract under the Cloud Depiction and Forecast System II program in the year 2000. These models improved resolution will improve cloud forecasting skill, but they do not address cloud changes due to non-advective processes.

To address boundary layer cloud depiction, we have been using the Oregon State University's IDPBL with the Ek and Mahrt (1991¹) cloud diagnosis algorithm. Our primary customers identified tropical regions as areas needing the most improvement, therefore, we began our development there. We recently concluded a pilot study where we ran the model over four separate radiosonde sites in Central and South America. The results indicated the model does a reasonable job forecasting daytime fractional cloud cover. However, running the model exclusively over radiosonde sites does not meet our spatial requirements. Therefore, we are beginning a new study where we will initialize all land grid points in a Central and South American domain with AFGWC's Relocatable Window Model (RWM) analysis fields instead of radiosondes. Cloud forecasts will be compared to satellite imagery, RTNEPH output, and surface observations. If this study is successful, we will integrate its output into the HRCF and ADVCLD, most likely with a weighted blending scheme.

Our final effort is to use cloud diagnosis schemes operating on output fields from NWP models. Since NWP models require a "spin-up" time for moisture fields, they are more suitable for longer range forecasts. Our initial work consisted of coding the Slingo (1987²) algorithm to apply to RWM output. Our validation showed it to be on par with ADVCLD forecasts by 12 hours and superior afterwards. Future work will be to evaluate this scheme against the Cloud Curve Algorithm (Mitchell and Hahn³) and select the best candidate to integrate into the RWM. We will also apply these algorithms to global NWP output.

CONCLUSIONS

We are pursuing a three part effort to improve our cloud forecasting capability at AFGWC. The three efforts of increasing horizontal resolution, adding physics to capture boundary layer clouds, and using cloud diagnosis algorithms provide a complimentary approach to build upon our existing cloud forecasting system. Preliminary results show each effort adds value. Our goal is to provide an interim capability for each effort within the next year and completely integrate within three years.

REFERENCES

- ¹Ek, M. and L. Mahrt, 1991: A formulation for boundary-layer cloud cover. *Annales Geophysicae*, **9**, 716-724.
- ²Slingo, J.M., 1987: The development and verification of a cloud prediction scheme for the ECMWF model. *Q. J. Roy. Meteorol. Soc.*, **113**, 899-927.
- ³Mitchell, K.E. and D.C. Hahn, 1989: *Development of a Cloud Forecast Scheme for the GL Baseline Global Model*. GL-TR-89-0343, Geophysics Laboratory (AFSC), Hanscom AFB, MA, 151 pp.

SHORT-TERM CLOUD FLUCTUATION STATISTICS FOR CENTRAL AMERICA USING GOES-8 IMAGERY

John DeVore
Visidyne, Inc.
Goleta, CA, 93117, USA

ABSTRACT

Short-range (0-12 h) cloud prediction must take into account both dynamics and advection. In this study spatial and temporal scales associated with cloud processes are inferred from GOES-8 band 4 imagery for a location in the tropics. The methods of one-point correlation and lag-correlation maps are applied to a dataset consisting of 1346 images taken over a 45 day period. The derived Eulerian correlation time, related to persistence, is approximately 2 h. The derived Lagrangian correlation time, associated with advection, is of the order of 4 days, but contributes less than half of the correlation.

1. INTRODUCTION

The Defense Nuclear Agency and the Air Weather Service are interested in the development of short-range (0-12 h) cloud prediction technology for all regions of the globe, and particularly for the tropics. Ramage¹ attributes the unexpectedly small improvement in forecasts associated with the increase in the supply of data from satellites to the dependence of local weather on changes in approaching systems rather than simply to their movement. Statistical analysis of satellite imagery can quantify the time scales of cloud systems and hence clarify the relative importance of advection and dynamics.

Cahalan, Short, and North², hereafter CSN, performed a space-time statistical analysis of total outgoing infrared radiation to determine the gross features of cloudiness fluctuations over the Pacific Ocean in summer and winter. They used AVHRR data in the 10.5-12.5 μm atmospheric window, averaged over 2.5° by 2.5° latitude-longitude areas and representing 45 consecutive months of twice daily data³. Fluctuations in the outgoing infrared radiation were attributed to both cloud advection and dynamical change. CSN defined the Eulerian correlation time as the lag time required for the autocorrelation of a fixed grid point signal to fall to 1/e and the corresponding correlation length to be the diameter of the area in which the zero-lag correlation exceeds 1/e. Advection of cloudiness causes the signal at a given point to be correlated with time-lagged signals at points downstream. The Lagrangian correlation time is the lag time required for the maximum downstream correlation to fall to 1/e; the distance to the downstream point is the advection length. For the North Pacific storm track CSN found values for the Eulerian correlation time from 12 to 24 hours, a correlation diameter of about 10°, a Lagrangian correlation time of about 24 hours, and an advection length of about 20°.

CSN's work addressed issues of relevance to climatology. For cloud forecasting shorter time and smaller spatial scales are important. GOES-8 offers half hourly coverage of the Northern Hemisphere to about 20° S with 4-km resolution in the long-wave infrared bands⁴. Following the lead of CSN, we used the methods of one-point correlation and lag-correlation maps to infer spatial and temporal scales. In contrast to the definitions of CSN, in the present study we considered non-zero lead times and upstream points.

2. THE DATASET

GOES-8 data were collected from the Space Science and Engineering Center (SSEC) of the University of Wisconsin on the Visidyne McIDAS workstation from February 21 through April 7 of 1995. The images consist of 4-km nominal resolution, band 4 infrared (10.2-11.2 μm) radiance values. Each set of 479 by 479 data values covers a nearly 2000 km square centered on Howard AFB, Panama (station MPH0). After culling images with missed or noisy scan lines or sections, 1346 datasets remained. Animation of the datasets showed the frequent occurrence of pronounced vertical shear in the cloud advection velocity, with low- and high-level clouds going in opposite directions. (Such shear poses a grave problem for any modeling of cloud advection that uses a single velocity.) Since the dataset statistics varied over the collection period, the data were divided into five time periods and the calculations of lead correlations were not allowed to cross the time boundaries. Linear trends were removed from the data at each grid point in order to assure the stationarity of the time series.

3. EULERIAN CORRELATION TIMES AND DIAMETERS

The autocorrelation function for the radiance at Howard AFB is shown in Figure 1. The peaks at 24 and 48 hours in Figure 1 are consequences of the diurnal thermal cycle on land.

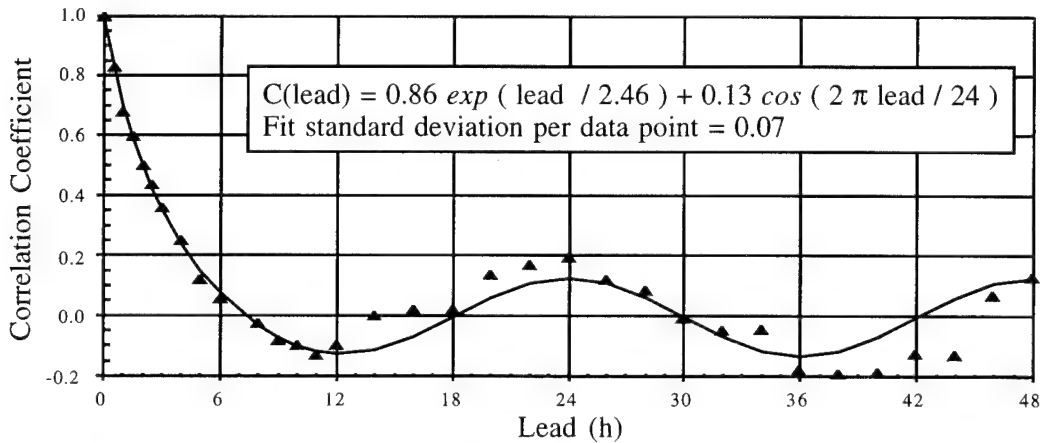


Figure 1. Autocorrelation of GOES-8 band 4 radiance time series at Howard AFB (triangles) and associated curve fit (solid line).

For comparison Figure 2 shows a similar calculation for a point 100 km South of Howard AFB in the Gulf of Panama. Note that the pronounced diurnal peak is missing for this point.

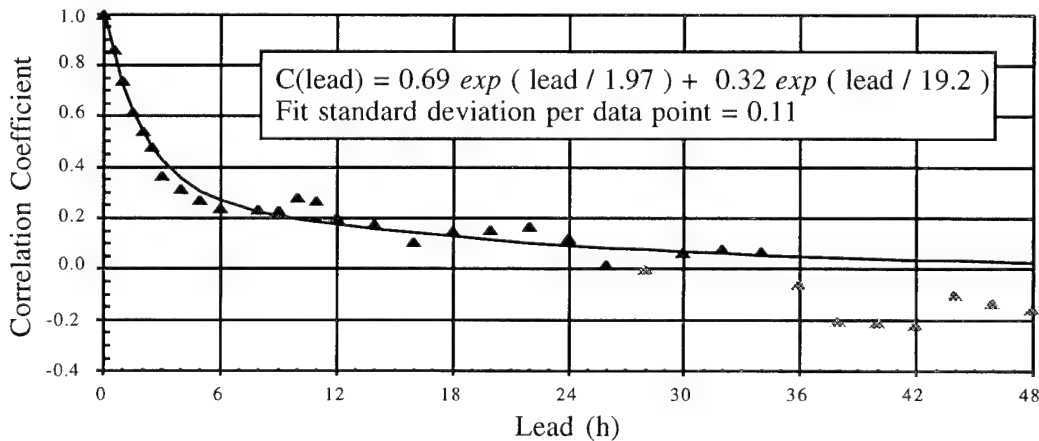


Figure 2. Autocorrelation of GOES-8 band 4 radiance time series for a point 100 km South of Howard AFB in the Gulf of Panama, (triangles) and associated curve fit (solid line).

Inspection of Figures 1 and 2 suggests that the Eulerian correlation times are roughly several hours. To derive a more quantitative measure the sum of an exponential and a cosine with a 24 hour period were fit to the data for Howard AFB (see Figure 1). This sum represents contributions to radiance fluctuations from both diurnal thermal variations, i.e., the cosine term, and, from stochastic processes, the exponential term. The derived Eulerian time scale for short term fluctuations is close to 2.5 hr. Taking this as the effective time between independent samples, the sampling fluctuations at large lead times are expected to be on the order of $(45 \times 24 / 2.5)^{-1/2} = 0.05$, consistent with the standard deviation of 0.07 (see also CSN). Similarly, the positive data in Figure 2 were fit with the sum of two exponentials (see Figure 2). The Eulerian time scale for the short term fluctuations is about 2.0 h while the longer time scale is 19 h.

The Eulerian correlation length may be found from examination of the contour plot of the unled cross correlation of the radiance time series at Howard AFB with the other points in the image datasets (Figure 3a). There are two distinct regions with correlation exceeding $1/e$: one is centered on Howard AFB, where the peak correlation is 1, and the other coincides with the Peninsula of Azuero. The second region and perhaps the elongation of the first appear to be associated with diurnal surface temperature effects. In Figure 3a 5,967 of the 229,441 grid points are enclosed by the two $1/e$ contours. Considering the first region only, and estimating from the plotted $1/e$ contour, the Eulerian correlation diameter is approximately 250 km.

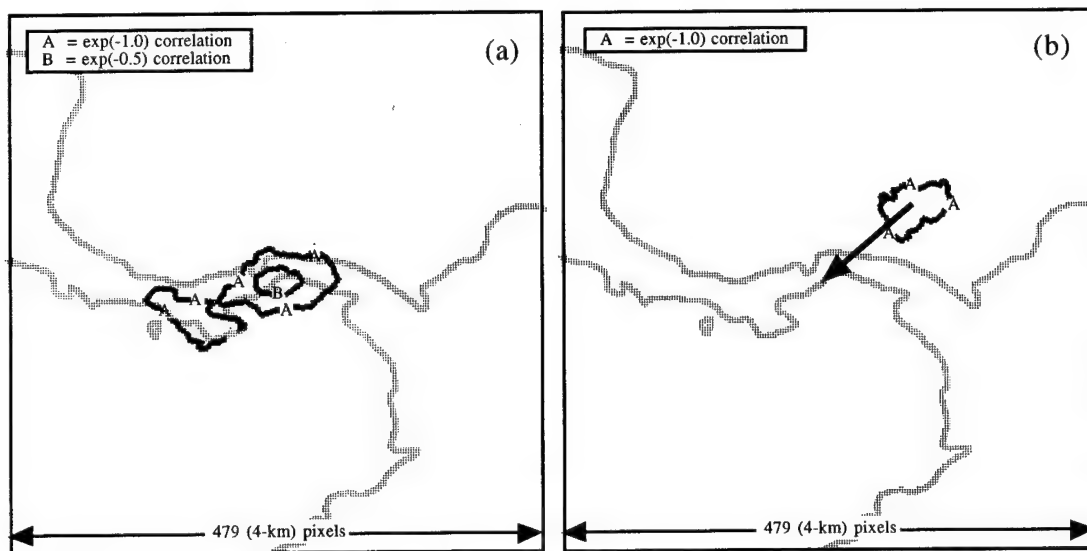


Figure 3. Contour map of the cross correlation between the radiance time series at Howard AFB and at other grid points (a) at the same time and (b) 8 h earlier (see Section 4 for an explanation).

CSN pointed out that the Eulerian correlation time increases with averaging area. Figure 4 compares the autocorrelation coefficient as a function of lead time for a single pixel with those for averages of various sizes. The 65 by 65 pixel area corresponds roughly to the Eulerian correlation diameter. The autocorrelation curves "saturate" at about 3 to 4 correlation diameters, suggesting that advective effects on the correlation time have been averaged out. Inspection of Figure 4 suggests that the characteristic initial decay time increases from a few hours for a single pixel to over half a day for areas of several Eulerian correlation diameters.

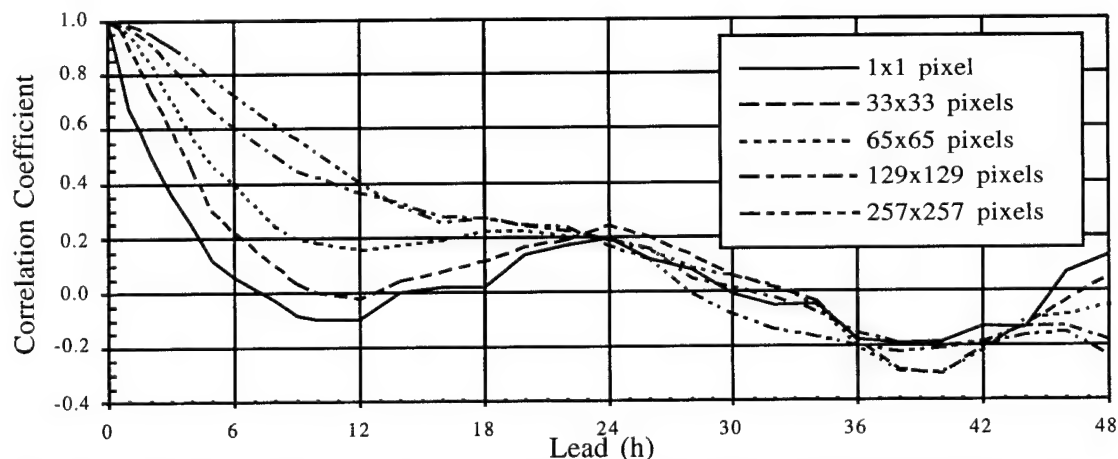


Figure 4. Autocorrelation of GOES-8 band 4 radiance time series for various averaging areas centered on Howard AFB.

4. LAGRANGIAN CORRELATION TIMES

Cross correlation maps of the radiance time series at Howard AFB were calculated with the time series at other grid points for lead times ranging from 30 min to over 4 days. Figure 3b shows a contour plot of the cross correlation for an 8 h lead. Note that the higher contour has disappeared and the maximum cross correlation is 0.47. The $1/e$ contour is located northeast of Howard AFB about 400 km. The peak cross correlation coefficient is plotted in Figure 5 as a function of lead time. Also shown is a fit using the sum of two exponentials. The peak cross correlation decays exponentially for the first few hours with a characteristic time of 1.6 h and then continues to decay much more slowly. The peak cross correlation with a point 100 km south of Howard AFB in the Gulf of Panama (not shown) behaves similarly.

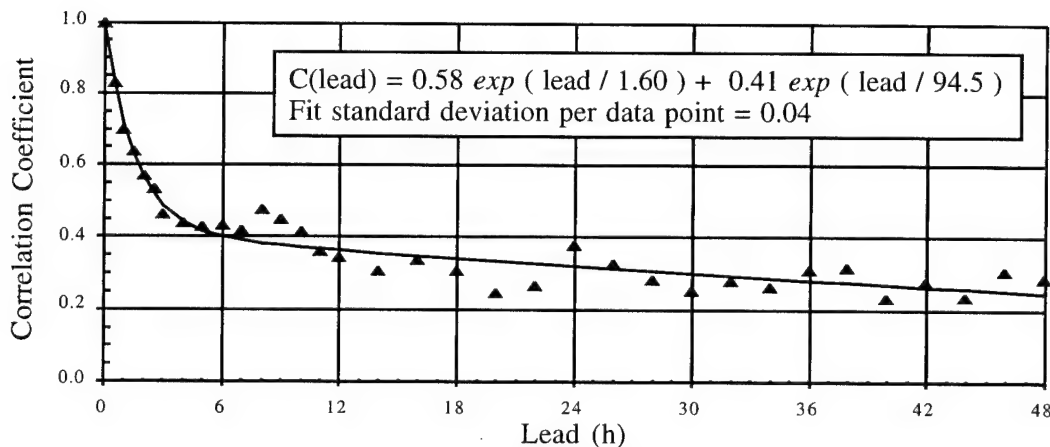


Figure 5. Peak cross correlation coefficient of GOES-8 band 4 radiance time series at Howard AFB with other grid points as a function of lead time (triangles) and associated curve fit (solid line).

5. DISCUSSION AND CONCLUSIONS

1) Eulerian correlation times are very short, on the order of 2 h. Although CSN found longer Eulerian correlation times, their study was based on twice-daily data averaged over 2.5° squares. As they showed, and as the present study confirmed, the Eulerian correlation time increases with averaging area.

2) At leads two to three times the initial Eulerian correlation time the autocorrelation curve follows a cosine function (Howard AFB) or a second exponential function (Gulf of Panama). The cosine function has a period of a day, an amplitude 15% of the initial exponential, and is associated with the diurnal thermal cycle of the land. The long-lead behavior of the autocorrelation coefficient over the ocean is exponential with a characteristic time of 19 h, more consistent with the results of CSN.

3) The Eulerian correlation diameter deduced for Howard AFB is approximately 250 km, which is roughly 2.5°, e.g., the grid size used by CSN.

4) The short-term cross correlation with Howard AFB decays rapidly; the long-term component decays much more slowly, with a characteristic time constant on the order of 4 days.

5) For an 8 h lead the centroid of the maximum in the cross correlation is located 400 km northeast of Howard AFB. This corresponds to an advection speed of $400 / 8 = 50$ km/h or about 14 m/s.

This work could be extended in a number of ways. (1) The same analysis could be performed for other climatic conditions. (2) The diurnal thermal cycle could be filtered from land locations. (3) As CSN suggested, the data could be filtered to separate low and high clouds. Finally, (4) image pairs could be segregated by wind direction before calculating the Lagrangian correlation times.

6. ACKNOWLEDGEMENTS

The author is pleased to acknowledge Mr. Scott Murdock for assistance in acquiring the GOES-8 images, Mr. Rick Kohrs for help with McIDAS, Prof. Kerry Emanuel for initially suggesting the use of lag correlation maps, Prof. Paul Joss for helpful review, and Maj. Rob Cox for his support. The work was sponsored by the Defense Nuclear Agency under contract DNA001-94-C-0145.

7. REFERENCES

- ¹ Ramage, C., 1993, "Forecasting in Meteorology", *Bull. Amer. Meteor. Soc.*, **74**, 1863-1871.
- ² Cahalan, R., D. Short, and G. North, 1982, "Cloud Fluctuation Statistics", *Mon. Wea. Rev.*, **110**, 26-43.
- ³ Gruber, A., and J. Winston, 1978, "Earth-Atmosphere Radiative Heating Based on NOAA Scanning Radiometer Measurements", *Bull. Amer. Meteor. Soc.*, **59**, 1570-1573.
- ⁴ Menzel, W., and J. Purdom, 1994, "Introducing GOES-I: The First of a New Generation of Geostationary Operational Environmental Satellites", *Bull. Amer. Meteor. Soc.*, **75**, 757-781.

IDENTIFICATION OF THUNDERSTORMS IN AN OPERATIONAL GLOBAL NEPHANALYSIS USING A CONVECTIVE-STRATIFORM TECHNIQUE

Thomas J. Kopp, Peter J. Broll, and Stephen G. Zahn
Headquarters Air Force Global Weather Central
Offutt AFB, NE 68113-4039

ABSTRACT

Identification of cloud types, including cumulonimbus, is one of many cloud parameters produced by the Real-Time Nephanalysis (RTNEPH). Cumulonimbus was frequently overanalyzed due to RTNEPH's threshold technique. We implemented a three-step process in RTNEPH to correct this deficiency. First, a surface temperature threshold is set to prevent cumulonimbus types over polar regions. Second, we apply a variation of Adler and Negri's (1988¹) Convective-Stratiform Technique (CST) to all remaining high cloud tops, with any overshooting cloud tops identified as cumulonimbus. Third, we use a latitude-dependent greyscale threshold to locate large convective clouds with smooth cloud tops. Comparisons of RTNEPH's cloud type with satellite imagery confirm the success of the CST.

1. INTRODUCTION

The Air Force Global Weather Central (AFGWC) provides customers with analyses of numerous cloud parameters through the Real-Time Nephanalysis (RTNEPH). One of these parameters is cloud type, which includes cumulonimbus. The original approach to identify cumulonimbus was through a single threshold; if a cloud top greyscale was less than 25 (approximately 237 K) then the cloud was labeled a cumulonimbus. This led to frequent overanalysis problems, especially over polar regions and extensive cloud bands associated with mid-latitude cyclones. Initial attempts to correct the problem, using information such as tropopause heights or cloud texture, were unsuccessful.

Adler and Negri, in an effort to determine rain rates based on satellite imagery for tropical cloud systems, produced a Convective-Stratiform Technique (CST). The ultimate objective of the CST is to produce rain rates, but the authors needed to differentiate between convective and stratiform cloud regimes. Hence, the first step in their CST is to locate convective clouds.

We recognized the CST would assist in reducing cumulonimbus overanalysis. Adjustments were required since the CST was designed using infrared temperatures from geostationary imagery over Florida, while the RTNEPH uses polar-orbiting imagery on a global scale and uses greyscales (1-63) in its analysis. We designed a three-step algorithm applying the principles of the CST, adjusted for use within the RTNEPH. The algorithm is discussed below.

2. METHOD

The first and simplest step removed cumulonimbus over polar regions. Since "polar" regions are not easily defined by latitude, RTNEPH defines a polar region as any location with a surface temperature colder than 277 K. While thunderstorms may occur at colder surface temperatures, they comprise a very small number of all cases.

The second step was to take all remaining cold cloud tops and apply the CST technique. The original convective identification scheme in Adler and Negri searched for overshooting cloud tops via a "slope parameter". Adler and Negri determined the slope parameter by taking a local temperature minima based on GOES pixel infrared temperatures and then subtracting the value from the average temperature of the six closest pixels surrounding the minima. The larger the slope parameter, the greater the likelihood the cloud was convective. The minimum slope parameter threshold for convective cloud varies with cloud top temperature.

RTNEPH uses polar orbiting imagery, compacted to a uniform 5 km resolution. We redefined the slope parameter within RTNEPH using the four adjacent satellite grid points. In order to determine the threshold for

the slope parameter used in RTNEPH, we performed a series of discriminant analyses using slope parameters and greyscale. An example is shown in Figure 1. Based on the results, the value which the slope parameter must exceed for a cloud to be identified as cumulonimbus is:

$$S = (0.1 * G_{\text{SMIN}}) + 2,$$

where S is the threshold and G_{SMIN} is the minima as a greyscale (1-63). This technique captures cumulonimbus embedded within extensive cloud systems.

Large convective complexes with generally smooth and cold cloud tops are not identified by the slope parameter. Convective systems such as hurricanes and mesoscale convective complexes exhibit such characteristics. In order to capture these types of systems, the third step identifies any cloud as a cumulonimbus that passes a latitude-dependent greyscale threshold. These thresholds are more restrictive than the single value used previously, since we assume marginal cases are captured by the slope parameter approach.

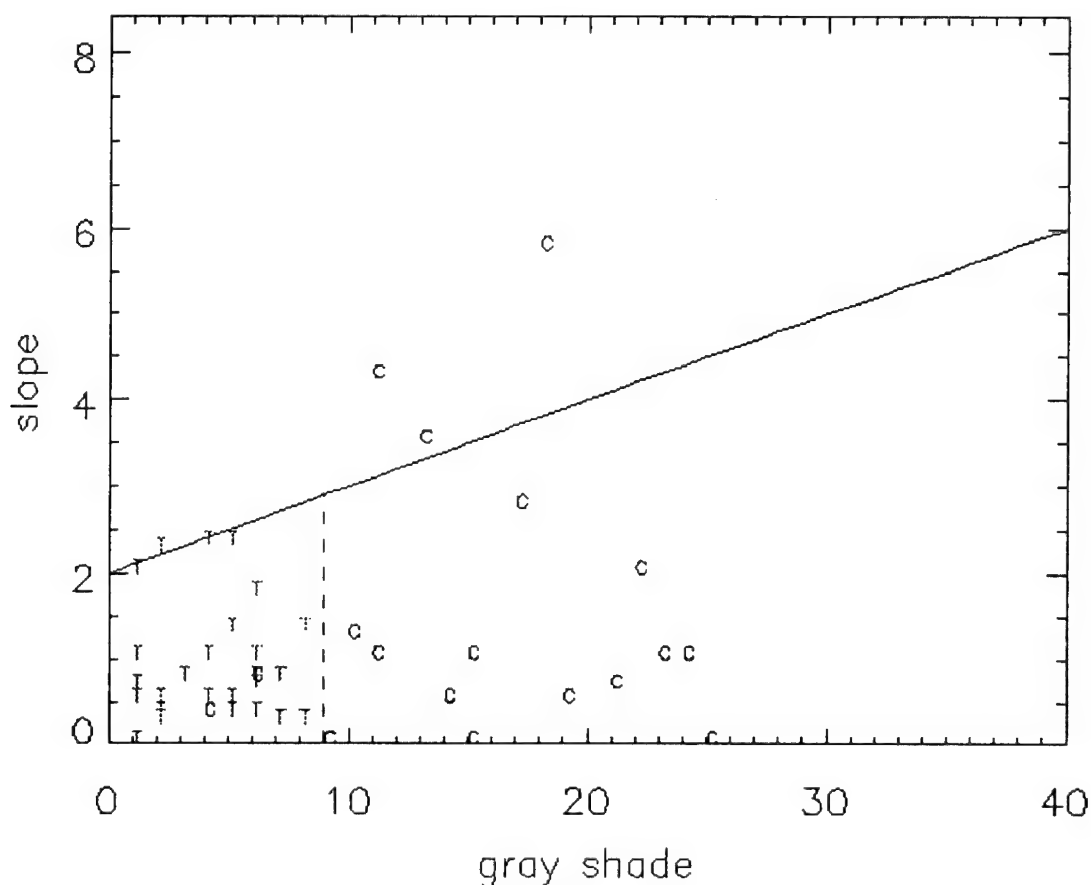


Figure 1

Distribution of thunderstorms (T) and cirrostratus (C) for two cases over the tropics. The solid line represents the slope threshold (S), the dotted line the latitude threshold for the tropics.

3. RESULTS

Figure 2 shows examples of cumulonimbus identification superimposed over satellite imagery. The "1's" indicate the location of cumulonimbus clouds. Figure 2a is a large thunderstorm complex over Oklahoma. Note the cirrus outflow is not identified as a thunderstorm. However some of the transverse bands to the north, due to their satellite signature, are misidentified.

Figure 2b shows a case of embedded thunderstorms within a large monsoon cloud band in the Arabian Sea. The success of the algorithm is evident, embedded thunderstorms are identified while surrounding cirrostratus is not. The previous method would have indicated the entire cloud field as cumulonimbus. Many other cases (not shown) give the same results.

Initial efforts comparing RTNEPH cumulonimbus locations and SSM/I rain rates have met with limited success.

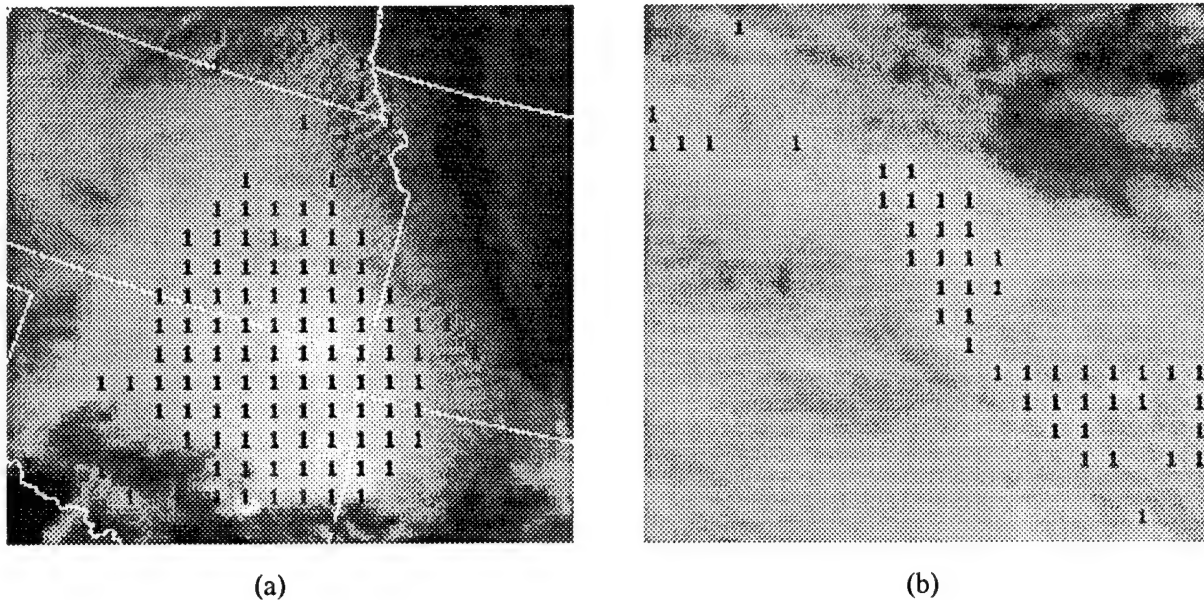


Figure 2

Thunderstorm identification in RTNEPH through the CST technique. The "1's" represent thunderstorm locations. Figure 2a is over Oklahoma, figure 2b over the Arabian Sea.

4. CONCLUSIONS

The application of a three-step algorithm, using a variation of the CST first presented in Adler and Negri, has vastly improved cumulonimbus identification within the RTNEPH. The algorithm eliminates the overanalysis problem over polar regions, and the overall distribution of thunderstorms within the RTNEPH is much more realistic. The algorithm has proven so successful it will likely be used even as newer cloud models are brought into AFGWC during the next decade.

ACKNOWLEDGEMENTS

We would like to thank Capt Louis Cantrell and TSgt Morris Friedman for their assistance in satellite interpretation and workstation expertise.

REFERENCES

¹Adler, R. F., and A. J. Negri, 1988: A Satellite Infrared Technique to Estimate Tropical Convective and Stratiform Rainfall. *J. Appl. Meteor.*, 27, 30-51

**SESSION VI:
CIRRUS AND CONTRAIL CLOUDS**

FOUR DECADES OF CIRRUS AND CONTRAIL OBSERVATIONS

Arnold A. Barnes, Jr.
PL/GPA
Hanscom AFB, MA 01731-3010

ABSTRACT

Since 1952 I have been encountering the effects of contrails and cirrus clouds on DoD operations and systems. B-47s conducting visual bombing runs over the Isle of Man for electronic scoring would leave contrails which rapidly spread out into a layer of cirrus so that only three runs could be conducted before the clouds obstructed visual sighting of the target. Anomalies in the flight characteristics of nosecones reentering the atmosphere at Kwajalein were traced to the presence of cirrus clouds along the reentry path. Visual observations from the ground and from jet aircraft, plus radar observations showed the almost continuous presence of cirrus clouds over Kwajalein. Detection of large (2 mm) cirrus particles in clear air led to modification of PMS (Particle Measuring Systems) probes and subsequent C-130 flights to characterize what is now known as sub-visual cirrus. Eight data reports were produced on flights into cirrus clouds over New Mexico in support of the Airborne Laser Laboratory (ALL) in an attempt to determine the effects of cirrus clouds on a laser beam trying to destroy an incoming ICBM (Intercontinental Ballistic Missile). For aircraft operating near the tropopause, sub-visual cirrus reduces the detection range of the IRST (InfraRed Search and Track) and the lethality near the ABL (AirBorne Laser). Gravitational settling of cirrus particles may be the mechanism required to remove the excess water vapor forecast for the upper tropopause by NWP (Numerical Weather Prediction) models, and the inclusion of both ice crystals and small drops in cirrus clouds may help in the resolution of the energy balance of the earth's atmosphere.

1. ENGLAND IN THE MID 1950'S

As an Air Weather Service (AWS) forecaster supporting B-47s operating from bases in England, I had to forecast cloud cover over the Isle of Man where SAC had an electronic bomb scoring range. The B-47s made visual bomb runs over the target and were scored for accuracy. Frequently only three or four runs could be made over the target before the contrails would spread precluding the visual bombing runs. Since consistent, outstanding scores within SAC were awarded with spot promotions, forecasting of contrails was a prime interest of the pilots we were supporting at that time.

Between rotating wings of B-47s and B-36s the Detachment had to catch up on AWS proficiencies. On one nice hazy day we started making pibal runs. The first balloon was lost at 23,000 ft. We assumed that the balloon burst, so we launched a second balloon which also disappeared at 23,000 ft. When the third pibal disappeared at the same level we became suspicious and contacted a plane flying in the area and the crew confirmed that there was a thin layer of cirrus clouds at that altitude which was readily visible from above but not noticed from below because of haze at lower levels.

2. KWAJALEIN IN THE MID 1970'S

The Kwajalein Atoll is located in the tropical Pacific between 8° and 9° N, just to the west of the international date line. The lagoon is used as a impact point for testing re-entry vehicles (RVs) launched from Vandenberg AFB. Our mission¹ was to forecast bad weather for the tests of the re-entry vehicles, and then to document the microphysics along the path of the RV after the fact. Because the tropopause is high, ~55,000 ft, Ed Uthe's SRI lidar was brought in for some of the first missions. During the checkout runs in nice weather, lidar returns between 50 to 60 thousand feet were attributed to turbulence near the tropopause, similar to the returns noticed on the high power tracking radars.

Anomalies in some of the RV trajectories had been noticed. An inspection of the movies taken during re-entry showed that these RVs passed through cirrus which did not obstruct the view of the glowing RV, but which momentarily lit up as the RV passed through the cirrus. Theoretical work indicated that ice particles larger than 80 microns would survive in their passage through the shock wave surrounding the vehicle, would impinge on the vehicle, roughen the surface and cause premature transition from laminar to turbulent flow thereby changing the RV flight characteristics.

At this point we had to start forecasting the occurrence of this high thin cirrus at nighttime when the re-entries were scheduled to occur for maximum photographic coverage. Kwajalein was near the edge of the view from the US western weather satellite, and this satellite could just be seen by our antennas at Hanscom AFB in Massachusetts. The radio/telephone conversations between our forecast team at Kwajalein and our AIMS satellite team at Hanscom were critical in our success in forecasting for both "clear air" and "weather erosion" missions. Needless to say, it was difficult to find areas clear of thin cirrus at night, even with the use of the instrumented WB-57F and the tracking radars².

A WB-57F was outfitted with PMS probes to obtain particle size distributions in clouds at altitudes up to 60,000 ft. It also had a replicator which encaptured cirrus particles. One thing we noticed, even at temperatures as cold as -60°C, was the occurrence of small round drops among the ice crystals. Lab experiments and text books said the homogeneous nucleation occurs at -40°C and that water droplets could not exist in the atmosphere at temperatures below -40°C. Because of the many problems with operating the replicator we concluded that we would never get this past any reviewers so we never wrote up our observations. A few years later it was reported that polarized lidar returns from very

cold cirrus indicated the presence of water. At a seminar I gave at SUNY Albany, Bernie Vonnegut suggested that these small droplets might be dilute sulfuric acid droplets.

Almost every sunrise and sunset at Kwajalein the sky seemed to be covered with cirrus. To see if cirrus was present during the day, we flew the PMS outfitted Learjet at maximum altitude during the middle of the day. At 45,000+ ft the sky was considerably darker and we could easily see "cirrus above-us" against the dark background of space. We also found that we could see this cirrus from the ground on a clear day by blocking out the sun with the corner of a building and then looking for structure movements which were not due to the low level tropical ocean haze which blew from east to west. I have used this technique in mid-latitudes to assess the full areal extent of cirrus clouds when they initially seem to be only scattered. If you use sunglasses and sun blocking, you will see a lot more cirrus from the ground.

3. STRATOSPHERIC HAZE

Pictures taken from the WB-57F when well into the stratosphere above Kwajalein consistently showed thin haze layers in the stratosphere. The pilots said that they often noticed these layers when flying in the stratosphere. They never seemed to be flying right in a layer, but they could see them off on the horizon. Apparently the concentrations in the layers was small, but because of the long paths through the layers they became visible.

4. CIRRUS PARTICLE SIZES

The flights of the cloud physics instrumented MC-130E from Wright-Patterson AFB in Ohio to Kwajalein was used for training the crews on the use, operation and in-flight maintenance. Glass and Varley³ reported on crystal types and sizes obtained in cirrus clouds over the southwestern US during a period of some striking optical phenomena.

The ASSP which detects particles in the 0.5 to 20 micron range checked out fine in the lab and in the aircraft when on the ground. However, when we were flying at altitude the smallest size channels were almost always registering particles. We conducted many shake tests in the lab to isolate the problem, but were never successful. On a west bound flight at 24,000 ft over Denver, Colorado the sky was clear, we could easily see the Air Force Academy north of Colorado Springs, we were getting returns in the smallest two ASSP channels, when we also began to pick up particles in the 2-D precip probe which detects particles in the 800 to 6400 micron range! This was very surprising since the buffer had to fill up with particles before they were displayed on the monitor. Subsequently we modified the 2-D probes so that when the internal clock, which measured the time between particles, overflowed a blank particle was entered into the buffer. This allowed us to see infrequent particles on the monitor and also gave us the exact time between particles.

We were able to conduct a couple of flights specifically into subvisible cirrus with the modified PMS equipment which were reported by Barnes^{4,5}. Crystals up to 2 mm in length were observed with densities as low as one particle per eight cubic meters. We also concluded that cirrus and subvisual cirrus clouds are composed primarily of two sizes of crystals, the micron/sub-micron size and the millimeter size particles⁶.

5. OTHER OBSERVATIONS OF CIRRUS PARTICLES

Anyone who has seen Cirrus Uncinus, commonly called "mares tails," has witnessed the fall of large cirrus crystals in the atmosphere. Braham and Spyres-Durand⁷ calculated that these large crystals could fall as much as 2 kilometers in dry air before sublimating. The hook on the lower end of cirrus uncinus is due to the fact that the crystals have lost much of their mass and are falling much slower.

In Arctic regions there are "Diamond Dust Falls" where, on a perfectly clear day, the sky twinkles and there are ice crystals blowing across the road and piling up in gutters and other low places. The same phenomena is called a "Blue Norther" in Texas when the cold wind blows from the north, the sky is a dark blue and twinkles as the large cirrus particles fall in the atmosphere. The only difference is that the crystals generally do not reach the ground in Texas.

6. CIRRUS DATA FOR THE AIRBORNE LASER LABORATORY

In 1977 the Airborne Laser Laboratory (ALL) asked us to take data in cirrus clouds over New Mexico. The ALL was designed to destroy incoming RVs with a powerful laser. AFOSR funded our flights to obtain cirrus particle size distributions and particle type information. These data were to be used as input to models being developed by Aerospace to predict the attenuation of the laser beam by cirrus which would be above the flight altitude of the ALL. The data in the eight reports on these flights⁸⁻¹⁵ have been used by Vernon Derr¹⁶ and others to describe cirrus clouds.

7. HORIZONTAL PATHS THROUGH CIRRUS

When the first InfraRed Search and Track (IRST) equipment was flight tested over a decade ago there was a ten fold reduction in detection range over what had been predicted. Subsequently this was attributed to unforecast thin cirrus clouds, aerosols and haze near the tropopause during the time of the flight tests. Subvisual cirrus will also cause some attenuation of the ABL beam which will require the beam to dwell on the target for a longer time to make a kill.

SAGE data are often used to estimate attenuation of a horizontal beam through the upper atmosphere. I believe that the SAGE data underestimates the attenuation when applied to systems such as the IRST, the AIRST and the ABL.

8. CONTRAILS

Contrails are an operational nuisance. Not only do they advertise the presence of high flying aircraft and UAVs during periods of sunlight and full moon, but they can spread out and thicken to make surveillance from high flying aircraft, UAVs and satellites difficult if not impossible. Self generated contrails might be a problem for the ABL as it loiters behind the front line of battle.

In-situ measurement of contrails is not easy. We tried it, with minimal success, using a PMS instrumented Learjet flying in a constant bank circle while letting the wind carry both the contrail and the aircraft. The Germans tried the same approach but switched to using two aircraft, one following the other.

9. REFERENCES

1. Barnes, A.A., L.D. Nelson and Lt. J.I. Metcalf, 1974: Weather Documentation at Kwajalein Missile Range, Preprints, 6th Conference on Aerospace and Aeronautical Meteorology, 66-99; also AFCRL-TR-74-0430. AD A000925.
2. Barnes, A.A., and Capt J.I. Metcalf, 1975: ALCOR High Altitude Weather Scans, AFCRL/A.N.T. Report No. 1, Air Force Surveys in Geophysics, No. 335, 31 Dec. 1975, AFCRL-TR-75-0645. AD B011588L.
3. Glass, M. and D.J. Varley, 1978: Observations of Cirrus Particle Characteristics Occurring with Halos, Preprints, Cloud Physics and Atmospheric Electricity Conference, Issaquah, Washington, 31 July - 4 August 1978.
4. Barnes, A.A., 1980: Ice Particles in Clear Air, Preprints of the 8th International Conference on Cloud Physics, Clermont-Ferrand, France, 15-19 July 1980, 189-190. AFGL-TR-81-0009. AD A094444.
5. Barnes, A.A., 1980: Observations of Ice Particles in Clear Air, Journal de Recherches Atmospherique, 14, No. 3-4, 311-315. AFGL-TR-81-0347. AD A108914.
6. Barnes, A.A., 1982: The Cirrus and Subvisible Cirrus Background, Preprints, 2nd Symposium on the Composition of the Nonurban Troposphere, Williamsburg, VA 25-28 May 1982, 170-175. AFGL-TR-82-0193. AD A117389.
7. Braham, R.R., and P. Spyres-Durand, 1967: Survival of Cirrus Crystals in Clear Air, Journal of Applied Meteorology, 6, 1053-1061.
8. Varley, D.J. 1978: Cirrus Particle Distribution Study, Part 1, Air Force Surveys in Geophysics, No. 394, 71 pp. AFGL-TR-78-0192. AD A061485.
9. Varley, D.J., and Brooks, D.M. 1978: Cirrus Particle Distribution Study, Part 2, Air Force Surveys in Geophysics, No. 411, 108 pp. AFGL-TR-78-0248. AD A063807.
10. Varley, D.J. 1978: Cirrus Particle Distribution Study, Part 3, Air Force Surveys in Geophysics, No. 404, 67 pp. AFGL-TR-78-0305. AD A066975.
11. Varley, Lt Col D.J., and A.A. Barnes, 1979: Cirrus Particle Distribution Study, Part 4, Air Force Surveys in Geophysics, No. 413, 18 June 1979, 91 pp. AFGL-TR-79-0134. AD A074763.
12. Cohen, I.D. 1979: Cirrus Particle Distribution Study, Part 5, Air Force Surveys in Geophysics, No. 414, 81 pp. AFGL-TR-79-0155. AD A077361.
13. Cohen, Capt I.D., and A.A. Barnes, 1980: Cirrus Particle Distribution Study, Part 6, Air Force surveys in Geophysics, No. 430, 4 September 1980, 106 pp. AFGL-TR-80-0261. AD A096772.
14. Varley, Lt Col D.J., Capt I.D. Cohen and A.A. Barnes, 1980: Cirrus Particle Distribution Study, Part 7, Air Force Surveys in Geophysics, No. 433, 16 October 1980, 82 pp. AFGL-TR-80-0324. AD A100269.
15. Cohen, I.D. (1981) Cirrus Particle Distribution Study, Part 8, Air Force Surveys in Geophysics, No. 437, 28 October 1981, 110 pp. AFGL-TR-81-0316. AD A118 715.
16. Derr, V.E., 1980: Attenuation of Solar Energy by High, Thin Clouds, Atmospheric Environment, 14, 719-729.

Retrieval of Cirrus Radiative and Spatial Properties Using Coincident Multispectral Imager and Sounder Satellite Data

Robert P. d'Entremont

*Atmospheric and Environmental Research, Inc.
840 Memorial Drive, Cambridge, MA 02139-3794*

Donald P. Wylie

*Space Science and Engineering Center
University of Wisconsin, Madison, Wisconsin 53706*

Szu-Cheng Ou and Kuo-Nan Liou

*Department of Meteorology / CARSS
University of Utah, Salt Lake City UT 84112*

In addition to the wide variability in properties common for other types of clouds, cirrus clouds have transmissivity values t_λ that span the entire possible domain $0 \leq t_\lambda \leq 1$. This variability adds complexity to the analysis of cirrus clouds. In comparison to opaque clouds, uncertainties exist in thin cirrus cloud amount, altitude, thickness, and optical properties as retrieved from satellite because the measured cirrus signal is affected additionally by an unknown radiation component from below.

Cirrus radiative and spatial properties are derived using HIRS CO₂ Slicing and multispectral AVHRR imager techniques. Each of these models is based on radiative transfer principles that intrinsically account for both the semi-transparent nature of thin cirrus clouds and the attenuation effect of atmospheric water vapor in the MWIR and LWIR thermal window regions.

Comparison is made of cirrus cloud attributes, both spatial and radiative, obtained for the same cloud scene using measurements from the independent AVHRR and HIRS sensors onboard the NOAA polar orbiting satellites. While the fundamental requirement is the same for both the HIRS and AVHRR models, i.e. to detect the presence of thin cirrus and to determine its radiative and spatial attributes, the capabilities of the two techniques depart from each other in

numerous respects. The most important distinctions are based on the differences in the spectral bandpass and spatial resolutions of the HIRS and AVHRR sensors.

Three cirrus retrieval algorithms, CO₂ Slicing, AVHRR, and SERCAA have been shown to complement one another for increasing the accuracy of the obtained cirrus parameters. New techniques will be presented that combine the strongest and most reliable attributes of the imager and sounder-based cirrus retrieval algorithms in combination with SERCAA-derived background analyses to generate an improved overall cirrus analysis. The "background" may be either the clear ground or an underlying water-droplet cloud. Improved SERCAA estimates of underlying cloud and surface temperature can significantly improve the AVHRR and HIRS CO₂ Slicing determination of cirrus bulk emissivity.

The SERCAA-derived cirrus fraction N is useful to CO₂ slicing in separating the effect of N from the effective emissivity $N\epsilon$ for those cirrus clouds whose optical attributes are uniform within a particular HIRS FOV, thus allowing for direct comparisons of the true thermal infrared cirrus bulk emissivities retrieved by each algorithm. On the other hand, the CO₂ slicing technique provides an independent determination of cirrus effective altitude z which obviates the need for the AVHRR parameterization of the variation of ϵ with wavelength.

Better cirrus emissivity analyses in turn will significantly improve the accuracy of cirrus radiative models.

AN ICE CRYSTAL GROWTH MODEL FOR CIRRUS CLOUD FORMATION

S.C. Ou, K.N. Liou, and D. Frankel

Department of Meteorology/CARSS

University of Utah

Salt Lake City, Utah 84112

ABSTRACT

In conjunction with the formation of cirrus clouds, we have developed a simplified ice crystal growth model, incorporating parameterizations of heterogeneous/homogeneous ice nucleations, diffusional growth, and gravitational accretion and settling adjustments. We demonstrate that the mean ice crystal size and ice water content derived from this theoretical model are dependent on temperatures and their values are comparable with those determined from aircraft measurements in midlatitude cirrus clouds.

1. INTRODUCTION

Regularly covering about 20 - 30 % of the globe, cirrus clouds have been recognized as an important regulator of the earth radiation budget and climate based on a number of observational and modelling studies (Liou 1986; Ou and Liou 1995). In particular, typical cirrus clouds are relatively opaque to thermal IR radiation but transparent to solar radiation. Their presence would tend to warm the underlying surface. The competition between the solar albedo and thermal IR greenhouse effects involving cirrus clouds is dependent on such factors as the cloud position, microphysics and their radiative properties. At this point, the role of cirrus clouds in weather and climate systems remains to be the least understood component.

Commonly observed ice crystals in cirrus clouds include columns, plates, bullet rosettes, dendrites, and aggregates with sizes ranging from 5 to about 600 μm . These ice crystals are initially formed by either heterogeneous or homogeneous freezing nucleations. Established cloud physics theories have shown that the rate of these nucleation mechanisms depends primarily on the relative humidity, the concentration of ice-forming nuclei or condensation nuclei, and temperature. The embryonic ice crystals are subject to diffusional growth, along with gravitational accretion (collision/coalescence) and settling.

In conjunction with our efforts to construct a physically based cirrus cloud formation model, we have developed an ice crystal growth model that includes heterogeneous and homogeneous ice nucleation processes; diffusional growth, accretion, and gravitational settling. In particular, we examine the temperature dependence of ice crystal growth in terms of ice water content (IWC) and mean effective ice crystal size.

2. THE DEPENDENCE OF ICE MICROPHYSICS ON TEMPERATURE

We have developed models for the diffusional and accretional growths of ice crystals. For the former we begin with the growth equation for ice crystal mass as follows:

$$\frac{dm}{dt} = \frac{4\pi C}{A+B} (S_1 - 1), \quad (1)$$

where C is the shape factor; A and B are thermal and mass diffusion coefficients, respectively; and S_i is the ice supersaturation, which can be solved by using the mass balance equation that involves IWC.

The initial ice crystal number concentration is prescribed based on the fundamental physical principles for ice nucleation. For temperatures above -35°C , it is assumed that heterogeneous nucleation dominates in which the empirical parameterization is used. For temperatures below -35°C , homogeneous freezing is the major ice forming mechanism. The number concentration follows the empirical relation derived from laboratory experiments.

Assuming that the ice crystals have the same size and shape and employing a time-marching numerical procedure, the IWC results are illustrated by the dashed line in Fig. 1a. Also shown in Fig. 1a are values of the averaged IWC derived from the aircraft dataset presented by Heymsfield and Platt (1984) for a temperature range from -20° to -60°C . The diffusional growth clearly shows that IWC is a function of temperature. The systematically higher IWC values from diffusional growth calculations as compared with parameterization results are due to the fact that gravitational settling initiated by accretion has not been accounted for.

The accretional growth for ice crystals due to collision and coalescence is modeled by using the conventional growth equation in the form

$$\rho_i \frac{dV}{dt} \approx \bar{A} \bar{E} \text{IWC}(w_T - w), \quad (2)$$

where ρ_i is the ice density, V is the ice crystal volume, A is the ice crystal cross sectional area, \bar{E} is the mean collision efficiency which is assumed to be 1 in this model, w_T is the crystal terminal velocity, and w is the updraft velocity, which for simplicity is assumed to be zero in the calculation. From laboratory and field experiments, the ice crystal volume, cross sectional area, and terminal velocity can be related to length as follows: $V = aL^3$, $A = bL^2$, $w_T = cL^d$, where a , b , c , and d , are coefficients determined from measured data. Numerical solutions can be obtained by performing the integration over time in terms of the crystal length.

The total ice water mass settled out of the cloud can be obtained from the vertical divergence of the ice mass flux integrated over time of ice crystal growth as follows (Heymsfield and Donner 1990):

$$\text{IWC} = - \int_0^t \frac{\partial}{\partial z} (\text{IWC} \cdot w_T) dt'. \quad (3)$$

The terminal velocity w_T is dependent on the ice crystal length which in turn is governed by accretion. The results of the mean D_e for diffusional growth only and for diffusion plus accretional growth are illustrated in Fig. 1b. With the inclusion of accretion, ice crystals become larger. For larger ice crystal sizes associated with warmer temperatures in diffusional growth, the accretion process further enhances their growth. In Fig. 1a, IWC is reduced by the incorporation of gravitational settling which follows accretion growth.

3. DISCUSSIONS

There has been significant progress toward incorporating a fully prognostic cloud scheme to evaluate cloud water content in GCMs. To be fully interactive with a radiation parameterization program, information on the mean effective cloud particle size is required. It is unlikely in the near future that cloud particle size distribution will be predicted in GCMs. In the previous section, we have demonstrated that the mean effective ice crystal size is dependent on temperature based on both aircraft observations and model simulations. Jakob and Morcrette (1995) have illustrated that the ECMWF model is sufficiently sensitive to the use of an interactive mean effective ice crystal size driven by temperature in regard

to the radiation budget at the top and surface. Analyses of numerous ice crystal size distributions that have been obtained during FIRE-II (midlatitude) and CEPEX and TOGA-COARE (tropics) are important in order to narrow down the uncertainty in the representation of ice crystal size distribution using large scale parameters such as temperature. In addition, more detailed theoretical analyses should be carried out for the simulation of ice crystal size distributions using one-dimensional parcel method to understand the critical parameters, besides temperature, that may affect the growth of ice crystals.

4. ACKNOWLEDGEMENTS

This research work has been supported by AFOSR Grant F49620-94-1-0142.

REFERENCES

- Heymsfield, A.J., and C.M.R. Platt, 1984: A parameterization of the particle size spectrum of ice clouds in terms of ambient temperature and ice water content. J. Atmos. Sci., 41, 846-855.
- Heymsfield, A.J., and L.J. Donner, 1990: A scheme for parameterizing ice-cloud water content in general circulation models. J. Atmos. Sci., 47, 1865-1877.
- Jakob, C., and J.-J. Morcrette, 1995: Sensitivity of the ECMWF model to the treatment of ice phase. Workshops on Microphysics in GCMs World Climate Research Program Proceeding, Calgary, Canada, May 23-25 1995.
- Liou, K.N., 1986: Influence of cirrus clouds on weather and climate processes: A global perspective. Mon. Wea. Rev., 114, 1167-1199.
- Ou, S.C., and K.N. Liou, 1995: Ice microphysics and climatic temperature perturbations. Atmos. Res., 35, 127-138.

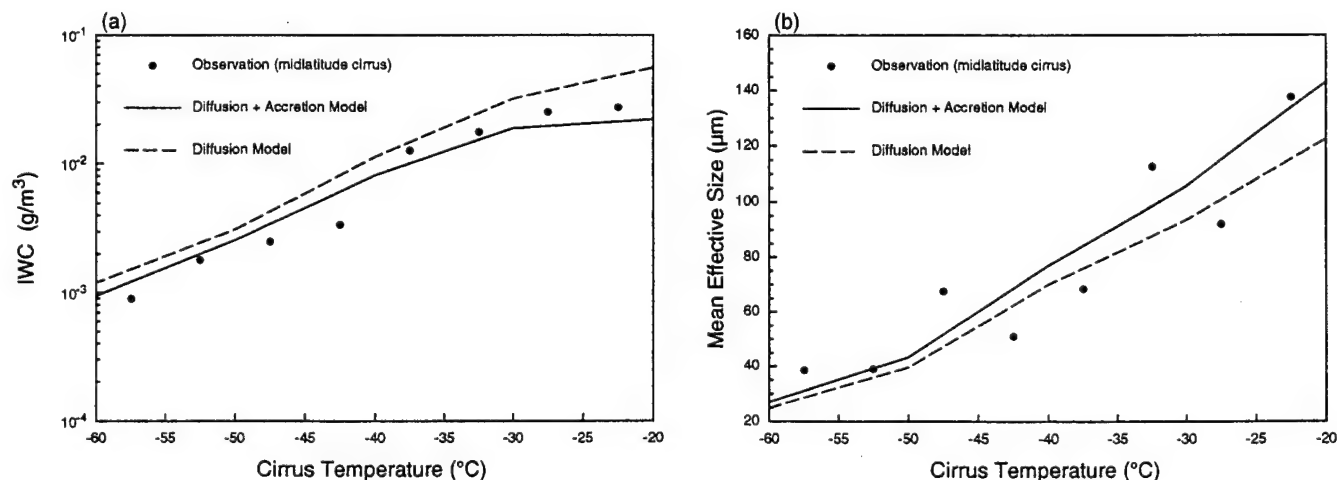


Figure 1. (a) IWC derived from aircraft measurements for midlatitude cirrus clouds as a function of temperature. (b) Ice crystal mean effective size (D_e) obtained from aircraft measurements for midlatitude cirrus clouds as a function of temperature. In both frames, the solid and dashed curves represent results computed from a diffusion plus accretion model and a diffusion model, respectively.

THIN CIRRUS EFFECTS ON HYPERSPECTRAL DETECTION OF TRACE GASES

P. Daniel Hestand and Kenneth B. MacNichol
TASC
Reading, Massachusetts USA 01867

ABSTRACT

A spectral simulation technique was formulated to quantify the effects of optically thin cirrus on the detection of fugitive gases using hyperspectral sensors. The purpose of the study was to determine the feasibility of using hyperspectral sensors in the detection of trace gases when thin cirrus is present. Three gases were studied: sulfur dioxide, sulfur hexafluoride, and methyl chloride. Spectral channels representing the strongest characteristics of the study gases at the sensor resolution were selected. Radiances computed in these detection channels with and without the gas present were used to determine a detection threshold and probability. The probability of detection was formulated to exploit the large number of detection channels provided by a hyperspectral sensor. The resulting scheme incorporates sensor noise effects and is suitable for computing probability of detection for a variety of detection scenarios and sensor models. Various detection scenarios were generated using the HITRAN 1992 database and FASCODE version 3's parameter set and internal aerosol and cirrus models. Attention focused on the effects of variation in gas concentration, gas layer temperature, cirrus optical depth, and atmospheric profile. Results indicate that using high-resolution data allows detection of gases with strong spectral signatures under unfavorable conditions (cirrus optical depths ≈ 0.2 , low concentrations, etc.).

1. INTRODUCTION

The use of infrared spectroscopy to detect the presence of trace gases in the lower atmosphere has been established in the literature (Zachor¹, et al.). However, detecting these gases in the presence of cirrus, particularly subvisual cirrus, has not been established. Cirrus can reduce the spectral signal of the trace gas relative to the atmospheric spectral signatures and introduce noise into the observed signal. Sensor noise further reduces this spectral signature causing weak signals to be nearly undetectable while stronger signals are easily detectable. This paper describes a study conducted at TASC to evaluate the effects of optically thin cirrus on the detection, using hyperspectral sensors, of fugitive gases near the earth's surface.

2. SCOPE AND APPLICABILITY

The primary objective of this effort was to study the feasibility of detecting trace gases in the presence of cirrus clouds using space-based hyperspectral sensors. To meet this objective, the study focused on simulating remote sensing to derive probability of detection as a function of parameters such as cirrus optical depth, gas concentration, and gas layer temperature. The study simulated nighttime detection in the 3 to 14 micron wavelength range using FASCODE² version 3 and the HITRAN 1992 spectral line database. The sensor was modeled as a hyperspectral type with resolution ranging from 3 cm^{-1} to 0.1 cm^{-1} . We assumed that the internal sensor noise was Gaussian and varied independently from channel to channel.

The study gases were sulfur dioxide, sulfur hexafluoride, and methyl chloride. Sulfur dioxide has absorption characteristics in three bands: 8 to 9.43 microns, 7.14 to 7.63 microns, and 3.95 to 4.07 microns. We used the 8 to 9.43 micron band from which to choose detection channels because it had the strongest absorption features in a spectral region where the atmosphere is largely transparent. Sulfur hexafluoride has a single strong absorption feature from 10.5 to 10.64 microns. Methyl chloride has absorption features from 3.14 to 3.45 microns.

3. TECHNICAL APPROACH

Our technical approach consisted of four parts to quantify the thin cirrus effects as shown in Figure 1. First, select the gas detection channels. Second, simulate the detection scenarios via FASCODE to provide simulated radiances in the selected channels. Third, establish a detection threshold based on sensor noise characteristics and the channel radiances. Finally, compute a probability of detection based on the established detection threshold.

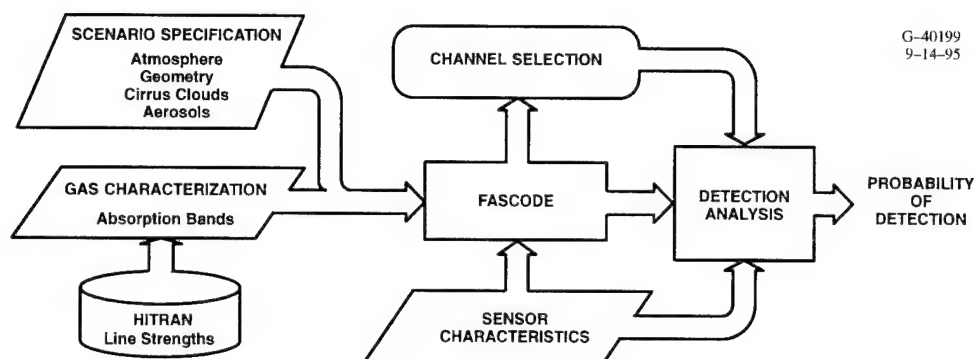


Figure 1 Technical Approach to Quantifying Thin Cirrus Effects on Gas Detection

We selected the gas detection channels by ratioing the radiances computed at 0.1 cm^{-1} resolution with no study gas present against the radiances computed in the same channels with the study gas present. Radiances were computed using a "standard" scenario consisting of the 1976 U.S. Standard Atmosphere, no clouds or aerosol, fixed surface temperature, emittance, and reflectance, fixed gas plume height, concentration, and temperature, and an atmosphere consisting of H_2O , CO_2 , O_3 , N_2O , CO , CH_4 , and O_2 . The channels used for gas detection were chosen as a fixed percentage of all channels showing a ratio different from unity.

The detection scenarios were constructed from a subset of the FASCODE input parameters. We used the mid-latitude summer, mid-latitude winter, and tropical model atmospheres. The surface emissivity and reflectance were set to 0.9 and 0.1, respectively, and surface temperatures were chosen to be consistent with the climate zone represented by the atmospheric model. A gas plume was modeled with a thickness of 0.1 km and a base altitude of 0.2 km. Plume temperatures were set at the surface temperature and the surface temperature ± 5 degrees. Gas concentrations were supplied by a plume model and we chose those concentrations representative of a point downwind close to the plume source. We used FASCODE's Subvisual Cirrus Model and set the cirrus base altitude at 10 km for all atmospheric models. The cirrus depth was set at 0.3 km and we used optical depths of 0.2 and 0.01. Finally, we chose the rural aerosol model for the troposphere and the background volcanic model for the stratosphere. All views were taken from space to the surface at nadir.

To quantify the results, we formulated a probability of detection (P_d) based on the computed radiances in the detection channels. We assumed that the radiances in the detection channels were normally distributed about a mean value with variance given by the variance of the sensor noise. We computed a test statistic as the natural logarithm of the ratio of the probability density functions of the without-gas radiances to the with-gas radiances. This test statistic formed the basis for the detection threshold. The P_d was then computed by assuming that the test statistic is normally distributed and specifying a probability of false alarm (P_{fa}). By fixing the P_{fa} , we also fixed the threshold value of the test statistic. Integration of the probability density function of the test statistic from minus infinity up to the threshold gave the P_d . This technique follows a derivation given in Anderson³. The key point is the relationship between the P_{fa} , the sensor noise, gas spectral signal, and P_d . For a given P_{fa} , a weak gas signal should exhibit low P_d . Under the same conditions, a strong gas signal with increased noise should also exhibit a low P_d .

4. RESULTS

We set up the scenarios and used FASCODE to derive the radiances for each scenario, both without the gas and with the gas present. The P_d results are shown in Figure 2. Gases with weaker spectral signals (SO_2 and CH_3Cl) relative to the atmospheric spectral signals gave non-zero P_d 's for the case with no cirrus and no aerosol and with either cirrus or aerosol only present. Addition of both cirrus and aerosol dropped the P_d 's for these gases to zero but did not for SF_6 . The effect of sensor resolution is obvious. Without hyperspectral resolution, the gas is undetectable. When there is contrast between the plume temperature and surface temperature, SF_6 is more easily detectable. The same applies for increased concentrations. Addition of thin cirrus and aerosol reduced the detectability significantly. There is also a strong dependence on the water vapor content of the column through which the gas is viewed. This is seen in the consistently lower P_d for the tropical model atmosphere and the consistently higher P_d for the mid-latitude winter model atmosphere.

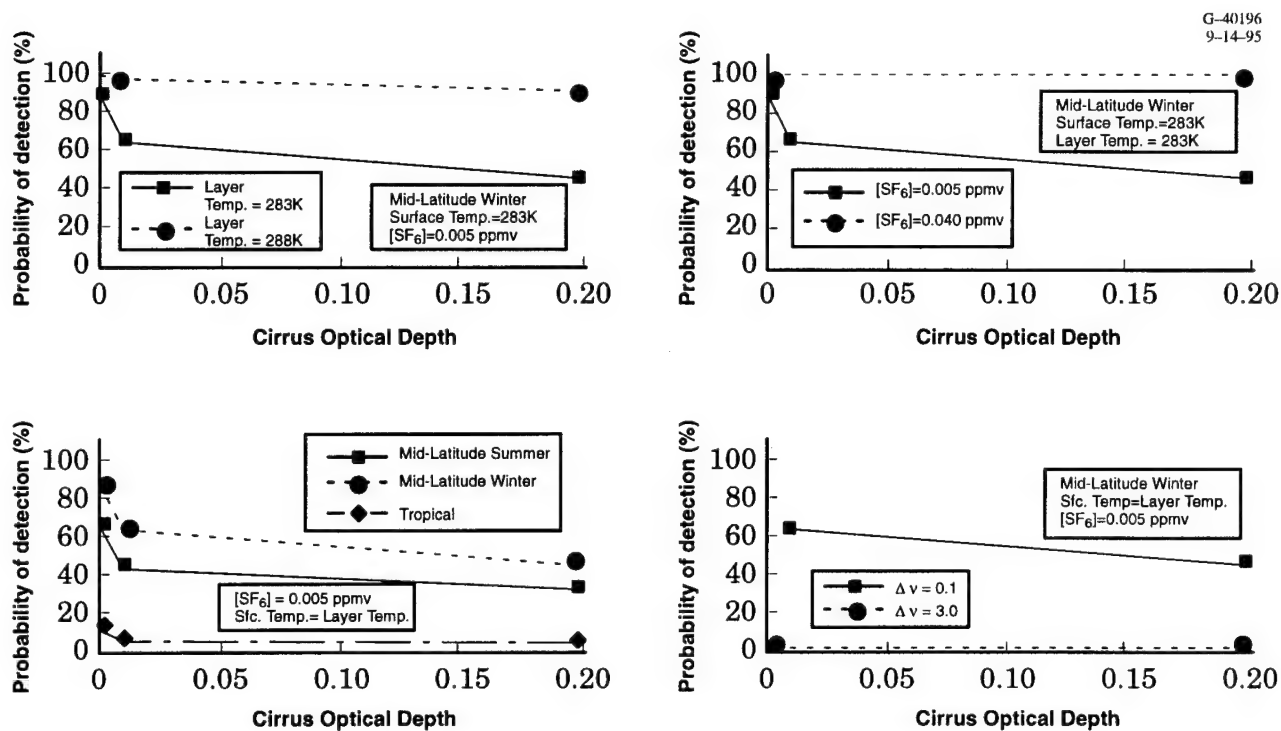


Figure 2 Probabilities of Detection for SF₆

5. CONCLUSIONS

Our simulation technique and method of detectability quantification indicate that thin cirrus can significantly impact the detection of fugitive gases in the lower atmosphere. In some cases, the presence of very thin cirrus can reduce the detectability to zero. Without the aid of hyperspectral resolution, the gases would be undetectable under most circumstances including those where no cirrus and only aerosols were present. Water vapor content appears to play an important role in the detectability of the gases and in some cases renders the gas undetectable.

6. ACKNOWLEDGMENTS

Special thanks to Dr. Eric Schmidt and Mr. Glenn Higgins for their kind advice and encouragement. Thanks also to Dr. Gail Anderson and Mr. Jim Chetwynd of the Phillips Laboratory for their assistance in using FASCODE.

7. REFERENCES

1. Zachor, A.S., Bartschi, B., and Ahmadjian, M., Limit on Fourier Transform Infrared (FTIR) Detection of Trace Gases, *Proceedings SPIE*, vol. 289, 1981, pp. 209-213.
2. Clough, S.A., et al., FASCOD3: Spectral Simulation, IRS '88: Current Problems in Atmospheric Radiation — *Proceedings of the 1988 International Radiation Symposium*, 1989.
3. Anderson, T.W., *An Introduction to Multivariate Statistical Analysis*, 2nd Edition, Wiley & Sons, New York, 1984.

SUBVISUAL CIRRUS CLOUDS ASSOCIATED WITH PROCESSES IN THE NATURAL ATMOSPHERE

E. Schmidt, D. Lynch, K. Sassen, G. Grams and J. Alvarez
TASC Inc., Reading, MA 01867, The Aerospace Corp., El Segundo, CA 90009,
University of Utah, Logan, UT, Clark-Atlanta University, Atlanta, GA 30314
NASA Langley Research Center, Hampton, VA 23665

ABSTRACT

Subvisual cirrus are defined as optically thin cirrus with zenith optical depth ≤ 0.05 in the visible. This includes threshold subvisual cirrus as defined in the literature. Subvisual cirrus are associated with at least five different dynamical phenomenon in the atmosphere. These associations are: equatorial, frontal, jet stream, orographic and other types. Characteristic properties of each cirrus association derived from reported observations are provided.

1. DEFINITION OF SUBVISUAL CIRRUS

The existence of subvisual cirrus has been documented by numerous investigators¹⁻⁷. We define subvisual cirrus as high, thin ice clouds with zenith optical depth, $\delta_{\text{ext}} \leq 0.05$ in the visible. This simple definition incorporates threshold-subvisible cirrus clouds⁸. Subvisual cirrus are typically invisible to ground-based observers, but may become visible under special conditions. These conditions include: high solar elevation angles, minimal boundary layer haze or turbulence, spatial variations in the cloud geometry and optical thickness. discrimination between subvisual cirrus and optically thick cirrus is established when an upper-bound threshold ($\delta_{\text{ext}} \leq 0.05$) is defined. This upper bound is based on the visual acuity of the human eye and the contrast between optically thin cirrus and the clear sky background. A caveat is that the discrimination of subvisual cirrus based on optical depth relaxes the "no physical manifestation" requirement historically imposed. Multi-level cloud systems are likely to have subvisual components (cloud edges or layers) and their presence is difficult or impossible to verify by ground-based observations.

2. SUBVISUAL CIRRUS ASSOCIATIONS

We define five types of associations between subvisual cirrus and the dynamic atmosphere: equatorial, jet stream, frontal, orographic and other types. The formation of a subvisual cirrus layer requires a high altitude moisture flux and turbulent conditions or wave action to initiate crystal growth. The vertical motion induced by gravity waves is attractive as a mechanism to initiate formation of optically thin clouds, particularly when banded structures are observed. Top-down convection processes at the tropopause are also possible formation mechanisms, as is motion due to lateral shearing equatorward of the jet stream core⁹. The intertropical convergence zone (ITCZ) and fronts are sources for gravity wave generation, while the jet core induces lateral shearing of similar magnitude to the Coriolis parameter on its flanks. Cloud formation is prevalent in all cases. A significant fraction of subvisual cirrus sightings are observations of cloud remnants. Orographically produced cloud remnants, material blown off anvil tops and diffuse contrails in regions with a high volume of air traffic are all examples. Rarer, more controversial observations of subvisual cirrus exist, but are beyond the scope of this paper. It is possible that subvisual cirrus are not caused by any of the suggested sources, but are merely an existing field of ice aerosols responding to their environment. However, we favor the interaction of moisture and

dynamic features of the environment as the sources for the associated subvisual cirrus. The interaction of gravity waves with moisture fields near the tropopause that are saturated with respect to ice is highly likely to cause cloud formation.

3. CHARACTERISTIC PROPERTIES OF SUBVISUAL CIRRUS

Table 1 summarizes the information cited in the following paragraphs. Nocturnal observations of subvisual cirrus have not been included, though they have been addressed⁸.

TABLE 1. Characteristics of associated subvisual cirrus clouds

	<i>Equatorial</i>	<i>Jet Stream</i>	<i>Frontal</i>	<i>Orographic</i>	<i>Other Types</i>
<i>Cloud Thickness</i>	≤ 1-2 km	1-2.5 km	0.5-1.0 km	1-4 km	≤ 0.5 km
<i>Horizontal Extent</i>	100-1000 km	10-100 km ^a , 10-20 km ^b	100-300 km	1-100 km	< 1-5 km
<i>Persistence</i>	days	< 1 day	1-4 hours	≤ 1 hour	minutes
<i>Composition</i>	ice hexagons	ice hexagons	variable	variable	variable
<i>Mass Density</i>	10 ⁻⁴ - 10 ⁻⁵ g/m ³	variable	10 ⁻² - 10 ⁻⁵ g/m ³	variable	variable, unknown
<i>Distance from Cloud-top to Tropopause</i>	1-5 km below	0.5-4 km below	1-2.5 km below	0.5-4 km below	0.5-2.5 below
<i>Comments</i>	largest extent, longest persistence	occur equatorward of jet core	observable under special conditions	glaciation processes require study	require further study

^aalong wind direction, ^bcross wind direction

Ground-based and airborne observers note the ubiquitous nature of thin cirrus in the Pacific²⁴. These cirrus are the result of deep convection, primarily at the ITCZ but including the warm pool. Subvisual cirrus associated with equatorial regions typically have the largest extent, longest persistence and are observed frequently. Subvisual cirrus associated with the jet stream is likely to be streak clouds due to the shear forces involved. A common scenario in the southern U.S. is the advection of subtropical moisture above 200-300 mb into the vicinity of a stationary jet stream. Jet stream subvisual cirrus can occur in tropical, mid-latitude and polar regions and in the upper- and lower-troposphere.

Subvisual cirrus are associated with the passage of fronts, particularly cold fronts. Pre-frontal bands of optically thin cirrus have a classic signature, as indicated in Table 1. These cirrus are generated by fronts, but do not appear to be strongly tied to them. This reinforces the concept of gravity wave propagation downstream as an activation mechanism. A limited number of cases where orographic lifting forces the formation of an optically thin cloud have been reported. There is a wide disparity in the observations reported, as reflected by the signature characteristics. There are two varieties of these clouds: streak clouds and vertically extensive clouds. The streak clouds tend to be elongated along the direction of the wind and of limited extent in the vertical and crosswind directions. Vertically extensive clouds have limited horizontal extent, but have highly variable geometrical thickness (typically 3-4 km).

Anvil tops are a source of optically thin clouds at high altitude. Whether the cloud objects observed are actually attached, subvisual cloud edges, or detached subvisual cloud remnants is uncertain. Contrails also form subvisual cloud objects as the water contained in the contrail diffuses horizontally to form a layer-like object. Anvil tops and contrail-generated subvisual cloud objects are typically composed of a complex variety of particles. These subvisual clouds are typically thin (≤ 0.5 km thick), highly transient and depend strongly on the atmospheric conditions. Other, more esoteric subvisual objects include "hotspots." Hotspots are typically detected just above or below extensive cirrus and stratus decks. These "hotspot" regions gain their name by the fact that they exhibit extremely strong backscattering of lidar signals, often exceeding backscatter ratios of 500:1. They are very thin (≤ 100 m thick) and persist for only ~ 10 minutes. It cannot be argued that hotspots are subvisual in all cases, as simultaneous measurement of the backscatter and depolarization in the presence of an extensive cloud object is difficult.

5. CONCLUSIONS

Subvisual cirrus clouds are important to understand as they can significantly affect the performance of airborne sensors. These clouds are difficult to detect by ground-based observers. These two factors lead us to the conclusion that it is necessary to understand how the presence of subvisual cloud objects is related to dynamic phenomena in the atmosphere. We have presented five such associations as a basis for analysis, further study and the impetus for forecast schemes.

6. REFERENCES

1. D.K. Lynch, "Subvisual Cirrus: What it is and where you find it," Proc. SPIE, Orlando, 1934, 264-274, 1993
2. Uthe, E.E. and P.B. Russell, "Lidar Observations of Tropical High-Altitude Cirrus Clouds," IAMAP Sym Radiation in the Atmos. Garmisch-Partenkirchen, Germany, 19-28 August 1976
3. A.A. Barnes, "Observations of Ice Particles in Clear Air," J. Rech. Atmos., 14, 311-315, 1980
4. A.A. Barnes, "The Cirrus and Sub-Visible Cirrus Background," AFGL-TR-82-0193, Hanscom AFB, MA, 1982
5. A. Heymsfield, "Ice particles observed in a cirriform cloud at -83° C and implications for polar stratospheric clouds," J. Atmos. Sci., 43, 851-855, 1986
6. Sassen, K., Griffin, M. and S. Dodd, "Optical Scattering and Microphysical Properties of Subvisual Cirrus Clouds, and Climate Implications," J. Appl. Met., 28, 91-98, 1989
7. Sassen, K., Grund, C.J., Spinhirne, J., Hardesty, M. and J.M. Alvarez, "The 27-28 October 1986 FIRE IFO cirrus case study: A five lidar overview of cloud structure and evolution," Mon. Wea. Rev., 118, 2288-2311, 1990
8. Sassen, K. and B.S. Cho, "Subvisual-thin cirrus lidar dataset for satellite verification and climatological research," J. Appl. Met., 31, 1275-1285, 1992
9. Browning, K.A. and C.W. Pardoe, "Structure of low-level jet streams ahead of mid-latitude cold fronts," Q. J. R. Met. Soc., 99, 619-638, 1973

VALIDATION OF THE APPLEMAN CONTRAIL FORECASTING SCHEME USING ENGINE-SPECIFIC AIRCRAFT DATA

David J. Speltz
USAF Environmental Technical Applications Center
859 Buchanan St
Scott AFB, IL 62225-5116 USA

ABSTRACT

In 1953 Herbert Appleman devised curves showing the contrail formation temperature as a function of atmospheric properties and jet engine characteristics. In this study pilot reports from KC-135A and U-2 aircraft and the latest engine characteristics are used to test the usefulness of the Appleman method in forecasting contrails. The Probability of Detection (POD) for the U-2 and KC-135A were 81.8% and 61.0%, respectively.

Differences in moisture amounts between the regions where U-2 and KC-135A pireps were gathered (stratosphere versus troposphere) lead to differences in forecast skill. Contrail forecast models must better predict moisture levels and temperature in the troposphere before they can improve.

1. INTRODUCTION

Even the most modern aircraft can produce condensation trails under certain atmospheric conditions. These contrails appear benign, but they can be a serious problem for aircraft trying to remain undetected. Contrail forecasting has been studied since World War II, beginning with the work of Goldie¹. Herbert Appleman advanced the field greatly in the 1950s when he developed a contrail prediction nomogram which showed the contrail formation temperature as a function of pressure, temperature, and relative humidity². The ambient air is heated by the engine, thereby lowering the relative humidity and hindering contrail formation. Combustion of fuel produces moisture, raising the mixing ratio (w) and making the formation of contrails more likely. The ratio of these two competing processes ($\Delta w/\Delta T$) is known as the contrail factor. In this study the latest contrail factors are used to make engine-specific contrail forecasts with the Appleman method.

2. METHODOLOGY

Data from 1031 U-2 pilot reports (pireps) and 318 KC-135A pireps were collected during 1989 and 1990 for contrail research. The U-2 pireps were primarily from the stratosphere (93.4%), while 91.5% of the KC-135A pireps were collected in the troposphere. Factors needed to compute the critical temperature (TC), or temperature *below* which contrails will form, include the ambient temperature (T), relative humidity (RH), aircraft altitude, and the contrail factor (CF). The ambient temperature was obtained from the pirep. Moisture sensors on radiosondes often do not function well at the altitudes used in this study, generally near 30,000 feet (300 mb) for the KC-135A and above 60,000 feet (70 mb) for the U-2. For these reasons assumptions of constant RH values in different regions of the atmosphere are used. RH values used are: 40% in the troposphere, 70% within 300 m of the tropopause, and 10% in the stratosphere³. Contrail factors were provided by P. Saatzer of Northrop Grumman Corporation⁴.

The calculation of TC has been explained by numerous authors in the past and will not be repeated here⁵. A FORTRAN program was written to calculate TC for each pirep and compare it to T. Hanssen and Kuipers' discriminant "V" score (VDS), recommended by Woodcock as an impartial measure of forecasting skill, is used to compare results⁶. VDS ranges from -1 (no skill) to 1 (total accuracy). Other measures of forecast skill used in

this study are the Probability of Detection (POD) and False Alarm Rate (FAR). The POD is the number of correct forecasts divided by the number of events observed and the FAR is the number of incorrect forecasts divided by the total number of forecasts.

3. RESULTS

The forecast results for the KC-135A are shown in Table 1. The forecast algorithm predicted "no contrails" 85.2% of the time, with 96.8% of the contrail non-occurrences being correctly forecast. Unfortunately, 43.9% of the null forecasts were incorrect. The program was not successful at forecasting contrail occurrences, with only 26.1% of the 161 contrails observed being forecast. Overall, contrail non-occurrences were greatly over-forecast, while most of the contrail occurrences were not predicted.

TABLE 1. KC-135A CONTRAIL FORECAST RESULTS

YES Forecasts		NO Forecasts	
Hits/POD	Misses/FAR	Hits/POD	Misses/FAR
42/26.1%	5/10.6%	152/96.8%	119/43.9%
VDS: 0.23 Total POD: 61.0% Total FAR: 39.0% Contrails observed: 161 (50.6%)			

The ambient temperature minus the critical temperature (ΔT) provides another method of visualizing the data. Figure 1 shows ΔT for each KC-135A pirez. Contrail reports are indicated by a "Y" and cases in which contrails were not observed are indicated by an "N". According to theory, contrails should only occur when ΔT is *negative*. The null events are well accounted for, with nearly all of the Ns appearing in the positive ΔT region. Most of the contrails are not predicted, with 73.9% of the observations laying in the *positive* ΔT region. In addition, most of the contrail observations lie several degrees away from the expected region.

Poor RH assumptions and errors in CF could account for some of the differences. If the actual RH were 90% instead of the assumed 40%, TC would increase by 4.0° C at 300 mb. Increasing CF from 0.030 to 0.036 g/kg-°C (value used by Peters)⁷ raises TC by 1.8° C at 300 mb. Combining these effects would raise TC by nearly 6° C at 300 mb. From Figure 1 we see that even a 6° C error could not account for many points in the positive ΔT region. The Y-points in error by more than about 10° C can only be explained by poor pirez temperatures, incorrect contrail reports, or a flaw in the Appleman theory. A recent study by Saatzer⁸ used an instrumented aircraft and a chase plane to provide compelling evidence that the Appleman theory is correct. Therefore, pirez errors appear to be the most likely cause of observations far outside of the "contrail zone". Table 2 shows forecast results for the U-2. The most obvious difference is the high POD for yes-forecasts: 89.5% compared to 26.1% for the KC-135A. Another major difference is that null events are not greatly over-forecast. The overall forecast results show a significantly higher POD and lower FAR than the KC-135A. Figure 2 is a plot of ΔT for the U-2. Although the null events are not accounted for as well, 89.5% of the contrails observed appear in the negative ΔT region. Positive contrail points which are on the wrong side of the zero line are not in error by as much as in the KC-135A plot.

RH levels in the stratosphere vary less than in the troposphere, making the assumption of constant RH a better one in the stratosphere. In addition, changes in *low* RH values have a smaller effect on TC than

TABLE 2. U-2 CONTRAIL FORECAST RESULTS

YES Forecasts		NO Forecasts	
Hits/POD	Misses/FAR	Hits/POD	Misses/FAR
560/89.5%	122/17.9%	283/69.9%	66/18.9%
VDS: 0.59 Total POD: 81.8% Total FAR: 18.2% Contrails observed: 626 (60.7%)			

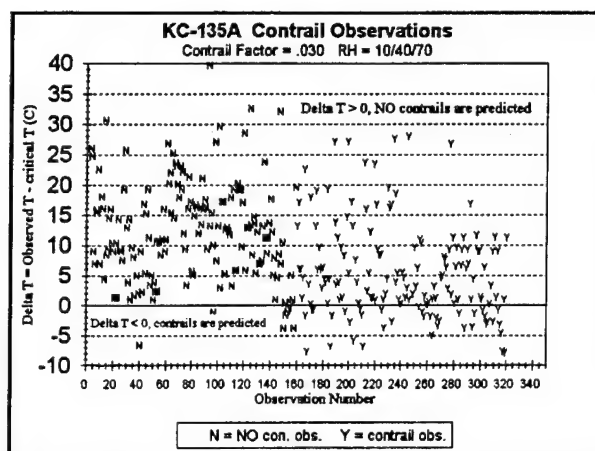


Figure 1. KC-135A ΔT plot.

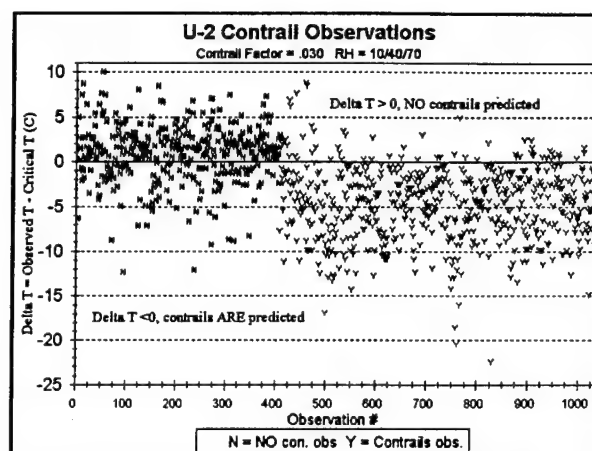


Figure 2. U-2 ΔT plot

changes in high RH values. For example, the difference in TC for RH values of 0% and 10% is 0.3°C , but TC increases by 3.7°C when RH increases from 90% to 100% ($\text{CF} = 0.030$ at 300 mb). These differences may be what makes the U-2 contrail forecasts better than those for the KC-135A. Forecast results for the mainly tropospheric B-52G and KC-135R (not shown) were also significantly worse than for the U-2. The total POD and FAR for the B-52G were 55.0% and 45.0%, respectively. The total POD and FAR for the KC-135R were 70.3% and 29.7%, respectively.

CONCLUSIONS

The performance of the contrail forecasting algorithm was marginal for the mainly tropospheric KC-135A, but was much better for the primarily stratospheric U-2. The relative humidity assumptions and contrail factors used lead to some of the errors. As the ΔT plots show, however, these errors are not large enough to account for many of the ΔT values observed. Incorrect contrail observations or faulty pirep temperatures are the most likely cause for the results obtained. Improvements in forecasting moisture amounts, especially at high humidity levels, must be made before contrail forecasts improve greatly. Obtaining another pirep database to further check the Appleman theory does not appear to be useful based on the results of Saatzer⁴ and this study.

ACKNOWLEDGMENTS

I wish to acknowledge the valuable suggestions of Captain Mark Schrader (HQ AWS/XTX).

REFERENCES

1. Goldie, A.H.R., *Formation of Cloud Behind Aircraft*, Gr. Br. Aer. Res. Comm., H.A.S. 42, 1941.
2. Appleman, H.S., *Derivation of Jet-Aircraft Contrail Formation Curves*, AWS/TR/105-145, HQ Air Weather Service (MATS), Washington D.C., 1957.
3. AWS/TR-81/001, *Forecasting Aircraft Condensation Trails*, HQ AWS, Scott AFB, IL, September 1981.
4. Contrail factors provided by personal contact with Pat Saatzer of Northrop Grumman Corp.
5. Schrader, M.L., *DRAFT, New Techniques for Contrail Forecasting*, HQ Air Weather Service, Scott AFB, IL, August 1994.
6. Woodcock, F., "The Evaluation of Yes/No Forecasts for Scientific and Administration Purposes", *Mon. Wea. Rev.*, 104, pp. 1209-1214, 1976.
7. Peters, J.L., *New Techniques for Contrail Forecasting*, AWS/TR-93/001, HQ Air Weather Service, Scott AFB IL, August 1993.
8. Saatzer, P., *Final Report - Pilot Alert System Flight Test*, Northrop Grumman Corp., B-2 Division, Pico Rivera CA, February 1995.

PREDICTING THE RADIATIVE PROPERTIES OF NON-SPHERICAL PARTICLES: APPLICATION TO CIRRUS CLOUDS

David L. Mitchell
Desert Research Institute
Reno, Nevada, 89506, USA

Andreas Macke
NASA-Goddard Institute for Space Studies
New York, New York, 10025, USA

ABSTRACT

This paper outlines a theoretical framework for understanding and predicting scattering and absorption by non-spherical particles. Although applicable in principle to any particle shape, the treatment has been applied to the radiative properties of cirrus clouds. The radiation scheme was tested against measurements from the laboratory and a cirrus cloud field study. Regarding the latter, the scheme retrieved the mean ice particle size and ice water paths from the observed cloud albedos and emittances, which agreed well with measurement derived values.

INTRODUCTION AND METHODS

Understanding and predicting the radiative properties of non-spherical particles should greatly advance our ability to explain the radiation which a satellite senses over cloudy atmospheres, or to estimate the physical properties of the clouds, since a large fraction of clouds viewed by satellite are composed primarily of ice. Such an ability should also enhance our knowledge of aerosol scattering and visibility degradation, since most insoluble aerosol appear either rough and spherical, irregular, or as chain-like aggregates¹.

A new treatment of cirrus cloud radiative properties has been developed, based on anomalous diffraction theory (ADT), which does not parameterize size distributions in terms of an effective radius². Rather, it uses the size distribution parameters directly, and explicitly considers the four ice particle shapes common in cirrus. There are four fundamental features which characterize this treatment: (1) the ice path radiation experiences as it travels through an ice crystal is parameterized, based on ADT and ray tracing results, (2) only the physical cross-section or projected area of the particle determines the amount of radiation scattered and absorbed, (3) the projected area of the size distribution, based on ice particle shape, is conserved, and (4) phase functions were calculated as a function of crystal shape, size and wavelength. Randomized second generation fractals were used as surrogates for irregular planar polycrystals regarding (4).

It may not be obvious that the second feature differs from Mie theory. However, Mie theory predicts that the absorption and extinction cross-section of a sphere can be (and often is) substantially greater than would be predicted from its physical cross-section. This appears to involve the capture of photons which have approximately tangential trajectories to the sphere. This process accounts for the wave resonance or surface wave phenomena discussed in van de Hulst³. By capturing photons which do not actually collide with the sphere, the absorption cross-section for a sphere may be greater than the sphere's physical cross-section. This physics is not included in ADT or our radiation scheme, and we postulate that resonance/surface wave phenomena does not apply to non-spherical particles.

RESULTS AND CONCLUSIONS

Measurements of extinction efficiency (Q_{ext}) were made in a laboratory ice cloud over wavelengths in the thermal infrared⁴. Q_{ext} is a measure of how efficient a particle is at removing radiation from the original beam. Figure 1 gives the results of this study for an ice cloud of hexagonal columns. The sizes and concentrations of the ice crystals were measured, and the estimated mean crystal length was 7 μm . The short-dashed curves depict the laboratory measurements. The solid curve was generated by the new ADT treatment, assuming a mean size for hexagonal columns of 7 μm . The minima shown are extremely sensitive to ice crystal size, and only occur when sizes are relatively small and the real index of refraction, n_r , approaches 1. The agreement of the measurements with the ADT curve indicates the ice crystal path of the radiation was well represented (feature 1 above). A method was developed to make ADT "act" like Mie theory, where the contribution of grazing photons to the extinction and absorption cross-section was parameterized. This parameterization generally matched the Mie theory result to within 10% for ice spheres and wavelengths in the solar and thermal IR. The new ADT treatment, after being modified in this way, was also compared to the measured Q_{ext} , as shown by the long-dashed curve. It is seen that when the effect of grazing photon capture is included, agreement between theory and observations becomes poorer away from the minima where $n_r > 1$. This indicates that for irregular ice particles, grazing photons might not be captured as surface waves, and that only the physical cross-section of the particle need be considered for predicting scattering and absorption of radiation. More laboratory measurements and analytical work are needed to test this hypothesis.

A cirrus cloud field study⁵ was used to test the radiation scheme, where broad-band albedos and emittances from a cirrus deck were measured from an aircraft at 33° zenith angle. These measurements are shown in Fig. 2 by the "+" signs. The mean ice crystal maximum dimension, based on the measured size distributions, was estimated as $\bar{D} = 6 \mu\text{m}$. Theoretical curves based on this scheme and a δ -Eddington two stream model are shown for $\bar{D} = 6 \mu\text{m}$, $\theta = 33^\circ$, for various ice crystal shapes. Although crystal habits were not measured, it appears that the curve for hexagonal plates fits the observations best. Also shown in Table 1 are ice water paths (IWP) predicted from the measured albedos and emittances, assuming hexagonal plates dominated. These values are compared against IWPs calculated from measured ice particle size spectra, assuming hexagonal plates. The average percent difference between predicted and measurement derived IWPs was 18%. This method is one of the first to obtain reasonable agreement between measurement derived IWPs and IWPs predicted from radiation transfer theory, and appears to be the first IWP retrieval scheme to consider more than one ice crystal shape.

ACKNOWLEDGMENTS

This work was funded by the Environmental Sciences Division of the U.S. Department of Energy, as part of the Atmospheric Radiation Measurement (ARM) Program. Financial support does not constitute an endorsement by this agency of the views expressed in this article.

REFERENCES

1. Cheng, R.L., 1979: Physical properties of atmospheric particulates. In *Light Scattering by Irregularly Shaped Particles*, edited by D.W. Schuerman, Plenum Press, New York, 334 pp.
2. Mitchell, D.L., A. Macke, and Y. Liu, 1995: Modeling cirrus clouds. Part II: Treatment of radiative properties. Revised for publication in *J. Atmos. Sci.*
3. van de Hulst, H., 1981: *Light Scattering by Small Particles*. Dover, 470 pp.
4. Arnott, W.P., Y. Dong and J. Hallett, 1995: Extinction efficiency in the infrared (2-18 μm) of laboratory ice clouds: observations of scattering minima in the Christiansen bands of ice. *Appl. Opt.*, **34**, 541-551.
5. Paltridge, G.W., and C.M.R. Platt, 1981: Aircraft measurements of solar and infrared radiation and the microphysics of cirrus cloud. *Quart. J. R. Met. Soc.*, **107**, 367-380.

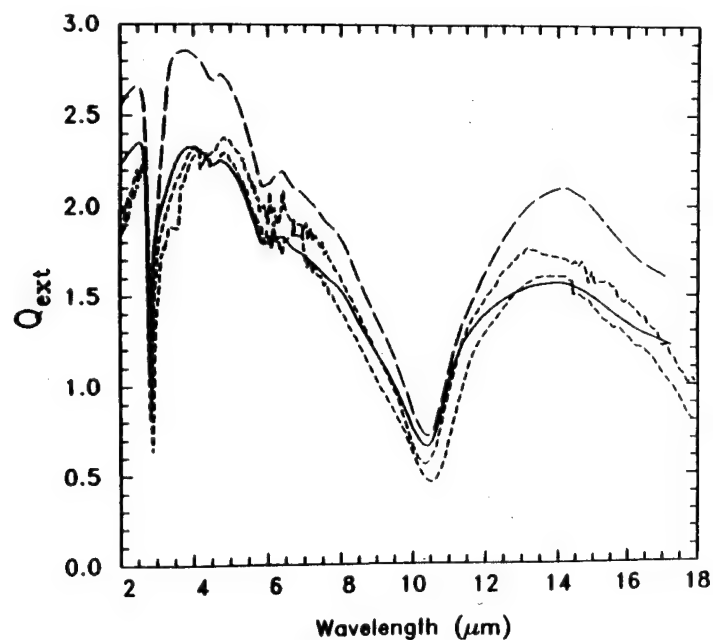


Fig. 1. Extinction efficiency measurements (short dashed curves) for an ice cloud of hexagonal columns. The solid curve was predicted from the observed crystal sizes by the new radiation scheme, while the long-dashed curve is based on the observed sizes and Mie theory.

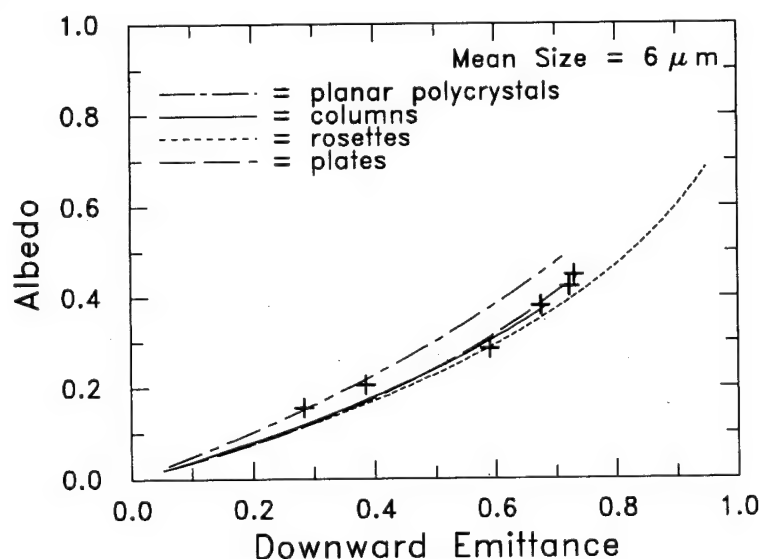


Fig. 2. Albedo-emittance data (+) from a cirrus cloud field study. Theoretical curves based on the new radiation scheme and observed mean ice crystal size are shown for various ice crystal types. All curves terminate at IWP = 13.5 g m⁻².

TABLE 1. COMPARISONS BETWEEN PREDICTED AND MEASURED IWP

Ice Water Path (g m ⁻²)		Percent Difference
Measurement Derived	Predicted	
1.8	2.2	20
4.0	3.5	13
5.2	8.0	42
7.9	10.7	30
13.2	13.2	0
14.4	13.5	6

STATISTICS ON THE OPTICAL PROPERTIES OF CIRRUS CLOUDS MEASURED WITH THE HIGH SPECTRAL RESOLUTION LIDAR

E. W. Eloranta and P. Piironen

University of Wisconsin

1225 W. Dayton St., Madison, WI 53706, USA

1. Abstract

This paper presents statistics derived from one year of cirrus cloud observations with the University of Wisconsin High Spectral Resolution Lidar (HSRL). The HSRL provides calibrated vertical profiles of atmospheric optical depth, backscatter cross section, extinction cross section and depolarization. The measurement technique allows rigorous computation of error bounds for all observations.

2. Instrumentation

The lidar signal backscattered from molecules is spectrally broadened by the Doppler shift resulting from the thermal motion of the molecules. Light scattered from aerosols shows little spectral broadening from the slow Brownian motion of the aerosols. The University of Wisconsin High Spectral Resolution Lidar (HSRL) measures backscatter cross sections and optical depth of clouds by separating the Doppler-broadened molecular backscatter return from the unbroadened aerosol return¹⁻³. The molecular signal is used as a calibration target with a backscatter cross section that can be computed from an independent temperature profile. This calibration avoids the need for information on the ratio of backscatter to extinction and boundary values of the extinction. It thus avoids the ambiguities and numerical instabilities encountered when calibrated measurements are attempted with traditional lidars.

3. Observation Schedule

The HSRL was operated when cirrus was present during the overpass of the NOAA 12 or 13 satellite. Observations were made between February 4, 1994 and December 8 1994. On each day, the decision to operate was based on the presence of visual cirrus clouds or an indication of approaching cirrus on GOES 7 imagery. Decisions to operate were made approximately two hours prior to the satellite pass. The data set includes nearly every case with visual cirrus. Only a few days with cirrus were missed during the entire year. Both AVHRR and GOES images were archived for nearly all data cases. Data from 51 days were used in this study. On each day the lidar was operated for at least one hour. The longest data session was 5 hours.

4. Analysis

The raw lidar data consists of 3 second integrations. For this study we have generated 3 minute averages of these profiles in order to increase the signal to noise ratio of the data and to decrease the total number of data points. The data set includes 1621 data profiles consisting of measurements at 15 meter intervals in the altitude range between 200 m and 35 km.

At first glance it appears easy to define what comprises a cloud. However, close examination shows that cloud cover statistics are very sensitive to how cloudy air is distinguished from clear air. Cloud boundaries are often not distinct and cloud elements that easily identified as clouds are joined by a gradation of cloud densities that merge smoothly with haze and other clear air aerosol clouds. In this study we use a threshold based on the ratio of backscattering from particulates to molecular backscattering to define the presence of cloud. Depolarization measurements allow identification of cloud phase⁴. Strong depolarization indicates the presence of non-spherical particles (ie. ice). Very small depolarizations indicate the presence of spherical scatters (ie. water droplets).

5. Results

Figure 1 shows the depolarization measured for this data set as a function of temperature. These data were used to determine depolarization thresholds which were used to distinguish ice, water, and mixed phase clouds.

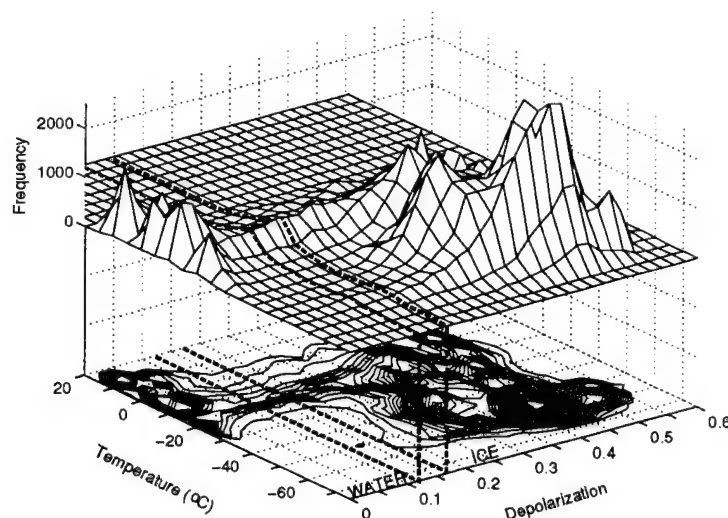


Figure 1. A contour plot and a 3-elevation map of depolarization as a function of temperature for all data points having an aerosol backscatter greater than the molecular backscatter.

Notice that at temperatures below -40°C , where water can not exist in the liquid state, all except one data point have depolarizations greater than 0.17. Also notice that at temperatures above freezing, the number of data points with depolarization above 0.12 become very small. Examination of HSRL altitude vs. time images suggest that those few points with temperatures above freezing and with depolarization greater than 0.12 represent snow falling into a melting layer or depolarization caused by multiple scattering in a dense water layer.

Based on this plot, all data points with depolarization greater than 0.17 have been classified as signal returns from ice clouds. Data points with depolarizations between 0.12 and 0.17 are identified as mixed phase clouds and points less than 0.12 are identified as water.

Figure 2 shows the probability distribution of backscatter cross sections observed in this experiment. Clouds are separated into ice, water and mixed phase clouds.

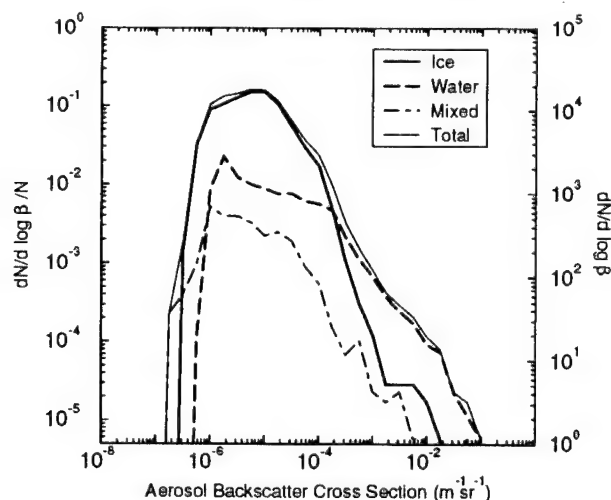


Figure 2. The probability distribution of backscatter cross sections in clouds measured in the current experiment. Only data points where the ratio of aerosol to molecular backscatter is greater than one are presented. Separate plots are shown for ice, water and mixed phase clouds. A combined curve for all cloud types is also presented.

Figure 2 shows a backscatter cross section of approximately $10^{-5} m^{-1} str^{-1}$ for most cirrus clouds. Very few cirrus clouds have backscatter cross sections of greater than $10^{-4} m^{-1} str^{-1}$. The probability of occurrence of water clouds continues to rise as the backscatter cross section decreases. This is due the presence of aerosol scattering in the profiles. Most aerosol particles are small solution droplets which generate small depolarizations and are thus classified as water clouds in this study. Probability distributions computed with a scattering ratio threshold of 0.1 show that the number of ice clouds continues to decrease with decreasing cross section and that the number of water clouds continues to increase.

Because observation days were selected on basis of cirrus cloud cover the combined probability distribution shows much smaller contributions from water clouds than would be found in an unbiased sample.

6. Other results

The oral paper will also present probability distributions of optical depth measurements, cloud altitudes and cloud temperatures. Measurements of multiply scattered lidar signals will be presented along with particle size measurements derived from these observations. Preliminary results from the recent SBIRS intensive observation period will also be presented.

-
1. S. T. Shipley, D.H. Tracy, E. W. Eloranta, J. T. Trauger, J. T. Sroga, F. L. Roesler, and J. A. Weinman, "High resolution lidar to measure optical scattering properties of atmospheric aerosols. 1: Theory and instrumentation," *Appl. Opt.* **22**, 3716-3724 (1983)
 2. P. K. Piironen, and E. W. Eloranta, "Demonstration of a high-spectral resolution lidar based on an iodine absorption filter," *Opt. Lett.* **19**, 234-236 (1994).
 3. C. J. Grund, and E. W. Eloranta, "University of Wisconsin High Spectral Resolution Lidar," *Optical Engineering* **30**, 6-12 (1991).
 4. K. Sassen, "The polarization technique for cloud research: a review and current assesment", *Bull. Am. Soc.*, **72**, 12, 1848-, (1991).

AN OPERATIONAL METHOD OF ICE-CONTAINING CLOUDS BASED ON LABORATORY AND OBSERVATIONAL DATA LEADING TO A NUMERICAL MODEL FOR PREDICTION OF RADIATIVE PROPERTIES

Darko Koracin and John Hallett
Desert Research Institute, P.O. Box 60220, Reno, NV89506-0220

ABSTRACT

An operational method that integrates laboratory-based representation of crystal growth and calculation of extinction coefficient in high-altitude clouds with and regional/mesoscale numerical model is presented. The numerical model supplies initial 3D fields of vertical velocity, temperature, humidity and dynamical trajectories of the parcels in the center of the domain to the laboratory-based method. The calculated radiative properties are then incorporated in an improved run of the numerical model. The procedure then iterates. The limits of iteration will be determined using data from the ARM field program.

1. INTRODUCTION

The model uses criteria derived from laboratory studies of crystal growth characteristics and the interaction of such particles with solar and thermal radiation. In order to achieve confidence in its performance, consistency is sought in aircraft observations of ice shape and spectra in recent field programs (FIRE, TOGA-COARE, ARM) and ultimately in the wavelength resolved spectra and emissivity. The former requires some estimate of spatial averaging required to go from a 'point' measurement (say over a 10 m path length) to an average over a much longer path length (some 10 km) as might be obtained from a satellite footprint. It is known that bimodal spectra occur on numerous occasions with small particles, sometimes dominating the radiation process whereas on other occasions spectra appear to fit a more generalized near linear curve on a log-log distribution (Foster et al. 1995).

2. MODEL INPUT

We list individually components of the model and the approach that we use for each component:

- a) Mean vertical velocity on a regional scale (of the order of 1000 km) from the regional or GCM.
- b) Local vertical velocity - particularly the large velocity tail of the spectrum. Use vertical doppler lidar data to establish distribution spread under different cirrus conditions and stability criteria to determine scales of motion.
- c) Cloud condensation nucleus (CCN) spectra from lidar real time analysis of CN distribution together with trajectory analysis of inflow air from the regional model with estimation of CCN characteristics - composition and spectra.
- d) Ice concentration from a knowledge of local vertical velocity, and the CCN spectra using the Kohler equation to estimate homogeneous ice nucleation on droplet dilution.
- e) Specify temperature of cirrus domain from regional model and estimate growth rates and habit of individual crystals as a function of temperature and supersaturation from direct simulation in laboratory experiments (Hallett 1987).

- f) Infer supersaturation on local scale and spatial distribution thereof using vertical velocity, ice concentration and particle growth rates. Compute growth rates and habit over whole domain.
- g) Use laboratory derived criteria to estimate extinction (Arnott et al. 1995) and laboratory data now being obtained to give emissivity with cm^{-1} wavenumber resolution.
- i) Provide domain of extinction and emissivity for both solar and thermal infrared radiation.
- j) Input to regional/GCM model for comparison with broad band flux measurements.

The greatest uncertainties lie in a knowledge of the vertical velocity tail (b). CCN measurements at these altitudes are sparse, but instrumentation is currently available and measurements are scheduled for April 1996 over Oklahoma. Meanwhile some measurements are available of CN over the Pacific and in TOGA COARE from the NASA DC-8. It is evident that these numbers are quite variable (concentrations range from <100 to $100,000 \text{ cm}^{-3}$). It will be necessary to build up some climatology to enable numbers to be provided on a regional or global basis from a knowledge of likely trajectories of cirrus forming. A further uncertainty lies in recycling of crystals as they fall out of cirrus, evaporate and break up. Laboratory studies are available which enable an estimate to be made.

3. INTEGRATION OF THE DESCRIBED METHOD WITH A NUMERICAL MODEL

There will be a two-way interaction between the described method and the regional/mesoscale model. The model will provide initial 3D fields of vertical velocity, temperature, humidity, and dynamical trajectories of the parcels that are located in the center of domain. The 'local' vertical velocity will be determined from the simulated turbulence kinetic energy and possible wave instabilities. The next step is estimation of the properties of ice crystals in cirrus clouds and the parameters of radiative heat transfer, based on the laboratory procedure described in section 2. Microphysical effects and extinction coefficients will then be transferred to improve the model run. The output fields from the numerical model will again drive laboratory method in another iteration cycle. The comparison with measurements will provide optimization of the iteration procedure and application of the entire method to actual atmospheric conditions.

The Regional/mesoscale Atmospheric Modeling System (RAMS, Pielke et al. 1992) will be used in the study. We have currently completed a test simulation of the case study during the ARM field program. The simulations compared well with radiosonde measurements and have reproduced a general structure of cirrus cloud (Fig. 1). The results from the analysis of spatial distribution of vertical velocity at levels where cirrus was observed and simulated are shown in Fig. 2. It can be inferred from the figure that the simulated tail of vertical velocity contributes to complexity of dynamics in cirrus. Moreover, the edge, between the upward motions and large subsidence area, corresponds to the cirrus region.

4. CONCLUSIONS

The method presented in this study offers an approach for efficient estimation of microphysical and radiative properties in cirrus. The method consists of a laboratory-based operational procedure for calculating extinction coefficient and integrating the results in a regional/mesoscale model which in turn supplies initial fields for local and regional scale vertical velocity, temperature and moisture fields, and dynamical trajectories of the parcels in the center of domain. The method improves simulations of cirrus and provides a guideline for an operational model.

REFERENCES

Arnott, W.P., Y.Y. Dong and J. Hallett, 1995: Extinction efficiency in the infrared (2-18 micrometers) of laboratory ice clouds: Observations of scattering minima in the Christiansen bands of ice. *Appl. Opt.*, **34**, 541-551

Foster, T., W.P. Arnott, J. Hallett, J. Hudson, and R. Pueschell: Measurements of ice particles in tropical cirrus anvils: Importance in radiation balance. *AMS Conference on Cloud Physics*, Jan. 15-20, 1995, Dallas, Texas, 419-424.

Hallett, J., 1987: Faceted snow crystals. *J. Opt. Soc. Amer.*, **4**, 581-588.

Pielke, R.A., W.R. Cotton, R.L. Walko, C.J. Tremback, W. Lyons, L. Grasso, M. Nicholls, M. Moran, D. Wesley, T. Lee and J. Copeland, 1992: A comprehensive meteorological modeling system-RAMS. *Meteorol. Atmos. Phys.*, **49**, 69-91.

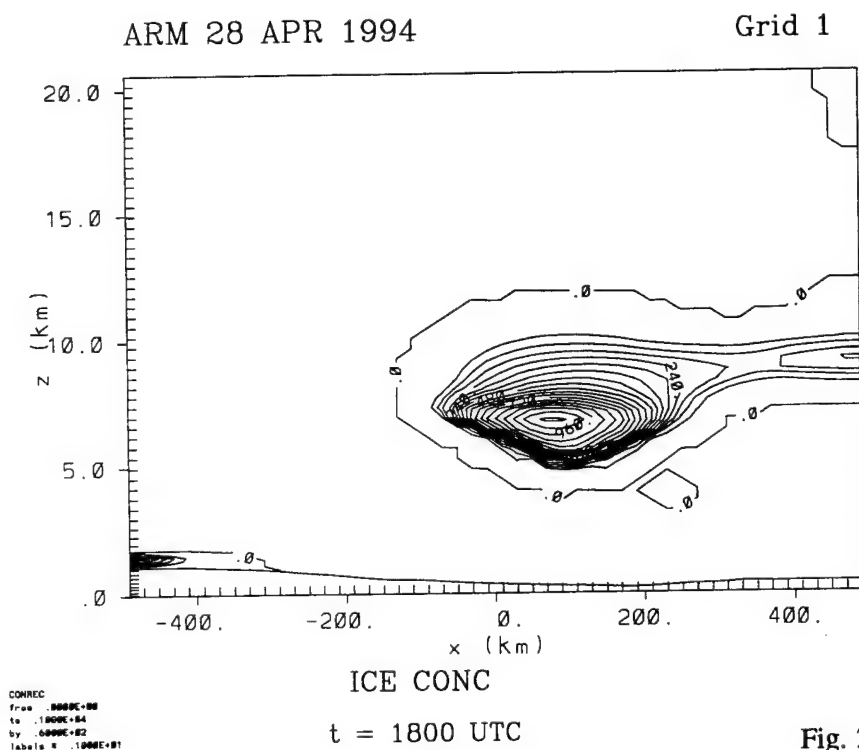
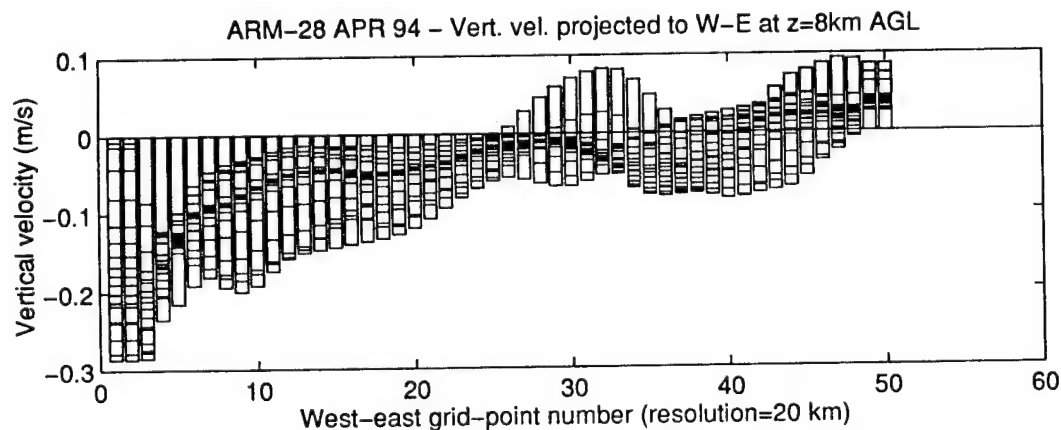


Fig. 1 Contour plot of simulated ice concentrations (#/l)

Fig. 2 Frequency distribution of simulated vertical velocity at 8 km AGL.



POSTER PRESENTATIONS

A SUMMARY OF VERTICAL CLOUD LAYER STATISTICS AS DERIVED FROM ECHO INTENSITIES RECEIVED BY A 35 GHz RADAR

James H. Willand
Hughes STX Corporation
Lexington, Massachusetts 02173

ABSTRACT

This paper summarizes an assortment of seasonal (winter and summer) vertical cloud layer statistics derived from echo intensities received from a 35 GHz radar. The unique capability of the radar's beam to "see" detailed cloud structures at discrete levels of the atmosphere up to 60,000 feet makes it possible to derive the types of statistics that are described here. The cloud statistics summarized include:

- 1) probability of clouds aloft,
- 2) diurnal cloud layer analysis,
- 3) probabilities of vertical cloud-free line-of-sight between two heights,
- 4) cloud layer correlation's between two heights,
- 5) serial correlation of clouds at specified altitudes,
- 6) probabilities of vertical cloud thickness,
- 7) probabilities of cloudy or clear run lengths.

The radar was housed within the U.S. Air Force Radar complex in Sudbury, MA. The radar data collection effort took place over a two and a quarter year period of record from April 1990 until radar site shutdown in mid July 1992. A much longer period of data collection would have been more desirable for deriving the statistics. However, the statistics summarized can provide useful information and insight toward simulating the physical reality of cloud structures aloft.

1. BACKGROUND

At the beginning of 1990, the Phillips Laboratory Atmospheric Structures Branch (GPAA) of Hanscom AFB initiated a project to collect 35-GHz radar data for purposes of deriving cloud layer statistics. The radar was housed at the U.S. Air Force Systems Command, Phillips Laboratory Radar site in Sudbury, MA. Vertical propagation of the beam extend from the surface to 60,000 ft. Each beam consisted of one second averages for 120 cells. Each cell has a pulse width of 492 ft. or 150m. The vertically pointing 35-GHz radar has the capability of "seeing" clouds and precipitation that pass over its beam through the atmosphere regardless of the number of cloud layers present. Since only heavy rain (rain rate > .75 inches/hr) will significantly degrade this capability, the 35-GHz radar is practical for deriving vertical cloud layer statistics.

Data collection began on April 26, 1990 and ended on July 17, 1992. This provided a 28 month or 2.25 year period of record. Data were collected over time period episodes of as little as 5 minutes to as long as 24 hours. Because of the high cost of radar operations, data collection episodes were chosen randomly for only two or three times a week. Thus, sample sizes used in generating monthly statistics were often small.

A simple DBz threshold technique determined weather or not a cell was cloudy or cloudless. By displaying the results of this cloud/no cloud discrimination process on a computer screen over the entire time period of an episode, a visual representation of the clouds passing over the radar was accomplished. A scene derived from data received on February 24, 1992 is shown in Figure 1.0 (A). Each display generated in the data processing activity was subjectively examined to ensure that the best cloud/no cloud threshold was being applied. A data file of these cloud/no cloud scenes was then created and subsequently utilized as the primary data for deriving the cloud layer statistics. A robust tetrachoric correlation technique was used to derive correlation statistics.

2. CLOUD LAYER STATISTICS

The types of cloud layer statistics derived and briefly discussed below provide useful information toward simulating and modeling the physical reality of clouds aloft.

Probability of clouds at altitude were derived from the winter and summer monthly and seasonal cloud/no cloud data sources. Probability of clouds at altitude for winter is shown in Figure 1.(B). (Statistics below about 5,000 feet were not computed because of very noisy data at lower levels.) The statistics show a sharp decrease in the probability of clouds from 5,000 to about 7,000 ft. followed by a rather steady linear decrease in probabilities up to 35,000 ft. Magnified versions of these graphs for probabilities of clouds aloft from 35,000 to 60,000 ft. show small probabilities ($<.01$) of cloud occurrences to as high as 55,000 ft. A diurnal cloud layer analysis of probabilities of clouds aloft was accomplished by stratifying these probabilities hourly. Results showed an intriguing decrease in the probability of mid and high cloud occurrences over the early and mid morning hours for both winter and summer cases.

Nomograms showing probabilities of vertical cloud-free line-of-sight and cloud layer correlation's between two heights were derived for both monthly and seasonal cases. The nomogram for extracting the probability of vertical CFLOS between two heights for December is shown in Figure 1.0 (C). The contours connect equal one tenth probability values of vertical CFLOS. Thus as shown in the figure the probability of a vertical CFLOS looking UP from an initial height of 15,000 ft. to an object at 20,000 ft. is estimated to be .72. Looking DOWN produces the same answer. Probability of CFLOS deduced from 35 GHz radar data is the same looking up as looking down. These results need not be the same at those frequencies where scattering into the beam can dominate the signal.

Serial correlation of clouds at altitude was derived for winter and summer cases. These statistics showed tighter packing of correlation contours at smaller time lags for middle and high clouds in the summer than those portrayed for winter cases. A tongue of rather high correlation values (.4 to .6) between altitudes from 28,000 to 32,000 ft. was prevalent over an 18 hour lag time in the winter. In the summer the phenomenon was very weak (.1 correlation) and lasted only for a 12 hour lag time.

Probabilities of vertical cloud thickness for seasonal winter and summer cases were assembled for 16 separate cloud base altitude levels. Figure 1.0 (D) shows the vertical cloud thickness presentation used for describing probable cloud thickness in meters for clouds having bases between 1950 to 2550 meters.

Probabilities of cloudy or clear run lengths were derived for winter and summer seasonal cases. Figure 1.0 (E) shows the rapidly decreasing probability of a cloudy run length greater than or equal to a specified run length of 0 to 60 minutes in the winter time. Another graph was produced showing a continuation of the results out to 24 hours.

ACKNOWLEDGMENTS

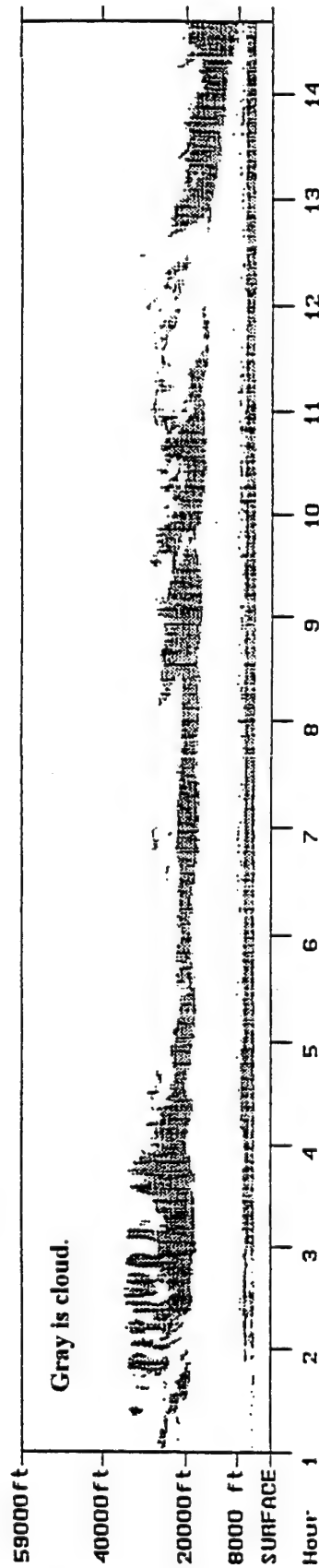
This work is supported by Geophysics Directorate of Phillips Laboratory with Mr. Donald Grantham as contract monitor for contract No. F19628-93-C-0051.

REFERENCES

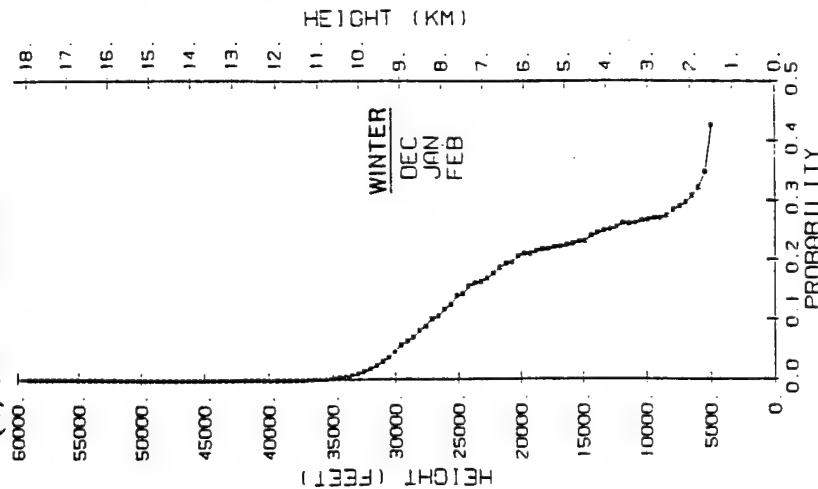
Willand, J.H. & A. Boehm, 1995: "Vertical Cloud Layer Statistics Derived From Echo Intensities Received By A 35 - GHz Radar." PL-TR-95-2034. Prepared by Hughes STX for the Phillips Laboratory, Air Force Systems Command, Hanscom AFB, MA. 01731-5000, AD-A294826.

(A) TPQ-11 Vertical Radar (35 GHz)

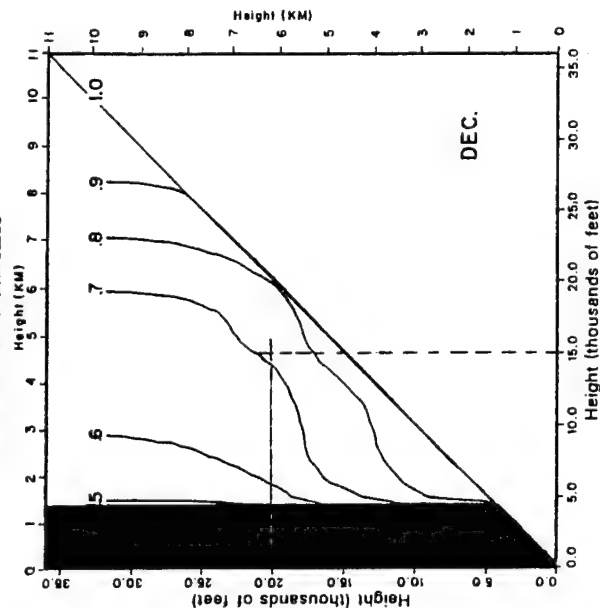
FEBRUARY 24, 1992



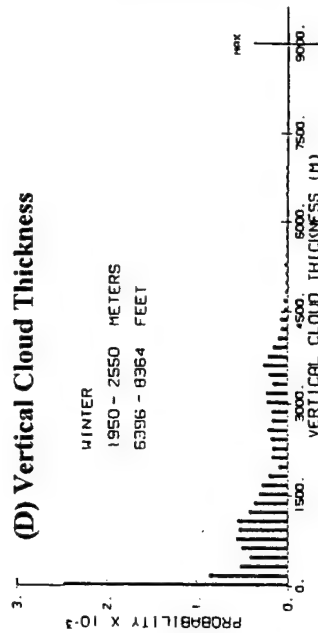
(B) Cloud at Altitude



(C) PROBABILITY OF VERTICAL CTLOS BETWEEN TWO HEIGHTS



(D) Vertical Cloud Thickness



(E) Cloudy or Clear Run Lengths

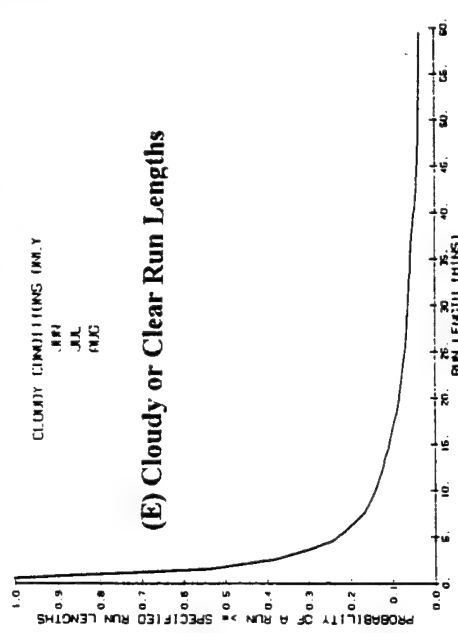


Figure 1.0
A cloud/no cloud scene from TPA-11 radar data. (B,C,D,E) are graphs showing some of the derived cloud layer statistics.

SWIR Cloud Modeling and Data Analysis For the SBIRS Program

Joseph G. Shanks, Frederick C. Mertz
Photon Research Associates, Inc.
10350 N. Torrey Pines Road, Suite 300
La Jolla, California 92037-1020 USA

Ian Robinson
The Aerospace Corporation
M4/041
P.O. Box 92957
Los Angeles, California 90009-2957 USA

William Blumberg
PL / GPOS
Hanscom AFB
Bedford, MA 01731-5000

Edward Eloranta
Dept. of Atmospheric Sciences, University of Wisconsin
1225 West Dayton
Madison, WI 53706

James Lisowski
SCITEC Corp.
100 Wall Street
Princeton, NJ 08540

ABSTRACT

The Space Based Infrared Systems (SBIRS) Program is a multi-satellite constellation designed to conduct global and regional surveillance using passive infrared detection. Clouds present a persistent and unpredictable source of clutter which can be the main degradation in the target detection process. Clutter has not been assessed using actual data thus a program is underway to collect cloud imagery spanning candidate spectral bands. This imagery will be used directly in assessing sensor performance and to evaluate the fidelity of cloud scene generation radiance models. The principal platform for near-term data collection is the multispectral sensor on the ARES aircraft. Additional data is to be collected by the MSTI-III and MSX platforms. In all cases supporting data will be provided by meteorological satellites, LANDSAT, and/or ground-based lidars. Examples of cloud imagery will be presented and discussed. A corollary effort will generate simulated imagery using the CLDSIM code, for comparison with data. For this effort, the shape of the cloud field will be determined with the University of Wisconsin Volume Imaging Lidar (VIL). The retrieval of cloud optical properties from the VIL will be calibrated with data measured coincidentally by the High Spectral Resolution Lidar, also developed at the University of Wisconsin.

1.0 INTRODUCTION

Modelling cloud radiance in the visible-infrared spectral band remains a challenging task, both because of the difficulty of characterizing the physical state of real clouds (water content and size distribution vs position, for example) and the intractability of the 3-D radiative transfer problem. Nonetheless, the CLDSIM (Cloud Scene Simulation Code) has been developed to produce high-fidelity, deterministic cloud radiance images for the design and assessment of high-altitude sensors. Missile detection and tracking sensors often operate in the H₂O and CO₂ absorption bands to optimize signal/noise, yet still find that small, bright features in clouds, especially high-altitude clouds, generate sufficient clutter to effect performance. Hence, the fidelity of a cloud radiance model should be assessed by measuring the clutter content in simulated cloud scenes [Shanks, et al., 1992; Shanks, et al., 1993]

The objective of the current program is two-fold. First, to gather cloud radiance imagery in spectral bands and geometries of interest to directly measure their clutter content. Platforms scheduled to collect such data include ARES, and MSTI-3 and MSX as they achieve orbit (scheduled for spring '96) [Lisowski, 1995;

To be presented at the "Cloud Impacts on DoD Operations and Systems, '95" conference, 24 - 26 October 1995, Hanscom AFB, Boston, MA

Thorwart, et al., 1995]. Second, to develop a sufficiently comprehensive physical description of the cloud to permit a detailed comparison of simulated cloud imagery with the data. The latter process is diagrammed in Figure-1. The baseline instruments to characterize the cloud are the VIL (Volume Imaging Lidar) and HSRL (High Spectral Resolution Lidar) based at the University of Wisconsin [Eloranta & Piironen, 1993; Wylie, et al., 1993], various aircraft-based sensors for *in-situ* measurements, and Landsat-5, GOES-8, 9, and the NOAA polar orbiters

The cloud-top map is a key input to the *CLDSIM* model, currently describing both the cloud-top shape and the optical depth of the cloud. This data base has historically been derived from LWIR remote-sensing imagery, an approach ill-suited to modelling thin or multi-layer clouds. The VIL offers the opportunity to develop this map from a database of 3-D cloud structure, as it can measure cloud-top and cloud-bottom altitude (defined as contours of constant backscatter cross-section), and cloud optical depth, independently. Various assumptions regarding the interpretation of the VIL data are illustrated in Figure 2. This is a mosaic of *CLDSIM* images generated with cloud-top altitude maps derived from (moving left-right) the cloud-top contour, the thickness of the cloud ($\text{cloud-top} - \text{cloud-bottom}$) and the cloud optical depth ($K_e = 2 \text{ (1/km)}$ assumed). Such comparisons with complete data sets are expected to reveal the limitations of the current model, and guide model development.

In summary, the SWIR imagery collected by ARES, in combination with the data collected by the

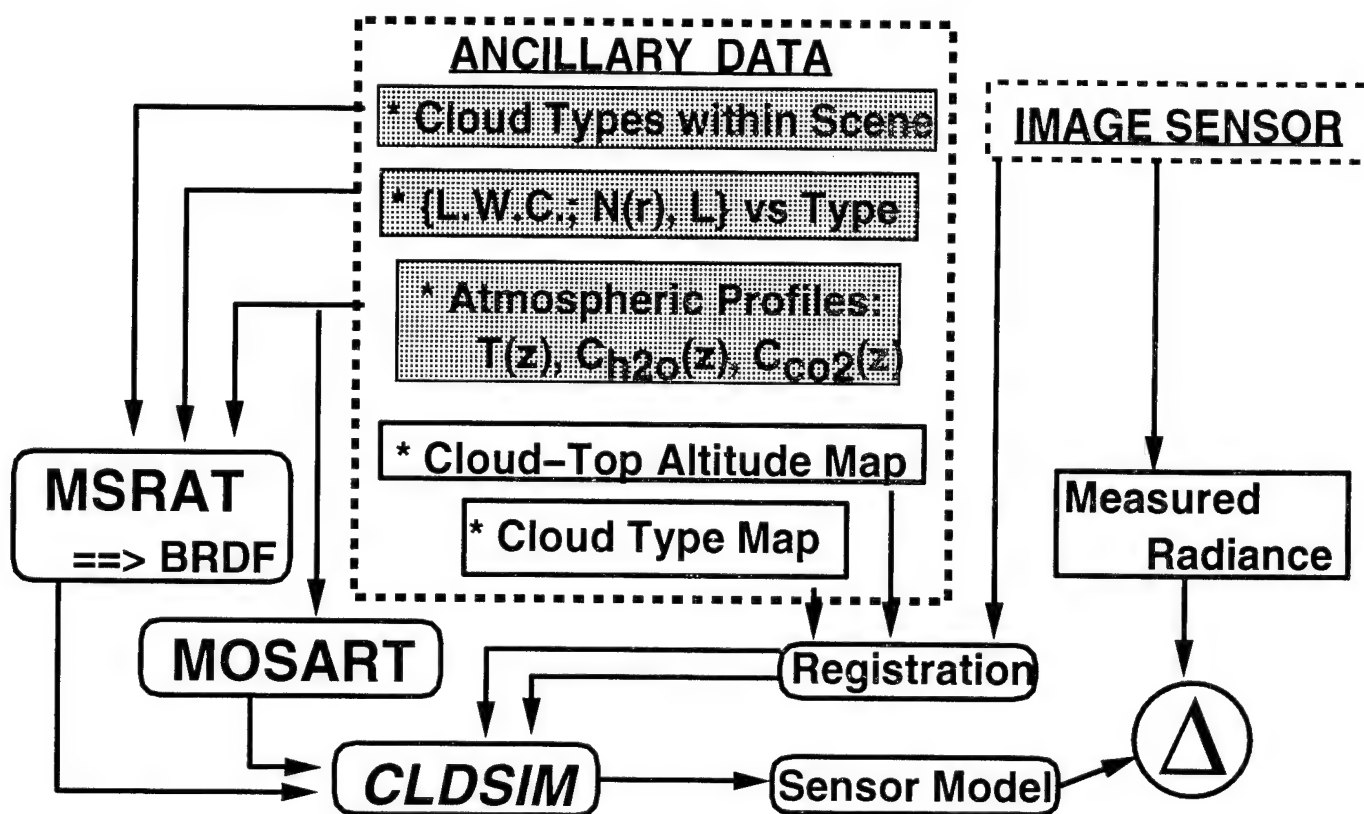


Figure 1. Schematic diagram illustrating the steps involved in comparing measured and modelled cloud radiance imagery

space-based sensors coming on line next year (providing a larger fields-of-view, and field-of-regard) together with coordinated collects of cloud data, will provide both a substantial data base of cloud radiance imagery for sensor development, and the opportunity to assess *CLDSIM* model accuracy.

REFERENCES

- Eloranta, E.W., Piironen, P.,
 "Remote Measurements of Cloud Optical Properties with a
 Robust High Spectral Resolution LIDAR"
 (Proc. of the Cloud Impact on Department of Defense Operations and
 Systems 1993, D. Grantham, W. Snow, eds., November 1993) page 184

$$(Alt = Z_{top})$$

$$(DBlalt = Z_{top} - Z_{lb} + 7500)$$

$$(DBlalt = \tau * 500 + 10,000)$$

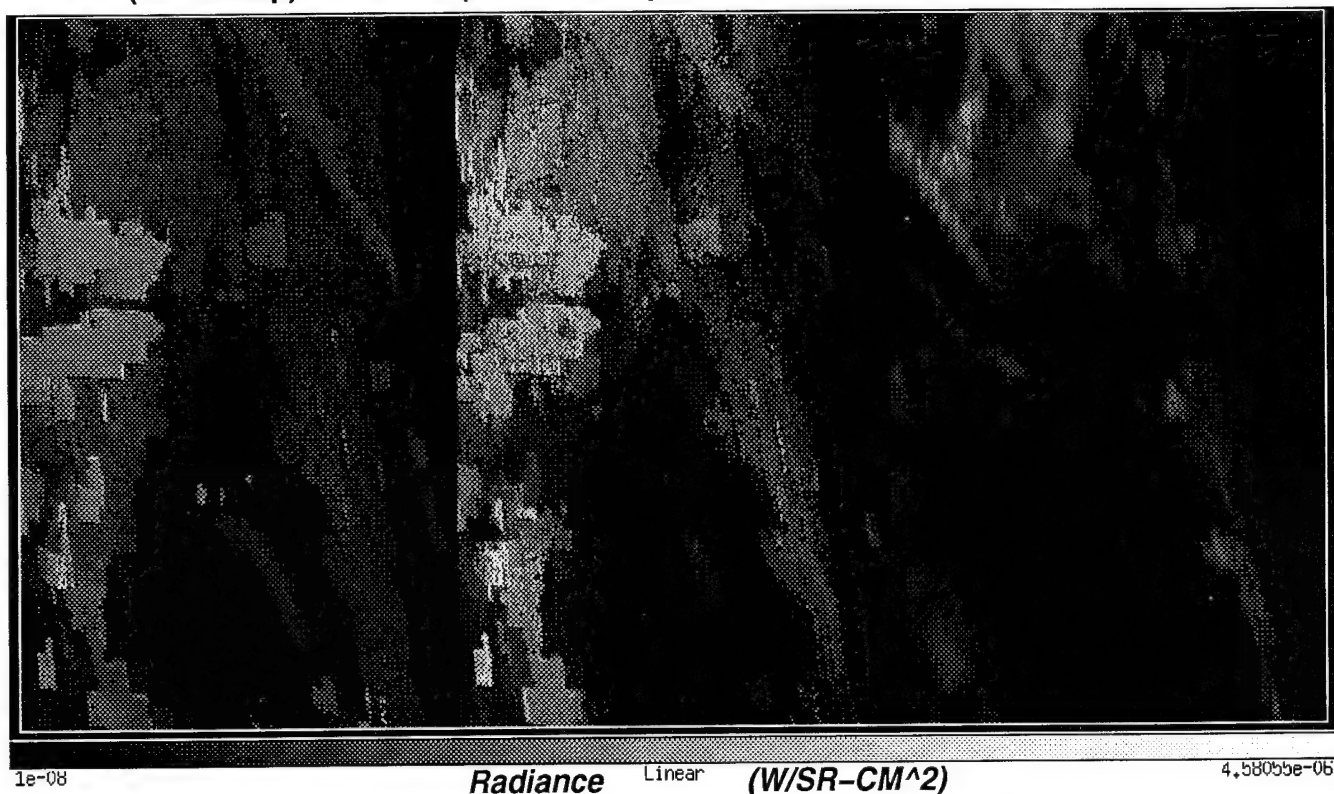


Figure 2. Mosaic of CLDSIM scenes generated with various cloud-top altitude maps. These maps were generated from the Pine Bluff data set collected by the Volume Imaging Lidar developed at the University of Wisconsin by Ed Eloranta and co-workers.

Lisowski, J., ed.,

"ARES Data Analysis Report, Cloud Specular Reflections"
(Preprint, SciTec, Inc., Princeton, N.J., 1995) 82 pages

Mertz, F.C., Blasband, C.B., Hendricks, L.W., Francis, R.J., Anding, D.C.,

"Validation of a Cloud Scene Simulation Model Using NOAA Multi-Spectral Imagery"
(Proc. of the Cloud Impact on Department of Defense Operations and Systems 1991, D. Grantham, W. Snow, eds., July 1991) page 261

Shanks, Joe, Mertz, Frederick C., Nadile, Richard M., Conley, Thomas D.,

"A Preliminary Comparison of CLDSIM Predictions with CIRRIS-1A Radiometer Data in SWIR and MWIR Spectral Bands"
(Proc. of the Cloud Impact on Department of Defense Operations and Systems 1993, D. Grantham, W. Snow, eds., November 1993) page 190

Shanks, Joe, Hendricks, Leif, Mertz, Fred, Moore, Richard, Patterson, Jim, Barry, Pat,

"DSP Response to Background Imagery: Measured and Modeled" (S)
(Proceedings for the 1992 IRIS Specialty Group on Targets, Backgrounds and Discrimination, Orlando, FL, 1992)

Thorwart, M.J., Lisowski, J.L., Shanks, J.G., Bishop, K.,

"Cloud Specular Data and Analysis for the Airborne Remote Earth Sensing (ARES) Program"
(Proceedings for the 1995 IRIS Specialty Group on Targets, Backgrounds and Discrimination, Cocoa Beach, FL, 1995)

Wylie, D.P., Wolf, W., Piironen, P., Eloranta, E.,

"Visible / Infrared Optical Depths of Cirrus as Seen by Satellite and Scanning LIDAR"
(Proc. of the Cloud Impact on Department of Defense Operations and Systems 1993, D. Grantham, W. Snow, eds., November 1993) page 355

GLOBAL CLOUD COVER AT ALTITUDE: SYSTEM IMPACTS

Ian S. Robinson and Susan L. Kafesjian
The Aerospace Corporation
Los Angeles, California

The Aerospace Corporation has been examining available global cloud climatologies in support of several Air Force programs. The primary statistics of interest are cloud frequency of occurrence (including thin clouds), cloud altitude, cloud opacity, and global coverage.

Data sets considered include ISCCP, University of Wisconsin at Madison (UW), SAGE-II, Nimbus-7, Bertoni, Warren, and RTNEPH. The sources found to best suit our application are the ISCCP, UW, and SAGE-II data sets. This paper will describe some of the comparisons that have been made amongst the data sets, describe some enhancements in process for the UW data set, and discuss the application of the UW data to systems' problems of cloud obscuration of targets at altitude and cloud-induced clutter at altitude.

Manuscript not available at time of printing. Please contact author for information.

THE CLOUD SCENE SIMULATION MODEL — PARAMETER ESTIMATION AND PRELIMINARY VALIDATION OF THE CUMULUS MODEL

Mark E. Raffensberger, Maureen E. Cianciolo, and Eric O. Schmidt
TASC
Reading, Massachusetts USA 01867

ABSTRACT

The Cloud Scene Simulation Model (CSSM), developed at TASC under the sponsorship of the Air Force Phillips Laboratory, generates synthetic, high-resolution four-dimensional liquid water content fields for a variety of cloud types based on large-scale atmospheric and cloud conditions. Aircraft-based observations of liquid water content (LWC) in cumuliform clouds are used to estimate the CSSM cumulus cloud model parameters that are used to simulate the spatial variability of cloud water. Independent observations of LWC along a path are compared with LWC paths derived from CSSM fields to validate the cumulus cloud model. Parameter estimation results and initial validation results are presented.

1. INTRODUCTION

TASC's CSSM,^{1,2} developed under contract to Phillips Laboratory, simulates high-resolution cloud structures and is used in applications involving scene visualization. The model produces realistic, high-resolution (on the order of meters) LWC fields for a variety of cloud types within domains described by larger-scale (on the order of kilometers) weather conditions. This paper describes one aspect of TASC's ongoing CSSM development effort — the use of aircraft-based observations of LWC to estimate cumulus model parameters and to validate the cumulus model.

2. CSSM CUMULUS MODEL OVERVIEW

The CSSM is an empirical model that generates high-resolution, four-dimensional (three spatial [3-D] and time), multi-layer cloud fields consistent with large-scale input weather conditions. That is, it simulates realistic structure of cloud water content (typical resolutions of 10 to 100 meters) within a spatial and temporal domain defined by general meteorological characteristics. One 3-D field is generated for each specified output time and contains cloud water content values arranged on a regular volumetric grid. The CSSM simulates a variety of cloud types including cirriform, stratiform, and cumuliform types.

The CSSM cumulus model uses a combination of stochastic field generation techniques and convection physics to produce four-dimensional LWC fields for cumuliform clouds. The model uses a fractal algorithm, known as the Rescale and Add (RSA) algorithm³, to simulate the spatial distribution of cloud elements and water density within these clouds. A one-dimensional convection model, driven by a time-varying heating field simulates the vertical growth of cumuliform clouds.

A number of parameters within the RSA and convection algorithms control the statistical characteristics of the resulting LWC fields. A limited set of cloud observations were used in a previous modeling effort¹ to estimate these parameters. LWC time series sampled using conventional hot-wire probes mounted on aircraft were compared to corresponding samples from the model output fields. A large number of additional observations spanning a wide range of climatological conditions have been collected in the current effort. A portion of these observations are used to estimate and tune model parameters and the remainder are used for model validation.

3. LIQUID WATER CONTENT DATA

The liquid water content data used in this study were obtained from the Federal Aviation Administration (FAA) cloud database. The database includes information on a variety of cloud-related variables, including LWC

data, originally collected from various research projects. Individual time series for cumuliform cloud types were selected from the database based on several criteria: length of series; type of flight path (slant or level); and supporting information, such as aircraft location, aircraft speed, cloud base and top, and freezing level. The data used in this study were collected during three projects located in Montana, South Africa, and France. LWC values reported in the database were either measured by a hot-wire meter (Johnson-Williams or CSIRO-King) and/or computed from the droplet size distributions indicated by the Forward Scattering Spectrometer Probe (FSSP). The hot-wire meter values were chosen for analysis in this study because the values appeared more reliable and consistent and because a greater number of hot-wire meter observations were available from the database. Information on aircraft speed and direction provide for the simple translation from time to spatial coordinates.

4. PRELIMINARY RESULTS

A total of 57 flight paths through cumulus clouds were selected from the database and analyzed. Of these, 19 were selected at random for use in estimating model parameters. The primary parameter of interest in this study is the Hurst parameter which is related to the fractal dimension and indicates the small-scale variability of LWC within the cloud. The Hurst parameter was estimated using TASC's Time Series Analysis Package (TSAP) software.⁴ The box estimator⁵ and the power spectral density estimator⁶ were used for long and short paths, respectively. The average Hurst parameter for the estimator paths was calculated to be 0.23. This value agrees quite well with the value of 0.2 that was estimated in the previous development effort¹ using a limited data set.

As a first step in validating the cumulus model, several paths were extracted from a LWC output field generated with the original baseline CSSM cumulus model parameterizations — in this case with Hurst parameter of 0.2. The average Hurst parameter, average LWC value, and standard deviation were calculated for the simulated paths and compared with the statistics for a sample observed LWC path. The results are shown in Table 1. Figures 1a and 1b show the autocorrelation functions for one of the simulated LWC paths and for the observed LWC path, respectively.

Table 1 Simulation vs. Observation Statistics

STATISTIC	SIMULATION	OBSERVATION
Hurst parameter	0.581	0.188
Average LWC (g kg ⁻¹)	0.95	0.65
Standard Deviation (g kg ⁻¹)	0.31	0.46

These comparisons show some agreement between the simulated LWC paths and the selected observed path, however some interesting differences exist. For example, the average simulated LWC along a path can vary significantly from that seen in the observations because of its strong dependence on the input moisture profile. Spatial variability of the LWC (as represented by the standard deviation and the Hurst parameter) is typically less in the simulations than that seen in the observations. Further model parameter tuning will address this difference.

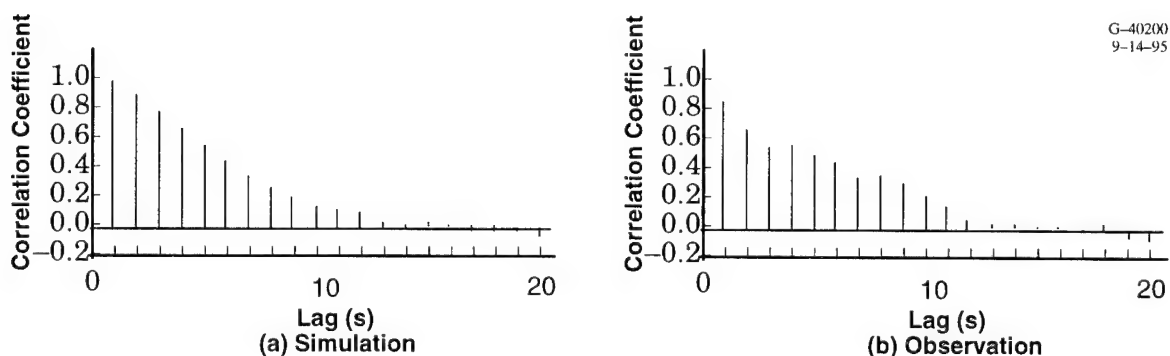


Figure 1 Autocorrelation Function for LWC Time Series for Simulation (a) and Observation (b)

5. CONCLUSIONS

The TASC/U.S. Air Force Phillips Laboratory Cloud Scene Simulation Model produces synthetic high-resolution liquid water content fields for use in applications involving scene visualization. Aircraft-based observations of liquid water content are used to estimate model parameters that control the statistical characteristics of the resulting LWC fields. The preliminary comparison presented here shows that simulated LWC fields produced using original estimates of cumulus model parameters in the original baseline CSSM produce LWC fields generally consistent with those seen in observations. Several differences noted in the comparison show that model parameters require additional tuning with information derived from the observed LWC data.

6. ACKNOWLEDGEMENTS

Special thanks to Don Grantham and Capt. Joseph Eicher of the U.S. Air Force Phillips Laboratory and Jeff Turner of the U.S. Army Topographic Engineering Center who sponsored this effort. Thanks to Dr. Richard Jeck of the Federal Aviation Administration who provided the liquid water content data.

7. REFERENCES

1. Cianciolo, M.E., and R.G. Rasmussen, Cloud Scene Simulation Modeling — The Enhanced Model, Technical Report PL-TR-92-2106, April 1992.
2. Cianciolo, M.E., J.S. Hersh, and M.P. Ramos-Johnson, Cloud Scene Simulation Modeling — The Interim Report, Technical Report PL-TR-91-2295, November 1991.
3. Saupe, D., Point Evaluation of Multi-Variable Random Fractals, *Visualisierung in Mathematik und Naturwissenschaft*, H. Jurgens and D. Saupe, Eds., Springer-Verlag, Heidelberg, 1989.
4. Medler, C.L., and R.G. Rasmussen, Fractal Models of Obscuration: Task 1 — Final Report, TASC Technical Report TR-5753-1, 20 April 1990.
5. Voss, R.F., "Fractals in Nature: From Characterization to Simulation," *IEEE Transactions on Pattern Analysis and Machine Intelligence*, v. PAMI-6, no. 6, November 1984, pp. 661-674.

PRODUCTION OF LONG-TERM GLOBAL MULTI-LAYER WATER VAPOR AND LIQUID WATER DATA SETS FROM MULTI-SATELLITE AND RADIOSONDE OBSERVATIONS

Thomas H. Vonder Haar, Mark A. Ringerud, David L. Randel, Graeme L. Stephens, Cynthia L. Combs,
Donald L. Reinke, and Thomas J. Greenwald
STC-METSAT
Fort Collins, Colorado, 80521, USA

ABSTRACT

A comprehensive and accurate global water vapor data set is critical to the adequate understanding of water vapor's role in the Earth's climate system. To satisfy this need, a blended global, five-year (1988-1992), one degree resolution, Precipitable Water Content (PWC) and Liquid Water Path (LWP) product consisting of both the daily total column integrated composite and multi-layered PWC products at three layers (sfc-700 mb, 700-500 mb, 500-300 mb) data set was produced. The analyses combines PWC retrievals from the Television and Infrared Operational Satellite (TIROS) Operational Vertical Sounder (TOVS), the Special Sensor Microwave/Imager (SSM/I), and radiosonde observations. The global layered water vapor data set is created by slicing the blended total water vapor data set using layered information from TOVS and radiosonde. Also produced were companion, over oceans only, integrated cloud liquid water and liquid water path data sets. The complete data set (all three products) has been named NVAP, an acronym for National Aeronautics and Space Administration (NASA) Water Vapor Project.

1. INTRODUCTION

There is a well documented requirement for a comprehensive and accurate global moisture data set to assist many important scientific studies in atmospheric science. This need is emphasized by the efforts of the U.S. Climate Research Program, the Global Energy and Water Cycle Experiment (GEWEX), the GEWEX Water Vapor Project (GVaP), and the GEWEX Continental-Scale International Project (GCIP). There is a tight correlation between water vapor and clouds. It may seem obvious, but knowing the distribution of water vapor in the atmosphere gives you an edge in predicting the onset, duration, and dissipation of clouds. Water vapor can be used to infer the presence or absence of clouds beneath an overcast cloud deck. The amount of water vapor in the column of air will also have an impact on visibility (i.e. the increased probability of fog and suspended aerosols). Lasers (or other optical transmission systems) are also affected by water (density) gradients in the atmosphere. Clouds are the single most significant detractor for laser guided and laser communications systems.

Currently, atmospheric water vapor measurements are made from a variety of sources including radiosondes, aircraft and surface observations, and in more recent years, by various satellite instruments. Creating a global data set from a single measuring system produces results which are useful and accurate only in specific situations or areas. Therefore, an accurate global moisture data set must be derived from a combination of these measurement systems.

2. DATA PROCESSING

The total PWC product is a weighted merging of SSM/I, TOVS and quality controlled radiosonde retrievals. Each of these measurement systems has limited data coverage. The radiosonde coverage is widely spaced and primarily over land, while TOVS retrievals are performed only in the absence of thick precipitating clouds. The SSM/I retrievals are made only over the oceans. The final integrated PWC product is created by combining these three input data sets using a hierarchical weighting scheme. This algorithm used radiosonde data when available as "truth", and then applies a weighting scheme to the TOVS and SSM/I. In the last step, linear and temporal interpolation routines are run to fill missing data points. Included as part of the PWC data set is a data source code map that describes the origin of each point in the blended product.

The vertical distribution of water vapor is important to moisture transport and radiation studies. Two of the three input data sets contain layered information, radiosonde and TOVS, and these were used to create the layered PWC. The TOVS data was retrieved in three layers: surface to 700 mb, 700-500 mb, and 500-300 mb and binned into a one by one degree grid. The radiosonde PWC retrievals were processed into identical matching layers. This layered information was then used to "slice" the total blended PWC product. This gives the layered product the advantage of including SSM/I information along with TOVS and radiosonde data.

Included as a companion data set are two atmospheric liquid water products, a quantity with increased importance of late since many global circulation models are beginning to include liquid water as an explicit variable. First the oceanic cloud LWP on a daily one by one degree grid from the SSM/I processing is available. The LWP product is the liquid water in any region, cloud or no cloud, and is based upon the physically based method of Greenwald et al. (1993), which covered ocean areas only. Also available are the monthly averages of cloud liquid water content which is the liquid water in cloudy-only regions using a specified threshold of liquid water retrieval.

3. RESULTS

General results from the layered PWC products show that in oceanic areas, roughly 75-85 percent of the total PWC is in the lowest layer. Depending on the surface elevation, elevated terrain has only around 50 percent in this layer. In some locations, the surface may be above 700 mb, such as over the Tibetan highlands, in which case the percent-of-the-total for this layer is zero.

The PWC annual cycle of the global and hemispheric daily averages for 1992, as shown in Figure 1, clearly shows the global PWC cycle is dominated by the Northern Hemisphere (NH). These variations were first reported by Wittmeyer and Vonder Haar (1994) using only the TOVS data. It is seen that the time series of global PWC averages are sinusoidal in shape and have a maximum during June-July-August (JJA). The NH values have a maximum during the summer months (JJA) and a minimum in the winter. The differences between the NH and the Southern Hemisphere (SH) are significant. The range of NH averages is twice that of the SH, the summer maximum being much greater for the NH. This variation is due mainly to land and ocean differences (the NH contains most of the Earth's land area). The large NH land areas produce much more of a seasonal temperature range than the oceans. The amount of water vapor in the air is related to temperature and in combination with the strong summer convective maximum, results in the larger NH seasonal range. Other factors include the severe summer monsoon season in India (NH) and the lower water vapor concentrations in the SH contributed by the cold and elevated Antarctic.

The annual cycles are also apparent in all layers. Upon examination of the annual maximum of the global and hemispheric averages, we see preliminary evidence that the time of the summer maximum increases with height. This would suggest the time delay of the moisture transport from the surface to upper layers is discernible in the data set.

4. ACKNOWLEDGMENTS

Data collection and processing for this project was sponsored by NASA under contract no. NASW-4715.

5. REFERENCES

- Greenwald, T.J., G.L. Stephens, T.H. Vonder Haar, D.L. Jackson, 1993: A physical retrieval of cloud liquid water over the global oceans using SSM/I observations. *J. Geophys. Res.*, **98**, 18471-18488.
- Wittmeyer, I.L. and T.H. Vonder Haar, 1994: Analysis of the global ISCCP TOVS water vapor climatology. *J. Climate*, **7**, 325-333.

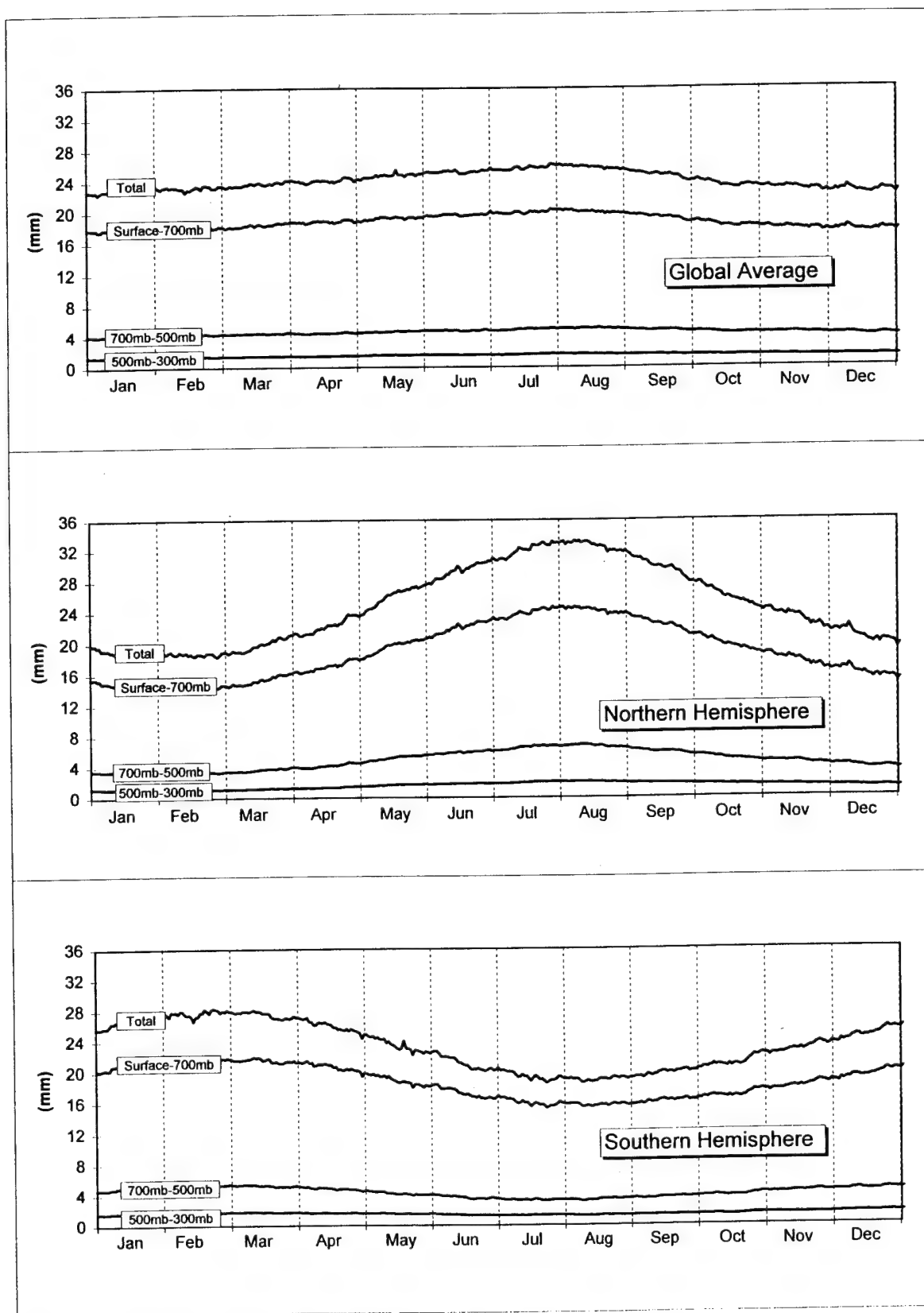


Figure 1. Total and Layered PWC annual cycle averages of the global, Northern Hemisphere, and Southern Hemisphere for 1992.

DEVELOPMENT OF A CLOUD COVER FORECAST MODEL

Roger D. Dickey
GENCORP/Aerojet
1100 W. Hollyvale
Azusa, CA 910702

William T. Kreiss
Georgia Tech Research Institute
Atlanta, GA 30332

ABSTRACT

Our objective was to develop a cloud cover forecast model for tactical applications that would execute on a small workstation with minimal inputs. The resultant Tactical Cloud Cover Forecast Model produces a representation of the predicted cloud fields in the 12-24 Hr. period for synoptic scale disturbances.

1. INTRODUCTION

A cloud cover forecasting technique based on a 500 mb barotropic atmosphere model and IR imagery has been developed for short-term forecast needs of operational forces. This technique has been developed from an earlier approach of R. Nagle¹. This implementation differs from that of Nagle's in that "ripping" of the forecast image has been prevented. The algorithm only requires a 700 mb temperature field, 500 mb height field and an infrared satellite image. The height field is filtered to extract the long wave component which is extrapolated into the future using conservation of vorticity and a barotropic model. The cloud fields are then identified and moved according to the predicted field.

1.1 SCALE SEPARATION AND PREDICTION

Atmospheric motions can be considered on two scales. A large scale quasi-stationary flow (Rosby Waves) and the perturbations on that flow, which produce inclement weather. Scale separation is achieved by recursively applying a weighted Laplacian operator to the height field, which produces a high pass spatial filter. This defines a short wave field, which is subtracted from the analysis field to produce an estimate of the long wave field. This is considered to be the steering field, which will propagate the disturbance represented in the satellite image. A 24 Hr. forecast is then produced from the smoothed (long wave) grid by assuming conservation of vorticity and a barotropic atmosphere. During the forecast process, the locations of the original grid points are extrapolated using geostrophic winds and output on an hourly basis.

1.2 CLOUD RECOGNITION AND EXTRAPOLATION

The pixels of an infrared image are classed as cloud/no cloud using the 700 mb temperature field. The pixels are loaded into rectangles corresponding to the 500 mb height grid and are moved to future locations using the advected 500 mb grid points. Rather than storing these pixels in a rectangular array, the relative coordinates along grid box's boundaries with respect to the nearest corner are stored. These corner relative coordinates are illustrated in Fig. 1. This implementation differs from that of R. Nagle in that the advected rectangles are allowed to deform

to quadrangles, and the pixels are plotted in these corner relative coordinates which prevents the “ripping” of the projected image, as will be shown in the associated video presentation.

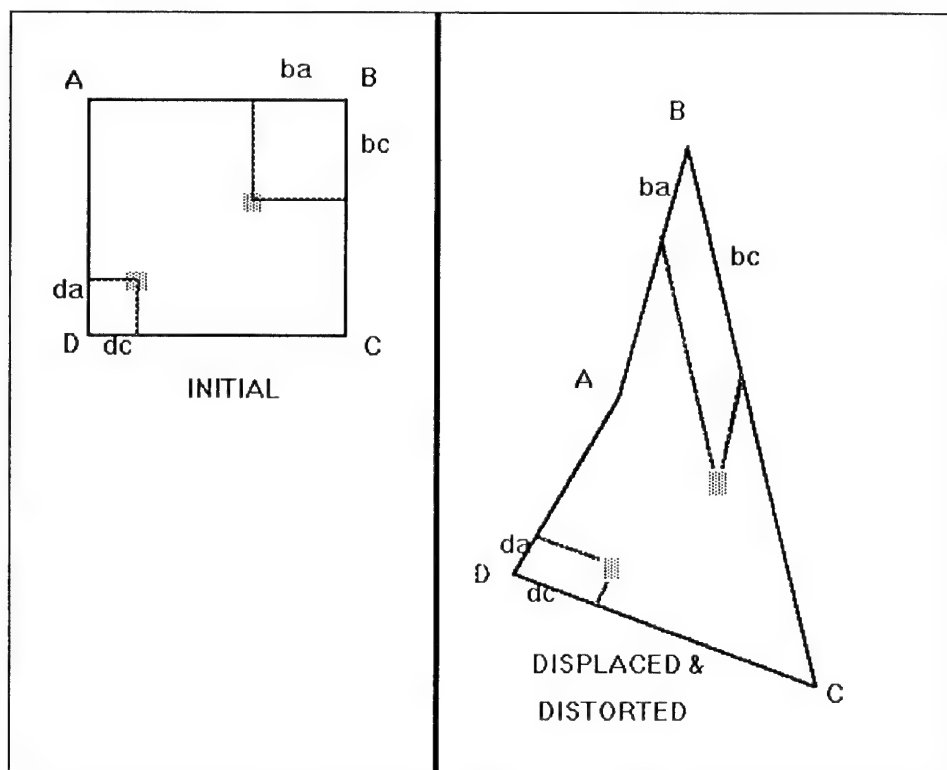


Figure 1. Corner relative coordinates.

While this method of generating the predicted image is robust under extreme distortions, it does produce holes in continuous cloud decks in divergent flows.

2.0 CONCLUSIONS

A workstation based cloud forecast model has been developed, with a robust method of generating predicted cloud images under conditions of distortion.

3.0 REFERENCES

- 1.) Nagle, R.E., 1992, A Kinematic Model for the Short-Term Prediction of Remotely Sensed Hydrometers, Technical Note 210, Naval Oceanographic and Atmospheric Research Laboratory

A NOVEL INFRARED IMAGING SPECTRORADIOMETER FOR PASSIVE REMOTE DETECTION OF CLOUDS

David M. Sonnenfroh, B. David Green, William J. Marinelli, and W. Terry Rawlins
Physical Sciences Inc., 20 New England Business Center, Andover, MA 01810

ABSTRACT

Physical Sciences Inc. is developing a compact, airborne, infrared *imaging* spectroradiometer with applications in passive, remote monitoring of clouds. The heart of the sensor is a tunable Fabry-Perot etalon operated in low order which produces a monochromatic, continuous image. The frequency agility of the sensor can be exploited to monitor different wavelengths with a common detector array. Sophisticated radiometric data processing algorithms have been created to fully exploit the power of multispectral imaging. We are developing such algorithms for detection of exhaust plumes, contrails, and cirrus clouds as well as aerosols, such as subvisible volcanic ash clouds.

1. INTRODUCTION

The IR Fabry-Perot Imager under development at Physical Sciences Inc. is a novel, tunable, infrared *imaging* spectroradiometer. The sensor is capable of operating in either the 3 to 5 or 8 to 13 μm atmospheric window. The frequency agility of the sensor allows it to tune around H_2O , CO_2 , and O_3 absorptions to capture images at several wavelengths, all with a common detector. This is a significant advantage over the use of multiple radiometers. The sensor can be readily deployed on air- or spaceborne platforms as it is compact, lightweight, and has minimal power requirements. The tunability and spectral resolution of this instrument, combined with advanced detection and data processing algorithms, create a unique sensor tailored for detection of clouds, aerosols, and contrails.

1.1 IR FABRY-PEROT IMAGER

The IR Fabry-Perot Imager is based on a unique application of Fabry-Perot interferometry. The heart of the instrument is a moderate resolution ($\sim 0.1\mu\text{m}$), high throughput, imaging Fabry-Perot interferometer configured to operate in low order. The interferometer utilizes mirror spacings which produce a monochromatic, *spatially continuous image* (compared to the familiar "bull's eye" ring pattern) and provide a wide-free spectral range while maintaining a high system finesse (spectral resolution). The close mirror spacings allow for a wide field-of-view without degradation of the spectral resolution. The interferometer then operates as a tunable interference filter with high radiant sensitivity. The main advantages of the Fabry-Perot interferometer, high optical throughput with good spectral resolution, are maintained. Piezoelectric transducers control the mirror spacing. Either an InSb or a HgCdTe focal plane array captures radiant intensity transmitted by the interferometer with high sensitivity, resulting in a true solid state sensor. Prototype systems operating at 4.3 and 10 μm have been field demonstrated; the MWIR instrument is pictured in Figure 1. A US patent is pending.

The IR FP Imager is sufficiently compact for deployment on airborne platforms including jet aircraft and UAVs, as well as satellites. For example, the IR FP Imager easily meets the payload constraints of the Perseus B UAV, requiring only a small fraction of the available payload resources.

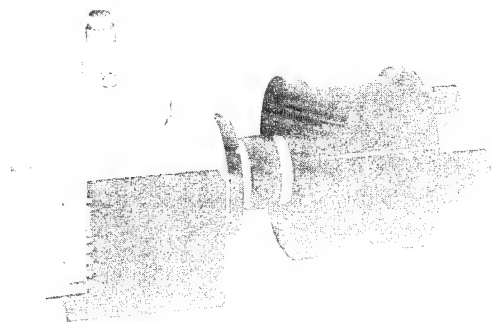


Figure 1. PSI IR FP imager.

1.2 DATA ALGORITHMS FOR MULTISPECTRAL IMAGERY

The IR FP Imager can acquire near-simultaneous two dimensional images at multiple wavelengths. The resulting data stream can stress the data acquisition, storage, and processing capabilities of current hardware. It can also tax the human ability to interpret the data on a useful time scale. We have developed data acquisition and processing methods which exploit the rapid tunability and spatial coregistration of the imager. These unique features are the key to the success of detection algorithms which employ ratios or differences of radiances at several wavelengths. They allow several wavelengths to be sampled nearly simultaneously. Ratios of these images at selected wavelengths can then be calculated to produce enhanced contrast images for target detection. Additional processing includes background frame subtraction to eliminate clutter and isolate the target. Background frames are acquired at wavelengths for which the target is transparent. Image processing is carried out with an on-board processor to decrease data downlink requirements.

1.3 EXAMPLE DATA

Algorithms have been developed to recover cloud top pressure and temperature, cloud opacity, and cloud emissivity from ratios of radiances in the MWIR and LWIR regions.^{1,2} Cloud microphysical properties can be recovered from reflected radiance in the NIR and visible regions.¹ No single satellite sensor has had the capability to monitor a suite of wavelengths throughout the MWIR and LWIR. We are currently pursuing interfacing existing radiometric algorithms with our IF FP Imager in order to create a sensor capable of monitoring most of the major cloud field parameters listed above.

To demonstrate volcanic ash cloud detection, we have applied a two color brightness temperature (BT) differencing algorithm to actual AVHRR satellite imagery of western Washington (Band 5, 12 μm). Separate images for wavelengths of 10, 11, 12, and 13 μm were generated by scaling the original image at 12 μm using Planck's equation. A model volcanic ash cloud was superimposed on the 10, 11, and 12 μm images near Mt. St. Helens. The cloud had a total number density of 50 cm^{-3} , an optical depth of 0.15 at 10 μm , a physical depth of 3 km, and was placed between 11 and 14 km altitude. The resulting images at 10 and 11 μm are shown in Figure 2a.

The BT differencing algorithm was then applied to these images. A background frame at 13 μm was subtracted from each of the images at 10, 11, and 12 μm . The background-subtracted frame for 10 μm was subtracted from that for 12 μm and normalized by the 12 μm frame to generate the difference frame in Figure 2b (top). Also illustrated is a similar difference frame for the 11 and 12 μm bands (bottom). The delta radiance values shown in Figure 2b are indicative of composition. If the cloud were composed of water, the delta radiances would have the opposite sign.

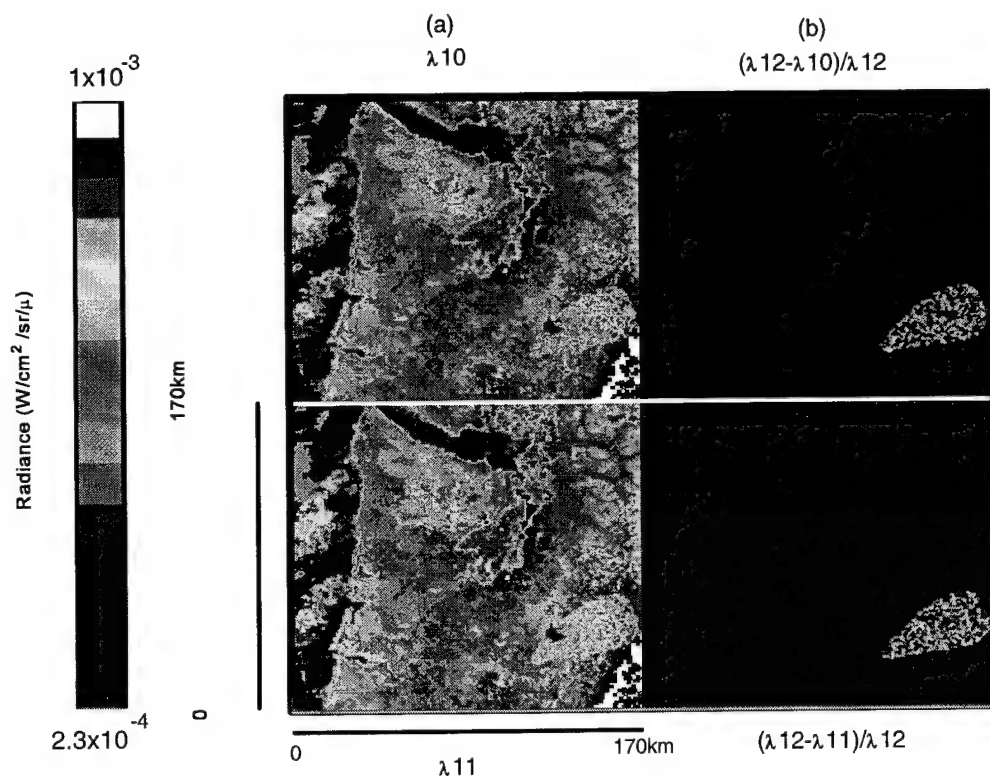


Figure 2. Simulated volcanic cloud over Mt. St. Helens. (a) Spectral radiance at 10 μm (top) and 11 μm (bottom), (b) Spectral radiance differences: $(N(12\mu\text{m}) - N(10\mu\text{m})) / N(12\mu\text{m})$ (top) and $(N(12\mu\text{m}) - N(11\mu\text{m})) / N(12\mu\text{m})$ (bottom).

2. CONCLUSIONS

Physical Sciences Inc. is developing a compact, airborne, infrared *imaging* spectroradiometer for passive, remote monitoring of clouds. The sensor is highly tunable so that multiple wavelengths can be monitored with a common detector. Sophisticated data processing algorithms have been created to fully exploit the unique features of the imager. The Imager is sufficiently compact for deployment on many different airborne platforms.

3. ACKNOWLEDGEMENTS

The authors acknowledge support from DOE under contract DE-FG02-94ER81830.

4. REFERENCES

- 1) M.D. King, et al., "Remote sensing of cloud, aerosol, and water vapor properties from the Moderate Resolution Imaging Spectrometer (MODIS)," *IEEE Trans. Geosci. Remote Sensing*, **30**, 2, (1992).
- 2) B.A. Baum, et al., "Multilevel cloud retrieval using multispectral HIRS and AVHRR data: Nighttime oceanic analysis," *J. Geophys. Res.*, **99**, 5499, (1994).

EXAMPLES OF CFLOSA (Cloud-Free Line-Of-Sight Aloft) OUTPUT

Albert R. Boehm, James H. Willand
and Marc A. Pereira
Hughes STX Corporation
Lexington, Massachusetts 02173

ABSTRACT

CFLOSA combines a variety of cloud climatologies, statistical cloud structure, complex retrieval and display algorithms to provide an assortment of cloud and cloud-free line-of-sight statistics. Climatological data bases include millions of surface, satellite, radar, aircraft observations. Cloud statistics are produced as a function of latitude, longitude, altitude elevation look angle, and distance.

1. CLIMATOLOGICAL DATA BASES

Mean total sky cover statistics compiled from surface observed cloud conditions are taken from the DOE/NCAR and DOD Burger data bases. Cloud ceiling data are extracted from the ISMC Summary stored on CD ROM. Mean cloud and high cloud cover from satellite observations are extracted from NIMBUS-7 CMATRIX data and ISCCP geosynchronous satellite data. Cloud layer data from satellites include the SAGE and HIRS CO₂ data. Mean cloud amounts, types, layers and particles are obtained from aircraft data such as GASP, and Bertoni LOS data. Other cloud layer statistics can be obtained from radar data such as the TPQ-11 data and compiled radar tops climatology.

Figure 1.0 (top) portrays typical mean cloud cover over the globe as derived from ISCCP data for July at 0900 Mean Apparent Solar Time (MAST). The bottom of the Figure shows mean sky cover over the globe as derived from DOE/NCAR/Burger summer season sky cover climatologies for 0900 MAST.

2. BLENDING DATA BASES

Cloud data comes in variety of formats and observational idiosyncrasies. Each data base has characteristic strengths and weaknesses. A combination of data bases provides a better overall estimate of cloud statistics. Before they can be combined, they must each be transformed to a uniform data structure. This process includes converting to MAST, spatial analysis, as well as finding and discarding incorrect values.

A third order Fourier series in time of day is used to convert data statistics from archived times to a common MAST time. A weighted spectral analysis (Fourier functions in longitude, fully normalized Legendre functions in latitude) with a triangular 18 set of coefficients provides spatial analysis. This type of analysis, for one data set for one time of day, can take over four hours of CPU on the mainframe CDC Amber computer. The number of coefficients was limited to the amount of detail the data could support without getting spurious results. This policy gives a uniform resolution over the globe.

The resulting coefficients are then blended using weights appropriate for the period of record and quality of the data set. The resulting set of coefficients is a rather compact set that allows rapid retrieval and is easily portable to other computers and programming languages. A more detailed description of the data base blending can be found in Willand (1992).

3. EIGENVALUE STRUCTURE

The probability of cloud at a point is only part of the problem. In order to calculate the probability of a cloud obscuring a line-of-sight, knowledge is needed of the structure of clouds. Correlation structure only gives information about pairs of points. A new type of analysis was needed. If the points in a domain are correlated,

the resulting correlation matrix can be characterized by its eigenvalues. Some straightforward equations relate eigenvalues to the correlation matrix,

$$\sum \lambda = \text{Tr}(\mathbf{R}), \quad \begin{array}{l} \lambda \text{ are eigenvalues} \\ \mathbf{R} \text{ is correlation matrix} \end{array} \quad (1)$$

$$\sum_i \sum_j r_{ij}^K = \text{Tr}(\mathbf{R}^K) = \sum \lambda^K \quad \begin{array}{l} r \text{ is element of } \mathbf{R} \\ K > 1 \end{array} \quad (2)$$

There also exists relations between the correlation matrix and coverage (Boehm, 1991) which allow the probability of a fractional coverage to be calculated. Also if the coverage distribution is known, the correlation structure can be inferred. These are very powerful tools. For example, they allow the probability of a cloud-free line-of-sight to be calculated knowing only the point probability of cloud and the correlation structure.

These tools also allow development and storage within CFLOSA of a global model of correlation structure for all altitudes.

TOPOLOGICAL EFFECTS

CFLOSA uses topology to quantify the point probability of clouds below 5000ft above ground level. Namely, a 10nm resolution elevation and land or sea data set delineates areas of low level cloudiness. Although there are topographic influences above 5000ft, for the most part the spectral spatial analysis resolves these adequately.

The 5000ft level was chosen not only on the extent of topographic effects, but also on weaknesses of certain data bases. Older ceilometer data is very poor above 5000ft while certain satellite data such as SAGE is very poor below 5000ft.

QUERY AND DISPLAY

Cloud effects are needed for a large number of scenarios and viewing geometries. Many archived data bases are designed to answer one question. CFLOSA is designed to answer a large variety of questions, quickly, and with tailored output. Individual values, graphs, and maps can be produced for a diverse selection of statistics. Data can be printed or sent to file for further analysis or for use in simulation or operational analysis. Certain conditional probabilities are useful as forecaster aids.

ACKNOWLEDGMENTS

This work is supported by Geophysics Directorate of Phillips Laboratory with Mr. Donald Grantham as contract monitor for contract No. F19628-93-C-0051.

REFERENCES

Boehm, A., 1992: CUB: A General Purpose Coverage Algorithm, 5th International Meeting On Statistical Climatology, American Meteorological Society, Boston, 595-598.

Willand, J. H., 1992: Database Blending for the Climatology of Cloud Statistics Program. PL-TR-92-2344, Geophysics Directorate of Phillips Laboratory with Mr. Donald Grantham as monitor for Contract F19628-88-C-0089, Hughes STX Corporation, AD-A265034.

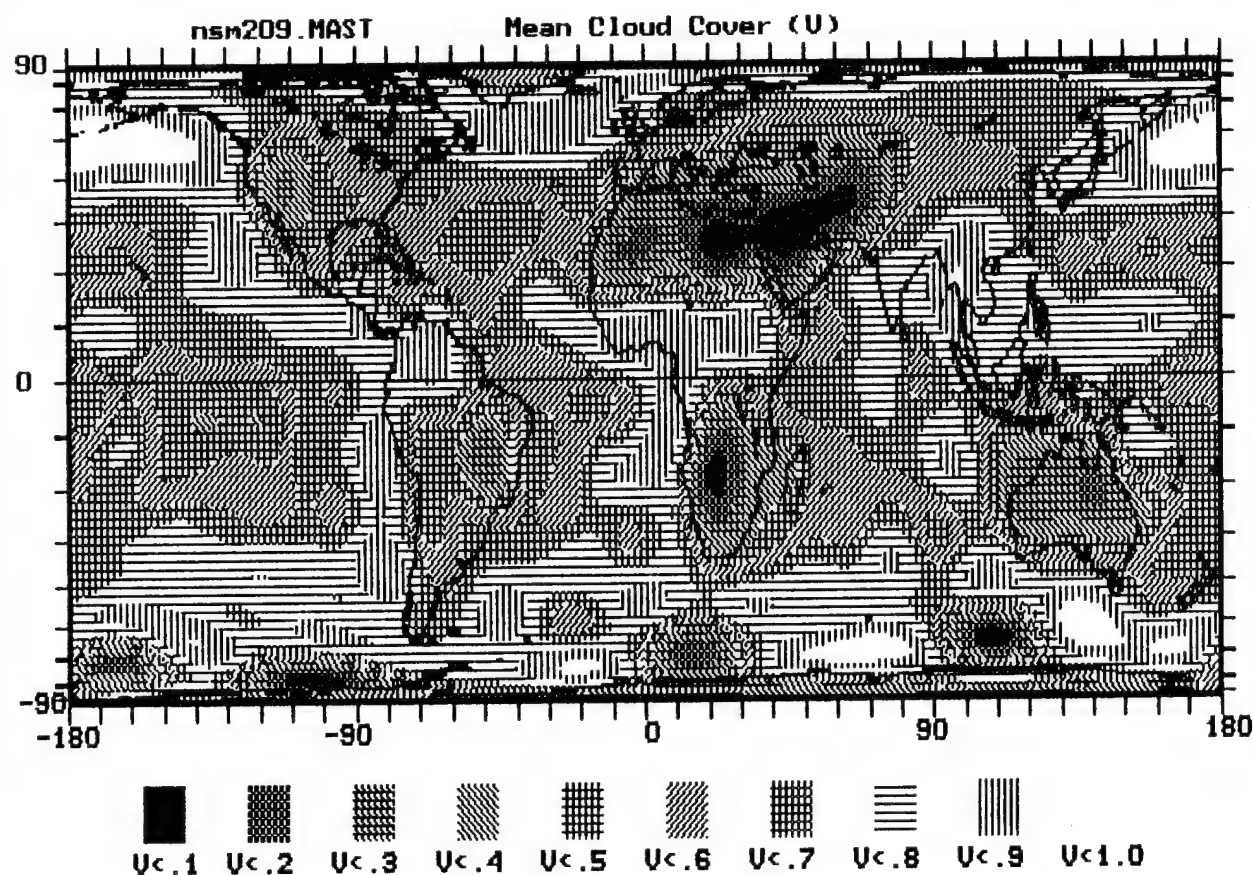
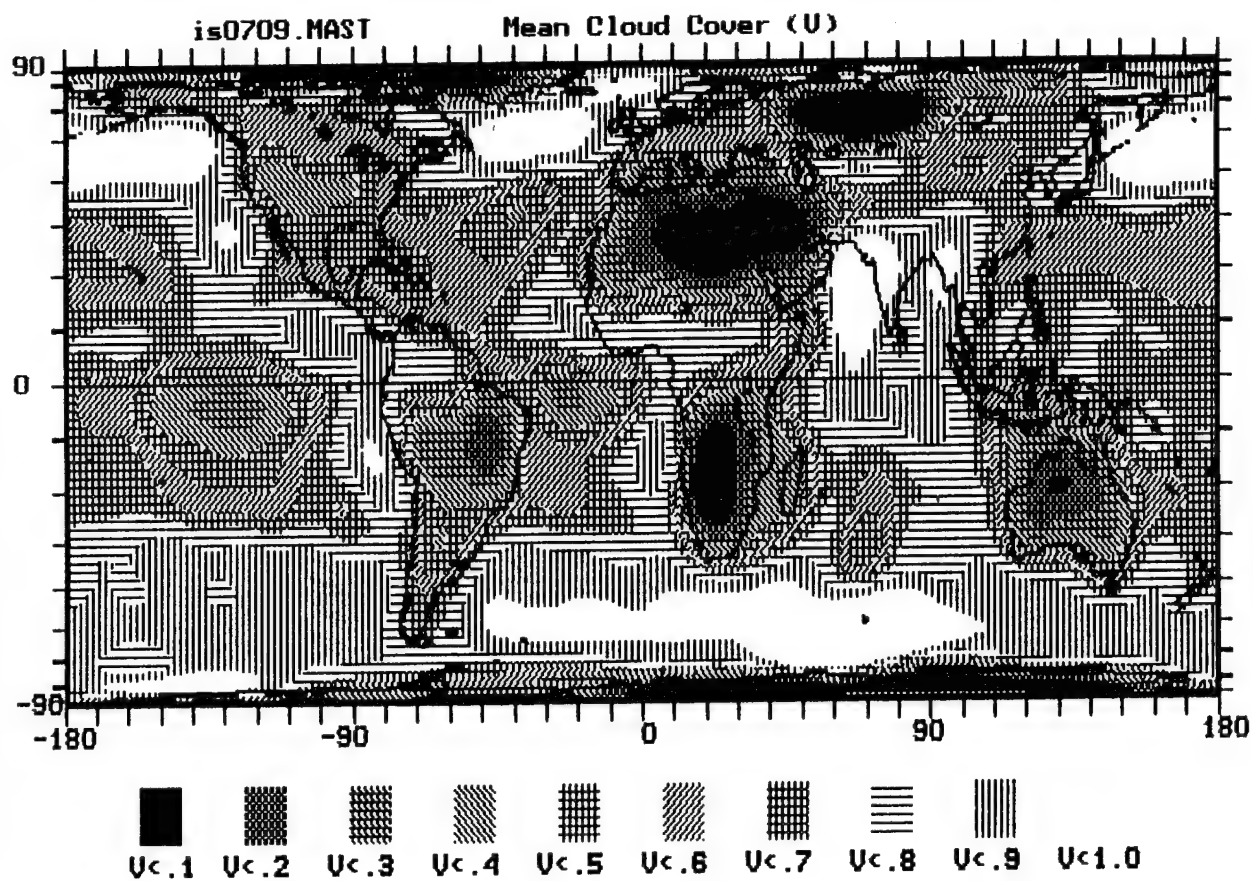


Figure 1.0 (TOP) Probability of mean cloud cover from ISCCP data for July at 0900 MAST and (BOTTOM) probability of mean sky cover from DOE/NCAR/DOD Burger data for the summer season at 0900 MAST.

LINE OF SIGHT CLOUD OBSERVATIONS FROM HALEAKALA

Russell H. Taft
Rockwell Power Systems
Kihei, Maui, Hawaii 96753

ABSTRACT

The High Performance CO₂ LADAR Surveillance Sensor (HI-CLASS) test planning required reliable estimates of the probability of cloud-free line-of-sight (CFLOS) from the summit of Haleakala (10K feet AMSL) to selected remote test sites. Candidate sites for the placement of remote targets to be used for cooperative testing and calibration had been initially identified as being in northeast Maui and along the southeastern section of the island of Lanai.

Two cameras and two time lapse video cassette recorders were set up at the Maui Space Surveillance Complex. One camera viewed the northeast side of Maui and the second camera viewed the southeast side of Lanai. Data were collected for 24 hours each day from February 15, 1994 through September 30, 1994.

The videotapes were reviewed and index numbers assigned to the observed viewing conditions at 15 minute intervals. Analysis indicated that the early morning hours from 2 a.m. through 10 a.m. had the least cloud cover of a 24-hour period and therefore provided the best opportunity to obtain CFLOS to these remote sites. Experience during the HI-CLASS remote sensing experiments in February through August 1995 verified these conclusions.

INTRODUCTION

The Maui Space Surveillance Complex (MSSC), located atop the 10,000 foot Haleakala mountain on the island of Maui, is operated by the Air Force Space Command and the Air Force Phillips Laboratory. The MSSC has a primary mission to conduct space surveillance and research and development activities for the U. S. Department of Defense (DoD).

With advanced sensor systems, excellent seeing conditions, dry weather, pristine environment, and mid-Pacific location, the site has established a reputation for excellence in space surveillance, missile tracking and imaging, atmospheric physics, and astronomy.

Another advantage of the unique location of the MSSC is to provide a testbed for simulating seeing conditions from an airborne platform for viewing from 10,000 feet with backgrounds including ocean, ocean/land interfaces, mountain terrain and clouds. Visibility ranges often exceed 100 km.

A current research program at the MSSC is the development of a High Performance CO₂ LADAR Surveillance Sensor (HI-CLASS) which uses the MSSC as a testbed to obtain laser radar data on low earth orbiting satellites. The program also provides DoD with a testbed for remote sensing of pollutants and airborne chemical agents. HI-CLASS test planning requires reliable estimates of the probability of CFLOS to selected test sites. Candidate sites for the placement of remote targets to be used for cooperative early testing and calibration of the prototype HI-CLASS laser system have been initially identified as northeast

Maui (Happy Valley, 10 miles distant, bearing 335°T from the transmitter site), and southern Lanai (Manele Bay, 30 miles, bearing 274°T from the transmitter site).

TEST CONFIGURATION AND SAMPLE RATE

Two cameras and two time-lapse video cassette recorders were set up for unattended 24-hour operations, such that one camera views the northeast side of Maui in the general direction of Wailuku town on towards Kahakuloa, and the second camera views the southeast side of Lanai near Manele Harbor as shown in Figure 1. The video data are overlaid with annotated time of day/night and provide passive visual coverage of the candidate test sites every 4 seconds (i.e., one standard 2-hour tape captured 240 hours of snapshot data). Videotapes are replaced typically every 10 days except during the latter part of the measurements when it was deemed appropriate to change the time lapse rate to one frame every eight seconds which yielded a 2-hour videotape every 20 days. Data were collected 24 hours each day, 7 days per week, from February 15, 1994 through September 30, 1994. There were occasions in April and May when observatory power failures precluded data collection.

The camera was a Canon 8 mm L1 Camera/Recorder with a CL-8-120 mm, f/1.4-2.1 zoom lens. The camera incorporated auto-iris zoom capability, selected to provide the appropriate fields-of-view for the targeted test sites and is capable of observing less than 1 lux minimum light illumination levels for night observations. The data recorder was a Sanyo TLS Time Lapse Video Cassette Recorder.

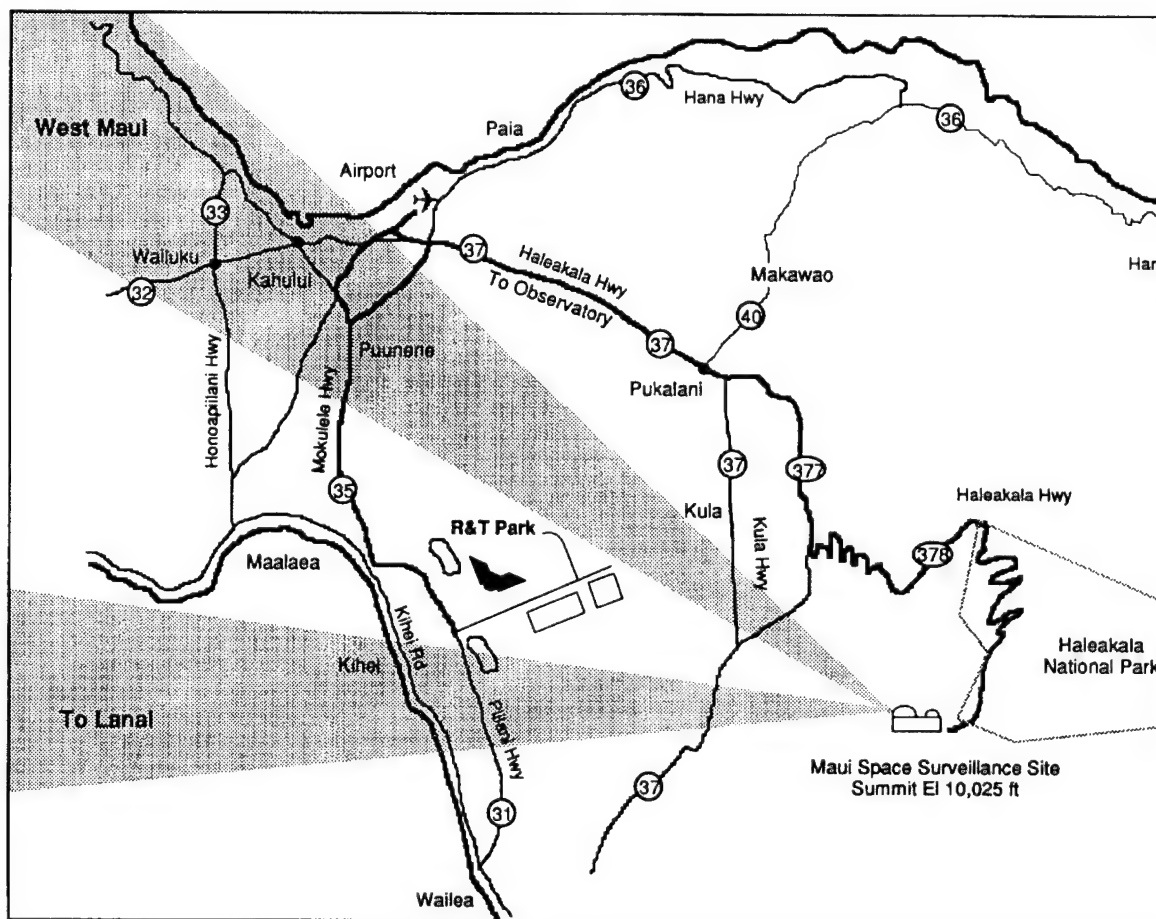


Figure 1 View Angles of Video Cameras

DATA REDUCTION

Two individuals were involved with viewing and reduction of the video data. Their basic task was to observe the TV monitor and at specific time intervals make a judgment of how much of the TV screen was obscured by clouds and to assign an index number in accordance with the following table.

TABLE 1. CLOUD INDEX CRITERION

Cloud Conditions	Visibility %	Cloud Index #
Clear	100	1
Partly cloudy - greater than 80% visibility	80-99	2
Cloudy - less than 80% visibility	1-80	3
Total obscuration	0	4

The videotapes were played back in their entirety. Every 15 minutes in the course of the 24 hour day, starting on the hour, the cloud index was estimated based upon the scene displayed at that time period. Inherent in these data is the subjective nature of this approach and also of the differences resulting from two individuals making estimates. However, the range of visibility for each index number is broad enough to minimize the subjective bias.

The reduced data were displayed using Microsoft Excel. All video and digital data have been archived and are available for future review and analysis. The results of the data indicate that it was not cost-effective to complete reduction of the additional data collected from July 9 through September 30, 1994.

DATA ANALYSIS

The first attempt to identify LOS cloud conditions was to plot the cloud index value for each 15-minute period as a function of time for each day. Results show that the mornings are generally clear; the base of the cloud layer starts generating at the 5,000 to 7,000 foot elevations in mid-morning. The clouds typically build up and obscure the summit from the valley from mid-morning until evening when the clouds dissipate. Afterwards it is usually clear again until mid-morning. During the day the northeasterly trade winds bring moist ocean air up the slopes of Haleakala where it rises to the cooler altitudes by mid-morning, at which time cloud formation takes place and is confined at these elevations because of the temperature inversion.

These clouds are typically formed as a band close to the land mass at these elevations. The cloud thickness and width is sufficient to obscure the land mass of the valley on the island. After sunset, when the land temperatures fall, the clouds dissipate and the LOS is generally clear until the cycle repeats. Figure 2 shows the diurnal trends in the LOS to West Maui and similar results were obtained with the Lanai data.

The data were also averaged over the entire data collection period of February through early July 1994 for each quarter hour of the 24-hour day. The typical diurnal cycle characteristic of the cloud cover is readily observed in the West Maui LOS averages plot, as shown in Figure 3. It was also observed in the Lanai data, but on a smaller scale. This is probably due to other cloud systems farther away from the slopes of Haleakala, in addition to the local cloud system, along the LOS from Haleakala to Lanai. There was only one light source available in the field of view on the eastern shore of Lanai, close to sea level. When the source was not observed in the video, the cloud conditions for the entire field of view could not be determined. In these cases no data are recorded.

Another approach in analyzing the cloud data was to obtain histograms to evaluate the frequency of observed times that the cloud conditions were clear, partly cloudy, cloudy or totally cloudy. Histograms for both the West Maui LOS and the Lanai LOS were generated for the months of February through July. They indicate clear conditions about 5.5% of the time, and complete obscuration by clouds around 57% of the

time. Figure 4 shows the Cloud Data Histogram for February through July for the West Maui Mountain. The histogram for the Lanai data is similar.

Figure 5 shows the Time-of-Day Distribution of Cloud Cover Measurements which show the Frequency of Occurrence of the seeing conditions for each hour of the day during the entire measurement period. The figure shows that the highest probability of clear LOS occurs between 2 a.m. and 10 a.m.

This agrees with the experience of the remote sensing measurement programs in February, May and August of 1995. The majority of the measurements were scheduled from the midnight to 8 a.m. time period for which clear LOS to the remote site located in the valley was available for 29 out of 38 scheduled periods.

CONCLUSIONS

Although Haleakala is considered one of the premier sights for optical observatories because of excellent seeing for satellite and astronomical observations, conditions are not as outstanding for low elevation. The temperature inversion that creates and maintains the cloud layer below the summit of Haleakala reduces the probability of CFLOS for elevation angles below 0 degrees. As a result, opportunities for propagating lasers to targets located in the valley of Maui or the West Maui Mountains, or any other nearby island are relatively few.

It is recommended that data collection continue for at least another six months, for at least one year of data, to evaluate annual changes. Even one year of data cannot be considered sufficient to generate reliable statistics from a meteorological perspective. Therefore, data presented within this brief report drawn from such a limited database should be approached with caution due to limited sampling and duration.

ACKNOWLEDGMENTS

The author is grateful for the efforts of E. Albetski and R. Fowler, for the tedious and time consuming process of viewing and reducing the videotapes.

SERCAA INTEGRATED CLOUD ANALYSIS VALIDATION

Kenneth F. Heideman

Phillips Laboratory / GPAB, Hanscom AFB, MA 01731-3010

Robert P. d'Entremont, Jeanne M. Sparrow, Tony S. Lisa, and Gary B. Gustafson
Atmospheric and Environmental Research, Inc.
840 Memorial Drive, Cambridge MA 02139-3794

1. INTRODUCTION

Support of Environmental Requirements for Cloud Analysis and Archive (SERCAA) is a large research and development program that has been underway at The Air Force Phillips Laboratory since FY93 (Isaacs, 1993 and Neu et al., 1994). The objective of Phase I of the project, completed during FY94, was to develop a global cloud detection and analysis model to replace the Air Force Global Weather Central (AFGWC) real-time nephanalysis (RTNEPH) as part of the Cloud Detection and Forecast System upgrade (CDFS II). The SERCAA algorithm is comprised of three cloud detection algorithms that independently analyze imagery from DMSP/OLS, NOAA/AVHRR and geostationary satellite platforms (Gustafson, 1992, d'Entremont et al., 1994, and Gustafson et al., 1994), a cloud layering and typing algorithm, and an analysis integration procedure. The motivation for the SERCAA Phase I effort was to address deficiencies in the RTNEPH product. For example, SERCAA incorporates the superior temporal coverage provided by geostationary satellites, and was designed to detect cirrus and low cloud more effectively than RTNEPH through the use of multispectral techniques. See Heideman et al. (1994) for an expanded comparison of RTNEPH and SERCAA cloud analysis model attributes.

While an important aspect of the SERCAA algorithm development program was testing of the individual satellite-specific cloud analysis algorithms that comprise it, the question of whether SERCAA should replace the incumbent nephanalysis required further study. Toward that end, a two-part systematic validation effort was initiated to compare the relative accuracy of the integrated SERCAA algorithm with the RTNEPH algorithm. The first part involved developing statistics to describe how often, and under what circumstances, the analyses significantly disagreed in assigning cloud fraction values. The second part provided an admittedly subjective but fair assessment of which algorithm provided the best cloud detection analysis under those circumstances. The procedure used for comparison of the two algorithms, as well as the results of the study, are described below. Details of the computer interface and validation database designed to facilitate collection and analysis of data can be found in Heideman et al. (1994).

2. PROCEDURE

2.1 Differences in SERCAA and RTNEPH-assigned cloud fraction values

SERCAA and RTNEPH fractional cloud amounts are both provided on the AFGWC polar stereographic hemispheric grid, but are performed at different spatial resolutions. SERCAA cloud amount is at 24-km resolution, while RTNEPH is at 48 km resolution. For comparisons with SERCAA results, RTNEPH resolution was artificially increased to 24-km using grid-cell replication. Limited time and resources restricted the validation to the May 1993 ten-day data set for three regions of interest (ROIs) within the northern hemisphere: Japan, the Himalayas, and Central America (see Figure 1). These ROIs were selected to stress the algorithms over a range of background conditions.

To minimize the minor differences in cloud fraction diagnosed due solely to the fundamental differences between the SERCAA and RTNEPH algorithms themselves (e.g., input satellite sensor data, temporal frequency of the analysis output, integration of multi-source data, etc.), the cloud amount (Ac) data from each source were stratified into three broad categories (clear-Ac<20%, partly cloudy-20%<Ac<80%, and cloudy-Ac>80%). Comparisons between the two analysis packages could then be based on cloud category differences. Because no ground truth was required for this portion of the validation it was carried out automatically. Results of these comparisons were used to determine whether the cloud fraction diagnoses of the two algorithms were significantly different for a variety of cloud and geographic conditions.

2.2 Relative algorithm performance when cloud fraction diagnoses diverged

In order to avoid ambiguity, only those situations in which one algorithm classified a grid cell as clear, while the other classified the same cell as cloudy (i.e., a two-category difference, hereafter referred to as a 'Level-2' difference), were subsequently evaluated by a human analyst to determine which algorithm was more representative of actual cloud conditions. Analysts made this determination through manual interpretation of the component raw satellite images used as input to the analysis products. The analyst first selected a 24-km grid cell centrally located within a Level-2 difference field (see Figure 2). The corresponding locations in the SERCAA and RTNEPH analyses were then identified and analysis-specific information was automatically entered in the validation database. This information included the latitude and longitude of the selected grid point; the SERCAA and RTNEPH cloud fractions assigned to the grid point; the resulting cloud fraction difference; the date and time of the original images (different for each platform); and the satellites involved. Table 1 shows the six categories that the analyst had to consider for each Level-2 grid cell selected. The first two categories, time of day and terrain, provided background information about the Level-2 difference scene in the area of interest. The third and fourth of each algorithm. The overall assessment category was used to quantify the value added by one algorithm over the other. For each grid cell selected the analyst chose one entry in each category, with the exception of Category 5, in which one or two entries could be chosen. This process was repeated for one grid point from each contiguous Level-2 difference area. All entries chosen for each selected grid point were then entered into the validation database for subsequent statistical analysis.

3. RESULTS AND SUMMARY

Space constraints preclude presentation and discussion of SERCAA vs. RTNEPH descriptive and cloud fraction difference statistics in this article; they will be shown in detail on the poster at the conference. Summary results of the SERCAA validation study for the three May 1993 ROIs are shown in Table 2. Note that the validation effort was extensive enough to allow night and day stratification in addition to the total-sample statistics. The advantage of using more timely multispectral (especially visible and near-IR) AVHRR and geostationary data in the daytime SERCAA cloud analyses is evident from Table 2; 70 out of 79 times when SERCAA and RTNEPH significantly disagreed during daylight hours, SERCAA was the more accurate of the two. During nighttime, however, the results do not suggest that one cloud analysis was significantly different than the other. The cause of poorer relative nighttime performance of SERCAA compared to RTNEPH was a failure to sufficiently persist AVHRR-derived low cloud in nighttime analyses. This problem has since been corrected. In summary, the results suggest that both the SERCAA and RTNEPH algorithms demonstrated skill in diagnosing cloud. However, when the two algorithms differed significantly in assigning cloud fractions (i.e., Level-2 differences), SERCAA routinely provided a more accurate analysis during daylight hours. The SERCAA improvement over RTNEPH was particularly dramatic in areas favorable to convective cloud development, such as the tropics.

4. REFERENCES

- d'Entremont, R. P., G. B. Gustafson, and B. T. Pearson, 1994: Analysis of geostationary satellite imagery using a temporal differencing technique. Proceedings, CIDOS-93, 243-246.
- Gustafson, G. B., 1992: Single channel and multispectral cloud algorithm development for TACNEPH. Preprints, Sixth AMS Conference on Satellite Meteorology and Oceanography, 5-10 January, 1992, Atlanta, Georgia.
- Gustafson, G. B., D. C. Peduzzi, and J. L. Moncet, 1994: Cloud cover determination using the DMSP OLS. Preprints, Seventh AMS Conference on Satellite Meteorology and Oceanography, 6-10 June, 1994, Monterey, California.
- Isaacs, R. G., 1993: Remote sensing of cloud defense and climate studies: an overview. Proceedings, SPIE, Passive Infrared Remote Sensing of Clouds and the Atmosphere, 13-15 April, 1993, Orlando, Florida.
- Neu, T. J., R. G. Isaacs, G. B. Gustafson, and J. W. Snow, 1994: Improved cloud analysis for CDFS II through the SERCAA research and development program. Preprints, Seventh AMS Conference on Satellite Meteorology and Oceanography, 6-10 June, 1994, Monterey, California.

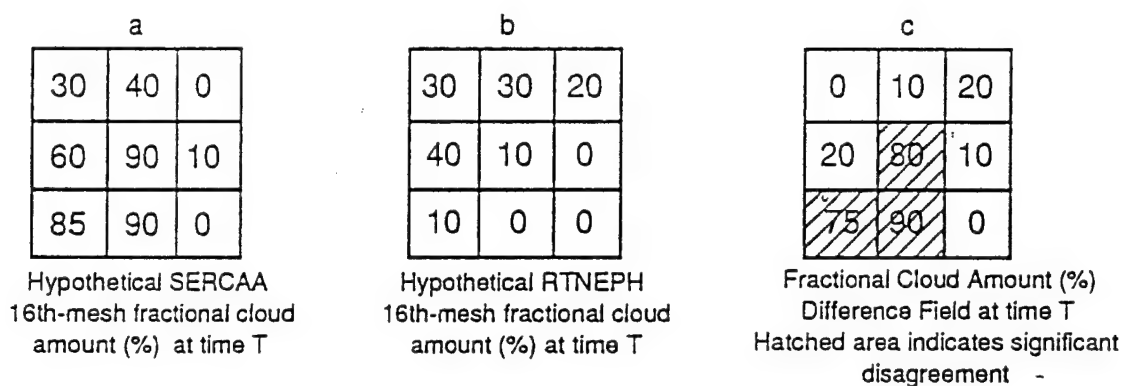


Figure 1. Cloud fraction analyses and difference fields for nine 16th mesh grid cells. (a) SERCAA analysis, (b) RTNEPH analysis, (c) difference analysis.

Table 1. Validation Database Categories. Categories 1-4 describe actual conditions around the grid point of interest; Categories 5 and 6 provide a measure of the accuracy of fractional cloud amounts analyzed by SERCAA and RTNEPH for that grid point.

CATEGORY 1 Cloud Amount a. None (0-20%) b. Partly Cloudy (21-80%) c. Cloudy (> 80%)	CATEGORY 2 Terrain a. Land b. Water c. Coastline d. Desert e. Mountains f. Ice/Snow g. Ice/Snow (Mountains)	CATEGORY 3 Cloud Type a. No Cloud b. Thin Cirrus c. Thick High Cloud d. Low Cloud e. Other
CATEGORY 4 Time of Day a. Day b. Night c. Terminator	CATEGORY 5 Algorithm Bias RTNEPH a. Over-Analysis b. Under-Analysis c. Acceptable SERCAA d. Over-Analysis e. Under-Analysis f. Acceptable	CATEGORY 6 Overall Assessment a. RTNEPH Better b. SERCAA Better

Table 2. Validation Statistics for Three ROIs from May 1993

	N _T	N _S	N _R	\bar{N}	sd	z	erf(z)	p(z)
Day	79	70	9	39.5	3.14	9.71	0.500	0.0001
Night	107	53	54	53.5	3.66	0.14	0.056	88.8
Total	186	123	63	93.0	4.82	6.22	0.500	0.0010

CLOUD CEILING CLIMATOLOGY ATLAS

Maj James R. Schaefer and Capt Bruce G. Shapiro
Air Force Combat Climatology Center
Scott AFB, Illinois 62225-5116

The *Cloud Ceiling Climatology (CCLIMO) Atlas* was developed at the Air Force Combat Climatology Center (formerly, USAF Environmental Technical Applications Center), Scott Air Force Base, Illinois, as a ready reference for mission planners developing warfighting strategies, tactics, and other operations. The color displays contained in the *CCLIMO Atlas* were developed to convey cloud ceiling information more quickly and easily than lengthy data charts and tables. This product is composed of a 2-disc CD-ROM set divided into 24 geographic regions for ease of use. It was developed using a 10-year period of record worldwide cloud analyses generated by the Real-Time Nephanalysis (RTNEPH) Model. *CCLIMO Atlas* provides, for each region, the ability to either display individually or animate through the climatological cloud ceiling displays for the following time periods/heights: Twelve months (January through December), four Zulu times (00Z, 06Z, 12Z, and 18Z), and eight heights in feet above mean sea level (500, 1500, 3000, 5000, 10000, 15000, 20000, and 75000 ["any ceiling"]). The percent frequency of occurrence of a cloud ceiling at and below a given mean sea level height is displayed using a graduated color scheme. Additionally, sunrise, sunset, beginning twilight, and ending twilight terminator lines are included in the displays where applicable.

Manuscript not available at time of printing. Please contact author for information.

APPENDIX A
Agenda

CLOUD IMPACTS ON DOD OPERATIONS AND SYSTEMS 1995 CONFERENCE (CIDOS-95)

U.S. Air Force Phillips Laboratory
Science Center, Building 1106
Hanscom Air Force Base, Massachusetts
24-26 October 1995

Theme

"CLOUD MODELING AND DATA FOR DEFENSE SIMULATION ACTIVITIES"

TUESDAY, 24 OCTOBER 1995

0800 – 0900 **REGISTRATION**

Phillips Laboratory, Science Center

SESSION I. INTRODUCTION AND PROGRAM REVIEWS

Conference Chair: **Donald D. Grantham**, Geophysics Directorate,
Phillips Laboratory, Air Force Materiel Command

0900 – 1000 **Welcome**

Dr. Hal Roth, Director, Geophysics Directorate, Phillips Laboratory

Introductory Address

Captain Bradley P. Smith, U.S. Navy, Assistant for Environmental Sciences,
Office of the Director, Defense Research and Engineering

Keynote Address – Future Direction of Modeling and Simulation in the Department of Defense

Captain James W. Hollenbach, U.S. Navy, Director, Defense Modeling and
Simulation Office

1000 – 1030 **BREAK**

1030 – 1100 **Invited Presentation – Overview of Satellite Systems and Cloud Data Product Trends**

Robert S. Winokur, DOC/NOAA/NESDIS

1100 – 1200 **Cloud Related Simulated Activities**

Overview of DOD Modeling and Simulation Executive Agency for the Air and Space

Natural Environment

LtCol(s) John M. Lanicci, Headquarters U.S. Air Force, Directorate of Modeling, Simulation,
and Analysis

Synthetic Environments in Synthetic Theater of War (STOW) 97

Jeffrey T. Turner, U.S. Army Topographic Engineering Center

Weather in Distributed Interactive Simulations (WINDS)

Vernon M. Stoltz, U.S. Army Topographic Engineering Center; Eric O. Schmidt, TASC

A Master Environmental Library (MEL) to Support Modeling and Simulation (Including Demo)
Richard A. Siquig, Naval Research Laboratory; Captain Bruce G. Shapiro, U.S. Air Force
Combat Climatology Center; Martin Miller, USAE Waterways Experiment Station

Dynamic Environmental Effects Model (DEEM)
John R. Hummel, Kathy L. Simunich and John H. Christiansen, Argonne
National Laboratory

1215 – 1330 **LUNCH BREAK**

SESSION I. INTRODUCTION AND PROGRAM REVIEWS
(continued)

1330 – 1400 The E²DIS Environmental Manager: Clouds
Harry M. Heckathorn, Naval Research Laboratory; **Stanley H. Grigsby**, ENFO, Inc.

Survey of Requirements for Effects of the Natural Environment in Military Models
and Simulations
Thomas M. Piwowar and John Burgeson, Science and Technology Corporation;
Donald D. Grantham, Geophysics Directorate, Phillips Laboratory;
Sam Brand, Naval Research Laboratory; Alan Wetmore, U.S. Army Research Laboratory

**SESSION II: CLOUD IMPACTS:
SIMULATIONS AND APPLICATIONS**
Co-Chairs: **Sam Brand**, Naval Research Laboratory
CDR Jeff Barker, Naval War College

1400 – 1500 Natural Environment Engineering Toolkit
Sandra K. Weaver, National Air Intelligence Center; William A. Lanich, U.S. Air Force
Wright Laboratory

Cloudscape™: Stochastic Cloud Visualization from Volumetric Descriptions
John G. DeVore, James H. Thompson and Ross Thornburg, Visidyne, Inc.

The Cloud Scene Simulation Model—Recent Enhancements and Additions
Maureen E. Cianciolo, Eric O. Schmidt and Mark E. Raffensberger, TASC

1500 – 1520 **BREAK**

1520 – 1700 Incorporation of Cloud Simulation Into Powerscene
Louis Hembree and Sam Brand, Naval Research Laboratory; Mark Deloura, Loral, Inc.;
Tom Hickey, Scott Randall and Chip Mayse, Cambridge Research, Inc.;
Maureen E. Cianciolo and Eric O. Schmidt, TASC

Cloud Depiction and Forecast System (CDFS) II Update
Major John D. Murphy, Major Don K. Rhudy and Major David J. Zdenek, HQ Air Weather
Service; 2Lt Jeff A. Baltes, Anna L. Lathrop and Captain Frank A. Leute IV, Air Force Global
Weather Central; Kevin J. Lunn, Michael J. Plonski and Bruce H. Thomas, The Aerospace
Corporation

SBIRS Cloud Measurements, Analysis and Model Validation
Captain Michael Pierce, SMC/MTAX; William Blumberg, Phillips Laboratory/GPOS;
Ian S. Robinson, The Aerospace Corporation

Simulated Cloudscapes with Fastview
Albert R. Boehm, Hughes STX Corporation

1800 – 2000 **ICEBREAKER**
Hanscom Air Force Base Officer's Club, Building 1425

WEDNESDAY, 25 OCTOBER 1995

**SESSION II: CLOUD IMPACTS:
SIMULATIONS AND APPLICATIONS**
(continued)

0830 – 0930 Radiative Transfer in Scenarios with Multiple Clouds
Patti Gillespie, **Alan Wetmore** and David Tofsted, U.S. Army Research Laboratory

Realistic Cloud Rendering Using an Auto-Regressive Moving Average (ARMA) Model
Robert A. Pilgrim, Murray State University; Andy Bevilacqua, Bevilacqua Research Corporation

Simulating Clouds Within a Space-Based Doppler Lidar Wind Sounder Simulation Model
G. David Emmitt and Sidney A. Wood, Simpson Weather Associates, Inc.

SESSION III: CLOUD DATABASES
Co-Chairs: **Major Lauraleen O'Connor**, NPOESS/IPO
Thomas E. Kotz, USAFETAC/OL-A

0930 – 1030 Application of Hypermedia and CD-ROM Technology to the Distribution of Navy Environmental Information for Satellite Image Analysis and Forecasting
Marie E. White, Pangaea; Robert Fett, Science Applications International Corporation;
Sam Brand, Naval Research Laboratory

Cloud Data Sets Derived from Combined Geostationary and Polar-Orbiting Environmental Satellite Sensors Using the SERCAA Cloud Model
Gary B. Gustafson, Robert P. d'Entremont and Daniel C. Peduzzi, Atmospheric and Environmental Research, Inc.

Climatological and Historical Analysis of Clouds for Environmental Simulations (CHANCES)—First Year of Products
Donald L. Reinke, **Thomas H. Vonder Haar**, Kenneth E. Eis, Jan L. Behunek,
Charles R. Chaapel, Cynthia L. Combs, John M. Forsythe and Mark A. Ringerud,
STC-METSAT

1030 – 1100 **BREAK**

- 1100 – 1200 Global Statistics on Cloud Optical Depths from Satellite and Lidar Observations
Donald P. Wylie, University of Wisconsin-Madison

Enhanced Satellite Cloud Analysis by the Development of a Higher Resolution (6-km) Global Geography Data Set

ILT R. Radburn Robb and Crystal L. B. Schaaf, Geophysics Directorate, Phillips Laboratory;
Daniel C. Peduzzi, Atmospheric and Environmental Research, Inc.;
Joan M. Ward, System Resources Corporation

Poster presenters will give two minute oral presentations

- 1200 – 1330 **LUNCH BREAK**

SESSION IV: MEASUREMENT SYSTEMS AND SENSORS

Co-Chairs: **Richard Shirkey**, U.S. Army Research Laboratory
George G. Koenig, U.S. Army Cold Regions
Research Engineering Laboratory

- 1330 – 1540 Detection and Retrieval of Cirrus Cloud Systems Using AVHRR Data: Verification Based on FIRE-II-IFO Composite Measurements

Kuo-Nan Liou, Szu-Cheng Ou, N. X. Rao and Y. Takano, University of Utah

Analysis of Test Results from a Mobile Profiling System

James Cogan and Edward Measure, U.S. Army Research Laboratory

Multi Spectral Pushbroom Imaging Radiometer (MPIR) for Remote Sensing Cloud Studies

Gary S. Phipps and Carter L. Grotbeck, Sandia National Laboratories

A Brief Description of Airborne InfraRed Measurement System (AIRMS)

William S. Helliwell, John R. Norris and Betty Rodriguez-Cottle, Science Applications International Corporation

Cloud Phenomenology Measured from Airborne InfraRed Measurement System (AIRMS) Data

William S. Helliwell, John R. Norris and **Betty Rodriguez-Cottle**, Science Applications International Corporation

Cloud Radiative and Spatial Properties Using a Ground-Based Infrared All-Sky Imager

Robert P. d'Entremont, Ronald G. Isaacs, Jean-Luc Moncet and **David B. Hogan**, Atmospheric and Environmental Research, Inc.

Upper Tropospheric Humidity Derived from SSM/T-2 Measurements

Michael K. Griffin, Geophysics Directorate, Phillips Laboratory; John D. Pickle, Atmospheric and Environmental Research, Inc.

- 1540 – 1600 **BREAK**

SESSION V: CLOUD AND CLOUD RELATED MODELS

Co-Chairs: **Major James T. Kroll**, AFOSR/NM

Kuo-Nan Liou, University of Utah

1600 – 1720 A Short-Term Cloud Forecast Scheme Using Cross Correlation: An Update
Kenneth F. Heideman and **ILT R. Radburn Robb**, Geophysics Directorate, Phillips Laboratory,

Cloud Detection Using Visible and Near-Infrared Bidirectional Reflectance Distribution Models
Robert P. d'Entremont, Atmospheric and Environmental Research, Inc.; **Crystal L. B. Schaaf**, Phillips Laboratory/GPAB; **Alan H. Strahler**, Boston University

SERCAA Phase II: Cloud Radiative, Microphysical, and Environmental Properties
Ronald G. Isaacs, **Gary B. Gustafson**, **Robert P. d'Entremont** and **David B. Hogan**, Atmospheric and Environmental Research, Inc.; **Major Michael Remeika** and **James T. Bunting**, Phillips Laboratory/GPAB

The Lattice Boltzmann Method: A New Approach to Radiative Transfer Through Clouds
Joel B. Mozer and **Thomas R. Caudill**, Geophysics Directorate, Phillips Laboratory

THURSDAY, 26 OCTOBER 1995

SESSION V: CLOUD AND CLOUD RELATED MODELS

(continued)

0830 – 1010 Cloud Forecasting Initiatives at Air Force Global Weather Central
Raymond B. Kiess and **Thomas J. Kopp**, Headquarters Air Force Global Weather Central

Short-Term Cloud Fluctuation Statistics for Central America Using GOES-8 Imagery
John G. DeVore, Visidyne, Inc.

Identification of Thunderstorms in an Operational Global Nephanalysis Using a Convective-Stratiform Technique
Thomas J. Kopp, **Peter J. Broll** and **Stephen G. Zahn**, Headquarters Air Force Global Weather Central

Layered Cloud Parameters: An Approach to Forecasting and Verification
Jeanne M. Sparrow, **Thomas Nehr Korn**, **Ross N. Hoffman** and **Christopher Grassotti**, Atmospheric and Environmental Research, Inc.

Cloud Forecasting Using Cross-Correlation Extrapolation Techniques: An Enhanced Approach Using NWP Model Information
Christopher Grassotti, **Ross N. Hoffman**, **Ronald G. Isaacs**, **Thomas Nehr Korn** and **Jeanne M. Sparrow**, Atmospheric and Environmental Research, Inc.

1010 – 1030 **BREAK**

<p>SESSION VI: CIRRUS AND CONTRAIL CLOUDS Co-Chairs: Arnold A. Barnes, Jr., Phillips Laboratory/GPA Eric O. Schmidt, TASC</p>
--

1030 – 1210 Four Decades of Cirrus and Contrail Observations
Arnold A. Barnes, Jr., Phillips Laboratory/GPA

Retrieval of Cirrus Radiative and Spatial Properties Using Coincident Multispectral Imager and Sounder Satellite Data

Robert P. d'Entremont, Atmospheric and Environmental Research, Inc.; Donald P. Wylie, University of Wisconsin; Szu-Cheng Ou and Kuo-Nan Liou, University of Utah

An Ice Crystal Growth Model for Cirrus Cloud Formation

Szu-Cheng Ou, Kuo-Nan Liou and D. Frankel, University of Utah

Thin Cirrus Effects on Hyperspectral Detection of Trace Gases

P. Daniel Hestand and Kenneth B. MacNichol, TASC

Subvisual Cirrus Clouds Associated with Processes in the Natural Atmosphere

Eric O. Schmidt, D. Lynch, K. Sassen, G. Grams and J. Alvarez, TASC

1210 – 1330 **LUNCH BREAK**

1330 – 1500 Validation of the Appleman Contrail Forecasting Scheme Using Engine-Specific Aircraft Data
Captain David J. Speltz, U.S. Air Force Environmental Technical Applications Center

Predicting the Radiative Properties of Nonspherical Particles: Application to Cirrus Clouds

David L. Mitchell, Desert Research Institute; Andreas Macke, NASA-Goddard Institute for Space Studies

Statistics on the Optical Properties of Cirrus Clouds Measured with the High Spectral Resolution Lidar

Edwin W. Eloranta and Paivi Piironen, University of Wisconsin-Madison

An Operational Method of Ice Containing Clouds Based on Laboratory and Observational Data Leading to a Numerical Model for Prediction of Radiative Properties

Darko Koracin and **John Hallett**, Desert Research Institute

1500 – 1600 **Wrap-Up Discussion/Opportunities for Cloud Research Funding**

1600 **CIDOS-95 ADJOURNS**

POSTER PRESENTATIONS

**POSTERS MAY REMAIN ON DISPLAY IN THE
SCIENCE CENTER
UNTIL ADJOURNMENT ON THURSDAY**

A Summary of Vertical Cloud Layer Statistics as Derived from Echo Intensities Received by a 35 Ghz Radar
James H. Willand, Hughes STX Corporation

SWIR Cloud Modeling and Data Analysis for the SBIRS Program

Joseph G. Shanks and Frederick C. Mertz, Photon Research Associates, Inc.;
Ian S. Robinson, The Aerospace Corporation; William Blumberg, Phillips Laboratory/GPOS;
Edwin W. Eloranta, University of Wisconsin-Madison; James Lisowski, Scitec Corporation

Global Cloud Cover at Altitude: System Impacts

Ian S. Robinson and Susan L. Kafesjian, The Aerospace Corporation

The Cloud Scene Simulation Model-Parameter Estimation and Preliminary Validation of the Cumulus Model

Mark E. Raffensberger, Maureen E. Cianciolo and Eric O. Schmidt, TASC

Production of Long-Term Global Multi-Layer Water Vapor and Liquid Water Data Sets from Multi-Satellite and Radiosonde Observations

Thomas H. Vonder Haar, Mark A. Ringerud, David L. Randel, Graeme L. Stephens, Cynthia L. Combs,
Donald L. Reinke and Thomas J. Greenwald, STC-METSAT

Development of a Cloud Cover Forecast Model

Roger D. Dickey, GENCORP/Aerojet; William T. Kreiss, Georgia Tech Research Institute

A Novel Infrared Imaging Spectroradiometer for Passive Remote Detection of Clouds

David M. Sonnenfroh, B. David Green, William J. Marinelli and W. Terry Rawlins, Physical Sciences, Inc.

Examples of CFLOSA (Cloud-Free Line-of-Sight Aloft) Output

Albert R. Boehm, James H. Willand and Marc A. Pereira, Hughes STX Corporation

Line of Sight Cloud Observations from Haleakala

Russell H. Taft, Rockwell Power Systems

Support of Environmental Requirements for Cloud Analysis and Archive (SERCAA) Integrated Cloud Analysis Validation

Kenneth F. Heideman, Phillips Laboratory/GPAB; **Robert P. d'Entremont**, Jeanne M. Sparrow,
Tony S. Lisa and Gary B. Gustafson, Atmospheric and Environmental Research, Inc.

Cloud Ceiling Climatology Atlas

Major James R. Schaefer and Captain Bruce G. Shapiro, Air Force Combat Climatology Center

On the Water

Jerry Tessendorf, Arete Associates

APPENDIX B
List of Registered Attendees

CIDOS-95 LIST OF REGISTERED ATTENDEES

B

Mr. Michael J. Baker
U.S. Space Command - J33W
250 S. Peterson Boulevard
Peterson AFB, CO 80914-3230
Tel: 719/554-6985
Fax: 719/554-6986

CDR Jeffrey Barker
Naval War College
686 Cushing Road
Newport, RI 02841
Tel: 401/841-6467
Fax: 401/841-3804

Dr. Arnold A. Barnes, Jr.
Phillips Laboratory/GPA
29 Randolph Road
Hanscom AFB, MA 01731-3010
Tel: 617/377-2939
Fax: 617/377-8892

Mr. Andy Bevilacqua
Bevilacqua Research Corporation
7501 South Memorial Parkway, Suite 204
Huntsville, AL 35802
Tel: 205/882-6229
Fax: 205/882-6239

CAPT Christopher Bjorkman
HQ Air Weather Service/XOS
102 West Losey Street, Rm 105
Scott AFB, IL 62225-5206
Tel: 618/256-5849
Fax: 618/256-6306

Mr. Albert R. Boehm
Hughes STX
PL/GPAA (HSTX)
29 Randolph Road
Hanscom AFB, MA 01731-3010
Tel: 617/377-2971
Fax: 617/377-2984

Mr. Sam Brand
Naval Research Laboratory
7 Grace Hopper Avenue
Monterey, CA 93943-5502
Tel: 408/647-4748
Fax: 408/656-4769

Mr. John Burgeson
Science and Technology Corp
23 Decatur Drive
Nashua, NH 03062
Tel: 603/891-4813
Fax: 603/891-4813

C

Dr. Thomas Caudill
PL/GPAB
29 Randolph Road
Hanscom AFB, MA 01731
Tel: 617/377-2943
Fax: 617/377-8892

Dr. Kenneth S.W. Champion
Phillips Laboratory/Geophysics Directorate
Atmospheric Sciences Division
29 Randolph Road
Hanscom AFB, MA 01731-3010
Tel: 617/377-3033
Fax: 617/377-8892

Ms. Maureen E. Cianciolo
TASC
2404 Cuenca Drive
San Ramon, CA 94583
Tel: 510/866-9123
Fax: 510/831-0880

Dr. James L. Cogan
US Army Research Laboratory
Battlefield Environment Directorate
AMSRL-BE-W
WSMR, NM 88002-5501
Tel: 505/678-2094
Fax: 505/678-3385

CIDOS-95 LIST OF REGISTERED ATTENDEES

D

Mr. Robert P. d'Entremont
Remote Sensing Group
Atmospheric & Environmental Research, Inc.
840 Memorial Drive
Cambridge, MA 02139-3794
Tel: 617/547-6207
Fax: 617/661-6489

Dr. Gilbert Davidson
PhotoMetrics, Inc.
4 Arrow Drive
Woburn, MA 01801
Tel: 617/935-6500
Fax: 617/935-0747

Mr. Richard E. Davis
Aerospace Electronic Systems Division
NASA Langley Research Center
MS 474
Hampton, VA 23681-0001
Tel: 804/864-1647
Fax: 804/864-8809

Dr. John DeVore
Visidyne, Inc.
5951 Encina Road, Suite 208
Goleta, CA 93117-2211
Tel: 805/683-4277
Fax: 805/683-5377

Mr. Roger D. Dickey
GenCorp/Aerojet
1100 W. Third Street
Azusa, CA 91702
Tel: 818/812-2671
Fax: 818/969-7750

E

Dr. Edwin W. Eloranta
Department of Atmospheric Sciences
University of Wisconsin
1225 W. Dayton Street
Madison, WI 53706
Tel: 608/262-7327
Fax: 608/262-5974

Dr. George D. Emmitt
Simpson Weather Associates, Inc.
809 E. Jefferson Street
Charlottesville, VA 22902
Tel: 804/979-3571
Fax: 804/979-5599

F

CAPT Fred Fahlbusch
NAIC/TATW
4180 Watson Way, Suite 31
WP AFB, OH 45433-5648
Tel: 513/257-7071
Fax: 513/257-9888

Mr. Randolph A. Fix
Pacific-Sierra Research Corp
1400 Key Boulevard, Suite 700
Arlington, VA 22209
Tel: 703/526-6323
Fax: 703/524-2420

G

Mr. Donald D. Grantham
AF Phillips Laboratory
PL/GPAA
29 Randolph Road
Hanscom AFB, MA 01731-3010
Tel: 617/377-2982
Fax: 617/377-2984

Mr. Christopher Grassotti
Atmospheric & Environmental Research, Inc.
840 Memorial Drive
Cambridge, MA 02139
Tel: 617/547-6207
Fax: 617/661-6479

Dr. Michael K. Griffin
Phillips Laboratory, Geophysics Directorate
Atmospheric Sciences Division
29 Randolph Road
Hanscom AFB, MA 01731-3010
Tel: 617/377-2961
Fax: 617/377-8892

CIDOS-95 LIST OF REGISTERED ATTENDEES

Mr. Stanley H. Grigsby
ENFRO, Inc.
1800 Diagonal Road, Suite 600
Alexandria, VA 22314
Tel: 703/802-8300
Fax: 703/802-0412

Dr. Carter Grotbeck
Sandia National Laboratories
P.O. Box 5800
MS 0980
Albuquerque, NM 87185-0980
Tel: 505/844-5312
Fax: 505/844-2057

Mr. Gary B. Gustafson
Atmospheric & Environmental Research, Inc.
840 Memorial Drive
Cambridge, MA 02139
Tel: 617/547-6207
Fax: 617/377-9638

H

Major Dewey E. Harms
HQ Air Weather Service/XOX
102 West Losey Street, Rm 105
Scott AFB, IL 62225-5206
Tel: 618/256-5631, x 423
Fax: 618/256-6306

Dr. Harry M. Heckathorn
Naval Research Laboratory
Code 7604
4555 Overlook Avenue SW
Washington, DC 20375-5352
Tel: 202/767-4198
Fax: 202/404-8445

Mr. Kenneth F. Heideman
Phillips Laboratory/GPAB
29 Randolph Road
Hanscom AFB, MA 01731-3010
Tel: 617/377-2955
Fax: 617/377-8892

Dr. Ken Heikes
Pacific-Sierra Research Corporation
2901 28th Street
Santa Monica, CA 90405
Tel: 310/314-2361
Fax: 310/314-2323

Dr. William S. Helliwell
Science Applications International Corp
10260 Campus Point Drive
San Diego, CA 92121
Tel: 619/546-6672
Fax: 619/546-6587

Mr. Louis Hembree
Naval Research Laboratory
7 Grace Hopper Avenue
Monterey, CA 93943-5502
Tel: 408/656-4787
Fax: 408/656-4769

Mr. P. Daniel Hestand
TASC
55 Walkers Brook Drive
Reading, MA 01867
Tel: 617/942-2000
Fax: 617/942-7100

Dr. R. F. Hickey
ITT Defense & Electronics
1919 West Cook Road
P.O. Box 3700
Fort Wayne, IN 46801
Tel: 219/487-6541
Fax: 219/487-6118

Mr. David B. Hogan
Remote Sensing Group
Atmospheric & Environmental Research, Inc.
840 Memorial Drive
Cambridge, MA 02139-3794
Tel: 617/547-6207
Fax: 609/737-2991

CIDOS-95 LIST OF REGISTERED ATTENDEES

CAPT James W. Hollenbach
Director, Defense Modeling & Simulation Office
1901 N. Beauregard Street, Suite 504
Alexandria, VA 22311
Tel: 703/998-0660
Fax: 703/998-0667

Dr. John R. Hummel
Argonne National Laboratory
9700 South Cass Avenue
Argonne, IL 60439
Tel: 708/252-7189
Fax: 708/252-5128

I

Mr. Robert E. Introne
TASC
55 Walker Brook Drive
Reading, MA 01867
Tel: 617/942-2000
Fax: 617/942-7100

Mr. Ronald G. Isaacs
Atmospheric & Environmental Research, Inc.
840 Memorial Drive
Cambridge, MA 02139-3794
Tel: 617/547-6207
Fax: 617/661-6479

J

Mr. Jimmy A. Jensen
Hughes Information Technology Corp
1620 Wilshire Drive, Suite 216
Bellevue, NE 68005
Tel: 402/294-2153
Fax: 402/294-8261

K

Mr. Raymond B. Kiess
HQ AFGWC/SYSM
106 Peacekeeper Drive, Suite 2N3
Offutt AFB, NE 68113-4039
Tel: 402/294-3373
Fax: 402/294-3505

Dr. George G. Koenig
USACRREL
72 Lyme Road
Hanover, NH 03755-1290
Tel: 603/646-4130
Fax: 603/646-4693

CAPT David J. Kohn
HQ Air Weather Service/XOXT
102 West Losey Street, Rm 105
Scott AFB, IL 62225-5206
Tel: 618/256-5631, x 422
Fax: 618/256-6306

Dr. Thomas J. Kopp
HQ, AFGWC/SYSM
106 Peacekeeper Drive, Suite 2N3
Offutt AFB, NE 68113-4039
Tel: 402/294-3533
Fax: 402/294-3505

Dr. Darko Koracin
Desert Research Institute
5625 Fox Avenue
Reno, NV 89506-0220
Tel: 702/677-3328
Fax: 702/677-3157

Dr. Thomas E. Kotz
OL-A, AFCCC
151 Patton Avenue, Room 120
Asheville, NC 28801
Tel: 704/271-4234
Fax: 704/221-4334

Major James T. Kroll
AFOSR/NM
110 Duncan Avenue, Suite B 115
Bolling AFB, DC 20332-0001
Tel: 202/767-7900
Fax: 202/404-7475

CIDOS-95 LIST OF REGISTERED ATTENDEES

L

LtCol(s) John M. Lanicci
 HQ USAF/XOMT
 1510 Air Force Pentagon
 Washington, DC 20030-1510
 Tel: 202/761-5341, x 139
 Fax: 202/761-5352

Mrs. Anna L. Lathrop
 AFGWC/SYPA
 106 Peacekeeper Drive, Suite 2N3
 Offutt AFB, NE 68113-4039
 Tel: 402/294-4233
 Fax: 402/294-3789

CAPT David Lawyer
 Aerospace Data Facility/WE
 18201 E Devils Thumb Avenue
 Buckley ANGB
 Aurora, CO 80011-9536
 Tel: 303/341-3579
 Fax: 303/341-3961

Mr. Kirk E. Lehneis
 WL/DOWA
 2690 C Street, STE 2
 WP AFB, OH 45433-7409
 Tel: 513/255-1978
 Fax: 513/255-7552

Dr. Bernard R. Lichtenstein
 GenCorp Aerojet
 Bldg 1, Dept. 8321
 PO Box 296
 Azusa, CA 91702
 Tel: 818/812-2347
 Fax: 818/812-1486

Prof. Kuo-Nan Liou
 Department of Meteorology/CARSS
 University of Utah
 Salt Lake City, UT 84112
 Tel: 801/581-3336
 Fax: 801/581-4065

Mr. James Lisowski
 SciTec, Inc.
 100 Wall Street
 Princeton, NJ 08540-1523
 Tel: 609/921-3892
 Fax: 609/921-1926

Mr. Kevin J. Lunn
 The Aerospace Corporation
 P.O. Box 819
 Bellevue, NE 68005
 Tel: 402/291-3140
 Fax: 402/291-3137

M

Mr. Kenneth B. MacNichol
 TASC
 55 Walkers Brook Drive
 Reading, MA 01833
 Tel: 617/942-2000, x 2278
 Fax: 617/942-7100

Mr. Peter Mantica
 ITT Aerospace/Communications Division
 1919 West Cook Road
 P.O. Box 3700
 Fort Wayne, IN 46801
 Tel: 219/487-6880
 Fax: 219/487-6033

Mr. John D. McGlynn
 Science Applications International Corp
 10260 Campus Point Drive
 MS C4
 San Diego, CA 92121
 Tel: 619/546-6853
 Fax: 619/546-6587

Captain Kris F. McKinney
 AFCC/SYT
 859 Buchanan Street
 Scott AFB, IL 62221-5116
 Tel: 618/256-4107
 Fax: 618/256-3772

CIDOS-95 LIST OF REGISTERED ATTENDEES

CAPT Stephen R. McMillan
46 OSS/OSW
601 W. Choctawhatchee Avenue, Ste 60
Eglin AFB, FL 32542
Tel: 904/882-5960
Fax: 904/882-3341

Dr. James Metcalf
Phillips Laboratory/GPAA
29 Randolph Road
Hanscom AFB, MA 01731-3010
Tel: 617/377-2972
Fax: 617/377-2984

Dr. David L. Mitchell
Desert Research Institute
5625 Fox Avenue
Reno, NV 89506-0220
Tel: 702/677-3151
Fax: 702/677-3157

Dr. Joel B. Mozer
Phillips Laboratory (AFMC)
PL/GPAA
29 Randolph Road
Hanscom AFB, MA 01731-3010
Tel: 617/377-2945
Fax: 617/377-2984

Major John Murphy
HQ AWS/SYA
102 W. Losey Street, Room 105
Scott AFB, IL 62225-5206
Tel: 618/256-4741, x 256
Fax: 618/256-6086

N

Mr. Thomas R. Newbauer
SMC/SDE LAAFB
160 Skynet Street
Los Angeles, CA 90245-4683
Tel: 310/363-5176
Fax: 310/363-2532

O

Major Laureleen O'Connor
Integrated Program Office/NPOESS
Centre Building, Suite 1450
8455 Colesville Road
Silver Springs, MD 20910
Tel: 301/427-2070
Fax: 301/427-2164

Dr. Szu-Cheng Ou
Department of Meteorology/CARSS
University of Utah
Salt Lake City, UT 84112
Tel: 801/581-3336
Fax: 801/581-4065

P

Mr. Marc Pereira
Hughes STX
PL/GPAA (HSTX)
29 Randolph Road
Hanscom AFB, MA 01731-3010
Tel: 617/377-2971
Fax: 617/377-2984

Mr. Gary S. Phipps
Sandia National Laboratories
P.O. Box 5800
MS0980/Dept 9225
Albuquerque, NM 87185-0980
Tel: 505/845-8269
Fax: 505/844-1362

Dr. Thomas M. Piwowar
Science and Technology Corporation
409 Third Street SW, Suite 203
Washington, DC 20024
Tel: 202/863-0012
Fax: 202/488-5364

Mr. Edward M. Powers
KTAADN, Inc.
1320 Centre Street, Suite 201
Newton, MA 02159-2453
Tel: 617/527-0054
Fax: 617/527-9321

CIDOS-95 LIST OF REGISTERED ATTENDEES

R

Dr. Lawrence F. Radke
NCAR/RAF
10800 W. 102th Avenue
Broomfield, CO 80021
Tel: 303/497-1032
Fax: 303/497-1092

Mr. Mark E. Raffensberger
TASC
55 Walkers Brook Drive
Reading, MA 01867
Tel: 617/942-2000, x 2438
Fax: 617/942-7100

Dr. W. Terry Rawlins
Physical Sciences, Inc.
20 New England Business Center
Andover, MA 01810
Tel: 508/689-0003
Fax: 508/689-3232

Mr. Donald L. Reinke
STC-METSAT
515 South Howes Street
Fort Collins, CO 80521
Tel: 303/221-5420
Fax: 303/493-3410

MAJ Don Rhudy
SAF/ST
1670 Air Force Pentagon
Washington, DC 20330-1670
Tel: 703/267-4651
Fax: 703/359-8234

Lt Col John R. Roadcap
Phillips Laboratory (WE)
3550 Aberdeen Avenue, S.E.
Kirtland AFB, NM 87117-5776
Tel: 505/846-4722
Fax: 505/846-4394

ILT R. Radburn Robb
Atmospheric Sciences Division
Geophysics Directorate
Air Force Phillips Laboratory
29 Randolph Road
Hanscom AFB, MA 01731-3010
Tel: 617/377-2973
Fax: 617/377-8892

Mr. Ian S. Robinson
The Aerospace Corporation
M4/041
PO Box 92957
Los Angeles, CA 90009-2957
Tel: 310/336-6142
Fax: 310/336-6316

Ms. Betty Rodriguez-Cottle
Science Applications International Corp
10260 Campus Point Drive
San Diego, CA 92121
Tel: 619/546-6355
Fax: 619/546-6587

S

Prof. Kenneth Sassen
Department of Meteorology
University of Utah
Salt Lake City, UT 84112
Tel: 801/581-6136
Fax: 801/585-3681

Major James R. Schaefer
AFCCC/SYT
859 Buchanan Street, Rm 309
Scott AFB, IL 62221-5116
Tel: 618/256-3902
Fax: 618/256-3772

Dr. Eric O. Schmidt
TASC
55 Walkers Brook Drive
Reading, MA 01867
Tel: 617/942-2000, x 3406
Fax: 617/942-7100

CIDOS-95 LIST OF REGISTERED ATTENDEES

Dr. Joseph G. Shanks
Photon Research Associates, Inc.
10350 N. Torrey Pines Road, Suite 300
La Jolla, CA 92037
Tel: 619/455-9741
Fax: 619/455-0658

Capt Bruce G. Shapiro
AFCCC/SYT
859 Buchanan Street
Scott AFB, IL 62221-5116
Tel: 618/256-5412
Fax: 618/256-3772

Dr. Richard Shirkey
US Army Research Laboratory
Battlefield Environment Directorate
AMSRL-BE-S
WSMR, NM 88002-5501
Tel: 505/678-5470
Fax: 505/678-4449

Dr. Richard A. Siquig
Naval Research Laboratory
7 Grace Hopper Avenue
MS 2
Monterey, CA 93943-5502
Tel: 408/647-4732
Fax: 408/656-4769

CAPT Bradley P. Smith
OSD/DDR&E/E&LS
3080 Defense Pentagon
Washington, DC 20301-3080
Tel: 703/695-9604
Fax: 703/693-7042

Capt Thomas J. Smith
DNA/SPWE
6801 Telegraph Road
Alexandria, VA 22310
Tel: 703/325-5421
Fax: 703/325-0398

Dr. David M. Sonnenfroh
Physical Sciences, Inc.
20 New England Business Center
Andover, MA 01810
Tel: 508/689-0003
Fax: 508/689-3232

Ms. Jeanne M. Sparrow
Atmospheric & Environmental Research, Inc.
840 Memorial Drive
Cambridge, MA 02139
Tel: 617/547-6207
Fax: 617/661-6479

Capt David J. Speltz
ESC/WE
11 Eglin Street
Hanscom AFB, MA 01731-2122
Tel: 617/377-5285
Fax: 617/377-9993

Dr. Timothy L. Stephens
Visidyne, Inc.
3322 South Memorial Parkway, Suite 223
Huntsville, AL 35801-5368
Tel: 205/880-3411
Fax: 205/880-3284

Mr. Vernon Stoltz
U.S. Army Topographic Engineering Center
7701 Telegraph Road
Alexandria, VA 22315
Tel: 703/755-2651
Fax: 703/355-3176

T

Mr. Russell H. Taft
Rockwell Power Systems
535 Lipoa Parkway, Suite 200
Kihei, Maui, HI 96784
Tel: 808/874-1557
Fax: 808/874-1600

CIDOS-95 LIST OF REGISTERED ATTENDEES

Dr. James W. Telford
Desert Research Institute
5625 Fox Avenue
P.O. Box 60220
Reno, NV 89506
Tel: 702/677-3201
Fax: 702/677-3157

Dr. Jerry Tessendorf
Arete Associates
PO Box 6024
Sherman Oaks, CA 91413
Tel: 818/501-2880
Fax: 818/501-2905

Dr. Ross J. Thornburg
Visidyne, Inc.
3322 South Memorial Parkway, Suite 223
Huntsville, AL 35801-5368
Tel: 205/880-3411
Fax: 205/880-3284

Dr. Paul D. Try
Science and Technology Corp
409 Third Street SW, Suite 203
Washington, DC 20024
Tel: 202/863-0012
Fax: 202/488-5364

Dr. Jeffrey T. Turner
U.S. Army Topographic Engineering Center
7701 Telegraph Road
Alexandria, VA 22315
Tel: 703/355-6651
Fax: 703/355-3176

Mr. Robert E. Turner
Science Applications International Corp
550 Camino El Estero, Suite 205
Monterey, CA 93940
Tel: 408/649-5242
Fax: 408/649-8048

Dr. Paul Twitchell
Science and Technology Corp
409 Third Street SW, Suite 203
Washington, DC 20024
Tel: 202/863-0012
Fax: 202/488-5364

V

Dr. Thomas H. Vonder Haar
Colorado State University
CIRA, Foothills Campus
Fort Collins, CO 80523
Tel: 970/491-8566
Fax: 970/491-8241

W

Mrs. Sandra K. Weaver
National Air Intelligence Center/TATW
4180 Watson Way, Suite 31
WP AFB, OH 45433-5648
Tel: 513/257-7071
Fax: 513/257-9888

Dr. Alan E. Wetmore
US Army Research Laboratory
Battlefield Environment Directorate
AMSRL-BE-S
WSMR, NM 88002-5501
Tel: 505/678-5563
Fax: 505/678-2432

Dr. Marie E. White
Pangaea
3032 Sherman Road
Pebble Beach, CA 93953
Tel: 408/656-0130
Fax: 408/656-0130

Mr. James H. Willand
Hughes STX
PL/GPAA (HSTX)
29 Randolph Road
Hanscom AFB, MA 01731-3010
Tel: 617/377-5951
Fax: 617/377-2984

Mr. Robert S. Winokur
DOC/NOAA/NESDIS
PB#4, Room 2069
Washington, DC 20233

CIDOS-95 LIST OF REGISTERED ATTENDEES

Dr. Donald P. Wylie
Space Science & Engineering Center
University of Wisconsin
1225 W. Dayton Street
Madison, WI 53706
Tel: 608/263-7458
Fax: 608/262-5974

Z

Dr. Bernard Zak
Sandia National Laboratories
MS 0755
Albuquerque, NM 87185
Tel: 505/845-8631
Fax: 505/844-0116

Lt Col Frank A. Zawada
Department of the Air Force
PL/GP-M
29 Randolph Road
Hanscom AFB, MA 01731
Tel: 617/377-8004
Fax: 617/377-5688

APPENDIX C
Author Index

CIDOS-95 AUTHOR INDEX

A

Alvarez, J. - 165

B

Baltes, 2Lt Jeff A. - 53
 Barnes, Jr., Arnold A. - 151
 Behunek, Jan L. - 81
 Bevilacqua, Andy - 65
 Blumberg, William - 57, 191
 Boehm, Albert R. - 59, 211
 Brand, Sam - 31, 49, 75
 Broll, Peter J. - 145
 Bunting, James T. - 131
 Burgeson, John - 31

C

Caudill, Thomas R. - 135
 Chaapel, Charles R. - 81
 Christiansen, John H. - 23
 Cianciolo, Maureen E. - 45, 49, 197
 Cogan, James - 101
 Combs, Cynthia L. - 81, 201

D

d'Entremont, Robert P. - 79, 117, 129, 131, 155, 219
 Deloura, Mark - 49
 DeVore, John G. - 41, 141
 Dickey, Roger D. - 205

E

Eis, Kenneth E. - 81
 Eloranta, Edwin W. - 177, 191
 Emmitt, G. David - 69

F

Fett, Robert - 75
 Forsythe, John M. - 81
 Frankel, D. - 157

G

Gillespie, Patti - 63
 Grams, G. - 165
 Grantham, Donald D. - xiii, 31
 Green, B. David - 207
 Greenwald, Thomas J. - 201
 Griffin, Michael K. - 119
 Grigsby, Stanley H. - 27
 Grotbeck, Carter L. - 105
 Gustafson, Gary B. - 79, 131, 219

H

Hallett, John - 181
 Heckathorn, Harry - 27
 Heideman, Kenneth F. - 125, 219
 Helliwell, William S. - 109, 113
 Hembree, Louis - 49
 Hestand, P. Daniel - 161
 Hickey, Tom - 49
 Hogan, David B. - 117, 131
 Hollenbach, Captain James W. - xvii, 5
 Hummel, John R. - 23

I

Isaacs, Ronald G. - 117, 131

K

Kafesjian, Susan L. - 195
 Kiess, Raymond B. - 205
 Kopp, Thomas J. - 139, 145
 Koracin, Darko - 181
 Kreiss, William T. - 139

L

Lanicci, John M. - 9
 Lanich, William A. - 35
 Lathrop, Anna L. - 53
 Leute IV, Captain Frank A. - 53
 Liou, Kuo-Nan - 95, 155, 157
 Lisa, Tony S. - 219
 Lisowski, James - 191
 Lunn, Kevin J. - 53
 Lynch, D. - 165

CIDOS-95 AUTHOR INDEX

M

Macke, Andreas – 173
 MacNichol, Kenneth B. – 161
 Marinelli, William J. – 207
 Mayse, Chip – 49
 Measure, Edward – 101
 Mertz, Fred – 191
 Miller, Martin – 21
 Mitchell, David L. – 173
 Moncet, Jean-Luc – 117
 Mozer, Joel B. – 135
 Murphy, Major John D. – 53

N

Norris, John R. – 109, 113

O

Ou, Szu-Cheng – 95, 155, 157

P

Peduzzi, Daniel C. – 79, 87
 Pereira, Marc A. – 211
 Phipps, Gary S. – 105
 Pickle, John D. – 119
 Pierce, Captain Michael – 57
 Piironen, Paivi – 177
 Pilgrim, Robert A. – 65
 Piwowar, Thomas M. – 31
 Plonski, Michael J. – 53

R

Raffensberger, Mark E. – 45, 197
 Randall, David L. – 201
 Randall, Scott – 49
 Rao, N. X. – 95
 Rawlins, W. Terry – 207
 Reinke, Donald L. – 81, 201
 Remeika, Major Michael – 131
 Rhudy, Major Don K. – 53
 Ringerud, Mark A. – 81, 201
 Robb, ILT R. Radburn – 87, 125
 Robinson, Ian S. – 57, 191, 195
 Rodriguez-Cottle, Betty – 109, 113

S

Sassen, K. – 165
 Schaaf, Crystal L. B. – 87, 129
 Schaefer, Major James R. – 223
 Schmidt, Eric O. – 17, 45, 49, 165, 197
 Shanks, Joseph G. – 191
 Shapiro, Captain Bruce G. – 21, 223
 Simunich, Kathy L. – 23
 Siquig, Richard A. – 21
 Smith, Captain Bradley P. – xv, 3
 Sonnenfroh, David M. – 207
 Sparrow, Jeanne M. – 219
 Speltz, Captain David J. – 169
 Stephens, Graeme L. – 201
 Stoltz, Vernon M. – 17
 Strahler, Alan H. – 129

T

Taft, Russell H. – 215
 Takano, Y. – 95
 Thomas, Bruce H. – 53
 Thompson, James H. – 41
 Thornsburg, Ross – 41
 Tofsted, David – 63
 Turner, Jeffrey T. – 13

V

Vonder Haar, Thomas H. – 81, 201

W

Ward, Joan M. – 87
 Weaver, Sandra K. – 35
 Wetmore, Alan – 31, 63
 White, Maire E. – 75
 Willand, James H. – 187, 211
 Winokur, Robert S. – xix
 Wood, Sidney A. – 69
 Wylie, Donald P. – 85, 155

Z

Zahn, Stephen G. – 145
 Zdenek, David J. – 53

CIDOS-95 NOTES

CIDOS-95 NOTES

CIDOS-95 NOTES

CIDOS-95 NOTES

CIDOS-95 NOTES

CIDOS-95 NOTES

CIDOS-95 NOTES

CIDOS-95 NOTES

CIDOS-95 NOTES

CIDOS-95 NOTES

CIDOS-95 NOTES

CIDOS-95 NOTES

CIDOS-95 NOTES

CIDOS-95 NOTES

CIDOS-95 NOTES

CIDOS-95 NOTES

CIDOS-95 NOTES

CIDOS-95 NOTES

CIDOS-95 NOTES

CIDOS-95 NOTES